

**GENERAL LORENTZ INVARIANT  
REPRESENTATION OF THE NN INTERACTION  
APPLIED TO QUASIELASTIC SCATTERING OF  
POLARIZED PROTONS**

**B. I. S. van der Ventel**



Dissertation submitted in partial fulfillment of the requirements  
for the degree of Doctor of Philosophy  
at the University of Stellenbosch

Supervisor: Dr G. C. Hillhouse

Co-supervisors: Prof P.R. De Kock and Prof H.B. Geyer

December 1999

## Declaration

I the undersigned hereby declare that the work contained in this dissertation is my own original work and has not previously in its entirety or in part been submitted at any university for a degree.

15/11/99

.....  
Date



# Abstract

In this dissertation a general Lorentz invariant representation (referred to as the IA2 representation) of the nucleon-nucleon (NN) scattering matrix,  $\hat{F}$  is applied to the calculation of complete sets of spin observables for quasielastic  $(\vec{p}, \vec{p}')$  and  $(\vec{p}, \vec{n})$  scattering in the context of the Relativistic Plane Wave Impulse Approximation (RPWIA). A complete expansion of the NN scattering matrix eliminates the arbitrariness of the previously used five-term representation (the IA1 or SPVAT form of the NN scattering matrix) and allows for a correct incorporation of effective-mass-type medium effects within the RPWIA framework and within the context of the Walecka model. The aim is to investigate how successful the Walecka-model effective nucleon mass concept is in describing quasielastic  $(\vec{p}, \vec{p}')$  and  $(\vec{p}, \vec{n})$  scattering data and whether it is possible to find a combination of effective projectile and target nucleon masses which can describe a complete set of quasielastic spin observables. Calculations are done for the energy range 200 MeV to 500 MeV and for the following targets:  $^{40}\text{Ca}$ ,  $^{12}\text{C}$ ,  $^{208}\text{Pb}$  and  $^{54}\text{Fe}$ .

Historically the first application of the IA1 representation of  $\hat{F}$  within the context of the RPWIA was to the reaction  $^{40}\text{Ca}(\vec{p}, \vec{p}')$  at  $T_{lab} = 500$  MeV and  $\theta_{lab} = 19^\circ$ . There it was found that the use of an effective mass for the external nucleons moved the theoretical calculation closer to the analyzing power data and below the free mass calculation. This was referred to as the 'quenching effect' in the analyzing power and was claimed to be a 'relativistic signature'. Employing the correct IA2 representation of  $\hat{F}$ , however, shows that the quenching effect in  $A_y$  is not as large as was initially predicted and in effect becomes negligible as the energy is lowered to 200 MeV for  $(\vec{p}, \vec{p}')$  scattering. The new calculations employing the IA2 representation therefore expose the danger of using an incomplete representation of  $\hat{F}$ . We also extract (individually for  $(\vec{p}, \vec{p}')$  and  $(\vec{p}, \vec{n})$  scattering) an optimal set of effective projectile and target nucleon masses which is defined as that combination which gives the best fit to all experimental spin observables for a specific reaction and incident laboratory kinetic energy  $T_{lab}$ . One finds that the optimal set for  $(\vec{p}, \vec{p}')$  and  $(\vec{p}, \vec{n})$  scattering are in general fairly the same and constant with  $T_{lab}$  and target nucleus. Numerical results indicate that the optimal set provides an adequate description of  $D_{\ell\ell}$ ,  $D_{s's}$ ,  $D_{s'\ell}$  and  $D_{\ell s}$  for the energy range 500 MeV to 200 MeV both at the quasielastic peak and as a function of energy transfer. The description of  $D_{nn}$  (for both the  $(\vec{p}, \vec{n})$  and  $(\vec{p}, \vec{p}')$  reaction) and  $A_y$  (for the  $(\vec{p}, \vec{p}')$  reaction only) becomes problematic, however, as the energy is lowered from 500 MeV to 200 MeV.

# Samevatting

Hierdie proefskrif bevat die toepassing van 'n algemene Lorentz invariante daarstelling (bekend as die IA2 daarstelling) van die nukleon-nukleon (NN) verstrooiingsmatriks,  $\hat{F}$  in die berekening van volledige stelle van spin waarneembare vir kwasi-elastiese  $(\vec{p}, \vec{p}')$  en  $(\vec{p}, \vec{n})$  verstrooiing binne die raamwerk van die Relatiewistiese Vlakgolf Impulsbenadering (RVI). 'n Volledige uitbreiding van die NN verstrooiingsmatriks verwyder die dubbelsinnighede wat inherent aan die sogenaamde IA1 of SPVAT daarstelling van  $\hat{F}$  is en bemaak sodoende 'n meer korrekte inagneming moontlik van die omringende kernmedium deur middel van effektiewe nukleonmassas volgens die Walecka model. Die doel is om vas te stel hoe suksesvol die konsep van 'n effektiewe nukleonmassa is in die beskrywing van kwasi-elastiese  $(\vec{p}, \vec{p}')$  en  $(\vec{p}, \vec{n})$  verstrooiingsdata en of dit moontlik is om 'n kombinasie van effektiewe massas vir die projektiel en teiken nukleone te verkry wat 'n volledige stel van kwasi-elastiese spin waarneembare kan bekryf. Berekeninge is gedoen vir laboratorium energieë tussen 200 MeV en 500 MeV en vir die volgende teikens:  $^{40}\text{Ca}$ ,  $^{12}\text{C}$ ,  $^{208}\text{Pb}$  en  $^{54}\text{Fe}$ .

Histories was die eerste toepassing van die IA1 daarstelling van  $\hat{F}$  op die reaksie  $^{40}\text{Ca}(\vec{p}, \vec{p}')$  by  $T_{lab} = 500$  MeV en  $\theta_{lab} = 19^\circ$ . Daar is toe gevind dat die gebruik van effektiewe massas die berekende analiseervermoë aansienlik verminder (relatief tot 'n vrye nukleon massa berekening: die sogenaamde 'quenching effect'.) en dat dit die gemete waardes kan reproduseer. Hierdie situasie is as 'n duidelike relatiewistiese effek geïnterpreteer. Die gebruik van die korrekte IA2 daarstelling van  $\hat{F}$  toon egter dat die dempingseffek nie so groot is as wat oorspronklik voorspel is nie en dat dit eintlik weglaatbaar klein word soos die energie verminder na 200 MeV vir  $(\vec{p}, \vec{p}')$  verstrooiing. Die nuwe berekeninge wat gebruik maak van die IA2 daarstelling wys dus die gevare en beperkings uit verbonde aan die gebruik van 'n onvolledige uitbreiding van  $\hat{F}$ . Verder word 'n optimale stel effektiewe projektiel en teiken massas (afsonderlik vir  $(\vec{p}, \vec{n})$  en  $(\vec{p}, \vec{p}')$  verstrooiing) afgelei wat gedefinieer word as daardie stel wat die beste passing gee vir alle eksperimentele spin waarneembare vir 'n spesifieke reaksie en invallende laboratorium energie  $T_{lab}$ . Berekeninge toon aan dat die IA2 daarstelling van  $\hat{F}$ , tesame met die effektiewe nukleonmassa as parameter, bevredigende resultate lewer vir die volgende spin waarneembare:  $D_{\ell\ell}$ ,  $D_{s's}$ ,  $D_{s'\ell}$  en  $D_{\ell's}$  vir beide  $(\vec{p}, \vec{p}')$  en  $(\vec{p}, \vec{n})$  verstrooiing vir die energieë 200 MeV tot 500 MeV. Die beskrywing van  $D_{nn}$  (vir beide die  $(\vec{p}, \vec{n})$  en  $(\vec{p}, \vec{p}')$  reaksies) en  $A_y$  (vir die  $(\vec{p}, \vec{p}')$  reaksie) word egter problematies soos die energie verlaag vanaf 500 MeV na 200 MeV.



# Acknowledgments

I am greatly indebted to the following people who contributed towards the successful completion of my dissertation:

- Prof P.R. De Kock and Dr G.C. Hillhouse. Thank you both for accepting me in your research team in 1996 which allowed me to study an interesting problem in Physics. Thank you Greg and Runan for your support, advice and constructive criticism in each aspect of the project.
- Prof H.B. Geyer for providing me with financial support from 1996 to 1998.
- Prof J.A. Tjon and Prof S.J. Wallace for helping me to understand the IA2 formalism.
- Prof S.J. Wallace and the rest of the Theory Group for Quarks, Hadrons, and Nuclei at the University of Maryland for the kind hospitality shown to me during my visit from March 1998 to May 1998.
- The National Accelerator Centre for the financial assistance for the period 1996 to July 1999.
- The South African FRD and the Harry Crossley Foundation for the financial support for my visit to the Universities of Utrecht and Maryland in 1998.

I wish to thank everyone below, who did not help with the Physics, but at least kept me sane:

- My good friend and fellow PhD-student, Hendrik De Waal.
- My parents for their love, support, prayers and encouragement through all my years of study.

Above all I wish to thank Almighty God who has guided me and helped me to achieve this milestone.

*Loof die Here, o my siel, en vergeet geeneen van sy weldade nie !*

*Psalm 103*

# Contents

<b>1</b>	<b>Introduction and motivation</b>	<b>1</b>
<b>2</b>	<b>General Lorentz invariant representation of the NN interaction applied to quasielastic scattering of polarized protons</b>	<b>5</b>
2.1	Introduction . . . . .	5
2.2	Inclusive quasielastic proton-nucleus scattering . . . . .	6
2.3	Relativistic Plane Wave Impulse Approximation . . . . .	11
2.4	Application of IA1 to quasielastic proton-nucleus scattering . . . . .	15
2.5	Application of IA2 to quasielastic proton-nucleus scattering . . . . .	17
2.5.1	General Lorentz invariant representation of the NN scattering matrix	17
2.5.2	Derivation of effective t-matrix . . . . .	34
2.5.3	Transformation from the invariant amplitudes $F_n^{\{\rho\}}$ ( $n = 1 \dots 13$ ) to the effective amplitudes $a_n$ ( $n = 1 \dots 8$ ) . . . . .	42
2.5.4	Expressions for spin observables in terms of effective amplitudes, $a_n$	46
2.6	Summary . . . . .	52
<b>3</b>	<b>IA2 predictions of quasielastic spin observables</b>	<b>53</b>
3.1	Introduction . . . . .	53
3.2	Numerical Checks . . . . .	54
3.3	Medium modifications of the effective amplitudes . . . . .	59
3.4	IA2 versus IA1 predictions without Fermi averaging . . . . .	67
3.4.1	Effective mass bands . . . . .	67
3.4.2	Optimal effective masses . . . . .	69
3.4.3	Discussion of results . . . . .	70
3.5	IA2 versus IA1 predictions with Fermi averaging . . . . .	81
3.6	Comparison of IA2 predictions to polarization data . . . . .	81
3.7	Summary and Conclusions . . . . .	83

<b>A Transformation properties of covariants, <math>\Gamma_n</math>, under charge symmetry and time-reversal transformations</b>	<b>101</b>
A.1 Transformation properties of covariants, $\Gamma_n$ under a charge symmetry transformation . . . . .	101
A.2 Transformation properties of the covariants, $\Gamma_n$ , under a time-reversal transformation . . . . .	102
<b>B Definition of matrices <math>t_i</math></b>	<b>104</b>
<b>C Explicit expressions for spin observables in terms of the effective amplitudes, <math>a_i (i = 1 - 8)</math></b>	<b>107</b>
<b>D Exchange covariants, <math>\tilde{S}, \tilde{P}, \tilde{V}, \tilde{A}</math> and <math>\tilde{T}</math> in terms of the <i>SPVAT</i> covariants</b>	<b>109</b>

# List of Figures

- 2.1 Double differential cross sections  $\frac{d\sigma}{d\Omega d\omega}$  (in  $\text{mb sr}^{-1} \text{MeV}^{-1}$ ) for inclusive  $^{12}\text{C}(p,n)$  and  $^{12}\text{C}(p,p)$  scattering as a function of energy transferred to the nucleus ( $\omega$ ), for a laboratory scattering angle of  $20^\circ$ , and incident proton energy of 392 MeV and 400 MeV respectively. The data are from Ref. [Ot97] . . . . . 8
- 2.2 Diagram illustrating the directions of the unit vectors  $\hat{\ell}, \hat{s}, \hat{n}, \hat{\ell}'$  and  $\hat{s}'$ . The vector quantities  $\vec{p}_1$  and  $\vec{k}_1$  are the incident and final three-momenta in the nucleon-nucleus laboratory frame respectively, and  $\theta_{\text{lab}}$  is the laboratory scattering angle. . . . . 9
- 2.3 Diagrammatic representation of the polarization transfer observables, showing with short arrows, the relevant pair of spin directions before and after scattering with respect to the beam direction. . . . . 10
- 2.4 Two-body scattering process with momentum, mass and spin labels for the external nucleons.  $\vec{p}_j$  and  $\vec{k}_j$  ( $j = 1, 2$ ) are the initial and final three-momenta of the external nucleons respectively.  $s_i$  and  $s_f$  are the spin four-vectors for the projectile and ejectile respectively. Similarly for nucleon 2 and nucleon 2'.  $M_j$  ( $j = 1, 2$ ) represents the effective nucleon mass.  $\hat{F}$  is the  $16 \times 16$  nucleon-nucleon scattering matrix. . . . . 12
- 2.5 Definition of polar ( $\beta$ ) and azimuthal ( $\alpha$ ) angles for the unit vector  $\hat{n}$  associated with the Pauli spinor  $\phi(\hat{n})$ . . . . . 14
- 2.6 A charge symmetry transformation on the left-hand figure produces the one on the right. . . . . 26
- 2.7 A time reversal transformation on the left-hand figure produces the one on the right. The tilde symbol ( $\sim$ ) on the momenta and spin denote time reversed quantities. . . . . 29
- 2.8 Laboratory kinematics for the scattering process of Fig. 2.4. . . . . 47
- 3.1 Here, in fact, two graphs of  $\Gamma''$ , calculated respectively from Eqs. 3.3 and 3.4 are plotted for the same kinematical configuration: A 200 MeV incident proton beam and no medium effects allowed on the projectile and target nucleons. Only one graph is visible which shows that the sets of  $\Gamma''$  values coincide exactly. It serves to illustrate the correct IA2 calculation based on Eq. 3.4. . . . . 56



- 3.2  $\Gamma''$  calculated via Pauli traces but including only one covariant (indicated by the subscript) to calculate the effective amplitudes as well as  $\Gamma''$  calculated via Dirac traces for the specific covariant. Only one line is present on the graph since the two curves coincide exactly. . . . . 60
- 3.3 Real parts of the isospin zero effective amplitudes for  $T_{lab} = 200$  MeV as a function of  $\theta_{lab}$ . The solid line represents the effective mass calculation for which  $\frac{M_1}{M} = 0.8$  and  $\frac{M_2}{M} = 0.8$  and the dashed line represents the free mass calculation. . . . . 61
- 3.4 Imaginary parts of the isospin zero effective amplitudes for  $T_{lab} = 200$  MeV as a function of  $\theta_{lab}$ . The solid line represents the effective mass calculation for which  $\frac{M_1}{M} = 0.8$  and  $\frac{M_2}{M} = 0.8$  and the dashed line represents the free mass calculation. . . . . 62
- 3.5 Real parts of the isospin one effective amplitudes for  $T_{lab} = 200$  MeV as a function of  $\theta_{lab}$ . The solid line represents the effective mass calculation for which  $\frac{M_1}{M} = 0.8$  and  $\frac{M_2}{M} = 0.8$  and the dashed line represents the free mass calculation. . . . . 63
- 3.6 Imaginary parts of the isospin one effective amplitudes for  $T_{lab} = 200$  MeV as a function of  $\theta_{lab}$ . The solid line represents the effective mass calculation for which  $\frac{M_1}{M} = 0.8$  and  $\frac{M_2}{M} = 0.8$  and the dashed line represents the free mass calculation. . . . . 64
- 3.7 Real parts of the charge exchange effective amplitudes for  $T_{lab} = 200$  MeV as a function of  $\theta_{lab}$ . The solid line represents the effective mass calculation for which  $\frac{M_1}{M} = 0.8$  and  $\frac{M_2}{M} = 0.8$  and the dashed line represents the free mass calculation. . . . . 65
- 3.8 Imaginary parts of the charge exchange effective amplitudes for  $T_{lab} = 200$  MeV as a function of  $\theta_{lab}$ . The solid line represents the effective mass calculation for which  $\frac{M_1}{M} = 0.8$  and  $\frac{M_2}{M} = 0.8$  and the dashed line represents the free mass calculation. . . . . 66
- 3.9 Values of  $A_y$  and  $D_{ij}$  versus  $\theta_{lab}$  for  $^{40}\text{Ca}(\vec{p}, \vec{p}')$  at  $T_{lab} = 500$  MeV. Solid and dashed lines represent the calculations with optimal effective mass values in respectively the IA2 and IA1 representations. The hatched bands denote the range of values which result from varying  $\frac{M_1}{M}$  and  $\frac{M_2}{M}$  over the full range (see text): The straight line hatch pattern denotes the IA1 model; the dotted hatch pattern the IA2 model. The long-dash-short-dash lines represent the free mass values. Data (at  $\theta_{lab} = 19^\circ$ ) are from Ref. [Ca84]. 73
- 3.10 Same as Fig. 3.9 but for the reaction  $^{12}\text{C}(\vec{p}, \vec{p}')$  at  $T_{lab} = 420$  MeV and  $\theta_{lab} = 24^\circ$ . The data are from Ref. [Ch90]. . . . . 74
- 3.11 Same as Fig. 3.9 but for the reaction  $^{12}\text{C}(\vec{p}, \vec{p}')$  at  $T_{lab} = 290$  MeV and  $\theta_{lab} = 30^\circ$ . The data are from Ref. [Ch90]. . . . . 75



- 3.12 Same as Fig. 3.9 but for the reaction  $^{54}\text{Fe}(\vec{p}, \vec{p}')$  at  $T_{lab} = 290$  MeV and  $\theta_{lab} = 20^\circ$ . The data are from Ref. [Hä88]. . . . . 76
- 3.13 For this reaction,  $^{40}\text{Ca}(\vec{p}, \vec{p}')$  at  $T_{lab} = 200$  MeV and  $\theta_{lab} = 30^\circ$  only a free mass calculation (denoted by the solid line) was performed due to the lack of a complete set of spin observables. The data are from Ref. [Ca95]. 77
- 3.14 Same as Fig. 3.9 but for the reaction  $^{40}\text{Ca}(\vec{p}, \vec{n})$  at  $T_{lab} = 495$  MeV and  $\theta_{lab} = 18^\circ$  and  $27^\circ$ . The data are from Ref. [Ta98]. . . . . 78
- 3.15 Same as Fig. 3.9 but for the reaction  $^{40}\text{Ca}(\vec{p}, \vec{n})$  at  $T_{lab} = 200$  MeV and  $\theta_{lab} = 24^\circ, 37^\circ$  and  $48^\circ$ . The data are from Ref. [Ha98]. . . . . 79
- 3.16 Same as Fig. 3.9 but for the reaction  $^{208}\text{Pb}(\vec{p}, \vec{n})$  at  $T_{lab} = 200$  MeV and  $\theta_{lab} = 24^\circ, 37^\circ$  and  $48^\circ$ . The data are from Ref. [Ha98]. . . . . 80
- 3.17 Values of  $A_y$  and  $D_{ij}$  versus  $\theta_{lab}$  for  $^{40}\text{Ca}(\vec{p}, \vec{p}')$  at  $T_{lab} = 500$  MeV. This figure includes the Fermi motion of the target nucleon. Compare the shape of the effective mass bands to Fig 3.9 which neglected the Fermi motion of the target nucleon. Solid and dashed lines represent the calculations with optimal effective mass values in respectively the IA2 and IA1 representations. The hatched bands denote the range of values which result from varying  $\frac{M_1}{M}$  and  $\frac{M_2}{M}$  over the full range (see text). The straight line hatch pattern denotes the IA1 model; the dotted hatch pattern the IA2 model. The long-dash-short-dash lines represent the free mass values. Data (at  $\theta_{lab} = 19^\circ$ ) are from Ref. [Ca84]. . . . . 87
- 3.18 Values of  $A_y$  and  $D_{ij}$  versus energy transfer,  $\omega$ , for the reaction  $^{40}\text{Ca}(\vec{p}, \vec{p}')$  at  $T_{lab} = 500$  MeV and  $\theta_{lab} = 19^\circ$ . The solid and dashed lines represent the IA2 optimal mass set and the free mass calculations respectively. The long-dash-short-dash line corresponds to the values  $\frac{M_1}{M} = M_{1SC}^*$  and  $\frac{M_2}{M} = M_{2SC}^*$  (see text and Ref. [Hi94]), calculated from self-consistent (SC) nuclear potentials. The peak is located at  $\omega \approx 63$  MeV and the data are from Ref.[Ca84]. . . . . 88
- 3.19 Similar to Fig 3.18 for the reaction  $^{12}\text{C}(\vec{p}, \vec{p}')$  at  $T_{lab} = 420$  MeV and  $\theta_{lab} = 24^\circ$ . The peak is located at  $\omega \approx 93$  MeV and the data are from Refs. [Ch89, Ch90]. . . . . 89
- 3.20 Similar to Fig 3.18 for the reaction  $^{12}\text{C}(\vec{p}, \vec{p}')$  at  $T_{lab} = 290$  MeV and  $\theta_{lab} = 30^\circ$ . The peak is located at  $\omega \approx 90$  MeV and the data are from Ref. [Ch90]. . . . . 90
- 3.21 Similar to Fig 3.18 for the reaction  $^{54}\text{Fe}(\vec{p}, \vec{p}')$  at  $T_{lab} = 290$  MeV and  $\theta_{lab} = 20^\circ$ . The peak is located at  $\omega \approx 40$  MeV and the data are from Ref. [Hä88]. . . . . 91

- 3.22 For this reaction,  $^{40}\text{Ca}(\vec{p}, \vec{p}')$  at  $T_{lab} = 200$  MeV and  $\theta_{lab} = 30^\circ$ , no optimal set was extracted due to the lack of a complete set of experimental spin observables. The solid line corresponds to the choice,  $\frac{M_1}{M} = M_{1SC}^*$  and  $\frac{M_2}{M} = M_{25C}^*$  (see Fig. 3.18) while the dashed line refers to the free calculation. The peak is located at  $\omega \approx 64$  MeV and the data are from Ref. [Ca95]. . . . . 92
- 3.23 Similar to Fig 3.18 for the reaction  $^{40}\text{Ca}(\vec{p}, \vec{n})$  at  $T_{lab} = 495$  MeV and  $\theta_{lab} = 18^\circ$ . The peak is located at  $\omega \approx 82$  MeV and the data are from Ref. [Ta98]. . . . . 93
- 3.24 Similar to Fig 3.18 for the reaction  $^{40}\text{Ca}(\vec{p}, \vec{n})$  at  $T_{lab} = 495$  MeV and  $\theta_{lab} = 27^\circ$ . The peak is located at  $\omega \approx 138$  MeV and the data are from Ref. [Ta98]. . . . . 94
- 3.25 Similar to Fig 3.18 for the reaction  $^{40}\text{Ca}(\vec{p}, \vec{n})$  at  $T_{lab} = 200$  MeV and  $\theta_{lab} = 24^\circ$ . The peak is located at  $\omega \approx 67$  MeV and the data are from Ref. [Ha98]. . . . . 95
- 3.26 Similar to Fig 3.18 for the reaction  $^{40}\text{Ca}(\vec{p}, \vec{n})$  at  $T_{lab} = 200$  MeV and  $\theta_{lab} = 37^\circ$ . The peak is located at  $\omega \approx 107$  MeV and the data are from Ref. [Ha98]. . . . . 96
- 3.27 Similar to Fig 3.18 for the reaction  $^{40}\text{Ca}(\vec{p}, \vec{n})$  at  $T_{lab} = 200$  MeV and  $\theta_{lab} = 48^\circ$ . The peak is located at  $\omega \approx 127$  MeV and the data are from Ref. [Ha98]. . . . . 97
- 3.28 Similar to Fig 3.18 for the reaction  $^{208}\text{Pb}(\vec{p}, \vec{n})$  at  $T_{lab} = 200$  MeV and  $\theta_{lab} = 24^\circ$ . The peak is located at  $\omega \approx 67$  MeV and the data are from Ref. [Ha98]. . . . . 98
- 3.29 Similar to Fig 3.18 for the reaction  $^{208}\text{Pb}(\vec{p}, \vec{n})$  at  $T_{lab} = 200$  MeV and  $\theta_{lab} = 37^\circ$ . The peak is located at  $\omega \approx 127$  MeV and the data are from Ref. [Ha98]. . . . . 99
- 3.30 Similar to Fig 3.18 for the reaction  $^{208}\text{Pb}(\vec{p}, \vec{n})$  at  $T_{lab} = 200$  MeV and  $\theta_{lab} = 48^\circ$ . The peak is located at  $\omega \approx 127$  MeV and the data are from Ref. [Ha98]. . . . . 100

# List of Tables

2.1	<i>Relation between rho-spin labels, <math>\rho_1, \rho'_1, \rho_2, \rho'_2</math> and pair indices, <math>ij</math> for the various subclasses.</i>	21
2.2	<i>Constraint condition for each rho-spin sector (or subclass) as well as the value of the parameter <math>\eta_{ij}</math>.</i>	23
2.3	<i>Transformation properties of the variables <math>s_i</math> as well as the gamma matrices under a parity transformation.</i>	25
2.4	<i>Transformation properties of the gamma matrices and <math>s_i</math> under a time-reversal transformation.</i>	33
2.5	<i>This table shows the number of independent amplitudes for each subclass, which arise due to constraint conditions. CS denotes charge symmetry, TR denotes time-reversal and OMS denotes on-mass-shell.</i>	35
2.6	<i>Continuation of Table 2.5 which shows the number of independent amplitudes for each subclass, which arise due to constraint conditions.</i>	36
2.7	<i>Values of kinematical quantities containing <math>\hat{s}_i</math> and/or <math>\hat{s}_f</math> for each non-zero polarization transfer observable.</i>	51
3.1	<i>Experimental data for which calculations were done at the quasielastic peak (as a function of laboratory scattering angle) and as a function of energy transfer.</i>	54
3.2	<i>Values of optimal effective mass combinations, <math>(\frac{M_1}{M}, \frac{M_2}{M})</math>, extracted at the quasielastic peak for the case where Fermi motion is neglected (the first set is the optimal IA1 set and the second is the optimal IA2 set) and for the case where Fermi motion of the target nucleon is taken into account (the first set is the optimal IA1 set and the second is the optimal IA2 set). The last column refers to the effective mass combinations which are calculated theoretically [Hi94].</i>	70
B.1	<i>t-matrices for the SPVAT covariants.</i>	105
B.2	<i>t-matrices for covariants <math>K_{10}</math> to <math>K_{11}</math>.</i>	105
B.3	<i>t-matrices for covariants <math>K_{12}</math> to <math>K_{13}</math>.</i>	106



# Chapter 1

## Introduction and motivation

Even though the neutron was discovered as long ago as 1932 by Chadwick [Ch32], the description of the nucleon-nucleon (NN) interaction from first principles remains to this day one of the most fundamental problems in physics. The NN interaction is dependent on the relative spin orientation of the two nucleons [Pa81] and hence it can best be studied if a beam of spin polarized protons is scattered and one measures the so-called spin observables describing the transition of the spin from some initial polarization to some final polarization.

This dissertation is concerned with the calculation of complete sets of spin observables for quasielastic  $(\vec{p}, \vec{p}')$  and  $(\vec{p}, \vec{n})$  scattering employing a general Lorentz invariant representation of the NN scattering matrix within the framework of the Relativistic Plane Wave Impulse Approximation (RPWIA). Eventually I calculate the associated complete set of spin observables for reactions in the energy range of 200 MeV to 500 MeV and the target nuclei include  $^{12}\text{C}$ ,  $^{40}\text{Ca}$ ,  $^{54}\text{Fe}$  and  $^{208}\text{Pb}$ . What follows is a brief motivation of the latter assignment.

For laboratory kinetic energies between 100 MeV and 500 MeV and moderate momentum transfers ( $|\vec{q}| < 2 \text{ fm}^{-1}$ ) quasielastic scattering is the dominant reaction mechanism in proton-nucleus scattering [Hi99]. It has the following characteristics which also explains why it is called a 'quasielastic' process: It manifests itself as a broad peak in the inclusive excitation spectrum: See Fig 2.1. The use of a polarized incident beam allows one to measure the following set of observables: the unpolarized double differential cross section, the induced polarization, the analyzing power and the spin transfer coefficients. Quasielastic scattering behaves like NN scattering inside the nuclear medium due to the following reasons:

1. The excitation energy associated with the centroid of the peak approximately obeys the conservation of momentum and energy of two colliding particles of equal mass.
2. The spin transfer coefficients are practically the same for scattering off closed shell nuclei within a large mass range ( $^2\text{H}$ ,  $^{12}\text{C}$ ,  $^{40}\text{Ca}$  and  $^{208}\text{Pb}$  [Wa99]), which indicates a general non-involvement of the other nucleons in the nucleus.

The most basic assumption is therefore that this type of scattering can be considered as mainly a single-step process whereby the projectile interacts with one target nucleon while the other nucleons remain inert. Thus it is considered to be effectively a single

NN scattering which occurs in the medium of the other nucleons of the nucleus and can therefore be called a quasielastic process. Deviations of any observables from their corresponding free NN values can thus be attributed to modifications of the free NN interaction due to the surrounding nuclear medium. Hence quasielastic scattering provides a way to study effects of the nuclear medium on the basic NN interaction. It is desirable to measure a complete set of spin observables since medium effects might show up differently for the different spin observables.

In this study we will be concerned with the calculation of the analyzing power and the polarization transfer observables. The unpolarized cross section represents an average over the spins and in a sense one 'washes out' any information relating to the spin, whereas the polarization transfer observables are sensitive to any changes in the spin dependence of the NN interaction in the nuclear medium. Distortions of the incoming and outgoing proton wave functions primarily reduce the cross section, whereas the spin observables (which are defined as ratios of polarized cross sections) are expected to be insensitive to distortion uncertainties. We consider both quasielastic ( $\vec{p}, \vec{p}'$ ) and ( $\vec{p}, \vec{n}$ ) scattering since these two reactions should yield complementary information about the different components of the NN interaction and hence provide further restrictions on any model of quasielastic proton-nucleus scattering. Measurements of complete sets of quasielastic spin observables are currently underway at the Research Center for Nuclear Physics (RCNP) in Osaka, Japan.

In a relativistic description of fundamental problems in Nuclear Physics the dynamical equation is the Dirac equation as opposed to the traditional Schrödinger-based formalism. Historically the Dirac-based description could successfully predict the spin observables for elastic scattering of 500 MeV protons by  $^{40}\text{Ca}$ . This was first illustrated in the work of Clark and collaborators [Cl73, Ar76, Ar79, Ar81, Cl82] who showed that one can obtain excellent quantitative results for elastic proton-nucleus spin observables if one solves the Dirac equation with large (attractive) scalar and (repulsive) vector phenomenological potentials [Cl82]. McNeil, Shepard and Wallace then showed [Mc83, Mc83a] that their parameter free theoretical description reproduces the qualitative features of the phenomenological approach of Clark et. al. A relativistic formulation of quasielastic proton-nucleus scattering was put forward by Horowitz and Murdock in 1988 [Ho88]. In their model, referred to as the Relativistic Plane Wave Impulse Approximation (RPWIA), they exploit the above-mentioned experimental features of quasielastic scattering and consider it to be a two-body scattering process in which the two nucleons participating in the reaction are described by four-component Dirac spinors, in which the nucleon mass is treated as a parameter. It is through the use of an effective nucleon mass that the effect of the spectator nucleons are taken into account, i.e. the fact that scattering takes place inside the nuclear medium. This effective nucleon mass is an intrinsically relativistic concept and was introduced in the work on nuclear structure and nuclear matter by Walecka [Wa74].

In order to calculate the spin observables the basic quantity of interest is the transition matrix element, defined as:

$$\mathcal{M} = \langle f | \hat{F} | i \rangle$$



where  $|i\rangle$  and  $|f\rangle$  denote initial and final nuclear states respectively and  $\hat{F}$  is the scattering operator that connects the initial and final states. In general these three components of  $\mathcal{M}$  namely  $|i\rangle$ ,  $|f\rangle$  and  $\hat{F}$  are very complicated entities since the nucleus is a complicated many-body system. The above-mentioned experimental features of quasielastic scattering allow one, however, to make certain assumptions which lead to a solvable model in the sense that theoretical numerical results can be obtained for the spin observables. Since the RPWIA reduces quasielastic scattering to a two-body scattering process one writes:

$$|i\rangle = |i_1\rangle \otimes |i_2\rangle$$

and

$$|f\rangle = |f_1\rangle \otimes |f_2\rangle.$$

Here  $|i_1\rangle$  and  $|i_2\rangle$  are free particle Dirac spinors with free nucleon masses replaced by effective nucleon masses (within the context of the Walecka model [Wa74]) for the two scattering nucleons. This is a huge simplification since the projectile does experience strong scalar and vector optical potentials in the nucleus before and after the one-step scattering event. Similarly the target nucleon experiences strong scalar and vector bound-state potentials. However, the experimental data [Wa99] indicate that at the momentum transfers of interest, the wave functions of the scattering nucleons in the nucleus can be adequately approximated by free particle wave functions. Therefore the nucleons are described in the present analysis by a Fermi gas model. The spin transfer coefficients are defined as ratios of polarized double differential cross sections and therefore as a first approximation, the effects of distortions on the projectile are neglected. (In a relativistic distorted wave impulse approximation one has to solve the Dirac equation with scalar and vector potentials. Not only is this complicated numerically but it could also obscure the basic aim of this project which is the investigation of the form of the NN scattering matrix which is employed in the theoretical calculations.)

In the direct product space of the two nucleons the relativistic NN scattering matrix is a  $16 \times 16$  matrix with 256 matrix elements. In the first application of the RPWIA [Ho88],  $\hat{F}$  was parameterised in terms of five invariant amplitudes (this is referred to as the IA1 representation of  $\hat{F}$ ) which could be directly obtained from the five Wolfenstein amplitudes parameterizing the non-relativistic NN scattering matrix. It is important to note that experimental data completely specify  $\hat{F}$  if one adopts a five-term representation. The IA1 representation of  $\hat{F}$  within the context of the RPWIA was applied to the reaction  $^{40}\text{Ca}(\vec{p}, \vec{p}')$  at  $T_{lab} = 500$  MeV and  $\theta_{lab} = 19^\circ$  [Ho88]. There it was found that the use of an effective mass for the external nucleons moved the theoretical calculation closer to the analyzing power data and below the free mass calculation. This was referred to as the 'quenching effect' in the analyzing power and was claimed to be a 'relativistic signature'. The polarization transfer observables, however, corresponded to the free mass calculation. Comparison of the limited data available with subsequent and more refined calculations [Hi94, Hi95, Hi98] revealed that quasielastic  $(\vec{p}, \vec{p}')$  and  $(\vec{p}, \vec{n})$  scattering prefer different five-term representations of  $\hat{F}$ .

One of the major goals of this dissertation is to address the latter ambiguity by considering a more rigorous representation of  $\hat{F}$ . There are two problems which can be identified with the IA1 representation of  $\hat{F}$ . Firstly, a five-term representation is necessarily ambiguous in the sense that one can exchange or even add covariants to  $\hat{F}$  if the only constraint is that one fits to free NN scattering data. Secondly, it can be shown that if one imposes the symmetries of the NN force, namely parity and time-reversal invariance as well as charge symmetry together with the on-mass-shell condition for the external nucleons then  $\hat{F}$  contains, in fact, 44 independent invariant amplitudes. This will be referred to as the IA2 representation of  $\hat{F}$  (and will be discussed in detail in Chapter 2). The remaining 39 amplitudes are then calculated via solution of the Bethe-Salpeter equation using a boson-exchange model for the NN force. It should always be kept in mind that the additional 39 amplitudes are based on a boson exchange model for the NN force. As emphasised by Horowitz [Ho91b], 'there is nothing sacred about a relativistic one boson exchange model'. The important point to note is that the *full* matrix structure of  $\hat{F}$  is *model-dependent*.

Further questions which will be addressed are the following:

1. How successful is the concept of an effective mass in describing quasielastic spin observables ?
2. Does there always exist an effective mass combination (i.e. a pair of effective projectile and target nucleon masses) which can describe a complete set of quasielastic spin observables ?
3. How do numerical results of quasielastic spin observables based on the IA1 representation of  $\hat{F}$  compare to those utilising the IA2 representation of  $\hat{F}$  ?

In this work we retain all the simplifying features of the RPWIA but the use of a complete set of amplitudes in  $\hat{F}$  now eliminates the arbitrariness of the original five-term representation, and also allows for an unambiguous incorporation of medium effects within the context of the Walecka model. This enables one to distinguish between experimental data which are genuine effective-mass-type medium effects and those which must be ascribed to other effects not taken into account by the RPWIA.

The organization of this thesis is as follows: In Chapter 2 we discuss some general experimental features of quasielastic scattering, review the IA2 representation of  $\hat{F}$  and present a formalism which applies the general Lorentz invariant representation of  $\hat{F}$  to quasielastic proton-nucleus scattering. The numerical results for quasielastic spin observables are presented in Chapter 3.



## Chapter 2

# General Lorentz invariant representation of the NN interaction applied to quasielastic scattering of polarized protons

### 2.1 Introduction

This chapter discusses in detail the general Lorentz invariant representation of  $\hat{F}$  and its application to quasielastic  $(\vec{p}, \vec{p}')$  and  $(\vec{p}, \vec{n})$  scattering within the framework of the Relativistic Plane Wave Impulse Approximation.

The work on elastic scattering of Refs. [Cl73, Ar76, Ar79, Ar81, Cl82, Mc83, Mc83a, Mu87] shows that the dominant terms in the optical potential for proton-nucleus elastic scattering are the large scalar and vector potentials with a small tensor contribution. Elastic scattering is therefore only sensitive to the scalar and vector pieces of the NN amplitude. There are two important aspects to quasielastic scattering. Firstly one needs a model for the scattering process itself. This is the Relativistic Plane Wave Impulse Approximation (RPWIA) which will be reviewed in Section 2.3. Secondly, since experimental data on the spin observables suggest that quasielastic scattering is essentially NN scattering inside the nuclear medium (see Section 2.2), quasielastic scattering provides a direct probe for studying medium modifications of the NN interaction. This is of fundamental importance since all studies in Nuclear Physics have to assume some form for the NN interaction. The fundamental quantity which must be evaluated in quasielastic scattering is the invariant matrix element  $\mathcal{M}$  already defined in Chapter 1. All observable quantities can be expressed in terms of the transition matrix element. All previous studies of quasielastic scattering have assumed a five-term representation (called the IA1 representation) of  $\hat{F}$ . This is an incomplete representation of  $\hat{F}$  and since it affects the calculation of spin observables it is necessary to improve on this simple model for  $\hat{F}$  by using a general Lorentz invariant representation of  $\hat{F}$  instead which is referred to as the IA2 representation.

In this chapter we review the Relativistic Plane Wave Impulse Approximation (RPWIA) as well as the general Lorentz invariant representation of the nucleon-nucleon scattering matrix. In Sections 2.5.2, 2.5.3 and 2.5.4 we discuss in detail the formalism which implements the IA2 representation in the RPWIA to calculate complete sets of spin observables for quasielastic proton-nucleus scattering. Before proceeding with the theoretical discussion we review some of the most important experimental features of quasielastic  $(\vec{p}, \vec{p}')$  and  $(\vec{p}, \vec{n})$  scattering, the purpose being to show that the simplifying assumptions



of the RPWIA are based on experimental considerations.

## 2.2 Inclusive quasielastic proton-nucleus scattering

Quasielastic proton-nucleus scattering is a complicated process since the nucleus is a very complicated many-body system. Experimental data on the spin observables, however, allow us to make simplifying assumptions in order to obtain a tractable model for the scattering process. A detailed discussion of the experimental status as well as a complete summary of the world data (until March 1999) for quasielastic  $(\vec{p}, \vec{p}')$  and  $(\vec{p}, \vec{n})$  scattering can be found in Ref. [Hi99]. Below we mention some experimental features of quasielastic scattering.

At incident proton energies between 100 and 500 MeV, the unpolarized double differential cross section (plotted as a function of energy transfer or excitation energy,  $\omega$ ) for inclusive  $(p, p')$  and  $(p, n)$  scattering at a fixed momentum transfer (corresponding to a fixed angle) has the typical form shown in Fig 2.1. The dominant broad bump or peak is called the quasielastic region. For  $(p, p')$  scattering the centroid corresponds to free NN kinematics, i.e.  $\omega_{peak} = \frac{\vec{q}^2}{2M}$  (where  $\vec{q}$  is the three-momentum transfer and  $M$  is the free nucleon mass), whereas for  $(p, n)$  scattering it is slightly shifted away from the peak for free NN kinematics [Wa94]. The width of the peak is attributed to the initial Fermi motion of the target nucleons. As the incident proton energy is increased, the quasielastic peak becomes more pronounced. As the scattering angle is increased, the width of the peak broadens and its magnitude drops. Further phenomenological studies [Ka90] have revealed the following empirical features:

- The position of the peak closely follows free NN kinematics.
- The shape is typically asymmetric.
- The quasielastic peak position does not vary significantly with the target mass.

The similarity between free NN and quasielastic peak positions motivates the assumption that quasielastic scattering can be considered to be a single-step process, whereby the projectile knocks out a single bound nucleon from the target nucleus, while the rest of the nucleons act as spectators. *Quasielastic proton-nucleus scattering can therefore be viewed as NN scattering inside the nuclear medium.* Since quasielastic scattering is essentially spin- $\frac{1}{2}$ -spin- $\frac{1}{2}$  scattering, the following complete set of observables can be measured [Hi99]

$$\left\{ \frac{d\sigma}{d\Omega d\omega}, P, A_y, D_{ij} \right\}$$

where

- $\frac{d\sigma}{d\Omega d\omega}$  is the unpolarized double differential cross section,

- $P$  is the induced polarization (perpendicular to the scattering plane) which results from the scattering of an unpolarized beam from an unpolarized target [Pa81],
- $A_y$  is the analyzing power which is a measure of the left-right asymmetry [Pa81] of the reaction products. Due to time-reversal invariance  $P = A_y$  [Ch90],
- $D_{i'j}$  represents the polarization transfer coefficients where  $j(i')$  is the initial (final) polarization direction where

$$\begin{aligned} j &\in \{\hat{\ell}; \hat{s}; \hat{n}\} & \text{and} \\ i' &\in \{\hat{\ell}'; \hat{s}'; \hat{n}\}. \end{aligned}$$

The longitudinal direction  $\hat{\ell}$  is defined as:

$$\hat{\ell} = \frac{\vec{p}_1}{|\vec{p}_1|}$$

where  $\vec{p}_1$  is the incident proton three-momentum in the laboratory frame; the sideways direction  $\hat{s}$  is perpendicular to  $\hat{\ell}$  and the normal direction,  $\hat{n}$  where  $\hat{n} = \hat{\ell} \times \hat{s}$ . Similar definitions hold for the primed directions. These unit vectors are illustrated in Fig. 2.2 where  $\vec{p}_1$  and  $\vec{k}_1$  are the incident and final three-momenta in the laboratory frame respectively, and  $\theta_{lab}$  is the laboratory scattering angle. The  $D_{i'j}$ 's describe the scattering of a proton with incident polarization  $j$  to polarization  $i'$ . Assuming parity and time-reversal invariance, there are five non-zero polarization transfer observables [Pa81], namely

$$\{D_{\ell\ell}, D_{s's}, D_{s'l}, D_{l's}, D_{nn}\}.$$

The polarization transfer observables are illustrated schematically in Fig. 2.3, where  $D, A, R, A'$  and  $R'$  refer to the so-called Wolfenstein parameters [Pa81, Hi90].

The systematics of the polarization data are discussed in Ref. [Hi99], but one of the outstanding features is that the  $D_{i'j}$ 's (except  $D_{nn}$ ) display almost no target dependence [Wa96].

Experimental data on the spin observables suggest that quasielastic scattering approximately simulates NN scattering in the nuclear medium and hence the observables allow one to study how the free NN interaction is modified by the surrounding nuclear medium. A medium effect on a spin observable can be observed if  $P, A_y$  or  $D_{i'j}$  for quasielastic scattering are different from the corresponding values for free NN scattering. This assumes that the scattering process is just a single-step process, i.e. NN scattering inside the nuclear medium [Hi89]. Not all spin observables, however, are sensitive to the medium effect. For  $(\vec{p}, \vec{p}')$  scattering from  $^{40}\text{Ca}$  at 500 MeV, it is found that the induced polarization deviates from the free value, whereas the other observables are insensitive to the nuclear medium [Ho88]. Complete sets of spin observables should therefore be measured for both  $(\vec{p}, \vec{p}')$  and  $(\vec{p}, \vec{n})$  scattering for the same target, incident proton energy and momentum transfer: Medium modifications might show up differently for these two complementary reactions since they probe different parts of the NN interaction.

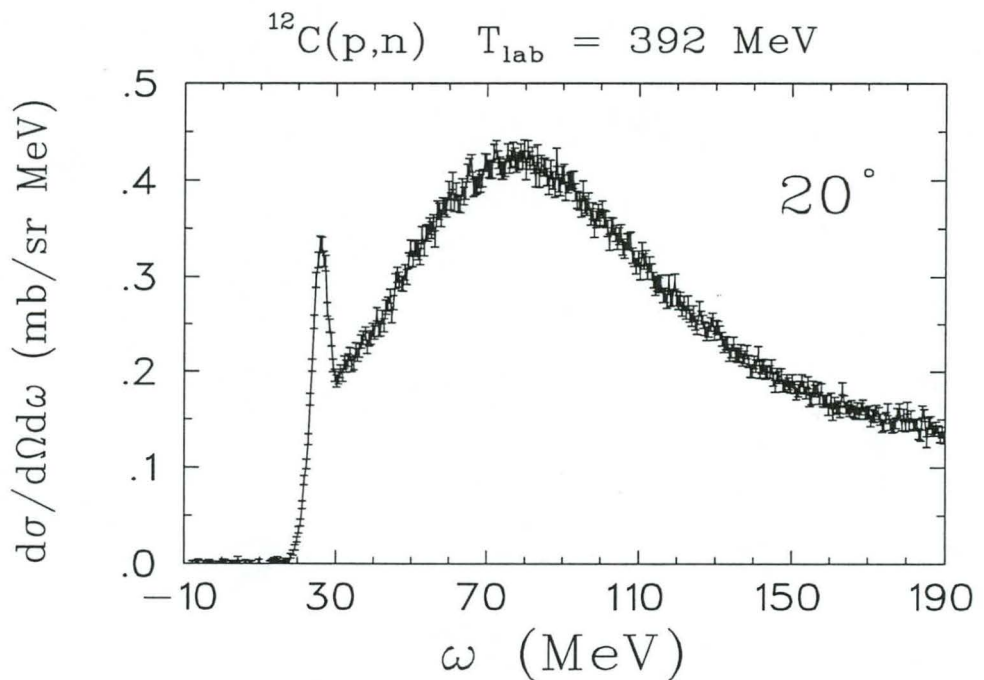
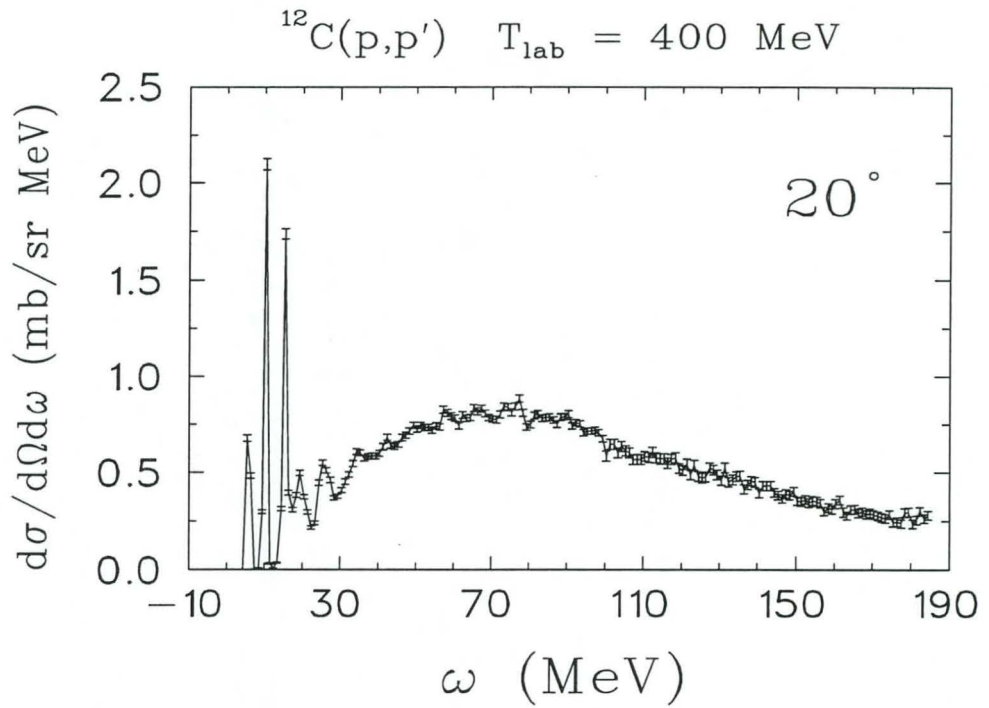


Figure 2.1: Double differential cross sections  $\frac{d\sigma}{d\Omega d\omega}$  (in  $\text{mb sr}^{-1} \text{MeV}^{-1}$ ) for inclusive  $^{12}\text{C}(p,n)$  and  $^{12}\text{C}(p,p)$  scattering as a function of energy transferred to the nucleus ( $\omega$ ), for a laboratory scattering angle of  $20^\circ$ , and incident proton energy of 392 MeV and 400 MeV respectively. The data are from Ref. [Ot97]



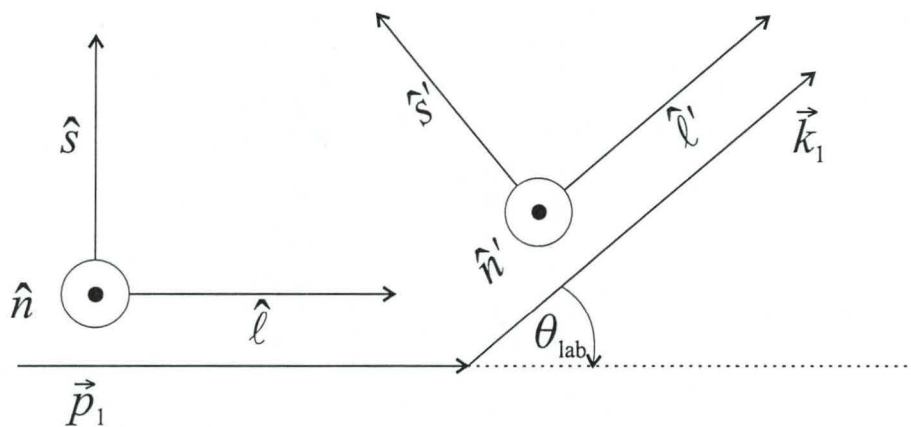


Figure 2.2: Diagram illustrating the directions of the unit vectors  $\hat{\ell}$ ,  $\hat{s}$ ,  $\hat{n}$ ,  $\hat{\ell}'$  and  $\hat{s}'$ . The vector quantities  $\vec{p}_1$  and  $\vec{k}_1$  are the incident and final three-momenta in the nucleon-nucleus laboratory frame respectively, and  $\theta_{lab}$  is the laboratory scattering angle.

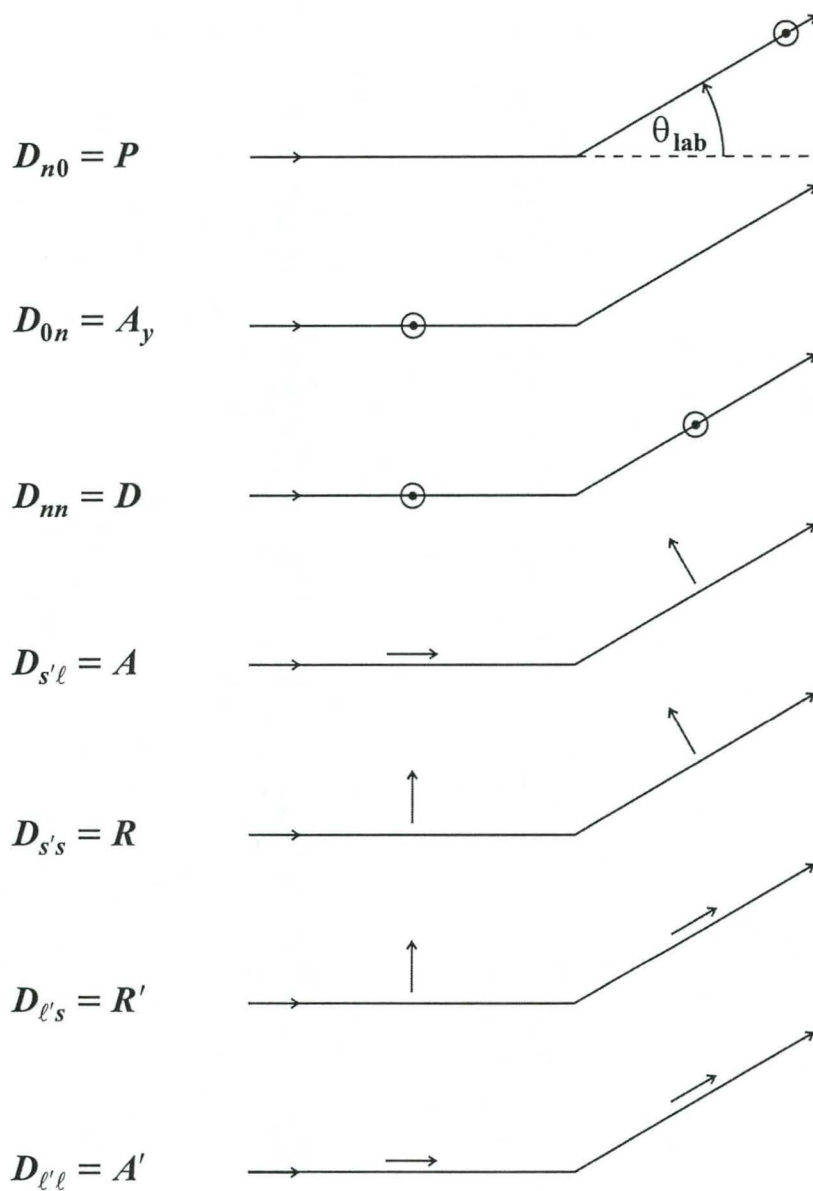


Figure 2.3: Diagrammatic representation of the polarization transfer observables, showing with short arrows, the relevant pair of spin directions before and after scattering with respect to the beam direction.

## 2.3 Relativistic Plane Wave Impulse Approximation

In Section 2.2 we emphasised the fact that experiment suggests that quasielastic scattering is essentially NN scattering inside the nuclear medium. This fact underpins the following basic assumption of the Relativistic Plane Wave Impulse Approximation: quasielastic scattering is considered to be a single-step process whereby the projectile knocks out a single bound nucleon from the target nucleus while the rest of the nucleons are assumed to remain inert. The effect of the other nucleons, i.e. the fact that the scattering process takes place inside the nuclear medium, is taken into account via the concept of an effective nucleon mass within the context of the Walecka model. Experimental data also suggest that at the momentum transfers of interest ( $1 \leq q \leq 2 \text{ fm}^{-1}$ ) the spin observables are target independent, and therefore the assumption of a non-interacting Fermi gas for the target nucleus is justified. The crux of the RPWIA is that it reduces quasielastic proton-nucleus scattering to a two-body scattering process with Dirac plane wave spinors (containing a constant effective mass) describing the external nucleons. A graphical representation of the scattering process is given in Fig. 2.4, where  $\hat{F}$  is the  $16 \times 16$  nucleon-nucleon scattering matrix.

The invariant matrix element for the scattering process in Fig. 2.4 is defined as:

$$\mathcal{M} = [\bar{U}(\vec{k}_1, M_1, s_f) \otimes \bar{U}(\vec{k}_2, M_2, s'_2)] \hat{F} [U(\vec{p}_1, M_1, s_i) \otimes U(\vec{p}_2, M_2, s_2)] \quad (2.1)$$

where  $\hat{F}$  is the  $16 \times 16$  nucleon-nucleon scattering matrix. Referring to Fig. 2.4, the projectile Dirac spinor is given by:

$$U(\vec{p}_1, M_1, s_i) = \left[ \frac{E_1^* + M_1}{2M_1} \right]^{\frac{1}{2}} \begin{pmatrix} \phi(s_i) \\ \frac{\vec{\sigma} \cdot \vec{p}_1}{E_1^* + M_1} \phi(s_i) \end{pmatrix} \quad (2.2)$$

where  $E_1^{*2} = \vec{p}_1^2 + M_1^2$  and the spinor is normalised to

$$\bar{U}(\vec{p}_1, M_1, s) U(\vec{p}_1, M_1, s') = \delta_{ss'}$$

where

$$\bar{U}(\vec{p}_1, M_1, s_i) = U^\dagger(\vec{p}_1, M_1, s_i) \gamma^0,$$

and the conventions of Bjorken and Drell are used for the gamma-matrices. In Eq. (2.2)  $M_1$  represents the constant effective nucleon mass to be discussed below. When medium effects are neglected the effective nucleon mass is replaced by the free nucleon mass, i.e.  $M_1 = M$ . The spinors associated with the other three external particles are defined in an analogous manner. The following four-momenta are also defined:

$$p_1^* = (E_1^*, \vec{p}_1) \quad p_2^* = (E_2^*, \vec{p}_2) \quad (2.3)$$

$$k_1^* = (E_1^{*'}, \vec{k}_1) \quad k_2^* = (E_2^{*'}, \vec{k}_2) \quad (2.4)$$

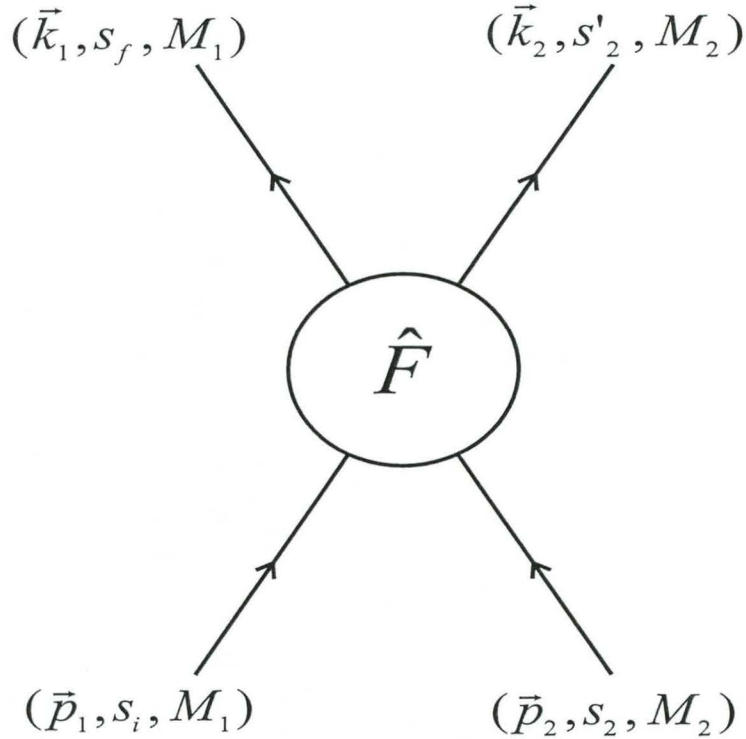


Figure 2.4: Two-body scattering process with momentum, mass and spin labels for the external nucleons.  $\vec{p}_j$  and  $\vec{k}_j$  ( $j = 1, 2$ ) are the initial and final three-momenta of the external nucleons respectively.  $s_i$  and  $s_f$  are the spin four-vectors for the projectile and ejectile respectively. Similarly for nucleon 2 and nucleon 2'.  $M_j$  ( $j = 1, 2$ ) represents the effective nucleon mass.  $\hat{F}$  is the  $16 \times 16$  nucleon-nucleon scattering matrix.

where  $p_j^{*2} = M_j^2$  and  $k_j^{*2} = M_j^2$  ( $j = 1, 2$ ).

To obtain some guidance in the calculation of the effective nucleon masses we turn to the Walecka model. In a mean-field approximation one replaces the position-dependent scalar and vector potentials with average values and hence the Dirac equation for the nucleon can be linearized, and the scalar field adds to the nucleon mass, giving an effective mass to the nucleon inside the nuclear medium. The concept of an effective mass therefore appears very naturally in a relativistic framework and is due to the fact that the mass term in the Dirac equation transforms as a scalar under Lorentz transformations. Following the Walecka model idea, the RPWIA assigns an effective mass to both the target and projectile nucleons to take into account the fact that the scattering takes place inside the nuclear medium. Consider the Dirac equation for the projectile [Mi75]

$$[\vec{p}_1 \cdot \vec{\alpha} + \beta(M + U^{(S)}(r)) - (E - U^{(V)}(r))]\psi = 0 \quad (2.5)$$

where spherically symmetric scalar and vector optical potentials,  $U^{(S)}(r)$  and  $U^{(V)}(r)$



have been assumed. When  $U^{(S)}(r)$  and  $U^{(V)}(r)$  are replaced by constant values,

$$U^{(S)}(r) \longrightarrow \langle U^{(S)} \rangle$$

and

$$U^{(V)}(r) \longrightarrow \langle U^{(V)} \rangle$$

where  $\langle \dots \rangle$  denotes an average over the whole nucleus (the averaging procedure is done within the eikonal approximation as discussed in Ref. [Ho86]) then Eq. (2.5) simplifies to the form of a free Dirac equation:

$$[\vec{p}_1 \cdot \vec{\alpha} + \beta M^*] \psi = E^* \psi \quad (2.6)$$

with a constant effective nucleon mass:

$$M^* = M + \langle U^{(S)} \rangle$$

and energy

$$E^* = E + \langle U^{(V)} \rangle$$

and therefore the solutions to Eq. (2.6) are free plane waves:

$$\psi \longrightarrow U(\vec{p}_1, M^*, s) \sim \begin{pmatrix} \phi(s) \\ \frac{\vec{\sigma} \cdot \vec{p}_1}{E^* + M^*} \phi(s) \end{pmatrix}.$$

*It is important to note that plane wave solutions are only possible if the scalar and vector potentials are replaced by constant values.* From Eq. (2.6) it follows that the effective mass for the projectile is given by

$$M_1 = M + \langle U^{(S)} \rangle \quad (2.7)$$

where  $\langle \dots \rangle$  represents the average over the whole nucleus. The average value of the scalar potential is defined as:

$$\langle U^{(S)} \rangle = \frac{\int d^3\vec{x} (\text{Re } U^{(S)}(r)) w(\vec{x})}{\int d^3\vec{x} w(\vec{x})} \quad (2.8)$$

with

$$w(\vec{x}) = \rho(\vec{x})T(\vec{x})$$

where  $\rho(\vec{x})$  is the baryon density and  $T(\vec{x})$  is the transmission probability, i.e. the probability that the nucleon will not be absorbed before reaching the position  $\vec{x}$ . The weighting function  $w(\vec{x})$  expresses the probability that both the projectile and target nucleons are present at position  $\vec{x}$ . Eq. (2.8) is therefore the weighted average of the scalar potential. The baryon density is calculated in a self-consistent Dirac-Hartree approximation as described in Ref. [Ho91a]. To obtain the scalar potential,  $U^{(S)}(r)$ , one has to fold



the scalar density (see Ref. [Ho91a]) with the nucleon-nucleon t-matrix obtained via the Horowitz-Love-Franey parameterisation [Ho85].

The effective mass of the target nucleon is given by

$$M_2 = M - g_s \langle \phi \rangle$$

where  $g_s$  is the scalar meson coupling constant and  $\langle \phi \rangle$  is the average value [averaging done as in Eq. (2.8)] of the scalar field  $\phi(\vec{x})$  for a bound particle which can be obtained via a self-consistent Dirac-Hartree calculation [Ho91a]. Values of  $M_1$  and  $M_2$  for specific targets and energies are listed in Table II of Ref. [Hi94].

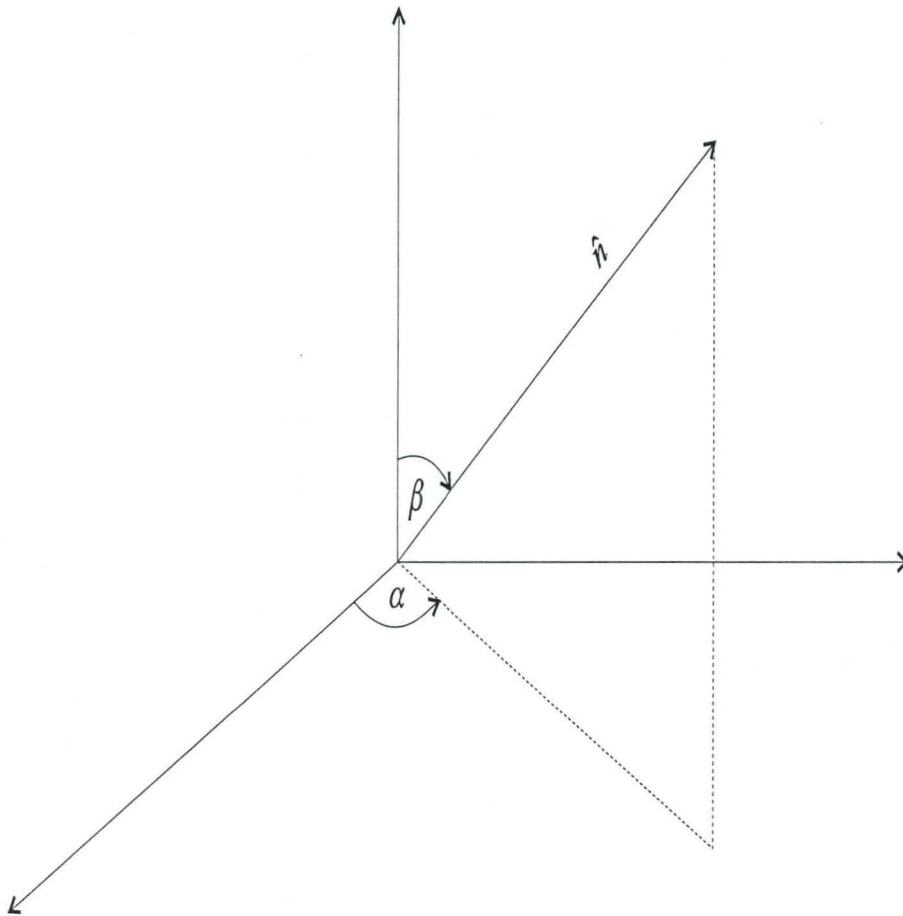


Figure 2.5: Definition of polar ( $\beta$ ) and azimuthal ( $\alpha$ ) angles for the unit vector  $\hat{n}$  associated with the Pauli spinor  $\phi(\hat{n})$ .

We now discuss how one describes the polarization of a nucleon which is represented by the Pauli spinor,  $\phi(s_i)$  in Eq. 2.2. For spin pointing in a direction specified by the

unit vector,  $\hat{n}$ , is associated a two-component Pauli spinor,  $\phi(\hat{n})$ , where

$$\phi(\hat{n}) = \begin{pmatrix} e^{-\frac{i\alpha}{2}} \cos \frac{\beta}{2} \\ e^{\frac{i\alpha}{2}} \sin \frac{\beta}{2} \end{pmatrix} \quad (2.9)$$

where  $\beta$  and  $\alpha$  are the polar and azimuthal angles respectively of the unit vector  $\hat{n}$ : See Fig. 2.5 [Sa85]. From the figure it follows that

$$\hat{n} = \begin{pmatrix} n_x \\ n_y \\ n_z \end{pmatrix} = \begin{pmatrix} \sin \beta \cos \alpha \\ \sin \beta \sin \alpha \\ \cos \beta \end{pmatrix}$$

with  $|\hat{n}|^2 = 1$  and  $\phi(\hat{n})$  satisfying the eigenvalue equation

$$(\vec{\sigma} \cdot \hat{n}) \phi(\hat{n}) = (+1) \phi(\hat{n})$$

with

$$\vec{\sigma} \cdot \hat{n} \equiv n_x \sigma_x + n_y \sigma_y + n_z \sigma_z.$$

The projection operator,  $P(\hat{n})$  for the direction  $\hat{n}$  is defined as:

$$P(\hat{n}) = \frac{1}{2} (I_2 + \vec{\sigma} \cdot \vec{n})$$

where  $I_2$  is the  $2 \times 2$  identity matrix. From Eq. (2.9) it can be shown that

$$P(\hat{n}) = \phi(\hat{n}) \phi^\dagger(\hat{n}) \quad (2.10)$$

and

$$\sum_{\hat{n}=\pm} \phi(\hat{n}) \phi^\dagger(\hat{n}) = I_2. \quad (2.11)$$

In Section 2.5.4 we show that the polarized double differential cross section can be calculated from the quantity  $|\mathcal{M}|^2$ . The question arises as to what is the form of  $\hat{F}$  to be used in Eq. (2.1) which is consistent with parity and time-reversal invariance as well as charge symmetry. In the next section we discuss the use of the IA1 representation of  $\hat{F}$  in the calculation of  $|\mathcal{M}|^2$  and summarise the results which were obtained. We will find that despite some encouraging results the SPVAT form will prove to be inadequate and hence we discuss in Section 2.5 the application of the general Lorentz invariant form of  $\hat{F}$  (also called the IA2 representation of  $\hat{F}$ ) to the calculation of spin observables for quasielastic proton-nucleus scattering.

## 2.4 Application of IA1 to quasielastic proton-nucleus scattering

In order to evaluate  $|\mathcal{M}|^2$  one needs to choose a representation of the NN scattering matrix,  $\hat{F}$ . All previous calculations of quasielastic spin observables have parameterised  $\hat{F}$  in terms of the five Fermi covariants [Ho88, Ho86, Hi94, Hi95, Hi98]:

$$\begin{aligned} \hat{F} = & F_S(I_4 \otimes I_4) + F_P(\gamma^5 \otimes \gamma^5) + F_V(\gamma^\mu \otimes \gamma_\mu) + \\ & F_A(\gamma^5 \gamma^\mu \otimes \gamma^5 \gamma_\mu) + F_T(\sigma^{\mu\nu} \otimes \sigma_{\mu\nu}). \end{aligned} \quad (2.12)$$

Eq. (2.12) is commonly called the SPVAT form or IA1 representation of  $\hat{F}$ . The subscripts  $S, P, V, A$  and  $T$  refer respectively to the scalar, pseudoscalar, vector, axial-vector and tensor components of the matrix  $\hat{F}$ . This is an incomplete representation of  $\hat{F}$  and, as will be discussed below, it gives inconsistent results for observable quantities. The amplitudes,  $F_L$  ( $L = S, P, V, A, T$ ) are obtained by fitting to free NN scattering data [Ho86]. This amounts to a relativistic parameterisation of the Arndt phases. One can also, however, write down analytical expressions for  $F_L$  using a meson-exchange model such as the Horowitz-Love-Franey (HLF) model [Ho85]. The advantage of the latter form is that it allows an explicit separation of direct and exchange terms, as well as a consistent investigation of the so-called pseudoscalar versus pseudovector ambiguity of the pion-nucleon coupling. Note that the parameters in the HLF model (the meson masses, meson coupling constants and cut-off parameters) are also obtained by fitting to free scattering data. Using Eqs. (2.1) and (2.12), formulas can be derived for the unpolarized double differential cross section, the analyzing power (which is equal to the polarization in this approximation) and the spin transfer coefficients. Explicit expressions for these quantities can be found in Ref. [Ho88]. A major success of the RPWIA was to successfully predict the analyzing power ( $A_y$ ) for  $^{40}\text{Ca}(\vec{p}, \vec{p}')$  and  $^{208}\text{Pb}(\vec{p}, \vec{p}')$  at 500 MeV, whereas all non-relativistic models totally fail [Ho88]. The use of an effective nucleon mass moved the theoretical calculation closer to the analyzing power data, as well as being below the calculation based on a free nucleon mass. This was referred to as the 'quenching effect' in the analyzing power and was claimed to be a 'relativistic signature'. The other observables ( $D_{\ell\ell}, D_{s's}, D_{s'l}, D_{l's}, D_{nn}$ ), however, seemed to favour the free mass calculation. The latter inconsistency (between  $M^*$ - and  $M$ -based RPWIA predictions) necessitated a critical review of the original RPWIA model. In this respect Refs. [Hi94, Hi95, Hi98] investigated the sensitivity of complete sets of quasielastic polarization transfer observables to the following ingredients of the RPWIA model:

1. different effective masses,
2. relativistic effects (i.e., the use of an effective mass versus a free mass),
3. pseudoscalar (PS) versus pseudovector (PV) forms of the  $\pi NN$  vertex, and
4. spin-orbit effects.

It was seen that the effective masses,  $M_1$  and  $M_2$  both increase as  $T_{lab}$  increases.  $M_1$  and  $M_2$  do not vary significantly with the mass number of the scattering nucleus. The effective masses for heavier nuclei like  $^{208}\text{Pb}$  are closer to the free mass than for light nuclei like  $^{12}\text{C}$ . Medium effects are therefore better studied by scattering from light nuclei. The RPWIA allows, in a very direct manner, the investigation of the pseudoscalar versus pseudovector ambiguity of the pion-nucleon coupling constant. In general it is found that the  $(\vec{p}, \vec{n})$  observables are much more sensitive to the  $PS$  versus  $PV$  form of the  $\pi NN$  vertex over the entire 200 to 500 MeV range. The ambiguity also affects the sensitivity of the spin observables to medium effects. The use of a  $PS$  vertex shows that the  $(\vec{p}, \vec{n})$  observables are much more sensitive to medium effects, whereas a  $PV$  vertex shows that the  $(\vec{p}, \vec{p}')$



observables are more sensitive. When the  $D_{ij}$ 's are calculated at the quasielastic peak, it is found that spin-orbit distortions are not entirely negligible, except for  $D_{nn}$ , which shows almost no sensitivity to spin-orbit effects over the entire energy range. The results in Refs. [Hi94, Hi95] must be viewed as being merely qualitative, since at the time HLF parameters only existed for 135, 200, 300, 400 and 500 MeV. In order to compare with actual experimental data new parameters were generated between 80 and 195 MeV in steps of 5 MeV using the procedure by Horowitz [Ho85], and between 200 and 500 MeV the Maxwell parameterisation [Ma96] of the NN amplitudes with both energy-dependent coupling constants and cut-off parameters were used. In Ref. [Hi98] the predictions of the RPWIA were compared to the following experimental data:

1.  $^{12}C(\vec{p}, \vec{n})$  at 186 MeV [Wa94]
2.  $^{12}C(\vec{p}, \vec{p}')$  at 290 MeV [Ch90].

For reaction (1) it was found that  $D_{nn}$  favours a  $PV$  to a  $PS$  vertex, while  $A_y$  fails to distinguish between the two. However, the free mass and  $PV(M^*)$  calculations describe the data equally well. For reaction (2),  $D_{nn}, D_{s's}, D_{s'l}$  and  $D_{l's}$  correspond to free mass calculations, and most of the data favour a  $PS$   $\pi NN$  vertex. Comparison to the limited data available therefore seem to suggest that  $(\vec{p}, \vec{p}')$  scattering favours a  $PS$  form, whereas  $(\vec{p}, \vec{n})$  data favour a  $PV$  form.

Despite the successes of the RPWIA the previous discussion shows that current relativistic models cannot consistently predict complete sets of spin observables for both quasielastic  $(\vec{p}, \vec{p}')$  and  $(\vec{p}, \vec{n})$  scattering. The next stage, therefore is to address the fact that an incomplete representation (IA1) of the NN scattering matrix was used in all these calculations. In the next section we discuss the general Lorentz invariant representation of the NN scattering matrix and the application thereof to quasielastic proton-nucleus scattering.

## 2.5 Application of IA2 to quasielastic proton-nucleus scattering

In this section we present a detailed discussion of the IA2 formalism of Tjon and Wallace as well as the new formalism which applies it to quasielastic scattering.

### 2.5.1 General Lorentz invariant representation of the NN scattering matrix

In the previous section we emphasised that ambiguities in the form of  $\hat{F}$  lead to different behaviour of the polarization transfer observables as well as inconsistent predictions of data for both  $(\vec{p}, \vec{p}')$  and  $(\vec{p}, \vec{n})$  scattering. The SPVAT form (originally presented in Ref. [Go60]) is a five-term representation consistent with parity and time-reversal invariance as well as charge symmetry. However, other five-term representations which respect the

above-mentioned symmetries are also possible. For example, there are the Goldberger, Nambu, Öhme (GNO) invariants [Go57]:

$$\begin{aligned}
 G_1 &= I_{16} = I_4 \otimes I_4 \\
 G_2 &= iP_\mu(\gamma^\mu \otimes I_4) + iK_\mu(I_4 \otimes \gamma^\mu) \\
 G_3 &= [iP_\mu(\gamma^\mu \otimes I_4)][iK_\nu(I_4 \otimes \gamma^\nu)] \\
 G_4 &= [iP_\mu(\gamma^5 \gamma^\mu \otimes I_4)][iK_\nu(I_4 \otimes \gamma^5 \gamma^\nu)] \\
 G_5 &= \gamma^5 \otimes \gamma^5
 \end{aligned}$$

where

$$\begin{aligned}
 K &= \frac{1}{2}(p_1 + k_1) \quad \text{and} \\
 P &= \frac{1}{2}(p_2 + k_2)
 \end{aligned}$$

and there are also the perturbative invariants [Br76]:

$$\begin{aligned}
 P_1 &= G_1 \\
 P_2 &= G_2 \\
 P_3 &= G_3 \\
 P_4 &= \gamma_\mu \otimes \gamma^\mu \\
 P_5 &= G_5.
 \end{aligned}$$

The invariant amplitudes in each of the representations of  $\hat{F}$  are connected via matrix relations given in Ref. [Br76]. They are obtained by fitting to free scattering data, since a matrix equation connects (for example) the Fermi covariants to the centre-of-mass helicity amplitudes [Tj85b]. *Physical NN scattering data therefore completely determine the amplitudes in a five-term representation of  $\hat{F}$ .* A priori there is no reason why one five-term representation should be chosen above another. The SPVAT form is very convenient since its amplitudes are free of kinematic singularities at  $\theta = 0$  and  $\theta = \pi$  ( $\theta$  is the centre-of-mass scattering angle) and the one-meson exchange contributions are naturally written in terms of Fermi covariants [Go60]. Up to this point all that was shown is that amplitudes in one representation are a linear combination of amplitudes in another representation. *The ambiguity lies in the fact that, even after a representation has been chosen, fitting to free scattering data does not uniquely fix the form of the matrix  $\hat{F}$ .* To see this we use the SPVAT form as an example and note that the pseudoscalar covariant,  $PS = \gamma^5 \otimes \gamma^5$ , has exactly the same matrix elements between positive energy free mass Dirac spinors as the pseudovector covariant,  $PV = \frac{\not{q} \gamma^5}{2M} \otimes \frac{\not{q} \gamma^5}{2M}$  i.e.

$$[\bar{U}_1(M) \otimes \bar{U}_2(M)] [PV - PS] [U_1(M) \otimes U_2(M)] = 0.$$

One can therefore *replace PS with PV* in Eq. (2.12) *without altering the amplitudes  $F_L$ .* This is called the equivalence theorem [Ha59]. Even though these two representations are equivalent on-shell, they give different results when sandwiched between *positive energy*



Dirac spinors containing an effective nucleon mass, since then matrix elements between negative energy states now also enter. This is because the effective mass spinor can always be expanded in a free mass basis:

$$U(\vec{p}_1, M_1, s_i) = \alpha_U U(\vec{p}_1, M, s_i) + \alpha_V V(\vec{p}_1, M, s_i) \quad (2.13)$$

where  $V(\vec{p}_1, M, s_i)$  is a negative-energy Dirac spinor [Bj64]. There also exists the relation [Hi94]

$$\mathcal{M}_{PV} = \frac{M_1 M_2}{M^2} \mathcal{M}_{PS} \quad (2.14)$$

where  $\mathcal{M}_{PS}$  and  $\mathcal{M}_{PV}$  are the contributions of the pseudoscalar covariant and pseudovector covariant respectively to the invariant matrix element in Eq. (2.1). Note that in Eq. (2.14) the pseudovector covariant is  $PV = \frac{\not{q} \gamma^5}{2M} \otimes \frac{\not{q} \gamma^5}{2M}$ , but where  $q = p_1^* - k_1^* = k_2^* - p_2^*$ , i.e., the momenta are on-mass-shell with respect to the effective masses,  $M_1$  and  $M_2$ . In the equivalence theorem, the momenta must be on-mass-shell with respect to the free mass. The replacement  $PS \rightarrow PV$  has been used in the RPWIA to investigate the so-called pseudoscalar versus pseudovector ambiguity in the pion-nucleon coupling constant [Ho88, Hi94, Hi95]. Comparison of the limited data available with subsequent and more refined calculations [Hi98] have also revealed that  $(\vec{p}, \vec{p}')$  scattering prefers a PS vertex, whereas  $(\vec{p}, \vec{n})$  scattering suggests a PV form. Additional parameters can also be included in  $\hat{F}$  which will not contribute on-shell, but which will still have an effect on observable quantities [Ra87, Ha87]. Despite the fact that the RPWIA formalism together with the IA1 representation of  $\hat{F}$  has given good quantitative predictions of spin observables [Hi98], it is not sufficient to unambiguously study effective-mass-type medium effects. The ambiguity which is inherent in any five-term (i.e. incomplete) representation of  $\hat{F}$  was first pointed out in Ref. [Ad84]. This leads to the conclusion that a general Lorentz invariant expansion of  $\hat{F}$  should rather be used.

Several authors [Pi86, Tj85, Tj87a] have addressed the problem of determining the general Lorentz invariant representation of  $\hat{F}$ . The formalism of Ref. [Pi86] was not employed in this study since the authors did not complete the numerical calculations which determine the invariant amplitudes used in their representation of  $\hat{F}$ . The formalism of Tjon and Wallace (which will be referred to as the IA2 representation of  $\hat{F}$ ) will be used in the present study due to the attractive feature that their representation includes the standard SPVAT form of  $\hat{F}$  as a special case. The numerical values of the invariant amplitudes contained in  $\hat{F}$  were also made available to the author of this thesis by Wallace.

Applications of the IA2 formalism to elastic proton-nucleus scattering can be found in Refs. [Tj85a, Tj85b, Tj87, Ke94].

In this section a fairly detailed discussion of the IA2 formalism [Tj85, Tj87a] will be given since it forms the basis of all subsequent work. The IA2 formalism comprises three problems:

1. The Lorentz covariant set constructed from the Dirac matrices which serve as a representation for  $\hat{F}$ .

2. The determination of the maximum number of independent invariant amplitudes which completely specify the general Lorentz invariant form of  $\hat{F}$  consistent with parity and time-reversal invariance as well as charge symmetry.
3. The determination of the numerical values of the invariant amplitudes.

In this section we will focus primarily on the first two problems since it will allow us to see how the symmetries of the nuclear force can reduce the number of independent amplitudes. Our approach will be to show how charge symmetry and time-reversal will lead to relationships amongst the invariant amplitudes. The third problem entails the solution of the Bethe-Salpeter equation for nucleon-nucleon scattering using a meson exchange model for the NN force. Since the latter also involves much numerical work, we will just refer to the relevant articles [Fa83, Fa84, Tj87a]. The main result will be the following: the nucleon-nucleon scattering matrix  $\hat{F}$  can be written in a general Lorentz invariant form which contains 44 independent invariant amplitudes, which are consistent with parity and time-reversal invariance, as well as charge-symmetry together with the on-mass-shell condition for the external nucleons.

We now discuss in detail how to implement the symmetries of the nuclear force, namely parity and time-reversal invariance as well as charge symmetry to reduce the number of independent amplitudes in  $\hat{F}$ .

In general, matrix elements of  $\hat{F}$  need to be calculated between positive and negative energy Dirac spinors, labelled as  $U^\rho(\vec{p}, M, s)$  where  $\rho = \pm$ . A general matrix element is therefore

$$[\bar{U}^{\rho'_1}(1') \otimes \bar{U}^{\rho'_2}(2')] \hat{F} [U^{\rho_1}(1) \otimes U^{\rho_2}(2)]. \quad (2.15)$$

From Eq. (2.15) it follows that  $\hat{F}$  contains 16 different rho-spin sectors. The use of covariant energy projection operators,  $\Lambda_\rho(\vec{p}, M)$ , allows the separation of the positive and negative energy sectors of the Dirac space and results in the following form for  $\hat{F}$ :

$$\hat{F} = \sum_{\rho_1, \rho'_1, \rho_2, \rho'_2} [\Lambda_{\rho'_1}(\vec{k}_1, M) \otimes \Lambda_{\rho'_2}(\vec{k}_2, M)] \hat{F}^{\rho_1 \rho'_1 \rho_2 \rho'_2} [\Lambda_{\rho_1}(\vec{p}_1, M) \otimes \Lambda_{\rho_2}(\vec{p}_2, M)] \quad (2.16)$$

where

$$\begin{aligned} \Lambda_\rho(\vec{p}, M) &= \frac{\rho \not{\vec{p}} + M}{2M} \\ &= \frac{\rho(E\gamma^0 - \vec{p} \cdot \vec{\gamma}) + M}{2M} \end{aligned} \quad (2.17)$$

with  $\rho = \pm$  and  $E^2 = \vec{p}^2 + M^2$ .  $\hat{F}^{\rho_1 \rho'_1 \rho_2 \rho'_2}$  is a  $16 \times 16$  matrix that acts only within a specific rho-spin sector (labelled by the rho-spin indices,  $\rho_1, \rho'_1, \rho_2, \rho'_2$ ) or subclass (labelled by the pair  $ij$ ). The association between rho-spin labels and subclass indices is given in Table 2.1. In general  $\hat{F}$  contains  $16^2 = 256$  independent elements which can be reduced if we impose parity invariance, time-reversal invariance and charge symmetry.

Table 2.1: *Relation between rho-spin labels,  $\rho_1, \rho_1', \rho_2, \rho_2'$  and pair indices,  $ij$  for the various subclasses.*

rho-spin labels: $\rho_1\rho_1'\rho_2\rho_2'$	subclass indices: $ij$ .
++ , ++	11
++ , +-	12
++ , -+	13
++ , --	14
+- , ++	21
+- , +-	22
+- , -+	23
+- , --	24
-+ , ++	31
-+ , +-	32
-+ , -+	33
-+ , --	34
-- , ++	41
-- , +-	42
-- , -+	43
-- , --	44



We first consider the case of parity invariance. The Dirac spinor can be labelled by the spin or the helicity,  $\lambda$ , i.e.

$$U = U_\lambda^\rho(\vec{p}, M)$$

where  $\lambda = \pm$ . Under a parity transformation  $\lambda$  changes to  $-\lambda$  [Ch98], and therefore invariance under parity can be stated as:

$$\mathcal{M}_{\lambda_1 \lambda'_1 \lambda_2 \lambda'_2}^{\rho_1 \rho'_1 \rho_2 \rho'_2} = \mathcal{M}_{-\lambda_1 -\lambda'_1 -\lambda_2 -\lambda'_2}^{\rho_1 \rho'_1 \rho_2 \rho'_2} \quad (2.18)$$

where

$$\mathcal{M}_{\lambda_1 \lambda'_1 \lambda_2 \lambda'_2}^{\rho_1 \rho'_1 \rho_2 \rho'_2} = [\bar{U}_{\lambda'_1}^{\rho'_1}(1') \otimes \bar{U}_{\lambda'_2}^{\rho'_2}(2')] \hat{F} [U_{\lambda_1}^{\rho_1}(1) \otimes U_{\lambda_2}^{\rho_2}(2)].$$

Eq. (2.18) relates all 256 matrix elements in pairs (involving  $\lambda_i$  and  $-\lambda_i$ ) and this forms 128 constraint conditions and therefore  $\hat{F}$  will contain 128 independent amplitudes if parity invariance is satisfied. Henceforth the notation

$$\{\rho\} = \rho_1 \rho'_1 \rho_2 \rho'_2$$

will be used. The matrix  $\hat{F}^{\rho_1 \rho'_1 \rho_2 \rho'_2}$  is expanded in terms of 9 parity invariant kinematic covariants  $\Gamma_n$  (constructed from the Dirac matrices) times invariant amplitudes, i.e.

$$\hat{F}^{\rho_1 \rho'_1 \rho_2 \rho'_2} = \sum_{n=1}^9 f_n^{\{\rho\}}(\underline{s}) \Gamma_n(\eta_{ij}). \quad (2.19)$$

In Eq. (2.19) there are 9 invariant amplitudes but only 8 are non-zero in a specific rho-spin sector. Each rho-spin sector therefore contains a constraint condition: see Table 2.2.  $\underline{s}$  is a collective index for the following Lorentz invariant quantities:

$$\underline{s} = \{s_1, s_2, s_3, s_4, s_5, s_6, s_7\}$$

where

$$s_1 = (p_1 + p_2)^2 = (k_1 + k_2)^2 \equiv \text{Mandelstam variable } s. \quad (2.20)$$

$$s_2 = (p_1 - k_1)^2 = (k_2 - p_2)^2 \equiv \text{Mandelstam variable } t. \quad (2.21)$$

$$s_3 = (p_1 - k_2)^2 = (k_1 - p_2)^2 \equiv \text{Mandelstam variable } u. \quad (2.22)$$

$$s_4 = \frac{1}{2}(p_1^2 + p_2^2) \quad (2.23)$$

$$s_5 = \frac{1}{2}(k_1^2 + k_2^2) \quad (2.24)$$

$$s_6 = \frac{1}{2}(p_1^2 - p_2^2) \quad (2.25)$$

$$s_7 = \frac{1}{2}(k_1^2 - k_2^2). \quad (2.26)$$

Table 2.2: Constraint condition for each rho-spin sector (or subclass) as well as the value of the parameter  $\eta_{ij}$ .

Rho-spin sector	Constraint condition	Value of $\eta_{ij}$ .
$\hat{F}^{11}$	$f_6 = 0$	+
$\hat{F}^{12}$	$f_6 = 0$	+
$\hat{F}^{13}$	$f_6 = 0$	-
$\hat{F}^{14}$	$f_9 = 0$	+
$\hat{F}^{21}$	$f_6 = 0$	+
$\hat{F}^{22}$	$f_8 = 0$	+
$\hat{F}^{23}$	$f_9 = 0$	-
$\hat{F}^{24}$	$f_6 = 0$	+
$\hat{F}^{31}$	$f_6 = 0$	-
$\hat{F}^{32}$	$f_9 = 0$	-
$\hat{F}^{33}$	$f_8 = 0$	-
$\hat{F}^{34}$	$f_6 = 0$	-
$\hat{F}^{41}$	$f_9 = 0$	+
$\hat{F}^{42}$	$f_6 = 0$	+
$\hat{F}^{43}$	$f_6 = 0$	-
$\hat{F}^{44}$	$f_6 = 0$	+

$\eta_{ij}$  is a parameter which can be  $\pm$  in a given subclass (see Table 2.2). Before we write down the matrices  $\Gamma_n$ , we first define:

$$\begin{aligned}
 S &= I_4 \otimes I_4 = I_{16} \\
 P &= \gamma^5 \otimes \gamma^5 \\
 V &= \gamma_\mu \otimes \gamma^\mu \\
 A &= \gamma^5 \gamma_\mu \otimes \gamma^5 \gamma^\mu \\
 T &= \sigma_{\mu\nu} \otimes \sigma^{\mu\nu}.
 \end{aligned} \tag{2.27}$$

We introduce the matrix  $\tilde{S}$  with matrix elements given by

$$(\tilde{S})_{ij,kl} = \delta_{il} \delta_{jk} \tag{2.28}$$

and with the properties:

$$\tilde{S}^2 = I_4 \otimes I_4 = I_{16} \tag{2.29}$$

$$\tilde{S}^\dagger = \tilde{S} \tag{2.30}$$

$$\tilde{S}(X \otimes Y) = (Y \otimes X)\tilde{S} \quad \text{if } X \text{ and } Y \text{ are } 4 \times 4 \text{ matrices} \tag{2.31}$$

$$\tilde{S}(X \otimes Y) = Y \otimes X \quad \text{if } X \text{ and } Y \text{ are } 4 \times 1 \text{ matrices} \tag{2.32}$$

as well as the matrices:

$$\begin{aligned}
 \tilde{P} &= \tilde{S}P = P\tilde{S} \\
 \tilde{V} &= \tilde{S}V = V\tilde{S} \\
 \tilde{A} &= \tilde{S}A = A\tilde{S} \\
 \tilde{T} &= \tilde{S}T = T\tilde{S}.
 \end{aligned} \tag{2.33}$$

The kinematic covariants are [Tj87a]:

$$\begin{aligned}
 \Gamma_1 &= S - \tilde{S} \\
 \Gamma_2 &= \frac{1}{2}(T + \tilde{T}) \\
 \Gamma_3 &= -A + \tilde{A} \\
 \Gamma_4 &= V + \tilde{V} \\
 \Gamma_5 &= P - \tilde{P} \\
 \Gamma_6 &= Q_{11,\mu}(I_4 \otimes \gamma^\mu) + Q_{22,\mu}(\gamma^\mu \otimes I_4) + \\
 &\quad (Q_{21,\mu}(\gamma^\mu \otimes I_4) + Q_{12,\mu}(I_4 \otimes \gamma^\mu))\tilde{S} \\
 \Gamma_7(\eta_{ij}) &= Q_{11,\mu}(I_4 \otimes \gamma^\mu) - Q_{22,\mu}(\gamma^\mu \otimes I_4) + \\
 &\quad \eta_{ij}(Q_{21,\mu}(\gamma^\mu \otimes I_4) - Q_{22,\mu}(\gamma^\mu \otimes I_4))\tilde{S} \\
 \Gamma_8(\eta_{ij}) &= \eta_{ij}(Q_{11,\mu}(\gamma^5 \otimes \gamma^5 \gamma^\mu) + Q_{22,\mu}(\gamma^5 \gamma^\mu \otimes \gamma^5)) + \\
 &\quad \eta_{ij}((Q_{21,\mu}(\gamma^5 \gamma^\mu \otimes \gamma^5) + Q_{12,\mu}(\gamma^5 \otimes \gamma^5 \gamma^\mu))\tilde{S}) \\
 \Gamma_9(\eta_{ij}) &= \eta_{ij}(Q_{11,\mu}(\gamma^5 \otimes \gamma^5 \gamma^\mu) - Q_{22,\mu}(\gamma^5 \gamma^\mu \otimes \gamma^5)) + \\
 &\quad (Q_{21,\mu}(\gamma^5 \gamma^\mu \otimes \gamma^5) - Q_{12,\mu}(\gamma^5 \otimes \gamma^5 \gamma^\mu))\tilde{S}.
 \end{aligned}$$



Table 2.3: Transformation properties of the variables  $s_i$  as well as the gamma matrices under a parity transformation.

$s_i$	$\hat{P}(s_i)\hat{P}^{-1} = s_i \quad \forall i = 1..7$
$S$	$\hat{P}I_4\hat{P}^{-1} = I_4$
$P$	$\hat{P}\gamma^5\hat{P}^{-1} = -\gamma^5$
$V$	$\hat{P}\gamma^\mu\hat{P}^{-1} = \gamma_\mu = -(-1)^{\delta_{\mu,0}}\gamma^\mu$
$A$	$\hat{P}\gamma^5\gamma^\mu\hat{P}^{-1} = -\gamma^5\gamma_\mu$
$T$	$\hat{P}\sigma^{\mu\nu}\hat{P}^{-1} = \sigma_{\mu\nu}$

An alternative set of covariants were defined in Ref. [Tj85] but those covariants lacked simple symmetries properties under particle exchange. The  $\Gamma_i$ 's defined above were specifically constructed so that each covariant is either odd or even under particle exchange. This ensures that the amplitudes can be conveniently represented by simple Yukawa forms.

Up to a phase factor the parity operator is given by [Bj64]:

$$\hat{P} = \gamma^0.$$

The transformation properties of the variables  $s_i$  and the gamma matrices under a parity transformation are summarised in Table 2.3 which can be used to explicitly verify the parity invariance of the covariants  $\Gamma_i$ . To summarise, assuming only parity invariance,  $\hat{F}$  contains  $16 \times 8 = 128$  independent invariant amplitudes. Substitution of Eq. (2.19) into Eq. (2.16) results in the following expression for  $\hat{F}$ :

$$\hat{F} = \sum_{\{\rho\}} \sum_{n=1}^9 f_n^{\{\rho\}}(\underline{s}) [\Lambda_{\rho'_1}(\vec{k}_1, M) \otimes \Lambda_{\rho'_2}(\vec{k}_2, M)] \Gamma_n(\eta_{ij}) [\Lambda_{\rho_1}(\vec{p}_1, M) \otimes \Lambda_{\rho_2}(\vec{p}_2, M)]. \quad (2.34)$$

We next consider the condition of charge symmetry. Consider the scattering process depicted in Fig. 2.6. The invariant matrix element for the scattering process on the left

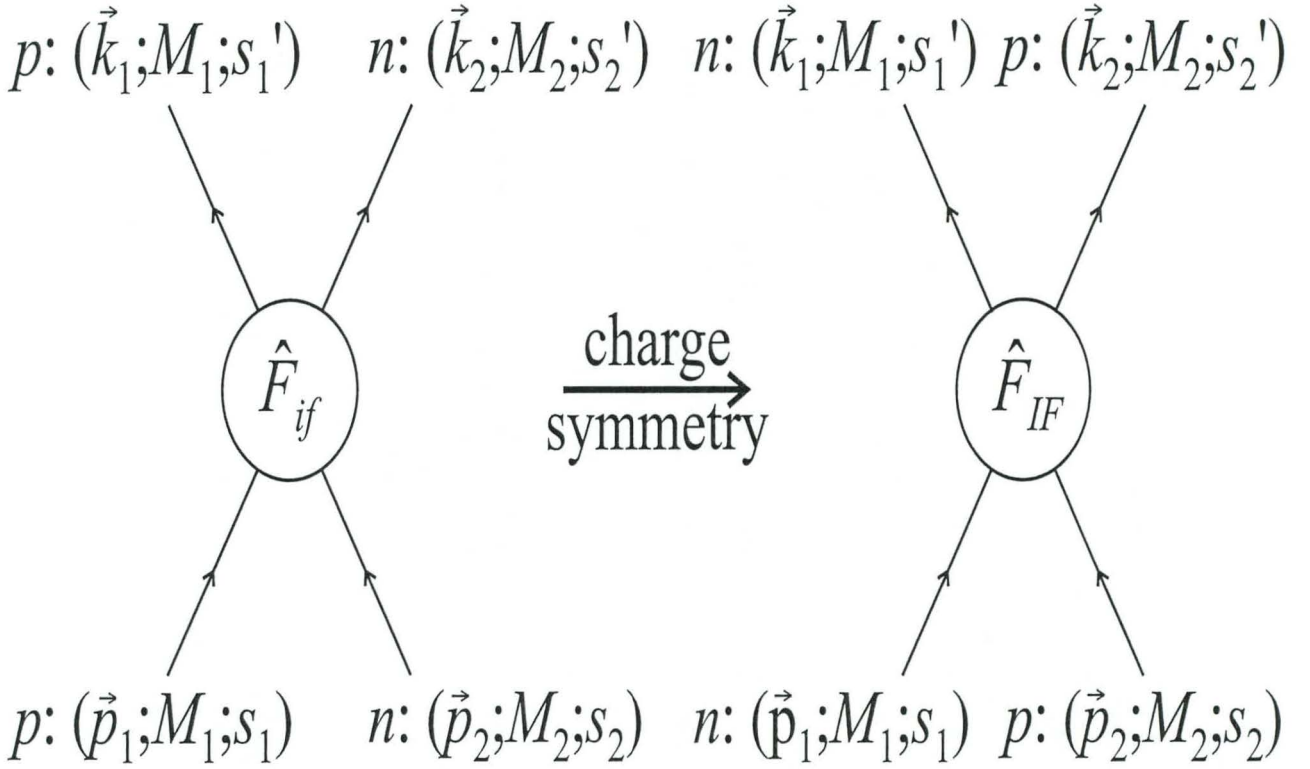


Figure 2.6: A charge symmetry transformation on the left-hand figure produces the one on the right.

of Fig. 2.6 is given by:

$$\mathcal{M}_{if} = [\bar{\psi}_p(1') \otimes \bar{\psi}_n(2')] \hat{F}((\vec{p}_1, \vec{p}_2) \longrightarrow (\vec{k}_1, \vec{k}_2)) [\psi_p(1) \otimes \psi_n(2)] \quad (2.35)$$

where

$$\left. \begin{aligned} \psi_p(1) &= \psi_p(\vec{p}_1, M, s_1) \\ \psi_p(1') &= \psi_p(\vec{k}_1, M, s_1') \end{aligned} \right\} \text{proton wavefunctions}$$

and

$$\left. \begin{aligned} \psi_n(2) &= \psi_n(\vec{p}_2, M, s_2) \\ \psi_n(2') &= \psi_n(\vec{k}_2, M, s_2') \end{aligned} \right\} \text{neutron wavefunctions.}$$

The invariant matrix element for the scattering process on the right is

$$\mathcal{M}_{IF} = [\bar{\psi}_n(1') \otimes \bar{\psi}_p(2')] \hat{F}((\vec{p}_1, \vec{p}_2) \longrightarrow (\vec{k}_1, \vec{k}_2)) [\psi_n(1) \otimes \psi_p(2)]. \quad (2.36)$$

We now aim to write Eq. (2.36) in such a form that the initial and final external states are exactly the same as in Eq. (2.35). To this end we introduce the substitution rule [Tj87a]  $\hat{P}_{12}$  which states that  $1 \rightleftharpoons 2$  for all spin and momentum labels. Application of  $\hat{P}_{12}$  to Eq. (2.36) results in:

$$\mathcal{M}_{IF} = [\bar{\psi}_n(2') \otimes \bar{\psi}_p(1')] \hat{P}_{1'2'} [\hat{F}((\vec{p}_1, \vec{p}_2) \longrightarrow (\vec{k}_1, \vec{k}_2))] \hat{P}_{12} [\psi_n(2) \otimes \psi_p(1)]. \quad (2.37)$$

Using Eq. (2.32) we can write Eq. (2.37) as

$$\mathcal{M}_{IF} = [\bar{\psi}_p(1') \otimes \bar{\psi}_n(2')] \tilde{S} \hat{P}_{1'2'} [\hat{F}((\vec{p}_1, \vec{p}_2) \longrightarrow (\vec{k}_1, \vec{k}_2))] \tilde{S} \hat{P}_{12} [\psi_p(1) \otimes \psi_n(2)]. \quad (2.38)$$

Invariance under charge symmetry demands that

$$\mathcal{M}_{if} = \mathcal{M}_{IF}$$

and therefore use of Eqs. (2.35) and (2.37) leads to the following charge symmetry condition on  $\hat{F}$ :

$$\hat{F}((\vec{p}_1, \vec{p}_2) \longrightarrow (\vec{k}_1, \vec{k}_2)) = \hat{P}_{1'2'} \tilde{S} \hat{F}((\vec{p}_1, \vec{p}_2) \longrightarrow (\vec{k}_1, \vec{k}_2)) \tilde{S} \hat{P}_{12} \quad (2.39)$$

where

$$[\tilde{S}, \hat{P}_{12}] = [\tilde{S}, \hat{P}_{1'2'}] = 0.$$

Note that the order of the momenta are the same on the left and right-hand side of Eq. (2.39). This will not be the case for the condition on  $\hat{F}$  due to time-reversal invariance [see Eq. (2.63)]. Substitution of Eq. (2.34) into Eq. (2.39) gives:

$$\hat{P}_{1'2'} \tilde{S} \hat{F}((\vec{p}_1, \vec{p}_2) \longrightarrow (\vec{k}_1, \vec{k}_2)) \tilde{S} \hat{P}_{12} = \sum_{\{\rho\}} \sum_{n=1}^9 \hat{P}_{1'2'} \tilde{S} [\Lambda_{\rho'_1}(\vec{k}_1, M) \otimes \Lambda_{\rho'_2}(\vec{k}_2, M)] f_n^{\{\rho\}} \Gamma_n(\eta_{ij}) [\Lambda_{\rho_1}(\vec{p}_1, M) \otimes \Lambda_{\rho_2}(\vec{p}_2, M)] \tilde{S} \hat{P}_{12}. \quad (2.40)$$

Keeping in mind that  $\hat{P}_{12}$  changes the spin and momentum labels and using Eq. (2.32) it follows that

$$[\Lambda_{\rho_1}(\vec{p}_1, M) \otimes \Lambda_{\rho_2}(\vec{p}_2, M)] \tilde{S} \hat{P}_{12} = \hat{P}_{12} [\Lambda_{\rho_1}(\vec{p}_2, M) \otimes \Lambda_{\rho_2}(\vec{p}_1, M)] \tilde{S} \quad (2.41)$$

$$= \hat{P}_{12} \tilde{S} [\Lambda_{\rho_2}(\vec{p}_1, M) \otimes \Lambda_{\rho_1}(\vec{p}_2, M)]. \quad (2.42)$$

Note that the rho-spin labels do not change under the action of  $\hat{P}_{12}$ , but that the operator  $\hat{P}_{12} \tilde{S}$  exchanges initial rho-spins. Similarly it follows that

$$\hat{P}_{1'2'} \tilde{S} [\Lambda_{\rho'_1}(\vec{k}_1, M) \otimes \Lambda_{\rho'_2}(\vec{k}_2, M)] = [\Lambda_{\rho'_2}(\vec{k}_1, M) \otimes \Lambda_{\rho'_1}(\vec{k}_2, M)] \hat{P}_{1'2'} \tilde{S}. \quad (2.43)$$

Use of Eqs. (2.41) and (2.43) in Eq. (2.40) gives:

$$\begin{aligned} \hat{P}_{1'2'} \tilde{S} \hat{F}((\vec{p}_1, \vec{p}_2) \longrightarrow (\vec{k}_1, \vec{k}_2)) \hat{P}_{12} \tilde{S} &= \sum_{\{\rho\}} \sum_{n=1}^9 [\Lambda_{\rho'_2}(\vec{k}_1, M) \otimes \Lambda_{\rho'_1}(\vec{k}_2, M)] \\ &[\hat{P}_{1'2'} \tilde{S} f_n^{\{\rho\}}(\underline{s}) \Gamma_n(\eta_{ij}) \hat{P}_{12} \tilde{S}] \\ &[\Lambda_{\rho_2}(\vec{p}_1, M) \otimes \Lambda_{\rho_1}(\vec{p}_2, M)]. \end{aligned} \quad (2.44)$$

The product in the second square brackets in Eq. (2.44) must now be evaluated for each covariant. The algebra is carried out in Section A.1 of Appendix A. The result is that:

$$\hat{P}_{1'2'} \tilde{S} (f_n^{\{\rho_1 \rho'_1 \rho_2 \rho'_2\}}(\underline{s}) \Gamma_n(\eta_{ij})) \hat{P}_{12} \tilde{S} = \chi_n f_n^{\{\rho_1 \rho'_1 \rho_2 \rho'_2\}}(\underline{s}) \Gamma_n(\eta_{ij}) \quad (2.45)$$



where  $\overleftrightarrow{s}$  is a collective index meaning:

$$\overleftrightarrow{s} = \{s_1, s_2, s_3, s_4, s_5, -s_6, -s_7\} \quad (2.46)$$

with

$$\chi_n = \begin{cases} 1, & n = 1 \dots 5, 6, 8 \\ -1, & n = 7, 9. \end{cases}$$

Substitution of Eq. (2.45) into Eq. (2.40) leads to:

$$\begin{aligned} \hat{P}_{1'2'} \tilde{S} \hat{F}((\vec{p}_1, \vec{p}_2) \longrightarrow (\vec{k}_1, \vec{k}_2)) \hat{P}_{12} \tilde{S} &= \sum_{\{\rho\}} \sum_{n=1}^9 [\Lambda_{\rho'_1}(\vec{k}_1, M) \otimes \Lambda_{\rho'_2}(\vec{k}_2, M)] \\ &\chi_n f_n^{\{\rho_2 \rho'_2 \rho_1 \rho'_1\}}(\overleftrightarrow{s}) \Gamma_n(\eta_{ij}) \quad (2.47) \\ &[\Lambda_{\rho_1}(\vec{p}_1, M) \otimes \Lambda_{\rho_2}(\vec{p}_2, M)]. \quad (2.48) \end{aligned}$$

Note that the order of the rho-spin labels are different in the amplitudes,  $f_n$ . Use of Eqs. (2.34) and (2.48) shows that the charge symmetry condition on  $\hat{F}$  [Eq. (2.39)] translates to the following charge symmetry condition on the amplitudes:

$$\begin{aligned} f_n^{\rho_1 \rho'_1 \rho_2 \rho'_2}(s_1, s_2, s_3, s_4, s_5, s_6, s_7) &= \chi_n f_n^{\rho_2 \rho'_2 \rho_1 \rho'_1}(s_1, s_2, s_3, s_4, s_5, -s_6, -s_7) \\ &\text{for } n = 1 \dots 9. \quad (2.49) \end{aligned}$$

Eq. (2.49) leads to symmetry relations between the amplitudes when the external nucleons are off-mass-shell for both diagonal and off-diagonal subclasses. If the external nucleons are on-mass-shell then Eq. (2.49) leads to constraint conditions for amplitudes in the diagonal subclasses. For diagonal subclasses Eq. (2.49) becomes:

$$\begin{aligned} f_n^{ii}(s_1, s_2, s_3, s_4, s_5, s_6, s_7) &= \chi_n f_n^{ii}(s_1, s_2, s_3, s_4, s_5, -s_6, -s_7) \\ &\text{for } n = 1 \dots 9. \quad (2.50) \end{aligned}$$

When the external nucleons are on-mass-shell then

$$s_4 = s_5 = M^2 \quad \text{and} \quad s_6 = s_7 = 0$$

and therefore

$$\begin{aligned} f_n^{ii}(s_1, s_2, s_3) &= \chi_n f_n^{ii}(s_1, s_2, s_3) \\ &\text{for } n = 1 \dots 9. \quad (2.51) \end{aligned}$$

Since  $\chi_n = -1$  for  $n = 7$  and  $n = 9$ , it follows from Eq. (2.51) that amplitudes 7 and 9 must vanish in all diagonal subclasses. The on-mass-shell condition for the external nucleons therefore leads to a further reduction in the number of independent invariant amplitudes. Eq. (2.49) leads to 48 relations between amplitudes in the on-shell case and Eq. (2.51) provide another 8 relations. These 56 relations reduce the number of amplitudes from 128 to 72. To summarise: When the parity invariance and charge

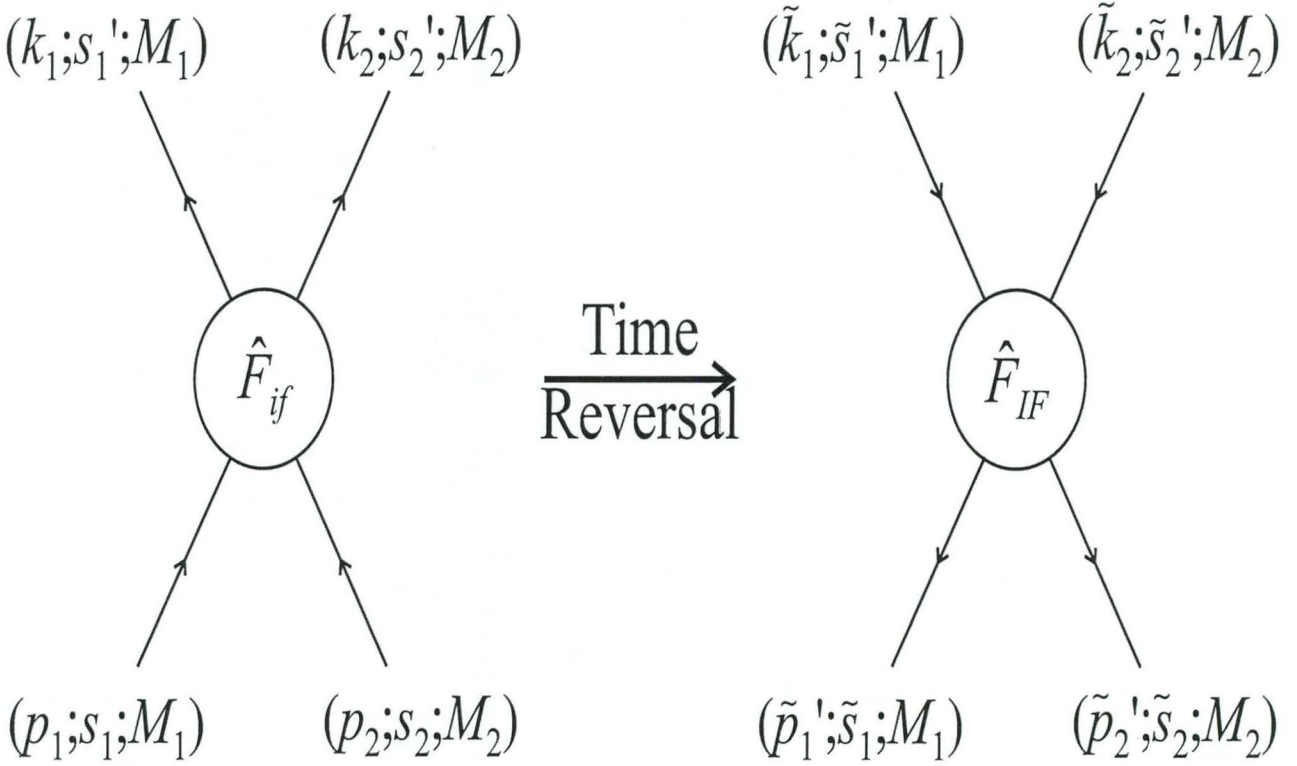


Figure 2.7: A time reversal transformation on the left-hand figure produces the one on the right. The tilde symbol ( $\sim$ ) on the momenta and spin denote time reversed quantities.

symmetry are obeyed, then  $\hat{F}$  will contain 72 independent amplitudes for the on-mass-shell case.

Next we study the time-reversal transformation. Consider the scattering process depicted in Fig 2.7. For the left-hand side of Fig 2.7 the initial state is given by

$$|i\rangle = \psi(p_1, s_1) \otimes \psi(p_2, s_2)$$

and the final state by

$$\langle f| = \bar{\psi}(k_1, s'_1) \otimes \bar{\psi}(k_2, s'_2).$$

The invariant matrix element is therefore

$$\begin{aligned} \mathcal{M}_{if} &= \langle f | \hat{F}((\vec{p}_1, \vec{p}_2) \rightarrow (\vec{k}_1, \vec{k}_2)) | i \rangle \\ &= [\bar{\psi}(k_1, s'_1) \otimes \bar{\psi}(k_2, s'_2)] \hat{F}((\vec{p}_1, \vec{p}_2) \rightarrow (\vec{k}_1, \vec{k}_2)) [\psi(p_1, s_1) \otimes \psi(p_2, s_2)] \\ &= (\psi^\dagger(1') \otimes \psi^\dagger(2')) (\gamma^0 \otimes \gamma^0) \hat{F}_{if}(\psi(1) \otimes \psi(2)) \end{aligned} \quad (2.52)$$

where the  $if$  subscript on  $\hat{F}$  denotes the scattering process:

$$(\vec{p}_1, \vec{p}_2) \rightarrow (\vec{k}_1, \vec{k}_2).$$

For the righthand side of Fig 2.7 the initial state is given by

$$|I\rangle = \psi(\tilde{k}_1, \tilde{s}'_1) \otimes \psi(\tilde{k}_2, \tilde{s}'_2)$$

and the final state by

$$\langle F| = \bar{\psi}(\tilde{p}'_1, \tilde{s}_1) \otimes \bar{\psi}(\tilde{p}'_2, \tilde{s}_2).$$

The invariant matrix element is therefore

$$\begin{aligned} \mathcal{M}_{IF} &= \langle F|\hat{F}((\tilde{k}_1, \tilde{k}_2) \longrightarrow (\tilde{p}'_1, \tilde{p}'_2))|I\rangle \\ &= [\bar{\psi}(\tilde{p}'_1, \tilde{s}_1) \otimes \bar{\psi}(\tilde{p}'_2, \tilde{s}_2)] \hat{F}((\tilde{k}_1, \tilde{k}_2) \longrightarrow (\tilde{p}'_1, \tilde{p}'_2)) [\psi(\tilde{k}_1, \tilde{s}'_1) \otimes \psi(\tilde{k}_2, \tilde{s}'_2)] \\ &= [\psi^\dagger(\tilde{p}'_1, \tilde{s}_1) \otimes \psi^\dagger(\tilde{p}'_2, \tilde{s}_2)] (\gamma^0 \otimes \gamma^0) \hat{F}_{IF} [\psi(\tilde{k}_1, \tilde{s}'_1) \otimes \psi(\tilde{k}_2, \tilde{s}'_2)] \end{aligned} \quad (2.53)$$

where the subscript  $IF$  on  $\hat{F}$  denotes the scattering process

$$(\tilde{k}_1, \tilde{s}'_1, \tilde{k}_2, \tilde{s}'_2) \longrightarrow (\tilde{p}'_1, \tilde{s}_1, \tilde{p}'_2, \tilde{s}_2).$$

Now employ Eq. (A.3) in Appendix A with

$$|\alpha\rangle = \psi(\tilde{k}_1, \tilde{s}'_1) \otimes \psi(\tilde{k}_2, \tilde{s}'_2) \quad (2.54)$$

and

$$\langle\beta| = \psi^\dagger(\tilde{p}'_1, \tilde{s}_1) \otimes \psi^\dagger(\tilde{p}'_2, \tilde{s}_2). \quad (2.55)$$

Then

$$\begin{aligned} |\tilde{\alpha}\rangle &= \mathcal{T}|\alpha\rangle \\ &= (\mathcal{T}_1 \otimes \mathcal{T}_2)[(\psi(\tilde{k}_1, \tilde{s}'_1) \otimes \psi(\tilde{k}_2, \tilde{s}'_2))] \end{aligned} \quad (2.56)$$

where  $\mathcal{T}_i$  is the time-reversal operator in the space of particle  $i$ . Therefore

$$|\tilde{\alpha}\rangle = \psi(k_1, s'_1) \otimes \psi(k_2, s'_2)$$

and thus

$$\langle\tilde{\alpha}| = \psi^\dagger(k_1, s'_1) \otimes \psi^\dagger(k_2, s'_2) \quad (2.57)$$

where we have used:

$$(A \otimes B)^\dagger = A^\dagger \otimes B^\dagger. \quad (2.58)$$

Use of Eq. (2.55) implies that

$$|\tilde{\beta}\rangle = \psi(p_1, s_1) \otimes \psi(p_2, s_2). \quad (2.59)$$

Substitution of Eqs. (2.54), (2.55), (2.57) and (2.59) into Eq. (A.4) with

$$\hat{X} = (\gamma^0 \otimes \gamma^0) \hat{F}_{IF} (\gamma^0 \otimes \gamma^0),$$



results in the following equation for  $\mathcal{M}_{IF}$ :

$$\begin{aligned}\mathcal{M}_{IF} &= [\psi^\dagger(\vec{p}'_1, \vec{s}_1) \otimes \psi^\dagger(\vec{p}'_2, \vec{s}_2)] (\gamma^0 \otimes \gamma^0) \hat{F}_{IF} [\psi(\vec{k}_1, \vec{s}'_1) \otimes \psi(\vec{k}_2, \vec{s}'_2)] \\ &= \{\psi^\dagger(k_1, s'_1) \otimes \psi^\dagger(k_2, s'_2)\} \mathcal{T} [(\gamma^0 \otimes \gamma^0) \hat{F}_{IF}]^\dagger \\ &\quad \mathcal{T}^{-1} \{\psi(p_1, s_1) \otimes \psi(p_2, s_2)\}.\end{aligned}\tag{2.60}$$

Invariance under time-reversal demands that

$$\mathcal{M}_{if} = \mathcal{M}_{IF}$$

and therefore the condition on the operator  $\hat{F}$  due to time-reversal invariance is:

$$\begin{aligned}(\gamma^0 \otimes \gamma^0) \hat{F}_{if} &= \mathcal{T} [(\gamma^0 \otimes \gamma^0) \hat{F}_{IF}]^\dagger \mathcal{T}^{-1} \\ &= \mathcal{T} \hat{F}_{IF}^\dagger (\gamma^0 \otimes \gamma^0) \mathcal{T}^{-1}\end{aligned}$$

and therefore

$$\hat{F}_{if} = (\gamma^0 \otimes \gamma^0) \mathcal{T} \hat{F}_{IF}^\dagger (\gamma^0 \otimes \gamma^0) \mathcal{T}^{-1}.\tag{2.61}$$

A matrix representation of the time-reversal operator in terms of Dirac matrices is given by [Bj64]:

$$\mathcal{T} = TK\tag{2.62}$$

where  $T = i\gamma^1\gamma^3$  and  $K$  is the complex conjugation operator. Use of Eq. (2.62) shows that

$$[\mathcal{T}, \gamma^0] = 0$$

and therefore Eq. (2.61) becomes

$$\begin{aligned}\hat{F}((\vec{p}_1, \vec{p}_2) \longrightarrow (\vec{k}_1, \vec{k}_2)) &= \mathcal{T} (\gamma^0 \otimes \gamma^0) \hat{F}^\dagger((-\vec{k}_1, -\vec{k}_2) \longrightarrow (-\vec{p}_1, -\vec{p}_2)) \\ &\quad (\gamma^0 \otimes \gamma^0) \mathcal{T}^{-1}\end{aligned}\tag{2.63}$$

where we have used

$$\begin{aligned}\vec{p}'_i &= \mathcal{T} p_i \\ &= \mathcal{T}(E_i, \vec{p}_i) \\ &= (E_i, -\vec{p}_i) \quad i = 1, 2\end{aligned}$$

and

$$\begin{aligned}\vec{k}_i &= \mathcal{T} k_i \\ &= \mathcal{T}(E'_i, \vec{k}_i) \\ &= (E'_i, -\vec{k}_i) \quad i = 1, 2.\end{aligned}$$

Eq. (2.63) is the condition for time-reversal invariance on the operator  $\hat{F}$ . Note also that the order of the momenta has changed [in contrast to the charge symmetry condition on  $\hat{F}$  given in Eq. (2.39)]. Use of Eq. (2.34) shows that

$$\begin{aligned} \hat{F}((- \vec{k}_1, - \vec{k}_2) \longrightarrow (- \vec{p}_1, - \vec{p}_2)) &= \sum_{\{\rho\}} \sum_{n=1}^9 f_n^{ij}(\underline{\tilde{s}}) [\Lambda_{\rho'_1}(- \vec{p}_1, M) \otimes \Lambda_{\rho'_2}(- \vec{p}_2, M)] \\ &\quad \tilde{\Gamma}_n(\eta_{ij}) [\Lambda_{\rho_1}(- \vec{k}_1, M) \otimes \Lambda_{\rho_2}(- \vec{k}_2, M)] \end{aligned} \quad (2.64)$$

where the  $\sim$  on  $\underline{\tilde{s}}$  and  $\Gamma_n$  indicate time-reversed quantities, where

$$\underline{\tilde{s}} = (s_1, s_2, s_3, s_5, s_4, s_7, s_6).$$

Note that the order of  $s_4$  and  $s_5$  has been interchanged as well as the order of  $s_6$  and  $s_7$  in  $\underline{\tilde{s}}$ . From Eq. (2.64) it follows that

$$\begin{aligned} \hat{F}^\dagger((- \vec{k}_1, - \vec{k}_2) \longrightarrow (- \vec{p}_1, - \vec{p}_2)) &= \sum_{\{\rho\}} \sum_{n=1}^9 (f_n^{ij}(\underline{\tilde{s}}))^* [\Lambda_{\rho_1}^\dagger(- \vec{k}_1, M) \otimes \Lambda_{\rho_2}^\dagger(- \vec{k}_2, M)] \tilde{\Gamma}_n^\dagger \\ &\quad [\Lambda_{\rho'_1}(- \vec{p}_1, M) \otimes \Lambda_{\rho'_2}(- \vec{p}_2, M)]. \end{aligned} \quad (2.65)$$

Using

$$\{\gamma^0, \gamma^i\} = 0$$

it follows that

$$\gamma^0 \Lambda_\rho^\dagger(\vec{p}, M) = \Lambda_\rho(\vec{p}, M) \gamma^0. \quad (2.66)$$

We therefore have

$$\begin{aligned} \mathcal{T}(\gamma^0 \otimes \gamma^0) \hat{F}_{IF}^\dagger(\gamma^0 \otimes \gamma^0) \mathcal{T}^{-1} &= \sum_{\{\rho\}} \sum_{n=1}^9 f_n^{ij}(\underline{\tilde{s}}) [\mathcal{T}_1 \gamma^0 \Lambda_{\rho_1}^\dagger(- \vec{k}_1, M) \otimes \mathcal{T}_2 \gamma^0 \Lambda_{\rho_2}^\dagger(- \vec{k}_2, M)] \\ &\quad \tilde{\Gamma}_n^\dagger(\eta_{ij}) [\Lambda_{\rho'_1}^\dagger(- \vec{p}_1, M) \gamma^0 \mathcal{T}_1^{-1} \otimes \Lambda_{\rho'_2}^\dagger(- \vec{p}_2, M) \gamma^0 \mathcal{T}_2^{-1}] \\ &= \sum_{\{\rho\}} \sum_{n=1}^9 f_n^{\rho_1 \rho'_1 \rho_2 \rho'_2}(\underline{\tilde{s}}) [\mathcal{T}_1 \gamma^0 \Lambda_{\rho_1}^\dagger(- \vec{k}_1, M) \gamma^0 \mathcal{T}_1^{-1} \otimes \\ &\quad \mathcal{T}_2 \gamma^0 \Lambda_{\rho_2}^\dagger(- \vec{k}_2, M) \gamma^0 \mathcal{T}_2^{-1}] \\ &\quad (\mathcal{T}_1 \gamma^0 \otimes \mathcal{T}_2 \gamma^0) \tilde{\Gamma}_n^\dagger(\eta_{ij}) (\gamma^0 \mathcal{T}_1^{-1} \otimes \gamma^0 \mathcal{T}_2^{-1}) \\ &\quad [\gamma^0 \mathcal{T}_1 \Lambda_{\rho'_1}(- \vec{p}_1, M) \gamma^0 \mathcal{T}_1^{-1} \otimes \gamma^0 \mathcal{T}_2 \Lambda_{\rho'_2}(- \vec{p}_2, M) \gamma^0 \mathcal{T}_2^{-1}] \end{aligned}$$

where we have used:

$$\begin{aligned} I_{16} &= I_4 \otimes I_4 \\ &= [(\gamma^0 \mathcal{T}_1)^{-1} \gamma^0 \mathcal{T}_1] \otimes [(\gamma^0 \mathcal{T}_2)^{-1} \gamma^0 \mathcal{T}_2]. \end{aligned}$$

Table 2.4: Transformation properties of the gamma matrices and  $s_i$  under a time-reversal transformation.

	$\mathcal{T}s_i\mathcal{T}^{-1} = s_i \quad i = 1, 2, 3$
$s_i$	$\mathcal{T}s_4\mathcal{T}^{-1} = s_5; \quad \mathcal{T}s_5\mathcal{T}^{-1} = s_4$ $\mathcal{T}s_6\mathcal{T}^{-1} = s_7; \quad \mathcal{T}s_6\mathcal{T}^{-1} = s_6$
$S$	$\mathcal{T}I_4\mathcal{T}^{-1} = I_4$
$P$	$\mathcal{T}\gamma^5\mathcal{T}^{-1} = \gamma^5$
$V$	$\mathcal{T}\gamma^\mu\mathcal{T}^{-1} = \gamma_\mu$
$A$	$\mathcal{T}\gamma^5\gamma^\mu\mathcal{T}^{-1} = \gamma^5\gamma_\mu$
$T$	$\mathcal{T}\sigma^{\mu\nu}\mathcal{T}^{-1} = -\sigma_{\mu\nu}$

The transformation properties of the gamma matrices and  $s_i$  under time-reversal are given in Table 2.4. From these properties it follows that:

$$\begin{aligned}
 \gamma^0\mathcal{T}\Lambda_\rho^\dagger(\vec{p}, M)\mathcal{T}^{-1}\gamma^0 &= \mathcal{T}\gamma^0\Lambda_\rho^\dagger(\vec{p}, M)\gamma^0\mathcal{T}^{-1} \\
 &= \mathcal{T}\Lambda_\rho(\vec{p}, M)\mathcal{T}^{-1} \quad (\text{Eq. (2.66)}) \\
 &= \frac{1}{2M}[\rho(E\gamma^0 + (-p_i)\gamma^i) + M] \\
 &= \Lambda_\rho(-\vec{p}, M).
 \end{aligned} \tag{2.67}$$

Use of Eq. (2.67) and the relabelling of the rho-spin indices according to

$$\rho_1 \rightleftharpoons \rho'_1 \quad \text{and} \quad \rho_2 \rightleftharpoons \rho'_2$$

results in

$$\begin{aligned}
 \mathcal{T}(\gamma^0 \otimes \gamma^0)\hat{F}_{IF}(\gamma^0 \otimes \gamma^0)\mathcal{T}^{-1} &= \sum_{\{\rho\}} \sum_{n=1}^9 f_n^{\rho'_1\rho_1\rho'_2\rho_2}(\underline{\underline{x}}) [\Lambda_{\rho'_1}(\vec{k}_1, M) \otimes \Lambda_{\rho'_2}(\vec{k}_2, M)] \\
 &\quad [\mathcal{T}(\gamma^0 \otimes \gamma^0)\tilde{\Gamma}_n^\dagger(\eta_{ij})(\gamma^0 \otimes \gamma^0)\mathcal{T}^{-1}] \\
 &\quad [\Lambda_{\rho_1}(\vec{p}_1, M) \otimes \Lambda_{\rho_2}(\vec{p}_2, M)].
 \end{aligned} \tag{2.68}$$

The matrix product in the second square bracket must now be evaluated for each covariant. The algebra is carried out in Section A.2 of Appendix A. The result is

$$\mathcal{T}(\gamma^0 \otimes \gamma^0)\tilde{\Gamma}_n^\dagger(\gamma^0 \otimes \gamma^0)\mathcal{T}^{-1} = \begin{cases} \Gamma_n & \text{if } n = 1 \dots 5, 6 \\ -\Gamma_n & \text{if } n = 8. \end{cases}$$



Covariants  $\Gamma_7$  and  $\Gamma_9$  do not transform simply under a time-reversal transformation. Only for  $n = 1..5, 6, 8$  can we therefore write down the following condition on the amplitudes due to time-reversal invariance:

$$\begin{aligned} f_n^{\rho_1 \rho_1' \rho_2 \rho_2'}(\underline{s}) &= f_n^{\rho_1 \rho_1' \rho_2 \rho_2'}(\tilde{\underline{s}}) & n = 1..5, 6 \\ f_8^{\rho_1 \rho_1' \rho_2 \rho_2'}(\underline{s}) &= -f_8^{\rho_1 \rho_1' \rho_2 \rho_2'}(\tilde{\underline{s}}). \end{aligned} \quad (2.69)$$

Imposing the charge symmetry and time-reversal conditions [Eqs. (2.49) and (2.69) respectively] on the amplitudes, allows one to construct Tables 2.5 and 2.6 for the case of on-mass-shell external nucleons.

To summarise: The IA2 representation of  $\hat{F}$  is given by

$$\begin{aligned} \hat{F} &= \sum_{\{\rho\}} \sum_{n=1}^9 f_n^{\{\rho\}}(\underline{s}) [\Lambda_{\rho_1'}(\vec{k}_1, M) \otimes \Lambda_{\rho_2'}(\vec{k}_2, M)] \Gamma_n(\eta_{ij}) \\ &[\Lambda_{\rho_1}(\vec{p}_1, M) \otimes \Lambda_{\rho_2}(\vec{p}_2, M)] \end{aligned} \quad (2.70)$$

where the independent subclasses are given in Table 2.5 and Table 2.6, which show that  $\hat{F}$  contains 44 independent invariant amplitudes consistent with parity and time-reversal invariance as well as charge symmetry when the external nucleons are on-mass-shell.

The next step is to determine the invariant amplitudes. Five amplitudes in subclass  $\hat{F}^{11}$  are completely specified by fitting to physical free NN scattering data and are therefore identical to the SPVAT amplitudes in the IA1 representation of  $\hat{F}$ . The remaining 39 off-shell amplitudes (contained in subclasses  $\hat{F}^{12}$  to  $\hat{F}^{44}$ ) are obtained by solving the Bethe-Salpeter equation in a three-dimensional quasi-potential reduction [Fa83, Fa84], with pure pseudovector pion-nucleon coupling, to determine a complete set of helicity amplitudes. The invariant amplitudes are related via matrix equations to the helicity amplitudes [Tj87a]. The IA2 representation is a complete and unambiguous expansion of  $\hat{F}$  since covariants cannot be added or changed arbitrarily without violating the above-mentioned symmetries. Amplitudes which are solely determined by physical scattering data are isolated in subclass  $\hat{F}^{11}$  while the remaining amplitudes are determined by solving a dynamical equation, the Bethe-Salpeter equation using a meson-exchange model for the NN force.

### 2.5.2 Derivation of effective t-matrix

In this section we discuss in detail the derivation of the effective t-matrix which will be employed to derive expressions for the quasielastic spin observables.

The exchange covariants  $\tilde{S}, \tilde{P}, \tilde{V}, \tilde{A}$  and  $\tilde{T}$  in Eq. (2.33) can be written in terms of the SPVAT covariants in Eq. (2.27) using Eq. (D.1) of Appendix D, and consequently Eq. (2.70) can be written as:

$$\begin{aligned} \hat{F} &= \sum_{\rho_1 \rho_1'; \rho_2 \rho_2'} \sum_{n=1}^{13} F_n^{\rho_1 \rho_1' \rho_2 \rho_2'} [\Lambda_{\rho_1'}(\vec{k}_1; M) \otimes \Lambda_{\rho_2'}(\vec{k}_2; M)] K_n \\ &[\Lambda_{\rho_1}(\vec{p}_1; M) \otimes \Lambda_{\rho_2}(\vec{p}_2; M)] \end{aligned} \quad (2.71)$$

Table 2.5: This table shows the number of independent amplitudes for each subclass, which arise due to constraint conditions. CS denotes charge symmetry, TR denotes time-reversal and OMS denotes on-mass-shell.

Subclass	Zero amplitude: redundant covariant	Constraints (CS,TR,OMS)	Zero amplitudes (CS,TR,OMS)	Number of independent amplitudes
$\hat{F}^{11}$	$f_6^{11}$		$f_7^{11}, f_8^{11}, f_9^{11}$	5
$\hat{F}^{12}$	$f_6^{12}$			8
$\hat{F}^{13}$	$f_6^{13}$	TR : $f_i^{13} = f_i^{12}; i = 1...5; 6$ $f_8^{13} = -f_8^{12}$		0
$\hat{F}^{14}$	$f_9^{14}$		$f_7^{14}, f_8^{14}$	6
$\hat{F}^{21}$	$f_6^{21}$	CS : $f_n^{21} = f_n^{12}; n = 1...5, 6, 8$ $f_n^{21} = -f_n^{12}; n = 7, 9$		0
$\hat{F}^{22}$	$f_8^{22}$		$f_7^{22}, f_9^{22}$	6
$\hat{F}^{23}$	$f_9^{23}$			6
$\hat{F}^{24}$	$f_6^{24}$			8
$\hat{F}^{31}$	$f_6^{31}$	CS : $f_i^{31} = f_i^{13}; i = 1...5, 6, 8$ $f_i^{31} = -f_i^{13}; i = 7, 9$ TR : $f_i^{31} = f_i^{21}; i = 1...5, 6$ $f_8^{31} = -f_8^{21}$		0
$\hat{F}^{32}$	$f_9^{32}$	CS : $f_i^{32} = f_i^{23}; i = 1...5, 6, 8$ $f_i^{32} = -f_i^{23}; i = 7, 9$ TR : $f_i^{32} = f_i^{23}; i = 1...5, 6$ $f_8^{32} = -f_8^{23}$		0
$\hat{F}^{33}$	$f_8^{33}$	TR : $f_i^{33} = f_i^{22}; i = 1...5, 6$ $f_8^{33} = -f_8^{22}$		0
$\hat{F}^{34}$	$f_6^{34}$	TR : $f_i^{34} = f_i^{24}; i = 1...5, 6$ $f_8^{34} = -f_8^{24}$		0

Table 2.6: Continuation of Table 2.5 which shows the number of independent amplitudes for each subclass, which arise due to constraint conditions.

Subclass	Zero amplitude: redundant covariant	Constraints (CS,TR,OMS)	Zero amplitudes (CS,TR,OMS)	Number of independent amplitudes
$\hat{F}^{41}$	$f_9^{41}$	CS : $f_i^{41} = f_i^{14}$ ; $i = 1...5, 6, 8$ $f_i^{41} = -f_i^{14}$ ; $i = 7, 9$		0
$\hat{F}^{42}$	$f_6^{42}$	CS : $f_i^{42} = f_i^{24}$ ; $i = 1...5, 6, 8$ $f_i^{42} = -f_i^{24}$ ; $i = 7, 9$		0
$\hat{F}^{43}$	$f_6^{34}$	CS : $f_i^{43} = f_i^{34}$ ; $i = 1...5, 6, 8$ $f_i^{43} = -f_i^{34}$ ; $i = 7, 9$ TR : $f_i^{43} = f_i^{42}$ ; $i = 1...5, 6$ $f_8^{43} = -f_8^{42}$		0
$\hat{F}^{44}$	$f_6^{44}$		$f_7^{44}, f_8^{44}, f_9^{44}$	5
Total				44



where the kinematic covariants  $K_n$  ( $n = 1\dots 13$ ) are

$$\begin{aligned}
K_1 &= S = I_4 \otimes I_4 \\
K_2 &= P = \gamma^5 \otimes \gamma^5 \\
K_3 &= V = \gamma^\mu \otimes \gamma_\mu \\
K_4 &= A = \gamma^5 \gamma^\mu \otimes \gamma^5 \gamma_\mu \\
K_5 &= T = \sigma^{\mu\nu} \otimes \sigma_{\mu\nu} \\
K_6 &= Q_{11,\mu}(I_4 \otimes \gamma^\mu) \\
K_7 &= Q_{22,\mu}(\gamma^\mu \otimes I_4) \\
K_8 &= Q_{11,\mu}(\gamma^5 \otimes \gamma^5 \gamma^\mu) \\
K_9 &= Q_{22,\mu}(\gamma^5 \gamma^\mu \otimes \gamma^5) \\
K_{10} &= Q_{12,\mu}(I_4 \otimes \gamma^\mu) \tilde{S} \\
K_{11} &= Q_{21,\mu}(\gamma^\mu \otimes I_4) \tilde{S} \\
K_{12} &= Q_{12,\mu}(\gamma^5 \otimes \gamma^5 \gamma^\mu) \tilde{S} \\
K_{13} &= Q_{21,\mu}(\gamma^5 \gamma^\mu \otimes \gamma^5) \tilde{S}
\end{aligned}$$

with

$$Q_{ij,\mu} = \frac{(p'_i + p_j)_\mu}{2M} \quad \text{and} \quad p'_1 = k_1 ; p'_2 = k_2.$$

The invariant amplitudes  $F_n^{\{\rho\}}$  are functions of the invariant amplitudes,  $f_n^{\{\rho\}}$  with

$$\begin{aligned}
F_1 &= \frac{3}{4}f_1 + \frac{3}{2}f_2 - f_3 + f_4 - \frac{1}{4}f_5 \\
F_2 &= -\frac{1}{4}f_1 + \frac{3}{2}f_2 + f_3 - f_4 + \frac{3}{4}f_5 \\
F_3 &= -\frac{1}{4}f_1 - \frac{1}{2}f_3 + \frac{1}{4}f_4 + \frac{1}{4}f_5 \\
F_4 &= \frac{1}{f_1} - \frac{3}{2}f_3 - \frac{1}{2}f_4 - \frac{1}{4}f_5 \\
F_5 &= -\frac{1}{8}f_1 + \frac{1}{4}f_2 - \frac{1}{8}f_5 \\
F_6 &= f_6^{\{\rho\}} + f_7^{\{\rho\}} \\
F_7 &= f_6^{\{\rho\}} - f_7^{\{\rho\}} \\
F_8 &= f_8^{\{\rho\}}\eta_{ij} + f_9^{\{\rho\}}\eta_{ij} \\
F_9 &= f_8^{\{\rho\}}\eta_{ij} - f_9^{\{\rho\}}\eta_{ij} \\
F_{10} &= f_6^{\{\rho\}} - \eta_{ij}f_7^{\{\rho\}} \\
F_{11} &= f_6^{\{\rho\}} + \eta_{ij}f_7^{\{\rho\}} \\
F_{12} &= f_8^{\{\rho\}}\eta_{ij} - f_9^{\{\rho\}} \\
F_{13} &= f_8^{\{\rho\}}\eta_{ij} + f_9^{\{\rho\}}
\end{aligned}$$

where the same rho-spin sector will appear on both sides of the equation above and the value of the parameter  $\eta_{ij}$  is given in Table 2.2 of Section 2.5.1 for each rho-spin sector. The relation between the rho-spin indices  $\{\rho\} = \{\rho_1\rho_1'\rho_2\rho_2'\}$  and the  $ij$  indices are given in Table 2.1 of Section 2.5.1. Using the short-hand notation,

$$\begin{aligned}\Lambda_\rho(\vec{p}_1, M, s_i) &= \Lambda_\rho(1) \\ \Lambda_\rho(\vec{p}_2, M, s_2) &= \Lambda_\rho(2) \\ \Lambda_\rho(\vec{k}_1, M, s_f) &= \Lambda_\rho(1') \\ \Lambda_\rho(\vec{k}_2, M, s_2') &= \Lambda_\rho(2')\end{aligned}$$

we can write down explicitly <sup>1</sup>:

$$\begin{aligned}\hat{F} &= (\Lambda_+(1')\Lambda_+(2'))\hat{F}^{11}(\Lambda_+(1)\Lambda_+(2)) + (\Lambda_+(1')\Lambda_-(2'))\hat{F}^{12}(\Lambda_+(1)\Lambda_+(2)) + \\ &(\Lambda_+(1')\Lambda_+(2'))\hat{F}^{13}(\Lambda_+(1)\Lambda_-(2)) + (\Lambda_+(1')\Lambda_-(2'))\hat{F}^{14}(\Lambda_+(1)\Lambda_-(2)) + \\ &(\Lambda_-(1')\Lambda_+(2'))\hat{F}^{21}(\Lambda_+(1)\Lambda_+(2)) + (\Lambda_-(1')\Lambda_-(2'))\hat{F}^{22}(\Lambda_+(1)\Lambda_+(2)) + \\ &(\Lambda_-(1')\Lambda_+(2'))\hat{F}^{23}(\Lambda_+(1)\Lambda_-(2)) + (\Lambda_-(1')\Lambda_-(2'))\hat{F}^{24}(\Lambda_+(1)\Lambda_-(2)) + \\ &(\Lambda_+(1')\Lambda_+(2'))\hat{F}^{31}(\Lambda_-(1)\Lambda_+(2)) + (\Lambda_+(1')\Lambda_-(2'))\hat{F}^{32}(\Lambda_-(1)\Lambda_+(2)) + \\ &(\Lambda_+(1')\Lambda_+(2'))\hat{F}^{33}(\Lambda_-(1)\Lambda_-(2)) + (\Lambda_+(1')\Lambda_-(2'))\hat{F}^{34}(\Lambda_-(1)\Lambda_-(2)) + \\ &(\Lambda_-(1')\Lambda_+(2'))\hat{F}^{41}(\Lambda_-(1)\Lambda_+(2)) + (\Lambda_-(1')\Lambda_-(2'))\hat{F}^{42}(\Lambda_-(1)\Lambda_+(2)) + \\ &(\Lambda_-(1')\Lambda_+(2'))\hat{F}^{43}(\Lambda_-(1)\Lambda_-(2)) + (\Lambda_-(1')\Lambda_-(2'))\hat{F}^{44}(\Lambda_-(1)\Lambda_-(2)).\end{aligned}\quad (2.72)$$

Use of Eq. (2.72) in Eq. (2.1) allows four cases concerning the combination of projectile and target nucleon masses to be distinguished:

1. No medium effect ( $M_1 = M_2 = M$ ): In this case only subclass  $\hat{F}^{11}$  will contribute to the invariant scattering amplitude. It is important to note that in this special case the IA2 representation of  $\hat{F}$  is equivalent to the SPVAT parameterisation of  $\hat{F}$ . This fact will be used later in Section 3.2 to perform numerical checks on the formalism presented in this chapter.
2. Projectile relativity ( $M_1 \neq M; M_2 = M$ ): Contributions to the invariant scattering amplitude arise from  $\hat{F}^{11}, \hat{F}^{21}, \hat{F}^{31}$  and  $\hat{F}^{41}$  where the latter three subclasses require *at least* projectile relativity for a contribution.
3. Target relativity ( $M_1 = M; M_2 \neq M$ ): Contributions to the invariant scattering amplitude arise from  $\hat{F}^{11}, \hat{F}^{12}, \hat{F}^{13}$  and  $\hat{F}^{14}$  where the latter three subclasses require *at least* target relativity for a contribution.
4. Target and projectile relativity ( $M_1 \neq M; M_2 \neq M$ ): Now all subclasses will contribute to the invariant scattering amplitude but  $\hat{F}^{22}, \hat{F}^{23}, \hat{F}^{24}, \hat{F}^{32}, \hat{F}^{33}, \hat{F}^{34}, \hat{F}^{42}, \hat{F}^{43}$  and  $\hat{F}^{44}$  require *at least* projectile *and* target relativity for a contribution.

---

<sup>1</sup>In this equation we dispense for notational simplicity of the  $\otimes$  symbol.

Note that due to the positive energy projection operators in the first term of Eq. (2.72) a medium effect can never occur in subclass  $\hat{F}^{11}$ , in contrast to the way in which medium effects are incorporated in the IA1 representation. Medium effects in the IA2 representation of  $\hat{F}$  arise only due to off-shell amplitudes (which are contained in the subclasses  $\hat{F}^{12}$  to  $\hat{F}^{44}$ ). One can now substitute Eq. (2.71) into Eq. (2.1) and proceed from there to calculate  $|\mathcal{M}|^2$  in terms of the invariant amplitudes  $F_n^{\{\rho\}}$ . We will, however, not follow this direct approach due to the following reasons:

1. Following the standard procedure (see Ref. [Bj64], for example) one finds that  $|\mathcal{M}|^2$  contains traces over at least eight gamma matrices. The number of gamma matrices increase as the covariants become more complicated. Since the number of terms generated by such a trace is given by  $\frac{N!}{(\frac{N}{2})! 2^{\frac{N}{2}}}$  (where  $N$  refers to the number of gamma matrices), and since there is a double sum over the rho-spin sectors, a very large number of terms will occur.
2. Since we are applying a relativistic formalism to a Nuclear Physics problem, it might be more instructive to rewrite the NN scattering matrix in a form which is more familiar to traditional Nuclear Physics.

We will therefore follow a similar approach to that in Ref. [Fu93] where an *effective t-matrix is derived* which is a  $4 \times 4$  matrix, but which still contains all the information coming from the relativistic analysis. From Eq. (2.2) we can write:

$$\begin{aligned} U(\vec{p}_1, M_1, s_i) &= \left( \frac{E_1^* + M_1}{2M_1} \right)^{\frac{1}{2}} \begin{pmatrix} \phi(s_i) \\ \frac{\vec{\sigma} \cdot \vec{p}_1}{E_1^* + M_1} \phi(s_i) \end{pmatrix} \\ &= \left( \frac{E_1^*}{M_1} \right)^{\frac{1}{2}} u^+(\vec{p}_1, M_1) \phi(s_i) \end{aligned}$$

where

$$\begin{aligned} u^+(\vec{p}_1, M_1) &= \left( \frac{E_1^* + M_1}{2E_1^*} \right)^{\frac{1}{2}} \begin{pmatrix} I_2 \\ \frac{\vec{\sigma} \cdot \vec{p}_1}{E_1^* + M_1} \end{pmatrix} \\ &\equiv 4 \times 2 \quad \text{matrix.} \end{aligned} \tag{2.73}$$

Similarly

$$\bar{U}(\vec{p}_1, M_1, s_i) = \left( \frac{E_1^*}{M_1} \right)^{\frac{1}{2}} \phi^\dagger(s_i) \bar{u}^+(\vec{p}_1, M_1) \tag{2.74}$$

where

$$\bar{u}^+(\vec{p}_1, M_1) = u^{+\dagger}(\vec{p}_1, M_1) \gamma^0 \tag{2.75}$$

$$\equiv 2 \times 4 \quad \text{matrix.} \tag{2.76}$$



$u^\rho(\vec{p})$  ( where  $\rho = \pm$  ) contains no reference to the spin and is normalised to

$$u^{\rho'\dagger}(\rho'\vec{p}')u^\rho(\rho\vec{p}) = \delta_{\rho'\rho}.$$

In terms of  $u^+$  the invariant matrix element is given by

$$\mathcal{M} = \left( \frac{E_1^* E_2^* E_1' E_2'^*}{M_1^2 M_2^2} \right)^{\frac{1}{2}} [\phi^\dagger(s_f) \bar{u}^+(\vec{k}_1, M_1) \otimes \phi^\dagger(s_2') \bar{u}^+(\vec{k}_2, M_2)] \hat{F} [\phi(s_i) u^+(\vec{p}_1, M_1) \otimes \phi(s_2) u^+(\vec{p}_2, M_2)].$$

Use of the identity

$$(A \otimes B)(C \otimes D) = AC \otimes BD \quad (2.77)$$

leads to the expression

$$\mathcal{M} = \left( \frac{E_1^* E_2^* E_1' E_2'^*}{M_1^2 M_2^2} \right)^{\frac{1}{2}} [\phi^\dagger(s_f) \otimes \phi^\dagger(s_2')] [\bar{u}^+(\vec{k}_1, M_1) \otimes \bar{u}^+(\vec{k}_2, M_2)] \hat{F} [u^+(\vec{p}_1, M_1) \otimes u^+(\vec{p}_2, M_2)] [\phi(s_i) \otimes \phi(s_2)]. \quad (2.78)$$

The *effective  $\hat{t}$ -matrix* is now defined as:

$$\hat{t} = [\bar{u}^+(\vec{k}_1, M_1) \otimes \bar{u}^+(\vec{k}_2, M_2)] \hat{F} [u^+(\vec{p}_1, M_1) \otimes u^+(\vec{p}_2, M_2)] \equiv 4 \times 4 \quad \text{matrix.} \quad (2.79)$$

Set

$$g_1 = \left( \frac{E_1^* E_2^* E_1' E_2'^*}{M_1^2 M_2^2} \right)^{\frac{1}{2}}.$$

Eq. (2.78) becomes:

$$\mathcal{M} = g_1 [\phi^\dagger(s_f) \otimes \phi^\dagger(s_2')] \hat{t} [\phi(s_i) \otimes \phi(s_2)]. \quad (2.80)$$

Since  $\hat{t}$  is a  $4 \times 4$  matrix, it can be expanded in terms of a basis constructed from the Pauli matrices and the momenta of the scattering process. Define

- the three-momentum transfer

$$\vec{q} = \vec{p}_1 - \vec{k}_1 = \vec{k}_2 - \vec{p}_2,$$

- the average momentum

$$\vec{p}_a = \frac{1}{2}(\vec{p}_1 + \vec{k}_1)$$

- and a vector orthogonal to both  $\vec{q}$  and  $\vec{p}_a$

$$\begin{aligned}\vec{N} &= \vec{q} \times \vec{p}_a \\ &= \vec{p}_1 \times \vec{k}_1.\end{aligned}$$

Note that

$$\vec{q} \cdot \vec{p}_a = \frac{1}{2}(\vec{p}_1^2 - \vec{k}_1^2).$$

For quasielastic scattering  $|\vec{p}_1| \neq |\vec{k}_1|$  and therefore  $\vec{q}$  and  $\vec{p}_a$  are not orthogonal, however,  $\vec{N} \cdot \vec{q} = \vec{N} \cdot \vec{p}_a = 0$ . Assuming only parity invariance  $\hat{t}$  can be written in terms of a set of eight linearly independent matrices:

$$\begin{aligned}\hat{t} &= a_1 I_4 + \frac{a_2}{M^4} (\vec{N} \cdot \vec{\sigma} \otimes \vec{N} \cdot \vec{\sigma}) + \frac{i}{M^2} a_3 (\vec{N} \cdot \vec{\sigma} \otimes I_2) + \\ &\frac{i}{M^2} a_4 (I_2 \otimes \vec{N} \cdot \vec{\sigma}) + \frac{1}{M^2} a_5 (\vec{q} \cdot \vec{\sigma} \otimes \vec{q} \cdot \vec{\sigma}) + \frac{1}{M^2} a_6 (\vec{p}_a \cdot \vec{\sigma} \otimes \vec{q} \cdot \vec{\sigma}) + \\ &\frac{1}{M^2} a_7 (\vec{q} \cdot \vec{\sigma} \otimes \vec{p}_a \cdot \vec{\sigma}) + \frac{1}{M^2} a_8 (\vec{p}_a \cdot \vec{\sigma} \otimes \vec{p}_a \cdot \vec{\sigma}).\end{aligned}\quad (2.81)$$

Therefore

$$\hat{t} = \sum_{n=1}^8 b_n (\chi_n^{(1)} \otimes \chi_n^{(2)}) \quad (2.82)$$

where

$$\begin{aligned}b_1 &= a_1, & \chi_1^{(1)} &= I_2, & \chi_1^{(2)} &= I_2 \\ b_2 &= \frac{a_2}{M^4}, & \chi_2^{(1)} &= \vec{N} \cdot \vec{\sigma}, & \chi_2^{(2)} &= \vec{N} \cdot \vec{\sigma} \\ b_3 &= \frac{i}{M^2} a_3, & \chi_3^{(1)} &= \vec{N} \cdot \vec{\sigma}, & \chi_3^{(2)} &= I_2 \\ b_4 &= \frac{i}{M^2} a_4, & \chi_4^{(1)} &= I_2, & \chi_4^{(2)} &= \vec{N} \cdot \vec{\sigma} \\ b_5 &= \frac{1}{M^2} a_5, & \chi_5^{(1)} &= \vec{q} \cdot \vec{\sigma}, & \chi_5^{(2)} &= \vec{q} \cdot \vec{\sigma} \\ b_6 &= \frac{1}{M^2} a_6, & \chi_6^{(1)} &= \vec{p}_a \cdot \vec{\sigma}, & \chi_6^{(2)} &= \vec{p}_a \cdot \vec{\sigma} \\ b_7 &= \frac{1}{M^2} a_7, & \chi_7^{(1)} &= \vec{q} \cdot \vec{\sigma}, & \chi_7^{(2)} &= \vec{p}_a \cdot \vec{\sigma} \\ b_8 &= \frac{1}{M^2} a_8, & \chi_8^{(1)} &= \vec{p}_a \cdot \vec{\sigma}, & \chi_8^{(2)} &= \vec{q} \cdot \vec{\sigma}.\end{aligned}$$

Eq. (2.81) [or Eq. (2.82)] is the central result of this section. It is important to note that *no approximations were made in deriving the  $4 \times 4$  form of the effective  $t$ -matrix*. The effective amplitudes still contain all the information which comes from the relativistic analysis, i.e. from the solution of the Bethe-Salpeter equation. We next have to do the following:

1. Derive the transformation from the invariant amplitudes,  $F_n^{\{\rho\}}$  ( $n = 1 \dots 13$ ) to the effective amplitudes,  $a_n$  ( $n = 1 \dots 8$ ).
2. Derive expressions for the spin observables in terms of the effective amplitudes,  $a_n$ .

### 2.5.3 Transformation from the invariant amplitudes $F_n^{\{\rho\}}$ ( $n = 1 \dots 13$ ) to the effective amplitudes $a_n$ ( $n = 1 \dots 8$ )

Define the following quantities:

$$Y_1 = \text{Tr}[\hat{t}] \quad (2.83)$$

$$Y_2(\vec{a}, \vec{b}) = \text{Tr}[(\vec{a} \cdot \sigma \otimes \vec{b} \cdot \sigma) \hat{t}] \quad (2.84)$$

$$Y_3 = -i \text{Tr}[(\vec{N} \cdot \vec{\sigma} \otimes I_2) \hat{t}] \quad (2.85)$$

$$Y_4 = -i \text{Tr}[(I_2 \otimes \vec{N} \cdot \vec{\sigma}) \hat{t}]. \quad (2.86)$$

The next step is derive equations for the effective amplitudes in terms of the Y-functions defined above. Taking the trace of Eq. (2.81) yields

$$a_1 = \frac{1}{4} Y_1. \quad (2.87)$$

Multiply Eq. (2.81) with  $(\vec{N} \cdot \vec{\sigma} \otimes \vec{N} \cdot \vec{\sigma})$  and take the trace of the resulting equation. Since  $\vec{N} \cdot \vec{q} = \vec{N} \cdot \vec{p}_a = 0$  there will be no contribution from the last four terms of Eq. (2.81) and therefore

$$a_2 = \frac{M^4}{4\vec{N}^4} Y_2(\vec{N}, \vec{N}). \quad (2.88)$$

Similar arguments lead to

$$a_3 = \frac{M^2}{4\vec{N}^2} Y_3 \quad (2.89)$$

and

$$a_4 = \frac{M^2}{4\vec{N}^2} Y_4. \quad (2.90)$$

If we follow the same reasoning as above, we can also derive a set of four coupled equations relating the amplitudes  $a_5$ ,  $a_6$ ,  $a_7$  and  $a_8$ . A set of coupled equations arise since the vectors  $\vec{q}$  and  $\vec{p}_a$  are not orthogonal for quasielastic scattering, (i.e.  $\vec{q} \cdot \vec{p}_a \neq 0$ ). The solutions are:

$$a_5 = \frac{r_2^2 Y_2(\vec{p}_a, \vec{p}_a) - r_2 r_3 Y_2(\vec{p}_a, \vec{q}) - r_2 r_3 Y_2(\vec{q}, \vec{p}_a) + r_3^2 Y_2(\vec{q}, \vec{q})}{(r_1 r_3 - r_2^2)^2} \quad (2.91)$$

$$a_6 = \frac{r_1^2 Y_2(\vec{p}_a, \vec{p}_a) - r_1 r_2 Y_2(\vec{p}_a, \vec{q}) - r_1 r_2 Y_2(\vec{q}, \vec{p}_a) + r_2^2 Y_2(\vec{q}, \vec{q})}{(r_1 r_3 - r_2^2)^2} \quad (2.92)$$

$$a_7 = \frac{-r_1 r_2 Y_2(\vec{p}_a, \vec{p}_a) + r_2^2 Y_2(\vec{p}_a, \vec{q}) + r_1 r_3 Y_2(\vec{q}, \vec{p}_a) - r_2 r_3 Y_2(\vec{q}, \vec{q})}{(r_1 r_3 - r_2^2)^2} \quad (2.93)$$

$$a_8 = \frac{-r_1 r_2 Y_2(\vec{p}_a, \vec{p}_a) + r_1 r_3 Y_2(\vec{p}_a, \vec{q}) + r_2^2 Y_2(\vec{q}, \vec{p}_a) - r_2 r_3 Y_2(\vec{q}, \vec{q})}{(r_1 r_3 - r_2^2)^2} \quad (2.94)$$



where

$$\begin{aligned} r_1 &= \frac{2\vec{q}^2}{M}, \\ r_2 &= \frac{2\vec{p}_a \cdot \vec{q}}{M} \quad \text{and} \\ r_3 &= \frac{2\vec{p}_a^2}{M}. \end{aligned}$$

The next step is to derive an expression for the  $\hat{t}$ -matrix which can be used in the definition of the  $Y$ -functions. To this end substitution of Eq. (2.71) into Eq. (2.79) leads to

$$\begin{aligned} \hat{t} &= \sum_{\{\rho\}} \sum_{n=1}^{13} F_n^{\{\rho\}} (\bar{\Gamma}_{\rho'_1}(\vec{k}_1, M, M_1) \otimes \bar{\Gamma}_{\rho'_2}(\vec{k}_2, M, M_2)) K_n \\ &\quad (\Gamma_{\rho_1}(\vec{p}_1, M, M_1) \otimes \Gamma_{\rho_2}(\vec{p}_2, M, M_2)) \end{aligned} \quad (2.95)$$

where we have used Eq. (2.77) and introduced the  $\Gamma$ -matrices defined as:

$$\begin{aligned} \Gamma_\rho(\vec{p}, M, M^*) &= \Lambda_\rho(\vec{p}, M) u^+(\vec{p}, M^*) \\ &\equiv 4 \times 2 \quad \text{matrix.} \end{aligned} \quad (2.96)$$

In Eq. (2.96)  $M^*$  denotes an effective mass and Eq. (2.73) has been generalized to:

$$u^+(\vec{p}, M^*) = \begin{pmatrix} I_2 \phi(\vec{p}_1, M^*) \\ \vec{\sigma} \cdot \vec{p} \chi(\vec{p}, M^*) \end{pmatrix}. \quad (2.97)$$

Eq. (2.97) reduces to Eq. (2.73) if one sets

$$\begin{aligned} \phi(\vec{p}_1, M_1) &= N(\vec{p}_1, M_1) \\ &= \left( \frac{E^*(\vec{p}_1) + M_1}{2E^*(\vec{p}_1)} \right)^{\frac{1}{2}} \end{aligned} \quad (2.98)$$

where  $E^*(\vec{p}_1) = \sqrt{\vec{p}_1^2 + M_1^2}$  and

$$\chi(\vec{p}_1, M_1) = N(\vec{p}_1, M_1) (E^*(\vec{p}_1) + M_1)^{-1}. \quad (2.99)$$

We can obtain an explicit expression for  $\Gamma_\rho$  as follows: From Eq. (2.97) we can write

$$u^+(\vec{p}, M^*) = \begin{pmatrix} I_2 \phi(\vec{p}, M^*) \\ 0 \end{pmatrix} + \begin{pmatrix} 0 \\ \vec{\sigma} \cdot \vec{p} \chi(\vec{p}, M^*) \end{pmatrix}$$

and therefore

$$u^+(\vec{p}, M^*) = \phi(\vec{p}, M^*) (\hat{e}_1 \otimes I_2) + \chi(\vec{p}, M^*) (\hat{e}_2 \otimes \vec{\sigma} \cdot \vec{p}) \quad (2.100)$$

where

$$\hat{e}_1 = \begin{pmatrix} 1 \\ 0 \end{pmatrix} \quad \text{and} \quad \hat{e}_2 = \begin{pmatrix} 0 \\ 1 \end{pmatrix}$$

with  $\hat{e}_i^\dagger \hat{e}_j = \delta_{ij}$ . To write the  $\rho$ -spin projection operator in  $(2 \times 2) \otimes (2 \times 2)$  form we recall that

$$\gamma^0 = \begin{pmatrix} I_2 & 0 \\ 0 & -I_2 \end{pmatrix} = \sigma_3 \otimes I_2 \quad \text{and} \quad (2.101)$$

$$\vec{p} \cdot \vec{\gamma} = \begin{pmatrix} 0 & \vec{p} \cdot \vec{\sigma} \\ -\vec{p} \cdot \vec{\sigma} & 0 \end{pmatrix} = i\sigma_2 \otimes \vec{p} \cdot \vec{\sigma}. \quad (2.102)$$

Substitution of Eqs. (2.101) and (2.102) into Eq. (2.17) leads to

$$\Lambda_\rho(\vec{p}, M) = \frac{\rho E_p}{2M}(\sigma_3 \otimes I_2) - \frac{i\rho}{2M}(\sigma_2 \otimes \vec{p} \cdot \vec{\sigma}) + \frac{1}{2}(I_2 \otimes I_2). \quad (2.103)$$

Substitution of Eqs. (2.100) and (2.103) into Eq. (2.96) and using Eq. (2.77) together with the properties of the Pauli matrices allows one to write:

$$\Gamma_\rho(\vec{p}, M, M^*) = \sum_{i=1}^2 h_\rho^{(i)}(\vec{p}, M, M^*) (\hat{e}_i \otimes A_i(\vec{p})) \quad (2.104)$$

where

$$A_i(\vec{p}) = \begin{cases} I_2; & i = 1 \\ \vec{p} \cdot \vec{\sigma}; & i = 2 \end{cases} \quad (2.105)$$

with

$$h_\rho^{(1)}(\vec{p}, M, M^*) = \frac{\rho E_p}{2M} \phi(\vec{p}, M^*) - \frac{\rho \vec{p}^2}{2M} \chi(\vec{p}, M^*) + \frac{1}{2} \phi(\vec{p}, M^*) \quad \text{and} \quad (2.106)$$

$$h_\rho^{(2)}(\vec{p}, M, M^*) = \frac{\rho}{2M} \phi(\vec{p}, M^*) - \frac{\rho E_p}{2M} \chi(\vec{p}, M^*) + \frac{1}{2} \chi(\vec{p}, M^*). \quad (2.107)$$

Similar steps lead to

$$\bar{\Gamma}_\rho(\vec{p}, M, M^*) = \sum_{i=1}^2 j_\rho^{(i)}(\vec{p}, M, M^*) (\hat{e}_i^\dagger \otimes A_i(\vec{p})) \quad (2.108)$$

where

$$j_\rho^{(1)}(\vec{p}, M, M^*) = h_\rho^{(1)}(\vec{p}, M, M^*) \quad \text{and} \quad (2.109)$$

$$j_\rho^{(2)}(\vec{p}, M, M^*) = -h_\rho^{(2)}(\vec{p}, M, M^*). \quad (2.110)$$

To calculate the effective amplitudes the contribution of each covariant to the  $Y$ -functions must be determined. This is done using Eq. (2.95) as well as Eqs. (2.83) to (2.86). These equations are then employed in Eqs. (2.87) to (2.94) to determine the effective amplitudes. This procedure requires the calculation of traces of a set of matrices,  $t_i$ , where  $i = 1 \dots 46$ . With each covariant is associated a set of  $t$ -matrices of which the trace must be taken. They are listed in Appendix B.  $t$ -matrices for covariants  $K_6$  to  $K_9$  need not be specified since we can use those already defined for the  $SPVAT$  covariants.

To illustrate how the  $t$ -matrices arise we calculate the contribution of the scalar covariant to each of the  $Y$ -functions. Substitution of  $K_1 = S = I_4 \otimes I_4$  into Eq. (2.95) and use of Eq. (2.77) leads to

$$\hat{t} = \sum_{\{\rho\}} F_1^{\{\rho\}} [\bar{\Gamma}_{\rho_1}'(\vec{k}_1, M, M_1) \Gamma_{\rho_1}(\vec{p}_1, M, M_1)] \otimes [\bar{\Gamma}_{\rho_2}'(\vec{k}_2, M, M_2) \Gamma_{\rho_2}(\vec{p}_2, M, M_2)]. \quad (2.111)$$

The matrix

$$[\bar{\Gamma}_{\rho_i}'(\vec{k}_i, M, M_i) \Gamma_{\rho_i}(\vec{p}_i, M, M_i)] \quad \text{for} \quad i = 1, 2$$

is the  $t$ -matrix,  $t_i$ , associated with the scalar covariant (see Table B.1). Therefore

$$\begin{aligned} Y_1 &= \text{Tr}(\hat{t}) \\ &= \sum_{\{\rho\}} F_1^{\{\rho\}} \text{Tr}(\bar{\Gamma}_{\rho_1}'(\vec{k}_1, M, M_1) \Gamma_{\rho_1}(\vec{p}_1, M, M_1)) \text{Tr}(\bar{\Gamma}_{\rho_2}'(\vec{k}_2, M, M_2) \Gamma_{\rho_2}(\vec{p}_2, M, M_2)). \end{aligned}$$

Use of Eqs. (2.104) and (2.108) shows that

$$\bar{\Gamma}_{\rho_i}'(\vec{k}_i, M, M_i) \Gamma_{\rho_i}(\vec{p}_i, M, M_i) = \sum_{r=1}^2 j_{\rho_i}^{(r)}(\vec{k}_i, M, M_i) h_{\rho_i}^{(r)}(\vec{p}_i, M, M_i) A_r(\vec{k}_i) A_r(\vec{p}_i)$$

for  $i = 1, 2$  and therefore [using Eq. (2.105)] it follows that

$$\begin{aligned} \text{Tr}(\bar{\Gamma}_{\rho_i}'(\vec{k}_i, M, M_i) \Gamma_{\rho_i}(\vec{p}_i, M, M_i)) &= 2j_{\rho_i}^{(1)}(\vec{k}_i, M, M_i) h_{\rho_i}^{(1)}(\vec{p}_i, M, M_i) + \\ &2j_{\rho_i}^{(2)}(\vec{k}_i, M, M_i) h_{\rho_i}^{(2)}(\vec{p}_i, M, M_i) \vec{p}_i \cdot \vec{k}_i \end{aligned}$$

for  $i = 1, 2$ . The contribution of the scalar covariant to  $Y_1$  is therefore

$$\begin{aligned} Y_1 &= 4 \sum_{\{\rho\}} F_1^{\{\rho\}} [j_{\rho_1}^{(1)}(\vec{k}_1, M, M_1) h_{\rho_1}^{(1)}(\vec{p}_1, M, M_1) + \\ &j_{\rho_1}^{(2)}(\vec{k}_1, M, M_1) h_{\rho_1}^{(2)}(\vec{p}_1, M, M_1) \vec{p}_1 \cdot \vec{k}_1] [j_{\rho_2}^{(1)}(\vec{k}_2, M, M_2) h_{\rho_2}^{(1)}(\vec{p}_2, M, M_2) + \\ &j_{\rho_2}^{(2)}(\vec{k}_2, M, M_2) h_{\rho_2}^{(2)}(\vec{p}_2, M, M_2) \vec{p}_2 \cdot \vec{k}_2]. \end{aligned} \quad (2.112)$$

Similarly we have that

$$\begin{aligned} Y(\vec{a}, \vec{b}) &= \text{Tr}[(\vec{a} \cdot \sigma \otimes \vec{b} \cdot \sigma) \hat{t}] \\ &= \sum_{\{\rho\}} F_1^{\{\rho\}} \{a_i b_j \text{Tr}[\sigma_i \bar{\Gamma}_{\rho_1}'(\vec{k}_1, M, M_1) \Gamma_{\rho_1}(\vec{p}_1, M, M_1)] \\ &\quad \text{Tr}[\sigma_j \bar{\Gamma}_{\rho_2}'(\vec{k}_2, M, M_2) \Gamma_{\rho_2}(\vec{p}_2, M, M_2)]\} \end{aligned}$$

where we have used Eq. (2.111) and where summation over the repeated indices,  $i$  and  $j$ , are implied. The matrix

$$[\sigma_i \bar{\Gamma}_{\rho_i}'(\vec{k}_i, M, M_i) \Gamma_{\rho_i}(\vec{p}_i, M, M_i)] \quad \text{for} \quad i = 1, 2$$



is the  $t$ -matrix,  $t_2$ , associated with the scalar covariant (see Table B.1). Using Eqs. (2.104), (2.108) and (2.105) it follows that

$$\text{Tr}(\sigma_i \bar{\Gamma}_{\rho'_l}(\vec{k}_l, M, M_l) \Gamma_{\rho_l}(\vec{p}_l, M, M_l)) = 2i(\vec{k}_l \times \vec{p}_l)_i j_{\rho'_l}^{(2)}(\vec{k}_l, M, M_l) h_{\rho_l}^{(2)}(\vec{p}_l, M, M_l)$$

for  $l = 1, 2$  and therefore

$$Y(\vec{a}, \vec{b}) = -4 \sum_{\{\rho\}} F_1^{\{\rho\}} [2i \vec{a} \cdot (\vec{k}_1 \times \vec{p}_1) j_{\rho'_1}^{(2)}(\vec{k}_1, M, M_1) h_{\rho_1}^{(2)}(\vec{p}_1, M, M_1) + 2i \vec{b} \cdot (\vec{k}_2 \times \vec{p}_2) j_{\rho'_2}^{(2)}(\vec{k}_2, M, M_2) h_{\rho_2}^{(2)}(\vec{p}_2, M, M_2)]. \quad (2.113)$$

Similarly it follows that

$$Y_3 = 4 \sum_{\{\rho\}} F_1^{\{\rho\}} [\vec{N} \cdot (\vec{k}_1 \times \vec{p}_1)] [j_{\rho'_2}^{(1)}(\vec{k}_2, M, M_2) h_{\rho_2}^{(1)}(\vec{p}_2, M, M_2) + j_{\rho'_2}^{(2)}(\vec{k}_2, M, M_2) h_{\rho_2}^{(2)}(\vec{p}_2, M, M_2) \vec{p}_2 \cdot \vec{k}_2] \quad (2.114)$$

and

$$Y_4 = 4 \sum_{\{\rho\}} F_1^{\{\rho\}} [\vec{N} \cdot (\vec{k}_2 \times \vec{p}_2)] [j_{\rho'_1}^{(1)}(\vec{k}_1, M, M_1) h_{\rho_1}^{(1)}(\vec{p}_1, M, M_1) + j_{\rho'_1}^{(2)}(\vec{k}_1, M, M_1) h_{\rho_1}^{(2)}(\vec{p}_1, M, M_1) \vec{p}_1 \cdot \vec{k}_1]. \quad (2.115)$$

Eqs. (2.112), (2.113), (2.114) and (2.115) can now be substituted into Eqs. (2.87) to (2.94) to determine the contribution of the scalar covariant to each effective amplitude. The other covariants are handled in a similar manner, but as they increase in complexity it becomes impractical to do the trace algebra by hand and therefore a program was written in the MATHEMATICA programming language [Wo88] to do the required trace algebra. The resulting expressions are very long and complicated and therefore we discuss in Section 3.2 various numerical checks that have been performed in order to ensure that the effective amplitudes are correctly implemented numerically.

Since the effective amplitudes are linear functions of  $F_n^{\{\rho\}}$ , i.e.

$$a_i = a_i(\{F_n^{\{\rho\}}\}) \quad \forall i = 1 \dots 8 \quad (2.116)$$

the isospin zero (isospin one) effective amplitudes are obtained by substituting the isospin zero (isospin one) invariant amplitudes into Eq. (2.116).

#### 2.5.4 Expressions for spin observables in terms of effective amplitudes, $a_n$

In this section we derive expressions for the unpolarized double differential cross section, the analyzing power and the polarization transfer observables in terms of the effective amplitudes,  $a_n$  for quasielastic  $(\vec{p}, \vec{p}')$  and  $(\vec{p}, \vec{n})$  scattering.

The kinematic quantities in the NN laboratory frame are depicted in Fig. 2.8 (which is identical to Fig. 2.2).

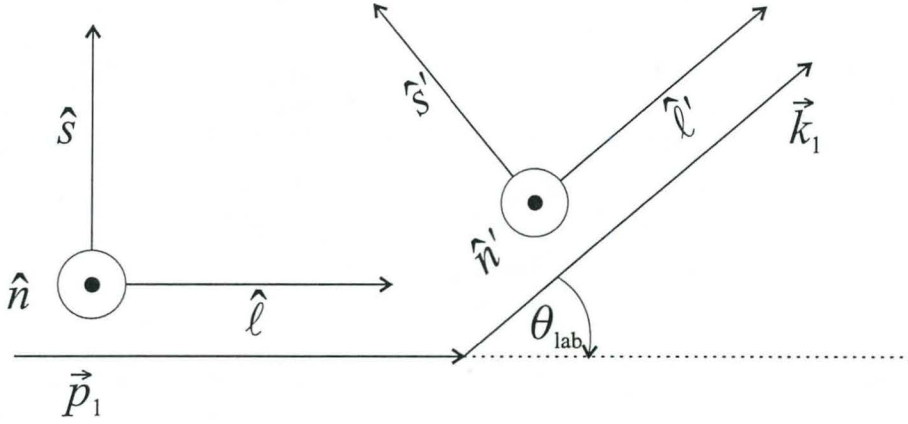


Figure 2.8: *Laboratory kinematics for the scattering process of Fig. 2.4.*

### 1. Unpolarized double differential cross section.

For the scattering process in Fig. 2.4 we can write down the expression for the differential cross section,  $d\sigma$  [Bj64]:

$$d\sigma = \frac{1}{|\vec{v}_1 - \vec{v}_2|} \left( \frac{M_1 M_2}{E_1^* E_2^*} \right) \left( \frac{M_1 M_2}{E_1'^* E_2'^*} \right) (2\pi)^4 \delta(p_1^* + p_2^* - k_1^* - k_2^*) \quad (2.117)$$

$$\frac{d^3 \vec{k}_1}{(2\pi)^3} \frac{d^3 \vec{k}_2}{(2\pi)^3} |\mathcal{M}|^2.$$

In this equation  $M_1$  and  $M_2$  refer to the effective masses of the external nucleons (see Section 2.3). The four-momenta  $p_1^*$ ,  $p_2^*$ ,  $k_1^*$  and  $k_2^*$  are defined in Eq. 2.3. As we consider the quasielastic scattering at energies much higher than the interaction energies amongst the target nucleons, we assume the latter to be practically non-interacting. Therefore, the momentum distribution of these nucleons can be obtained in a Fermi gas model. Following the same arguments as in Ref. [Ho88] allows one to write down the following expression for the *double differential cross section*:

$$\frac{d\sigma}{d\Omega_1 dE_1'} = \frac{|\vec{k}_1| E_1'}{|\vec{q}| E_1'^*} \int_{p_{min}}^{k_f} d|\vec{p}_2| d\phi |\vec{p}_2| f(p_1^*, p_2^*, k_f) |\mathcal{M}|^2$$

where  $k_f$  is the Fermi momentum,

$$f(p_1^*, p_2^*, k_f) = \frac{3}{16\pi^3 k_f^3} \frac{M_1^2 M_2^2}{[(p_1^* \cdot p_2^* - M_1^2 M_2^2)^2]^{\frac{1}{2}}} \quad (2.118)$$

and

$$p_{min} = \left| \frac{q}{2} - \frac{\omega^*}{2} \left[ 1 - \frac{4M_2^2}{q_\mu q^\mu} \right]^{\frac{1}{2}} \right|. \quad (2.119)$$

In Eq. (2.119),  $q^\mu$  is the four-momentum transfer  $q^\mu = (\omega^*, \vec{q})$  where

$$\omega^* = E_1^* - E_1'^* = E_2'^* - E_2 \quad \text{and} \quad \vec{q} = \vec{p}_1 - \vec{k}_1 = \vec{k}_2 - \vec{p}_2.$$

Define the function

$$\Gamma''(\vec{p}_1, \vec{p}_2, \vec{k}_1, \vec{k}_2) = \sum_{s_i, s_f} \sum_{s_2, s_2'} |\mathcal{M}|^2. \quad (2.120)$$

Substitution of Eq. (2.82) into Eq. (2.80) leads to

$$\mathcal{M} = g_1 \sum_{n=1}^8 b_n [\phi^\dagger(s_f) \chi_n^{(1)} \phi(s_i)] [\phi^\dagger(s_2') \chi_n^{(2)} \phi(s_2)]$$

and therefore one can write

$$\Gamma''(\vec{p}_1, \vec{p}_2, \vec{k}_1, \vec{k}_2) = g_1^2 \sum_{m,n=1}^8 b_m^* b_n \text{Tr}[\chi_n^{(1)} \chi_m^{(1)}] \text{Tr}[\chi_n^{(2)} \chi_m^{(2)}]. \quad (2.121)$$

An explicit expression for  $\Gamma''(\vec{p}_1, \vec{p}_2, \vec{k}_1, \vec{k}_2)$  is given in Appendix C. To obtain the unpolarized cross section, one sums over the initial spins and averages over the final spins, which leads to:

$$\left( \frac{d\sigma}{d\Omega_1' dE_1'} \right)_{\text{unpol}} = \frac{|\vec{k}_1| E_1'}{4|\vec{q}| E_1'^*} \int_{p_{\min}}^{k_f} d|\vec{p}_2| d\phi |\vec{p}_2| f(p_1^*, p_2^*, k_f) \times \Gamma''(\vec{p}_1, \dots, \vec{k}_2). \quad (2.122)$$

Eq. 2.122 is defined to yield zero when  $|\vec{k}_1| \leq k_F$  or  $|\vec{k}_2| \leq k_F$ . This effect is called Pauli blocking. For  $(\vec{p}, \vec{p}')$  scattering

$$\left( \frac{d\sigma}{d\Omega_1' dE_1'} \right)_{\text{unpol}}^{(p,p')} = \frac{|\vec{k}_1| E_1'}{4|\vec{q}| E_1'^*} \int_{p_{\min}}^{k_f} d|\vec{p}_2| d\phi |\vec{p}_2| f(p_1^*, p_2^*, k_f) \times (Z_{eff} \Gamma''(\vec{p}_1, \dots, \vec{k}_2, \{b_i(I=1)\}) + N_{eff} \Gamma''(\vec{p}_1, \dots, \vec{k}_2, \{b_i^{ave}\}))$$

where

$$b_i^{ave} = \frac{1}{2}(b_i(I=0) + b_i(I=1)).$$

For the  $(\vec{p}, \vec{n})$  charge-exchange reaction

$$\left( \frac{d\sigma}{d\Omega_1' dE_1'} \right)_{\text{unpol}}^{(p,n)} = \frac{|\vec{k}_1| E_1'}{4|\vec{q}| E_1'^*} \int_{p_{\min}}^{k_f} d|\vec{p}_2| d\phi |\vec{p}_2| f(p_1^*, p_2^*, k_f) \times N_{eff} \Gamma''(\vec{p}_1, \dots, \vec{k}_2, \{b_i^{ch-ex}\})$$

where the charge-exchange amplitudes are defined as:

$$b_i^{ch-ex} = \frac{1}{2}[b_i(I=1) - b_i(I=0)].$$

For employing these expressions one needs the following quantities:



- (a) The Fermi momentum  $k_f = \left[ \frac{3}{2} \pi \langle \rho \rangle \right]^{\frac{1}{3}}$ , where the average nuclear density  $\langle \rho \rangle$  can be calculated, spatially weighted for this reaction, in an eikonal approximation of the incoming beam. More refined values of  $k_f$  for specific target nuclei can be found in Table II of Ref. [Hi94].
- (b) The effective number of participating protons and neutrons  $Z_{eff}$  and  $N_{eff}$ , also follow from the  $\langle \rho \rangle$ -value and the nuclear  $\frac{Z}{N}$  ratio.

## 2. Analyzing power

The definition of the analyzing power is given in terms of polarized double differential cross sections as [Ho88]:

$$A_y = \frac{\frac{d\sigma}{d\Omega'_1 dE'_1}(\hat{s}_f = +\hat{n}) - \frac{d\sigma}{d\Omega'_1 dE'_1}(\hat{s}_f = -\hat{n})}{\frac{d\sigma}{d\Omega'_1 dE'_1}(\hat{s}_f = +\hat{n}) + \frac{d\sigma}{d\Omega'_1 dE'_1}(\hat{s}_f = -\hat{n})} \quad (2.123)$$

where, for example,

$$\frac{d\sigma}{d\Omega'_1 dE'_1}(\hat{s}_f) = \frac{|\vec{k}_1| E'_1}{|\vec{q}| E_1^*} \int_{p_{min}}^{k_f} d|\vec{p}_2| d\phi |\vec{p}_2| f(p_1^*, p_2^*, k_f) \frac{1}{2} \tilde{\Gamma}'(\hat{s}_f)$$

is averaged over incident spin directions  $\hat{s}_i$ , and the target particles' initial and final spin as contained in the factor:

$$\begin{aligned} \tilde{\Gamma}'(\vec{p}_1, \dots, \vec{k}_2, \hat{s}_f) &= \sum_{s_i, s_2, s'_2} |\mathcal{M}|^2 \\ &= \text{Tr}[\chi_m^{(1)} \hat{P}(\hat{s}_f) \chi_n^{(1)}] \text{Tr}[\chi_m^{(2)} \chi_n^{(2)}] \end{aligned} \quad (2.124)$$

where use was made of Eqs. (2.10) and (2.11). A calculation of the traces in Eq. (2.124) shows that  $\tilde{\Gamma}'(\vec{p}_1, \dots, \hat{s}_f)$  has the following structure:

$$\begin{aligned} \tilde{\Gamma}'(\vec{p}_1, \dots, \hat{s}_f) &= f_1(\vec{p}_1, \dots, \vec{k}_2) + f_2(\vec{p}_1, \dots, \vec{k}_2) \vec{N} \cdot \hat{s}_f + \\ &f_3(\vec{p}_1, \dots, \vec{k}_2) \vec{p}_a \cdot (\vec{q} \times \hat{s}_f). \end{aligned} \quad (2.125)$$

Defining the combination function

$$\Gamma'(\vec{p}_1, \dots, \vec{k}_2, \hat{s}_f) = \tilde{\Gamma}'(\vec{p}_1, \dots, \vec{k}_2, \hat{s}_f) - \tilde{\Gamma}'(\vec{p}_1, \dots, \vec{k}_2, -\hat{s}_f) \quad (2.126)$$

and using Eq. (2.125) in Eq. (2.126) yields

$$\Gamma'(\hat{s}_f) = 2(f_2(\vec{p}_1, \dots, \vec{k}_2) \vec{N} \cdot \hat{s}_f + f_3(\vec{p}_1, \dots, \vec{k}_2) \vec{p}_a \cdot (\vec{q} \times \hat{s}_f)).$$

The explicit forms of the functions  $f_2$  and  $f_3$  can be inferred from Eq. (C.2) in Appendix C. If  $\hat{s}_f = \hat{n}$  then

$$\vec{N} \cdot \hat{n} = p_1 k_1 \sin \theta_L$$

and

$$\vec{p}_a \cdot (\vec{q} \times \hat{n}) = -p_1 k_1 \sin \theta_L.$$

The analyzing power (which is equal to the polarization in the RPWIA model) for the  $(\vec{p}, \vec{p}')$  reaction is given by

$$A_y(\vec{p}, \vec{p}') = \frac{\int_{p_{min}}^{k_f} d|\vec{p}_2| d\phi |\vec{p}_2| f(p_1^*, \dots, p_2^*, k_f) (Z_{eff} \Gamma'(\hat{n}, \{b_i(I=1)\}) + N_{eff} \Gamma'(\hat{n}, \{b_i^{ave}\}))}{\int_{p_{min}}^{k_f} d|\vec{p}_2| d\phi |\vec{p}_2| f(k_f) (Z_{eff} \Gamma''(\{b_i(I=1)\}) + N_{eff} \Gamma''(\{b_i^{ave}\}))}$$

and the analyzing power (which is equal to the polarization in the RPWIA model) for the  $(\vec{p}, \vec{n})$  reaction is given by

$$A_y(\vec{p}, \vec{n}) = \frac{\int_{p_{min}}^{k_f} d|\vec{p}_2| d\phi |\vec{p}_2| f(k_f) \Gamma'(\hat{n}, \{b_i^{ch-ex}\})}{\int_{p_{min}}^{k_f} d|\vec{p}_2| d\phi |\vec{p}_2| f(k_f) \Gamma''(\{b_i^{ch-ex}\})}. \quad (2.127)$$

Since a  $(\vec{p}, \vec{n})$  reaction implies that the incident proton could only have scattered off a neutron, we set  $Z_{eff} = 0$ . Now  $N_{eff}$  cancels between the numerator and denominator (both being cross sections) rendering  $A_y(\vec{p}, \vec{n})$  independent of  $N_{eff}$ .

### 3. Polarization transfer observables

The polarization transfer observables are defined in terms of linear combinations of polarized double differential cross sections as follows [Ho88]:

$$D_{ij} = \frac{\frac{d\sigma}{d\Omega_1 dE_1'}(\hat{s}_i, \hat{s}_f) - \frac{d\sigma}{d\Omega_1 dE_1'}(-\hat{s}_i, \hat{s}_f) - \frac{d\sigma}{d\Omega_1 dE_1'}(\hat{s}_i, -\hat{s}_f) + \frac{d\sigma}{d\Omega_1 dE_1'}(-\hat{s}_i, -\hat{s}_f)}{\frac{d\sigma}{d\Omega_1 dE_1'}(\hat{s}_i, \hat{s}_f) + \frac{d\sigma}{d\Omega_1 dE_1'}(-\hat{s}_i, \hat{s}_f) + \frac{d\sigma}{d\Omega_1 dE_1'}(\hat{s}_i, -\hat{s}_f) + \frac{d\sigma}{d\Omega_1 dE_1'}(-\hat{s}_i, -\hat{s}_f)}. \quad (2.128)$$

In Eq. (2.128) a typical polarized double differential cross section is:

$$\frac{d\sigma}{d\Omega_1 dE_1'}(\hat{s}_i, \hat{s}_f) = \frac{|\vec{k}_1| E_1'}{|\vec{q}| E_1^*} \int_{p_{min}}^{k_f} d|\vec{p}_2| d\phi |\vec{p}_2| f(p_1^*, p_2^*, k_f) \frac{1}{2} \tilde{\Gamma}(\hat{s}_i, \hat{s}_f) \quad (2.129)$$

where

$$\begin{aligned} \tilde{\Gamma}(\vec{p}_1, \dots, \vec{k}_2, \hat{s}_i, \hat{s}_f) &= \sum_{s_2, s_2'} |\mathcal{M}|^2 \\ &= g_1^2 \sum_{m,n=1}^8 b_m^* b_n [\text{Tr}(\hat{P}(\hat{s}_i) \chi_m^{(1)} \hat{P}(\hat{s}_f) \chi_n^{(1)})][\text{Tr}(\chi_m^{(2)} \chi_n^{(2)})] \\ &= f_1(\vec{p}_1, \dots, \vec{k}_2) + \vec{A}_1 \cdot \hat{s}_i + \vec{A}_2 \cdot \hat{s}_f + \\ &\quad (\hat{s}_i \cdot \vec{A}_3)(\hat{s}_f \cdot \vec{A}_4) + (\hat{s}_i \cdot \hat{s}_f)(\vec{A}_6 \cdot \vec{A}_7) + \hat{s}_i \cdot (\hat{s}_f \times \vec{A}_5) \end{aligned}$$

with  $\vec{A}_i$  functions of only the three-momenta, (i.e.  $\vec{p}_1$ ,  $\vec{p}_2$ ,  $\vec{k}_1$  and  $\vec{k}_2$ ) of which the explicit form can be inferred from Eq. (C.1). Define again, now dictated by the form of Eq. (2.128), a function:

$$\begin{aligned} \Gamma(\vec{p}_1, \dots, \vec{k}_2, \hat{s}_i, \hat{s}_f) &= \tilde{\Gamma}(\hat{s}_i, \hat{s}_f) - \tilde{\Gamma}(-\hat{s}_i, \hat{s}_f) - \tilde{\Gamma}(\hat{s}_i, -\hat{s}_f) + \\ &\quad \tilde{\Gamma}(-\hat{s}_i, -\hat{s}_f). \\ &= 4[(\hat{s}_i \cdot \vec{A}_3)(\hat{s}_f \cdot \vec{A}_4) + \hat{s}_i \cdot (\hat{s}_f \times \vec{A}_5) + \\ &\quad (\hat{s}_i \cdot \hat{s}_f)(\vec{A}_6 \cdot \vec{A}_7)]. \end{aligned} \quad (2.130)$$

Table 2.7: Values of kinematical quantities containing  $\hat{s}_i$  and/or  $\hat{s}_f$  for each non-zero polarization transfer observable.

kinematical quantity	$D_{\ell\ell}$	$D_{s's}$	$D_{nn}$	$D_{s'l}$	$D_{V_s}$
$\vec{q} \cdot \hat{s}_i$	$p_1 - k_1 \cos \theta$	$-k_1 \sin \theta$	0	$p_1 - k_1 \cos \theta$	$-k_1 \sin \theta$
$\vec{q} \cdot \hat{s}_f$	$p_1 \cos \theta - k_1$	$-p_1 \sin \theta$	0	$-p_1 \sin \theta$	$p_1 \cos \theta - k_1$
$\vec{p}_a \cdot \hat{s}_i$	$\frac{1}{2}(p_1 + k_1 \cos \theta)$	$\frac{1}{2}k_1 \sin \theta$	0	$\frac{1}{2}(p_1 + k_1 \cos \theta)$	$\frac{1}{2}k_1 \sin \theta$
$\vec{p}_a \cdot \hat{s}_f$	$\frac{1}{2}(p_1 \cos \theta + k_1)$	$-\frac{1}{2}p_1 \sin \theta$	0	$-\frac{1}{2}p_1 \sin \theta$	$\frac{1}{2}(p_1 \cos \theta + k_1)$
$\vec{N} \cdot \hat{s}_i$	0	0	$p_1 k_1 \sin \theta$	0	0
$\vec{N} \cdot \hat{s}_f$	0	0	$p_1 k_1 \sin \theta$	0	0
$\hat{s}_i \cdot \hat{s}_f$	$\cos \theta$	$\cos \theta$	1	$-\sin \theta$	$\sin \theta$
$\vec{N} \cdot (\hat{s}_i \times \hat{s}_f)$	$p_1 k_1 \sin^2 \theta$	$p_1 k_1 \sin^2 \theta$	0	$p_1 k_1 \cos \theta \sin \theta$	$-p_1 k_1 \cos \theta \sin \theta$

The explicit expression for  $\Gamma$  contains various kinematic parameters which are presented in the first column of Table 2.7. The other columns contain the values of these quantities, in the laboratory frame, for each spin transfer coefficient.  $\theta$  refers to the laboratory scattering angle,  $p_1 = |\vec{p}_1|$  and  $k_1 = |\vec{k}_1|$ . Use of Eqs. (2.129), (2.130) and (2.122) leads to

$$D_{i'j} = \frac{\int_{p_{\min}}^{k_f} d|\vec{p}_2| d\phi |\vec{p}_2| f(p_1^*, p_2^*, k_f) 4\Gamma(\hat{s}_i, \hat{s}_f)}{\int_{p_{\min}}^{k_f} d|\vec{p}_2| d\phi |\vec{p}_2| f(p_1^*, p_2^*, k_f) \Gamma''(\vec{p}_1, \dots, \vec{k}_2)}. \quad (2.131)$$

The polarization transfer observables for the  $(\vec{p}, \vec{p}')$  reaction are given by

$$D_{i'j}[(\vec{p}, \vec{p}')] = \frac{\int_{p_{\min}}^{k_f} d|\vec{p}_2| d\phi |\vec{p}_2| f(k_f) (4Z_{eff}\Gamma(\hat{s}_i, \hat{s}_f, \{b_i(I=1)\}) + 4N_{eff}\Gamma(\hat{s}_i, \hat{s}_f, \{b_i^{ave}\}))}{\int_{p_{\min}}^{k_f} d|\vec{p}_2| d\phi |\vec{p}_2| f(k_f) (Z_{eff}\Gamma''(\{b_i(I=1)\}) + N_{eff}\Gamma''(\{b_i^{ave}\}))}$$

and the corresponding observables for the  $(\vec{p}, \vec{n})$  reaction are given by

$$D_{i'j}[(\vec{p}, \vec{n})] = \frac{\int_{p_{\min}}^{k_f} d|\vec{p}_2| d\phi |\vec{p}_2| f(k_f) 4\Gamma(\hat{s}_i, \hat{s}_f, \{b_i^{ch-ex}\})}{\int_{p_{\min}}^{k_f} d|\vec{p}_2| d\phi |\vec{p}_2| f(k_f) \Gamma''(\{b_i^{ch-ex}\})}. \quad (2.132)$$

Once again, as in Eq. (2.127), the effective number of neutrons does not appear in Eq. (2.132).



## 2.6 Summary

We have presented a formalism to calculate polarization transfer observables for quasielastic proton-nucleus scattering using a general Lorentz invariant representation of the nucleon-nucleon scattering matrix. In this way we avoid the ambiguities which are inherent in the previously-used five-term representation (the *SPVAT* form) of  $\hat{F}$ . In the process we have derived an effective t-matrix which is a  $4 \times 4$  matrix (and therefore more familiar to Nuclear Physics) but which still contains all the information coming from the relativistic analysis. This necessitates the transformation from the 44 invariant amplitudes to a set of eight effective amplitudes as well as the derivation of new expressions for the spin observables in terms of the effective amplitudes. By staying within the framework of the RPWIA (with its many simplifying features)<sup>2</sup> and using a general Lorentz invariant representation of  $\hat{F}$ , allows one to do an unambiguous investigation of effective-mass-type medium effects via quasielastic proton-nucleus scattering. In the next chapter numerical results for the spin observables based on the formalism developed in this chapter will be presented.

---

<sup>2</sup>all of which are motivated by experimental data on the spin observables

## Chapter 3

# IA2 predictions of quasielastic spin observables

### 3.1 Introduction

In this chapter we present the numerical results for the quasielastic spin observables employing a general Lorentz invariant representation of the NN scattering matrix within the framework of the RPWIA (we will refer to this as the RPWIA2 formalism). Our aim is to perform a systematic study of the predictive power of RPWIA2 for complete sets of spin observables for both quasielastic  $(\vec{p}, \vec{p}')$  and  $(\vec{p}, \vec{n})$  scattering.

Recall (see Section 2.4) that, despite a number of significant improvements on the original RPWIA model (such as the inclusion of more refined effective masses and a more rigorous treatment of the  $\pi$ NN vertex), its predictions could still not consistently describe both quasielastic  $(\vec{p}, \vec{p}')$  and  $(\vec{p}, \vec{n})$  spin observables. The latter shortcoming is one of the main reasons for developing the RPWIA2 model discussed in Chapter 2. Some of the questions we hope to address in this chapter are the following:

1. How successful is the effective mass concept in describing quasielastic  $(\vec{p}, \vec{p}')$  and  $(\vec{p}, \vec{n})$  scattering data ?
2. Is it possible to find *a combination of effective projectile and target nucleon masses*<sup>1</sup>  $(\frac{M_1}{M}, \frac{M_2}{M})$  which can describe a *complete set of spin observables*  $\{A_y, D_{ij}\}$  for  $(\vec{p}, \vec{p}')$  and  $(\vec{p}, \vec{n})$  scattering ? Will this set be the same for the two types of reactions ?
3. How do numerical results based on the IA1 representation of  $\hat{F}$  compare to those utilising the IA2 representation of  $\hat{F}$  ?

We attempt to address the first two questions in Sections 3.4.1 and 3.4.2, where we introduce the idea of an effective mass band and the concept of an optimal effective mass. Table 3.1 lists all the reactions for which calculations are done in this survey. Complete sets of spin observable data exist for all the energies and targets used, except  $^{40}\text{Ca}(\vec{p}, \vec{n})$  at  $T_{lab} = 495$  MeV for which no analyzing power data is available and  $^{40}\text{Ca}(\vec{p}, \vec{p}')$  at  $T_{lab} = 200$  MeV for which only  $A_y$  and  $D_{nn}$  data are available. The reaction  $^{40}\text{Ca}(\vec{p}, \vec{n})$  at  $T_{lab} = 495$  MeV is included since data exist at two different laboratory angles and furthermore it is complementary to the reaction  $^{40}\text{Ca}(\vec{p}, \vec{p}')$  at  $T_{lab} = 500$  MeV. The  $(\vec{p}, \vec{p}')$  data at  $T_{lab} = 200$  MeV are complementary to the  $(\vec{p}, \vec{n})$  data at

---

<sup>1</sup>this of course includes the possibility:  $M_1 = M_2 = M$

$T_{lab} = 200$  MeV and are therefore also included. In Section 3.6 we compare predictions

Table 3.1: *Experimental data for which calculations were done at the quasielastic peak (as a function of laboratory scattering angle) and as a function of energy transfer.*

Reaction	$T_{lab}$ (MeV)	$\theta_{lab}$ (degrees)	Reference
$^{40}\text{Ca}(\vec{p}, \vec{p}')$	500	19	[Ca84]
$^{12}\text{C}(\vec{p}, \vec{p}')$	420	24	[Ch90]
$^{12}\text{C}(\vec{p}, \vec{p}')$	290	30	[Ch90]
$^{54}\text{Fe}(\vec{p}, \vec{p}')$	290	20	[Hä88]
$^{40}\text{Ca}(\vec{p}, \vec{p}')$	200	30	[Ca95]
$^{40}\text{Ca}(\vec{p}, \vec{n})$	495	18, 27	[Ta98]
$^{40}\text{Ca}(\vec{p}, \vec{n})$	200	24,37,48	[Ha98]
$^{208}\text{Pb}(\vec{p}, \vec{n})$	200	24,37,48	[Ha98]

of the RPWIA2 formalism with spin observable data as a function of energy transfer,  $\omega$ . Before proceeding, we first discuss the various numerical checks that were performed on the RPWIA2 formalism developed in Chapter 2.

## 3.2 Numerical Checks

This section discusses the numerical checks that were performed to ensure that the transformation from invariant amplitudes,  $F_n^{\{\rho\}}$  ( $n = 1, \dots, 13$ ) [Eq. 2.71] to effective amplitudes,  $a_i$  ( $i = 1, \dots, 8$ ) [Eq. 2.81] done in Section 2.5.3 have been carried out correctly.

The IA1 representation of  $\hat{F}$  is given by [Ho86, Ho88]:

$$\hat{F}_{IA1} = \sum_{n=1}^5 F_n^{IA1} (\lambda^n \otimes \lambda_n) \quad (3.1)$$

where

$$\lambda^n \in \{S, P, V, A, T\}$$

and the IA2 representation of  $\hat{F}$  [see Eq. (2.71)] is given by

$$\hat{F} = \sum_{\rho_1 \rho'_1; \rho_2 \rho'_2} \sum_{n=1}^{13} F_n^{\rho_1 \rho'_1 \rho_2 \rho'_2} [\Lambda_{\rho'_1}(\vec{k}_1; M) \otimes \Lambda_{\rho'_2}(\vec{k}_2; M)] K_n [\Lambda_{\rho_1}(\vec{p}_1; M) \otimes \Lambda_{\rho_2}(\vec{p}_2; M)]. \quad (3.2)$$



Substitution of Eq (3.1) into Eq. (2.1) yields [using Eq. (2.120)]

$$\Gamma''_{IA1}(\vec{p}_1, \vec{p}_2, \vec{k}_1, \vec{k}_2) = \sum_{n,n'=1}^5 (F_n^{IA1})^* (F_{n'}^{IA1}) \text{Tr} \left[ \left( \frac{\vec{k}_1 + M_1}{2M_1} \right) \lambda^n \left( \frac{\vec{p}_1 + M_1}{2M_1} \right) \lambda^{n'} \right] \text{Tr} \left[ \left( \frac{\vec{k}_2 + M_2}{2M_2} \right) \lambda_n \left( \frac{\vec{p}_2 + M_2}{2M_2} \right) \lambda_{n'} \right]. \quad (3.3)$$

An explicit expression for Eq. (3.3) is given in Eq. (2.26) of Ref. [Ho88]. For the IA2 representation of  $\hat{F}$ , we have from Eq. (2.121):

$$\Gamma''(\vec{p}_1, \vec{p}_2, \vec{k}_1, \vec{k}_2) = g_1^2 \sum_{m,n=1}^8 b_m^* b_n \text{Tr}[\chi_n^{(1)} \chi_m^{(1)}] \text{Tr}[\chi_n^{(2)} \chi_m^{(2)}]. \quad (3.4)$$

From Eq. (2.72) we see that only subclass  $\hat{F}^{11}$  contributes when  $M_1 = M_2 = M$  (when medium effects are neglected, i.e. only free masses are used instead of effective masses), then Eqs. (3.3) and (3.4) must give exactly the same results when the same amplitudes are used. When, for a given  $T_{lab}$ ,  $\Gamma''_{IA1}$  and  $\Gamma''$  give exactly the same numerical value, then we know that the transformation from invariant amplitudes to effective amplitudes, for only the *SPVAT* covariants have been carried out correctly. In Fig. 3.1 we show a graph of  $\Gamma''$  versus  $\theta_{lab}$ . Only one line is visible on the graph since the curves for  $\Gamma''$  calculated via Eq.(3.4) (but using a free mass for the projectile and target nucleon which implies that only subclass  $\hat{F}^{11}$  will contribute and is therefore equivalent to a free mass IA1 calculation) and  $\Gamma''$  calculated using the *SPVAT* form of  $\hat{F}$ , i.e. directly from Eq. (3.3), coincide exactly.

We now investigate whether the transformation from invariant amplitudes to effective amplitudes have been carried out correctly for covariants  $K_6$  to  $K_{13}$ . This will be done as follows: The effective amplitudes in Eq. (3.4) are determined by the choice of the covariant and the traces in this equation are over Pauli matrices. On the other hand one can also calculate  $\Gamma''$  directly in terms of invariant amplitudes but in this case the traces will be over Dirac matrices. One therefore has two independent ways to calculate  $\Gamma''$  for the choice of a specific covariant. The two expressions one obtains (one in terms of effective amplitudes and one in terms of invariant amplitudes) must give exactly the same numerical answer for the same incident laboratory kinetic energy as a function of the laboratory scattering angle. We will illustrate this procedure for the covariant  $K_6$ . Covariants  $K_6$  and  $K_8$  are of the form:

$$L_\mu(A \otimes B^\mu) \quad (3.5)$$

where for

$$K_6 : \quad L_\mu = Q_{11,\mu} \quad A = I_4 \quad B^\mu = \gamma^\mu \quad (3.6)$$

and for

$$K_8 : \quad L_\mu = Q_{22,\mu} \quad A = \gamma^5 \quad B^\mu = \gamma^5 \gamma^\mu. \quad (3.7)$$

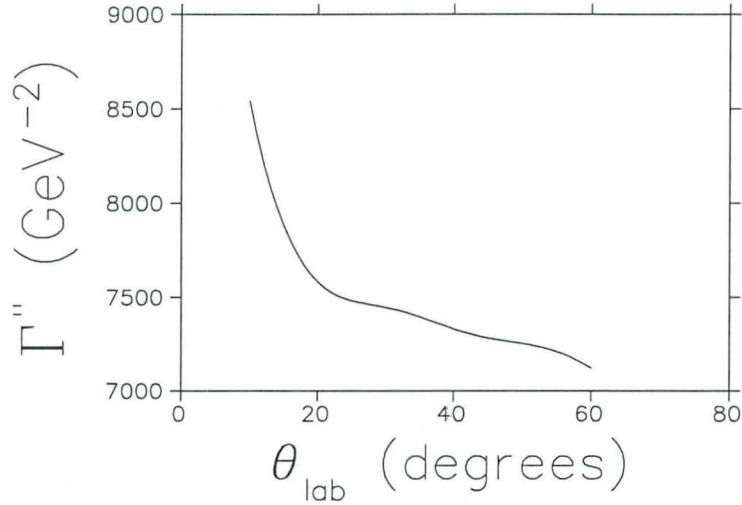


Figure 3.1: Here, in fact, two graphs of  $\Gamma''$ , calculated respectively from Eqs. 3.3 and 3.4 are plotted for the same kinematical configuration: A 200 MeV incident proton beam and no medium effects allowed on the projectile and target nucleons. Only one graph is visible which shows that the sets of  $\Gamma''$  values coincide exactly. It serves to illustrate the correct IA2 calculation based on Eq. 3.4.

The contribution of either covariant  $K_6$  or covariant  $K_8$  to Eq. (2.71) is therefore:

$$\hat{F}_{6;8} = \sum_{\{\rho\}} F_{6;8}^{\{\rho\}} L_{\mu} (\Lambda_{\rho'_1}(1') \otimes \Lambda_{\rho'_2}(2')) (A \otimes B^{\mu}) (\Lambda_{\rho_1}(1) \otimes \Lambda_{\rho_2}(2)). \quad (3.8)$$

The subscript '6;8' in Eq. (3.8) indicates that either covariant  $K_6$  or covariant  $K_8$  will make a contribution of this form to  $\hat{F}$ . Eq. (3.8) can also be written as:

$$\hat{F}_{6;8} = \sum_{\{\rho\}} F_{6;8}^{\{\rho\}} L_{\mu} (A_{\rho'_1\rho_1} \otimes B_{\rho'_2\rho_2}^{\mu}) \quad (3.9)$$

where we have used Eq. (2.77) and

$$A_{\rho'_1\rho_1} = \Lambda_{\rho'_1}(1') A \Lambda_{\rho_1}(1) \quad (3.10)$$

and

$$B_{\rho'_2\rho_2}^{\mu} = \Lambda_{\rho'_2}(2') B^{\mu} \Lambda_{\rho_2}(2). \quad (3.11)$$

The contribution of either covariant  $K_6$  or  $K_8$  to the invariant amplitude can then be found by substituting Eq. (3.9) into Eq. (2.1) to obtain:

$$\mathcal{M}_{6;8} = \sum_{\{\rho\}} F_{6;8}^{\{\rho\}} L_{\mu} (\bar{U}(1') A_{\rho'_1\rho_1} U(1)) (\bar{U}(2') B_{\rho'_2\rho_2}^{\mu} U(2)). \quad (3.12)$$

Therefore

$$\mathcal{M}_{6;8}^* = \sum_{\{\rho\}} (F_{6;8}^{\{\rho\}})^* (\bar{U}(1) \overline{A_{\rho'_1 \rho_1}} U(1')) (\bar{U}(2) \overline{B_{\rho'_1 \rho_1}^\mu} U(1')) \quad (3.13)$$

where

$$\overline{A_{\rho'_1 \rho_1}} = \gamma^0 A_{\rho'_1 \rho_1}^\dagger \gamma^0 \quad (3.14)$$

and

$$\overline{B_{\rho'_1 \rho_1}^\mu} = \gamma^0 (B_{\rho'_1 \rho_1}^\mu)^\dagger \gamma^0. \quad (3.15)$$

The contribution of either  $K_6$  or  $K_8$  to

$$\Gamma'' = \sum_{s_i s_f s_2 s'_2} |\mathcal{M}|^2 \quad (3.16)$$

is therefore

$$\Gamma''_{6;8} = \sum_{s_i s_f s_2 s'_2} |\mathcal{M}_{6;8}|^2. \quad (3.17)$$

The use of standard techniques [Bj64] leads to

$$\begin{aligned} \Gamma''_{6;8} = & \sum_{\{\rho\}\{\alpha\}} F_{6;8}^{\{\rho\}} (F_{6;8}^{\{\alpha\}})^* L_\mu L_\nu \text{Tr} \left[ \left( \frac{\not{p}_1^* + M_1}{2M_1} \right) \overline{A_{\alpha'_1 \alpha_1}} \left( \frac{\not{k}_1^* + M_1}{2M_1} \right) A_{\rho'_1 \rho_1} \right] \\ & \text{Tr} \left[ \left( \frac{\not{p}_2^* + M_2}{2M_2} \right) \overline{B_{\alpha'_2 \alpha_2}^\nu} \left( \frac{\not{k}_2^* + M_2}{2M_2} \right) B_{\rho'_2 \rho_2}^\mu \right]. \end{aligned} \quad (3.18)$$

Notice in Eq. (3.18) that there is a double sum over the positive and negative energy sectors, indexed by

$$\{\rho\} = \{\rho_1 \rho'_1 \rho_2 \rho'_2\}$$

and

$$\{\alpha\} = \{\alpha_1 \alpha'_1 \alpha_2 \alpha'_2\}.$$

For covariant  $K_6$ , use of Eq. (3.6), shows that

$$\begin{aligned} A_{\rho'_1 \rho_1} &= \Lambda_{\rho'_1}(\vec{k}_1, M) \Lambda_{\rho_1}(\vec{p}_1, M) \\ \overline{A_{\alpha'_1 \alpha_1}} &= \Lambda_{\alpha_1}(\vec{p}_1, M) \Lambda_{\alpha'_1}(\vec{k}_1, M) \\ B_{\rho'_2 \rho_2}^\mu &= \Lambda_{\rho'_2}(\vec{k}_2, M) \gamma^\mu \Lambda_{\rho_2}(\vec{p}_2, M) \\ \overline{B_{\alpha'_2 \alpha_2}^\nu} &= \Lambda_{\alpha_2}(\vec{p}_2, M) \gamma^\nu \Lambda_{\alpha'_2}(\vec{k}_2, M) \end{aligned}$$



where we have used Eq. (2.17) and Eq.(2.66), and therefore the contribution of covariant  $K_6$  to  $\Gamma''$  is:

$$\begin{aligned} \Gamma_6''(\vec{p}_1, \vec{p}_2, \vec{k}_1, \vec{k}_2) &= \sum_{\{\rho\}\{\alpha\}} F_6^{\{\rho\}} F_6^{\{\alpha\}*} Q_{11,\mu} Q_{11,\nu} \\ &\text{Tr} \left[ \left( \frac{\not{p}_1^* + M_1}{2M_1} \right) \left( \frac{\alpha_1 \not{p}_1 + M}{2M} \right) \left( \frac{\alpha'_1 \not{k}_1 + M}{2M} \right) \right. \\ &\quad \left. \left( \frac{\not{k}_1^* + M_1}{2M_1} \right) \left( \frac{\rho'_1 \not{k}_1 + M}{2M} \right) \left( \frac{\rho_1 \not{p}_1 + M}{2M} \right) \right] \\ &\text{Tr} \left[ \left( \frac{\not{p}_2^* + M_2}{2M_2} \right) \left( \frac{\alpha_2 \not{p}_2 + M}{2M} \right) \gamma^\nu \left( \frac{\alpha'_2 \not{k}_2 + M}{2M} \right) \right. \\ &\quad \left. \left( \frac{\not{k}_2^* + M_2}{2M_2} \right) \left( \frac{\rho'_2 \not{k}_2 + M}{2M} \right) \gamma^\mu \left( \frac{\rho_2 \not{p}_2 + M}{2M} \right) \right] \end{aligned} \quad (3.19)$$

where

$$\begin{aligned} p_1 &= (E_1, \vec{p}_1) & p_2 &= (E_2, \vec{p}_2) \\ k_1 &= (E'_1, \vec{k}_1) & k_2 &= (E'_2, \vec{k}_2) \end{aligned}$$

with  $E_i^2 = \vec{p}_i^2 + M^2$  and  $E_i'^2 = \vec{k}_i^2 + M^2$  for  $i = 1, 2$ . Eqs. (3.19) and (2.121) provide a check whether the transformation from invariant amplitudes to effective amplitudes has been carried out correctly for only covariant  $K_6$ , since Eqs. (3.19) and (2.121) must give (for chosen  $T_{lab}$ ) exactly the same numerical value, when only  $K_6$  is included to calculate the effective amplitudes [which is then used in Eq. (2.121)]. It is worth appreciating that Eq. (2.121) requires traces over Pauli matrices, whereas Eq. (3.19) requires traces over Dirac matrices. It is impractical to do the Dirac traces in Eq. (3.19) by hand and therefore a code was written using MATHEMATICA [Wo88] to do the required trace algebra. To check that this program works correctly we have verified that we can reproduce Eqs. (2.26), (2.27), (A.1) and (A.2) of Ref. [Ho88]. Exactly the same reasoning can be applied to covariants  $K_7$  to  $K_9$ . For covariants  $K_{10}$  to  $K_{13}$  the presence of the exchange covariant,  $\tilde{S}$  leads to traces with respect to particle 1 *and* particle 2, as well as particle 1' *and* particle 2'. For example, the contribution of  $K_{10}$  or  $K_{12}$  to  $\Gamma''$  is

$$\begin{aligned} \Gamma_{10;12}'' &= \sum_{\{\rho\}\{\alpha\}} F_{10;12}^{\{\rho\}} (F_{10;12}^{\{\alpha\}})^* Q_{12,\mu} Q_{12,\nu} \text{Tr} \left[ \left( \frac{\not{p}_1^* + M_1}{2M_1} \right) \overline{B_{\alpha'_2 \alpha_1}^\nu} \left( \frac{\not{k}_2^* + M_2}{2M_2} \right) B_{\rho'_2 \rho_1}^\mu \right] \\ &\text{Tr} \left[ \left( \frac{\not{p}_2^* + M_2}{2M_2} \right) \overline{A_{\alpha'_1 \alpha_2}} \left( \frac{\not{k}_1^* + M_1}{2M_1} \right) A_{\rho'_1 \rho_2} \right]. \end{aligned} \quad (3.20)$$

Notice in Eq. (3.20) that particle 1 and particle 2 appear within the same trace (this is due to the exchange covariant,  $\tilde{S}$ ). In Fig. 3.2 we show a plot of  $\Gamma''$  calculated via Eq. (3.4) [but including only one covariant at a time, indicated by the subscript on  $\Gamma''$ , to calculate the effective amplitudes] and  $\Gamma''$  calculated using Dirac traces, with  $\frac{M_1}{M} = 0.8$  and  $\frac{M_2}{M} = 0.8$ . The specific choice of  $\frac{M_1}{M} = 0.8$  and  $\frac{M_2}{M} = 0.8$  corresponds to the *optimal*

*value* (see Chapter 3) for the reaction  $^{40}\text{Ca}(\vec{p}, \vec{n})$  at  $T_{lab} = 200$  MeV. Any choice of effective masses will of course be valid. Only one line is visible on the graph since the resulting curves coincide exactly.

In this section we have verified numerically that the transformation from invariant amplitudes to effective amplitudes have been carried out correctly and that the formulas derived for the spin observables are correct.

### 3.3 Medium modifications of the effective amplitudes

The purpose of this section is to show, by way of illustration, how medium effects influence the individual effective amplitudes due to the IA2 representation of  $\hat{F}$ . Figs 3.3 to 3.8 show real and imaginary parts of all the effective amplitudes for isospin zero ( $T = 0$ ) and isospin one ( $T = 1$ ) as well as the charge exchange effective amplitudes for  $T_{lab} = 200$  MeV as a function of laboratory scattering angle. The solid line represents the effective mass calculation for which  $\frac{M_1}{M} = 0.8$  and  $\frac{M_2}{M} = 0.8$  and the dashed line represents the free mass calculation. The specific choice of  $\frac{M_1}{M} = 0.8$  and  $\frac{M_2}{M} = 0.8$  corresponds to the *optimal value* (see Chapter 3) for the reaction  $^{40}\text{Ca}(\vec{p}, \vec{n})$  at  $T_{lab} = 200$  MeV. Any choice of effective masses will yield similar qualitative results. We note the following:

1. Medium effects on the individual effective amplitudes at this low energy are in general not very large. The only two amplitudes which do display a comparatively larger medium effect are  $a_3$  and  $a_4$  for isospin one: See Figs 3.5 and 3.6.
2. The behavior of the charge-exchange amplitudes (which are used in the  $(\vec{p}, \vec{n})$  reaction) are completely different from the individual isospin zero and isospin one amplitudes (which are used in the  $(\vec{p}, \vec{p}')$  reaction). This illustrates the fact that  $(\vec{p}, \vec{p}')$  and  $(\vec{p}, \vec{n})$  scattering sample different parts of the NN interaction in the nuclear medium.
3. Since the spin observables are complicated functions of the effective amplitudes, medium effects on the individual amplitudes do not necessarily translate into medium effects on the spin observables (see Sections 3.4.3 and 3.6).

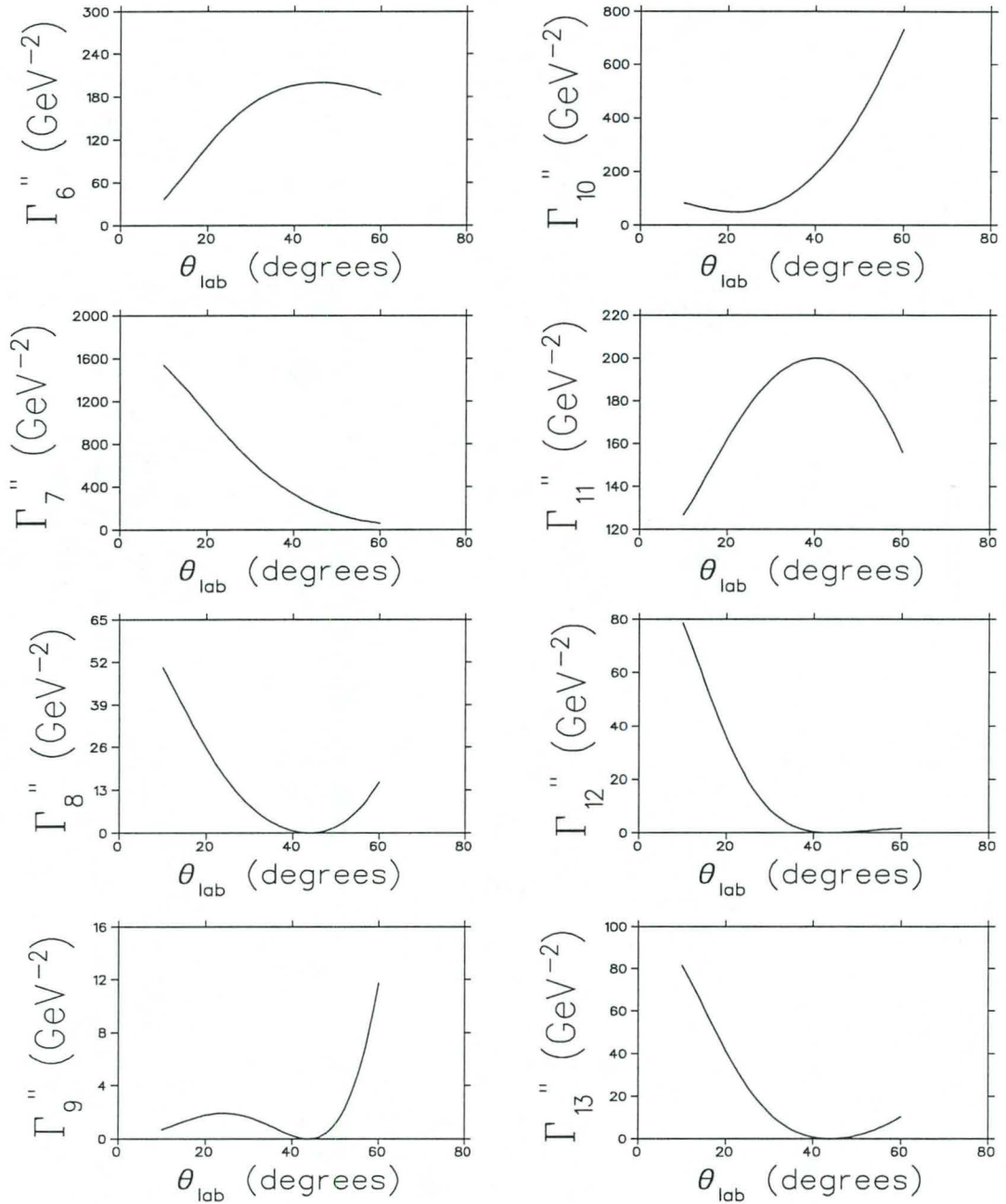


Figure 3.2:  $\Gamma''$  calculated via Pauli traces but including only one covariant (indicated by the subscript) to calculate the effective amplitudes as well as  $\Gamma''$  calculated via Dirac traces for the specific covariant. Only one line is present on the graph since the two curves coincide exactly.



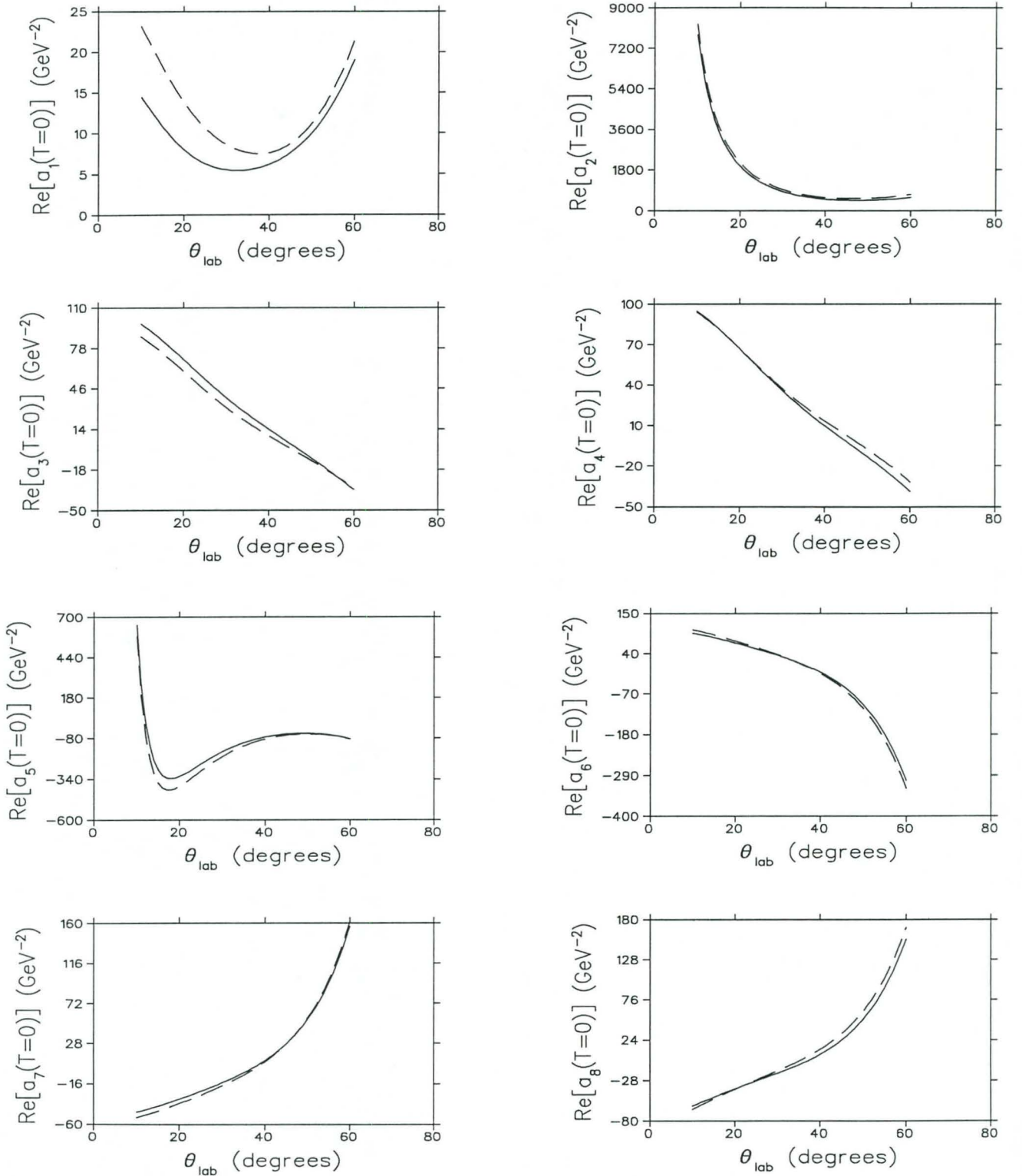


Figure 3.3: Real parts of the isospin zero effective amplitudes for  $T_{\text{lab}} = 200$  MeV as a function of  $\theta_{\text{lab}}$ . The solid line represents the effective mass calculation for which  $\frac{M_1}{M} = 0.8$  and  $\frac{M_2}{M} = 0.8$  and the dashed line represents the free mass calculation.

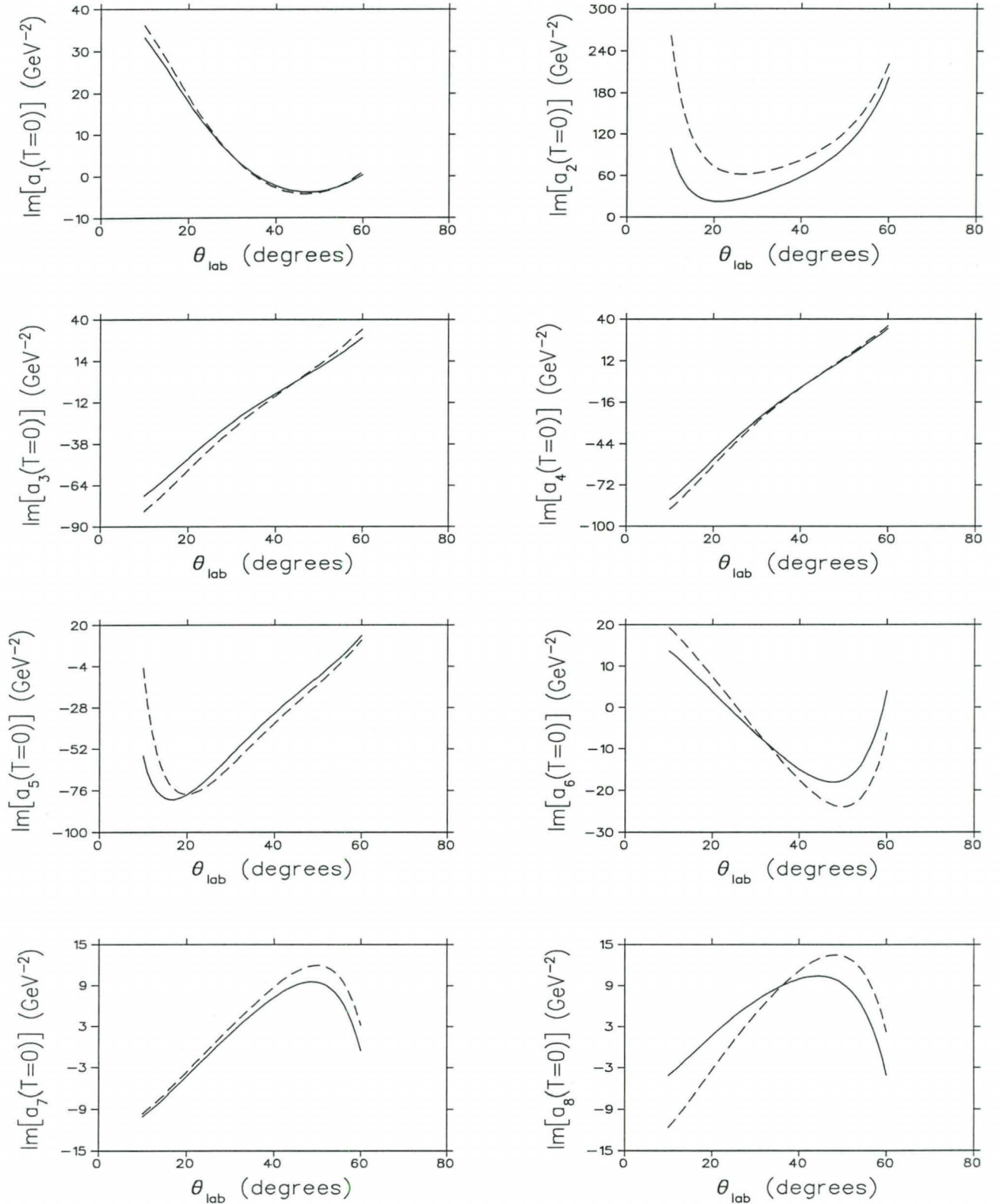


Figure 3.4: Imaginary parts of the isospin zero effective amplitudes for  $T_{\text{lab}} = 200$  MeV as a function of  $\theta_{\text{lab}}$ . The solid line represents the effective mass calculation for which  $\frac{M_1}{M} = 0.8$  and  $\frac{M_2}{M} = 0.8$  and the dashed line represents the free mass calculation.

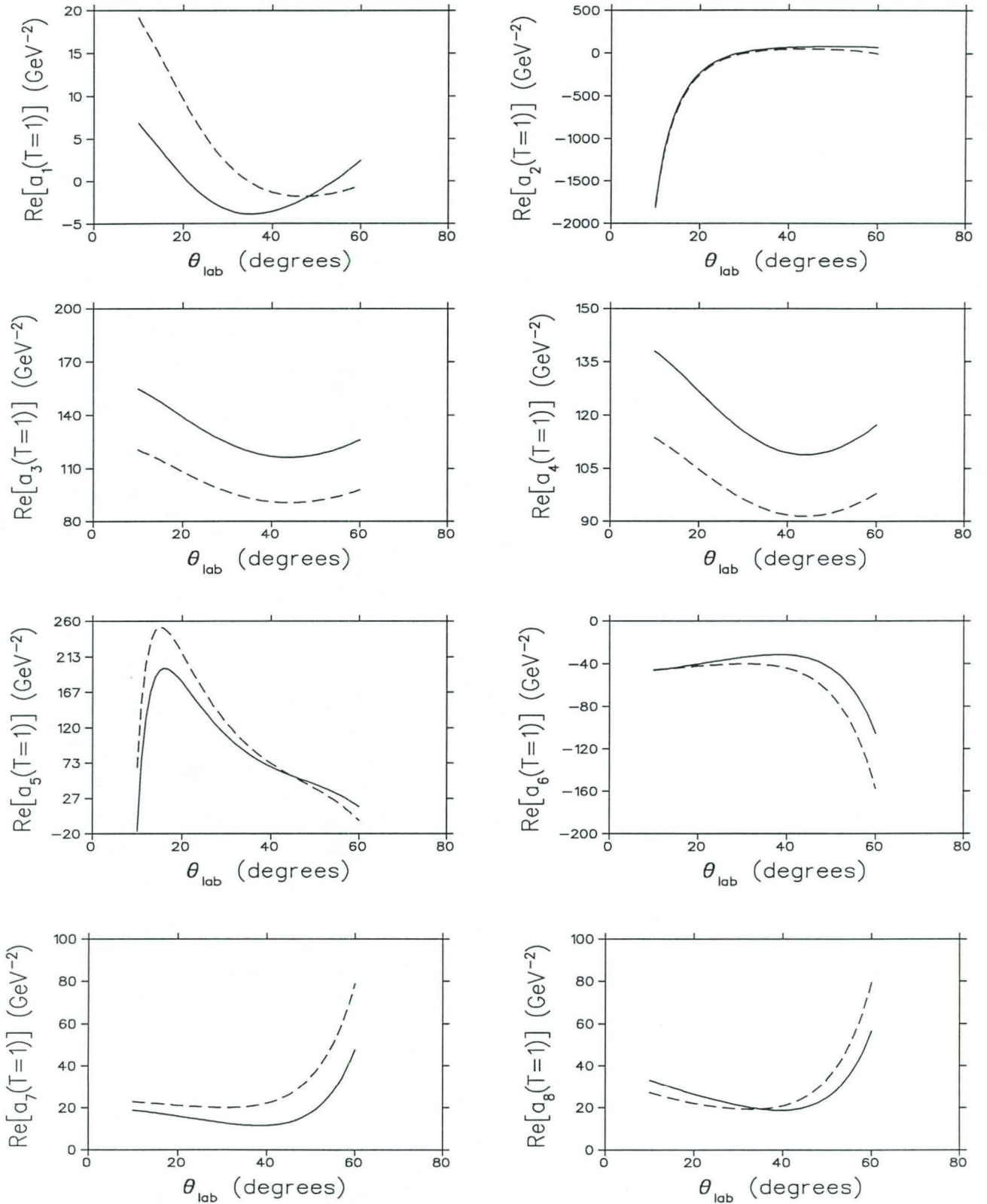


Figure 3.5: Real parts of the isospin one effective amplitudes for  $T_{\text{lab}} = 200$  MeV as a function of  $\theta_{\text{lab}}$ . The solid line represents the effective mass calculation for which  $\frac{M_1}{M} = 0.8$  and  $\frac{M_2}{M} = 0.8$  and the dashed line represents the free mass calculation.



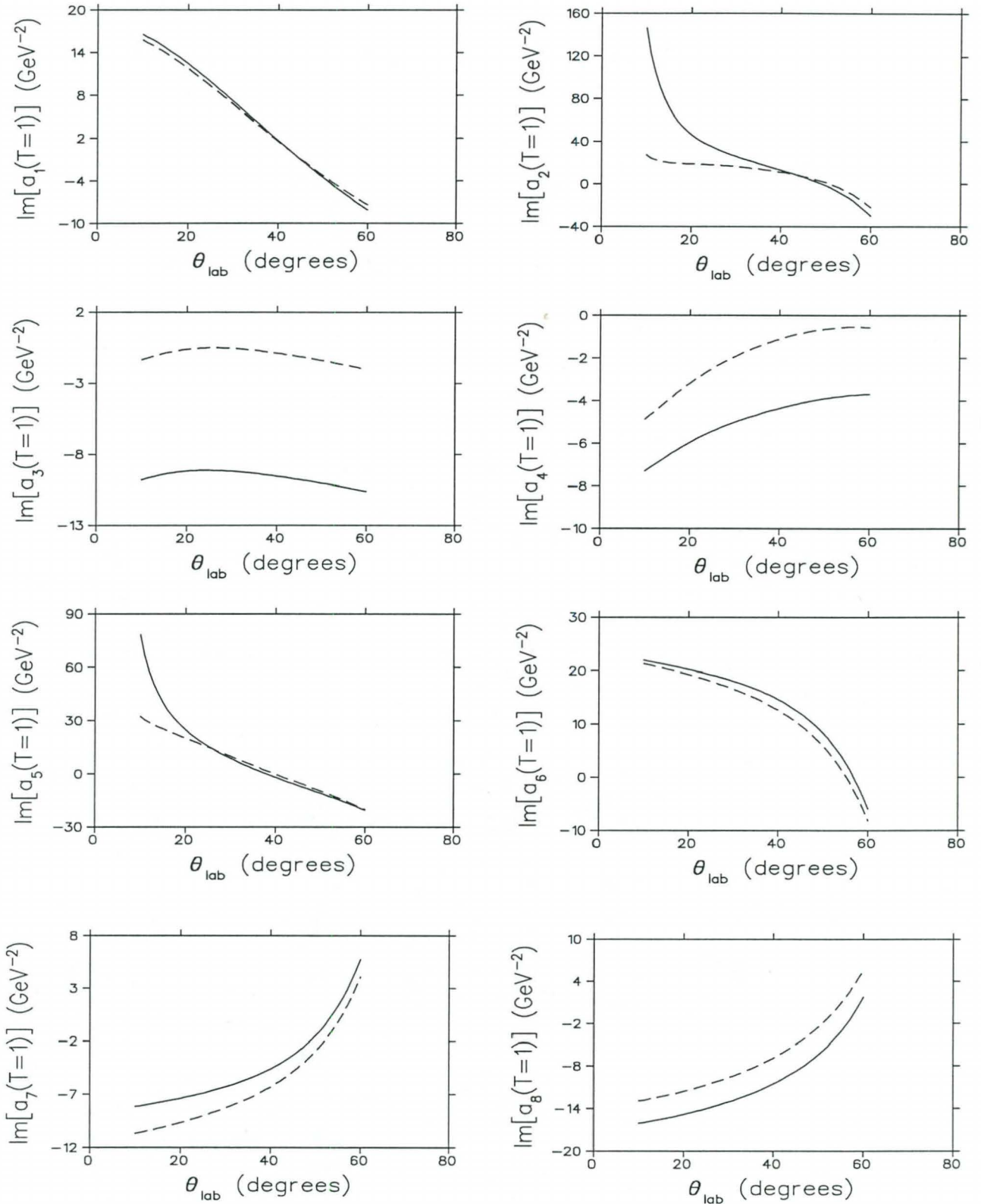


Figure 3.6: Imaginary parts of the isospin one effective amplitudes for  $T_{\text{lab}} = 200$  MeV as a function of  $\theta_{\text{lab}}$ . The solid line represents the effective mass calculation for which  $\frac{M_1}{M} = 0.8$  and  $\frac{M_2}{M} = 0.8$  and the dashed line represents the free mass calculation.

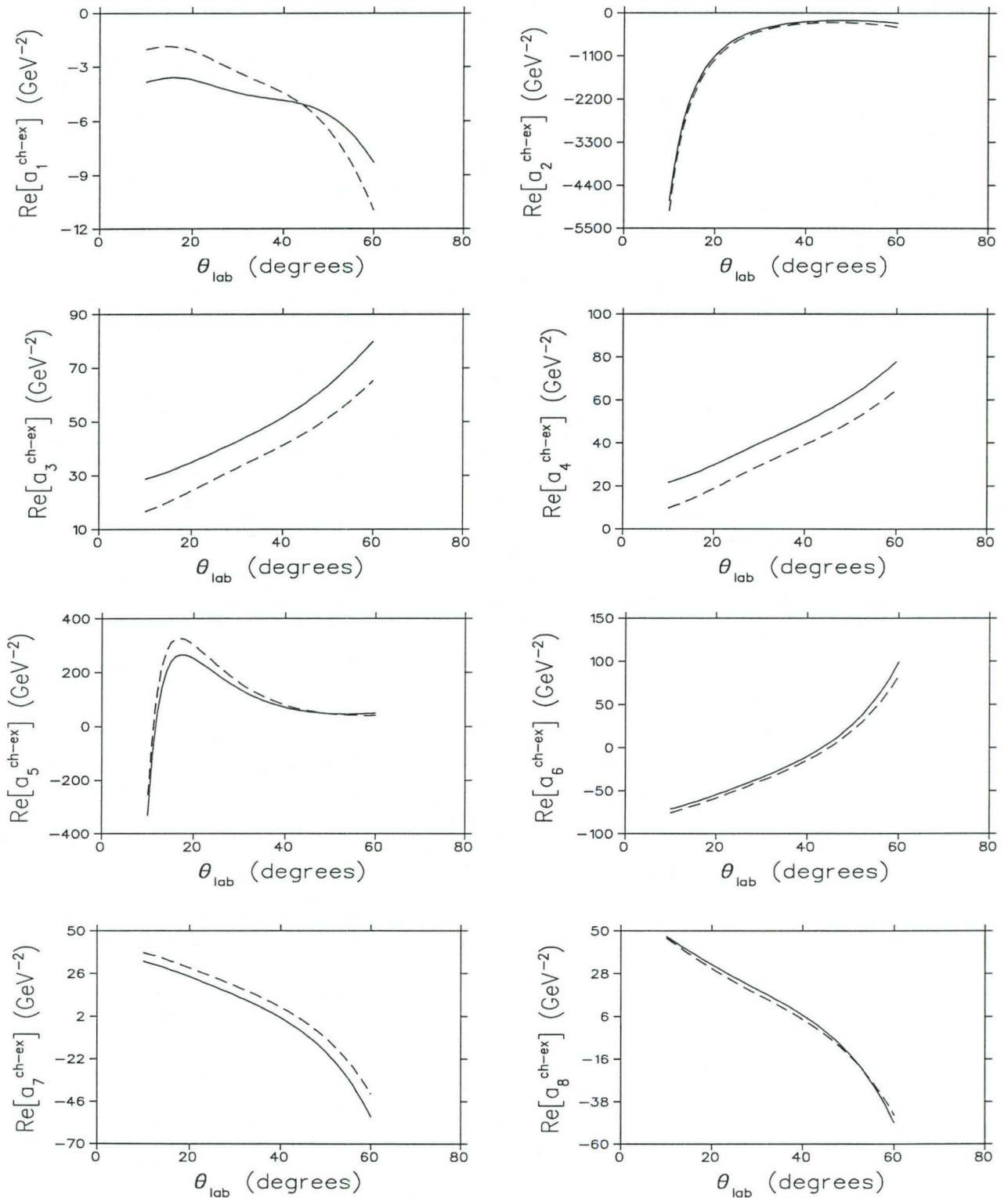


Figure 3.7: Real parts of the charge exchange effective amplitudes for  $T_{\text{lab}} = 200$  MeV as a function of  $\theta_{\text{lab}}$ . The solid line represents the effective mass calculation for which  $\frac{M_1}{M} = 0.8$  and  $\frac{M_2}{M} = 0.8$  and the dashed line represents the free mass calculation.

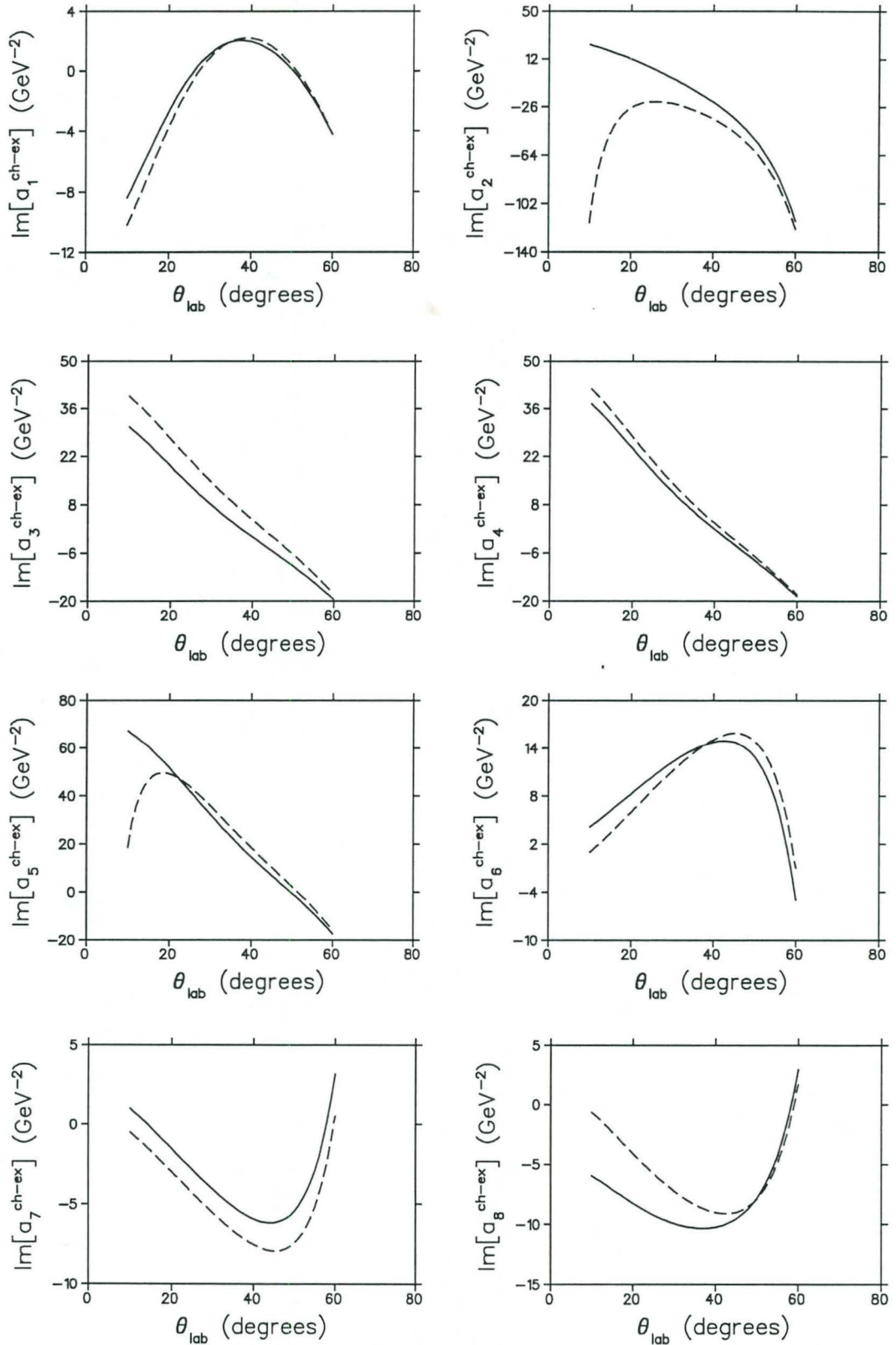


Figure 3.8: Imaginary parts of the charge exchange effective amplitudes for  $T_{\text{lab}} = 200$  MeV as a function of  $\theta_{\text{lab}}$ . The solid line represents the effective mass calculation for which  $\frac{M_1}{M} = 0.8$  and  $\frac{M_2}{M} = 0.8$  and the dashed line represents the free mass calculation.



### 3.4 IA2 versus IA1 predictions without Fermi averaging

In this section we compare IA1-based predictions of spin observables to those utilising the IA2 representation of  $\hat{F}$ . In parallel with this we address the questions as to whether the effective mass concept can describe all experimental data and if there exists *one combination of effective masses* which can describe *a complete set* of spin observables. Experimental data on the spin observables are generally fairly constant with energy transfer [Hi99]. For this reason we compare IA1 and IA2 representations of  $\hat{F}$  *at the quasielastic peak* (hence as a function of laboratory scattering angle,  $\theta_{lab}$ ). For the reaction at the quasielastic peak we assume that, on average, the target nucleon is at rest, i.e.  $|\vec{p}_2| = 0$  and hence we first ignore the Fermi motion of the target nucleon and proceed to plot the effective mass bands and extract the optimal effective masses for the various reactions listed in Table 3.1. We ignore Fermi motion in order to do a first order calculation to compare IA1 with IA2 results. In Section 3.5 we include the Fermi motion of the target nucleon in the extraction of the optimal effective masses.

#### 3.4.1 Effective mass bands

In this section we introduce the concept of an effective mass band for a particular reaction listed in Table 3.1. The effective mass band will immediately give an indication if a particular spin observable can be described, at the quasielastic peak, by the effective nucleon mass concept.

In the RPWIA2 formalism the effective mass in the Dirac spinor plays a central role. Due to the free mass projection operators in the general expansion for  $\hat{F}$  [see Eq. (2.72)], the subclasses  $\hat{F}^{12}$  to  $\hat{F}^{44}$  can only contribute if the Dirac spinor contains an effective mass. As stated previously, medium effects in the RPWIA2 arise only due to off-shell amplitudes contained in subclasses  $\hat{F}^{12}$  to  $\hat{F}^{44}$ . We refer to these amplitudes as off-shell since they cannot be fixed by experimental NN scattering data. This is in contrast to the SPVAT parameterisation of  $\hat{F}$  which contains no projection operators and medium effects therefore occur together with the on-shell amplitudes determined from free NN scattering data. As explained in Section 2.3, the projectile and target effective mass can be calculated in a well-defined manner, however, the approach here will be to consider them as free parameters which can be varied over a range of physically acceptable values, i.e.

$$(0.5; 0.5) \leq \left(\frac{M_1}{M}; \frac{M_2}{M}\right) \leq (1.0; 1.0) \quad (3.21)$$

in step sizes of 0.1. Theoretical calculations of the effective projectile and target nucleon masses [Hi94] indicate that  $M_2$  is in general less than  $M_1$ . This constraint leads to 21 different effective mass combinations coming from Eq. (3.21). Recall from Section 2.5.4 that the RPWIA models quasielastic scattering as a two-body scattering process where initially the target nucleon has a momentum  $\vec{p}_2$  with

$$p_{min} \leq |\vec{p}_2| \leq k_f$$

where  $k_f$  is the Fermi momentum and

$$p_{min} = \left| \frac{q}{2} - \frac{\omega^*}{2} \left[ 1 - \frac{4M_2^2}{q_\mu q^\mu} \right]^{\frac{1}{2}} \right|.$$

For the reaction at the quasielastic peak we assume that, on average, the target nucleon is at rest, i.e.  $|\vec{p}_2| = 0$ . This condition means that the integration over  $\vec{p}_2$  can be neglected, i.e. we are considering free NN kinematics. The formulas for the spin observables then simplify to

$$A_y(\vec{p}, \vec{n}) = \frac{\Gamma'(\hat{n}, \{a_i^{ch-ex}\})}{\Gamma''(\{a_i^{ch-ex}\})} \quad (3.22)$$

and

$$D_{i'j}[(\vec{p}, \vec{n})] = \frac{4\Gamma(\hat{s}_i, \hat{s}_f, \{a_i^{ch-ex}\})}{\Gamma''(\{a_i^{ch-ex}\})} \quad (3.23)$$

and for the  $(\vec{p}, \vec{p}')$  reaction to

$$A_y(\vec{p}, \vec{p}') = \frac{(Z_{eff}\Gamma'(\hat{n}, \{a_i(I=1)\}) + N_{eff}\Gamma'(\hat{n}, \{a_i^{ave}\}))}{(Z_{eff}\Gamma''(\{a_i(I=1)\}) + N_{eff}\Gamma''(\{a_i^{ave}\}))} \quad (3.24)$$

and

$$D_{i'j}[(\vec{p}, \vec{p}')] = \frac{(4Z_{eff}\Gamma(\hat{s}_i, \hat{s}_f, \{a_i(I=1)\}) + 4N_{eff}\Gamma(\hat{s}_i, \hat{s}_f, \{a_i^{ave}\}))}{(Z_{eff}\Gamma''(\{a_i(I=1)\}) + N_{eff}\Gamma''(\{a_i^{ave}\}))}. \quad (3.25)$$

The spin observables are now functions of the laboratory scattering angle,  $\theta_{lab}$ , since we are working at a fixed energy transfer namely  $\omega = \omega_{peak}$ . If we have experimental data for a given reaction then we take  $\omega_{peak}$  to be equal to the experimental peak value. The spin observables are of course also functions of the effective mass combinations, i.e.

$$A_y = A_y(\theta_{lab}; \frac{M_1}{M}; \frac{M_2}{M})$$

and

$$D_{i'j} = D_{i'j}(\theta_{lab}; \frac{M_1}{M}; \frac{M_2}{M}).$$

For a **fixed**  $\theta_{lab}$  each spin observable ( $A_y, D_{i'j}$ ) can be calculated successively for each of the 21 different effective mass combinations in Eq. (3.21). This is repeated for  $10^\circ \leq \theta_{lab} \leq 60^\circ$  and therefore each effective mass combination generates a curve as a function of  $\theta_{lab}$ . Instead of plotting all the different curves on one graph, we calculate, for a **fixed**  $\theta_{lab}$  the minimum and maximum values for a spin observable, for example:

$$(A_y)_{min}(\theta_{lab}) = \text{Min}[A_y(\theta_{lab}; 1.0; 0.5), A_y(\theta_{lab}; 1.0; 0.6), \dots, A_y(\theta_{lab}; 1.0; 1.0)]$$



and

$$(A_y)_{max}(\theta_{lab}) = \text{Max}[A_y(\theta_{lab}; 1.0; 0.5), A_y(\theta_{lab}; 1.0; 0.6), \dots, A_y(\theta_{lab}; 1.0; 1.0)].$$

As  $\theta_{lab}$  is varied between  $10^\circ$  and  $60^\circ$ ,  $(A_y)_{min}(\theta_{lab})$  traces out a lower curve and  $(A_y)_{max}(\theta_{lab})$  traces out an upper curve on the graph: All effective mass combinations given by Eq. (3.21) will lie between these limits. This is how the effective mass bands are generated for each spin observable. The advantage of the effective mass band plots is that it immediately gives an indication whether a particular spin observable can be described **at the quasielastic peak** via the concept of an effective-mass medium effect. If the data point falls outside an effective mass band it means that no effective mass combination can describe that particular data point. Both the IA1 and IA2 representations of  $\hat{F}$  were used to generate these effective mass bands. For the IA1 representation we employ the phenomenological Horowitz-Love-Franey [Ho85] model with pseudovector coupling incorporated as explained in Ref. [Hi94]. The bands in Figs 3.9 to 3.16 represent the range of values of the spin observable in question, which are found by varying  $\frac{M_1}{M}$  and  $\frac{M_2}{M}$  over the full range specified in Eq. (3.21). The legends are: IA1 (straight line hatch pattern) or IA2 (dotted hatch pattern). The data points on these figures represent the value of the particular spin observable extracted at the quasielastic peak for a specific laboratory scattering angle. The solid and dashed lines represent the values calculated using the optimal set (see Section 3.4.2) for respectively the IA2 and the IA1 representation of  $\hat{F}$ ; the long-dash–short-dash line represents the free mass values. The systematic behaviour of the effective mass bands when Fermi motion is neglected for the various reactions listed in Table 3.1 is discussed in Section 3.4.3.

### 3.4.2 Optimal effective masses

In this section we introduce the concept of an optimal effective mass for spin observables at the quasielastic peak.

We start by defining:

$$\Delta\left(\frac{M_1}{M}, \frac{M_2}{M}\right) = \sum_{i=1}^{n_1} \sum_{j=1}^{n_2} (w_{theory}^{(j)}(\theta_i) - w_{expr}^{(j)}(\theta_i))^2 \quad (3.26)$$

where  $w_{theory}^{(j)}(\theta_i)$  is the theoretical value of the spin observable evaluated at the laboratory scattering angle  $\theta_i$  at which the experimental data are available. Similarly  $w_{expr}^{(j)}(\theta_i)$  is the experimental value of the spin observable.  $n_1$  and  $n_2$  denote the number of laboratory scattering angles at which data exist and the number of spin observables which were measured, respectively. For example: For the reaction  $^{40}\text{Ca}(\vec{p}, \vec{p}')$  at  $T_{lab} = 500$  MeV,  $n_1 = 1$  (data measured only at one angle),  $n_2 = 6$  ( $A_y$ ,  $D_{\ell', \ell}$ ,  $D_{s', s}$ ,  $D_{\ell', s}$ ,  $D_{s', \ell}$  and  $D_{nn}$ ) and  $\theta_i = 19^\circ$ . To calculate  $w_{theory}^{(j)}(\theta_i)$  we used Eqs. (3.22) and (3.23) for the  $(\vec{p}, \vec{n})$  reaction and Eqs. (3.24) and (3.25) for the  $(\vec{p}, \vec{p}')$  reaction. The optimal set for a particular reaction is defined as that combination of effective masses for which  $\Delta$  is a minimum, i.e. the optimal set is that combination of effective masses which best describe



all the spin observable data for a particular reaction at a particular energy. Table 3.2 displays optimal effective mass combinations for the case where Fermi motion is neglected and for the case when Fermi motion of the target nucleon is taken into account. The differences between the two sets of optimal effective masses will be discussed in Section 3.5.

Table 3.2: Values of optimal effective mass combinations,  $(\frac{M_1}{M}, \frac{M_2}{M})$ , extracted at the quasielastic peak for the case where Fermi motion is neglected (the first set is the optimal IA1 set and the second is the optimal IA2 set) and for the case where Fermi motion of the target nucleon is taken into account (the first set is the optimal IA1 set and the second is the optimal IA2 set). The last column refers to the effective mass combinations which are calculated theoretically [Hi94].

Reaction	$T_{lab}$ (MeV)	No Fermi motion		Fermi motion of target		Theory [Hi94]
$^{40}\text{Ca}(\vec{p}, \vec{p}')$	500	(0.9;0.9)	(1.0; 0.6)	(1.0; 1.0)	(1.0;0.9)	(0.8;0.8)
$^{12}\text{C}(\vec{p}, \vec{p}')$	420	(0.9;0.9)	( 0.9;0.6)	(0.9;0.9)	(0.9;0.8)	(0.8;0.7)
$^{12}\text{C}(\vec{p}, \vec{p}')$	290	(0.9;0.9)	( 1.0;0.7)	(0.9;0.9)	(1.0;0.9)	(0.8;0.7)
$^{54}\text{Fe}(\vec{p}, \vec{p}')$	290	(0.9;0.9)	( 0.9;0.6 )	(0.9;0.9)	( 0.9;0.7)	( 0.8; 0.7)
$^{40}\text{Ca}(\vec{p}, \vec{n})$	495	(0.8;0.8)	(0.9;0.9)	(0.8;0.8)	(0.9;0.9)	(0.8;0.8)
$^{40}\text{Ca}(\vec{p}, \vec{n})$	200	(1.0;1.0)	( 0.8; 0.8)	(1.0;0.9)	(0.9;0.9)	(0.8;0.7)
$^{208}\text{Pb}(\vec{p}, \vec{n})$	200	(0.9;0.9)	(0.7;0.7)	(0.9;0.8)	(0.9;0.9)	(0.8;0.8)

### 3.4.3 Discussion of results

In this section we discuss in some detail the effective mass bands and the optimal effective masses for the reactions listed in Table 3.1. A summary of our findings is presented in Section 3.7.

Referring to Fig 3.9 we see that for all spin observables the IA1 and IA2 effective mass bands overlap and that the data point always lies within this overlapping region, except for  $A_y$  where it lies on the boundary of the IA2 effective mass band. For all  $D_{ij}$ 's the optimal IA1 and IA2 curves describe the single data point very well. For  $D_{\nu l}$ ,  $D_{s's}$  and  $D_{s'l}$ , IA2 does slightly better than IA1. Only  $D_{s'l}$  and  $D_{\nu s}$  show big differences between IA2 medium effects and a free mass calculation for large angles. Both IA1 and IA2 as well as the free mass calculation totally fail to describe the  $A_y$  data point: The optimal curves do, however, display a slight quenching effect. In Fig 3.10 the optimal IA1 and IA2 curves describe the  $D_{ij}$ 's very well but  $A_y$  now falls outside the IA2 effective mass band. This implies that no effective mass combination in the RPWIA2 formalism can give  $A_y$ .



For large angles it is really only  $D_{s'l}$  which shows big differences between a free mass and an IA2 optimal mass calculation. For  $^{12}\text{C}(\vec{p}, \vec{p}')$  at  $T_{lab} = 290$  MeV and  $\theta_{lab} = 30^\circ$  (Fig 3.11), both  $A_y$  and  $D_{nn}$  fall outside the IA2 effective mass band. This is also true for  $^{40}\text{Ca}(\vec{p}, \vec{p}')$  at  $T_{lab} = 200$  MeV and  $\theta_{lab} = 30^\circ$  (Fig 3.13). We can therefore make the following general statement: As the energy is lowered, the prediction of  $A_y$  and  $D_{nn}$  at the quasielastic peak become poorer for  $(\vec{p}, \vec{p}')$  using the RPWIA2 formalism. The remaining observables are still excellently described, however, by the IA2 optimal curve.  $D_{s'l}$  for  $(\vec{p}, \vec{p}')$  scattering consistently exhibits a strong sensitivity to the IA2 medium effect, as the energy is lowered, for large angles.  $D_{l'l}$  for  $(\vec{p}, \vec{p}')$  displays increased sensitivity to IA2 medium effects, as the energy is lowered, for angles less than  $30^\circ$ , and is insensitive to medium effects for angles larger than  $30^\circ$  for  $200 \text{ MeV} \leq T_{lab} \leq 500 \text{ MeV}$ .  $D_{s's}$  shows little sensitivity to medium effects over the entire energy range and for all angles. Compared to  $A_y$  and  $D_{nn}$ , the effective mass bands for the other  $D_{ij}$ 's are much wider. This means that there are indeed certain effective mass combinations which show large deviations from the free mass calculation, but this is not necessarily the optimal set. It is interesting to note that as the energy is lowered, the width of the IA2 effective mass band decreases, while the IA1 effective mass band stays roughly the same. The consequence is that at  $T_{lab} = 420$  MeV, there is still some effective mass combination for which IA1 will give the  $A_y$  data, whereas IA2 will fail. This must not be interpreted, however, as a true  $M^*$ -medium effect. However, as the energy is lowered, the  $A_y$  data point now falls outside both IA1 and IA2 effective mass bands. The successes of the effective mass idea does therefore not carry over to lower energies for the description of  $A_y$  at the peak for  $(\vec{p}, \vec{p}')$  scattering.

Referring to Fig 3.15 we see that in contrast to  $(\vec{p}, \vec{p}')$  scattering, the optimal curves (IA1 and IA2) as well as the free mass calculation describe the analyzing power very well, except for  $48^\circ$  where the data point falls outside the effective mass band. This shows that for  $(\vec{p}, \vec{n})$  scattering,  $A_y$  is not a good observable to measure if medium effects are to be studied, since both the free mass and the optimal curves describe the data equally well. As for  $(\vec{p}, \vec{p}')$  scattering, the effective mass bands overlap for all observables except for  $D_{s's}$ . This observable is therefore sensitive to the difference in using the incomplete IA1 representation or the more correct IA2 representation of  $\hat{F}$ . The data clearly favours the IA2 calculation, for which the optimal IA2 curve describe the trend very well. The data, as well as the theoretical calculation show strong variation with respect to angle for  $D_{l'l}$  and  $D_{s's}$ . The data for  $D_{l's}$  have a slight slope with respect to angle and, even though it follows the trend, the theoretical calculation misses the data completely. No medium effects can therefore predict this observable.  $D_{nn}$  is a very interesting observable since the data are quite flat whereas the theoretical calculation varies strongly with respect to angle. Even though the data points at  $24^\circ$  and  $37^\circ$  lie inside the IA2 effective mass band, the optimal curves miss the data completely. This shows that there might be some combination of effective masses which describe  $D_{nn}$  better than the optimal set. Both IA1 and IA2 theoretical calculations are totally incorrect at  $48^\circ$ . We notice, however, that for the heavier  $^{208}\text{Pb}$  target, the variation with respect to angle of  $D_{nn}$ , is not quite as dramatic as for  $^{40}\text{Ca}$ . The data point at  $24^\circ$  is described fairly well by the optimal IA2 curve. The  $D_{nn}$  data do not exhibit the oscillatory motion of the theoretical curves. On

the other hand, the other observables are described fairly well by the optimal IA2 curve. This shows the importance of measuring a complete set of spin observables, since as was pointed out in Refs. [Hi94, Hi95, Hi98], the  $D_{ij}$ 's are sensitive to different aspects of the model and therefore provide very stringent tests for any assumptions that are made. The data and the theoretical calculation do not display much difference for the heavier  $^{208}\text{Pb}$  target compared to  $^{40}\text{Ca}$  for  $(\vec{p}, \vec{n})$  at 200 MeV. It is really only  $D_{\nu l}$  which display for angles  $\geq 30^\circ$  some notable difference between a free mass and an IA2 optimal mass calculation. For  $^{40}\text{Ca}$  at 495 MeV, the IA2 optimal curve does not describe the data so well, even though it does give the trend of the two data points, except for  $D_{\nu s}$ . The spin observables show totally different behaviour for the  $(\vec{p}, \vec{p}')$  reaction compared to the  $(\vec{p}, \vec{n})$  reaction. The theoretical calculation of the polarization transfer observables for  $(\vec{p}, \vec{p}')$  scattering are more monotonic than the  $D_{jj'}$ 's for  $(\vec{p}, \vec{n})$  scattering, especially  $D_{\nu l}$ ,  $D_{s's}$  and  $D_{nn}$  (which exhibits a very strong oscillatory motion with respect to laboratory scattering angle).



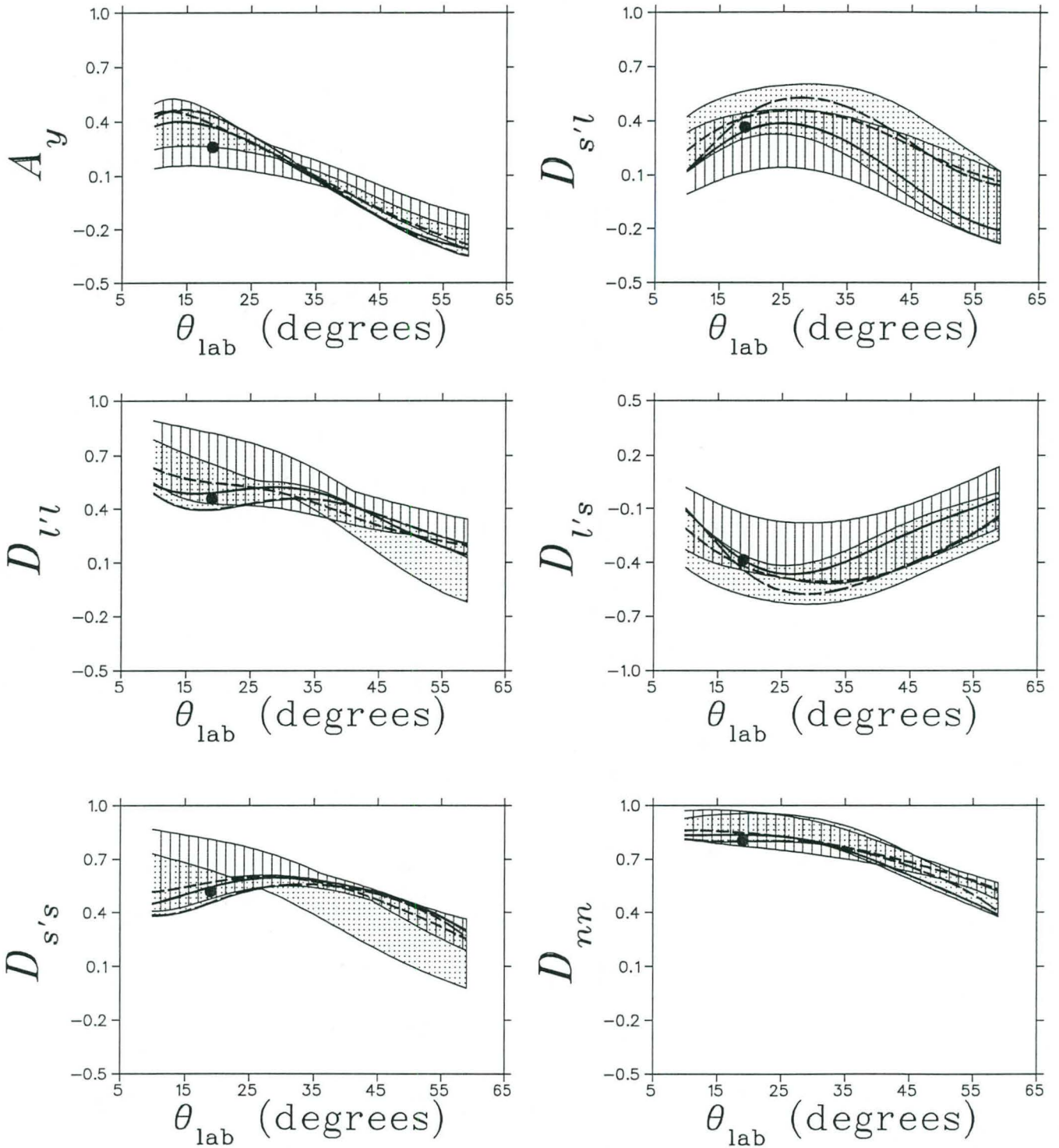


Figure 3.9: Values of  $A_y$  and  $D_{ij}$  versus  $\theta_{lab}$  for  $^{40}\text{Ca}(\vec{p}, \vec{p}')$  at  $T_{lab} = 500$  MeV. Solid and dashed lines represent the calculations with optimal effective mass values in respectively the IA2 and IA1 representations. The hatched bands denote the range of values which result from varying  $\frac{M_1}{M}$  and  $\frac{M_2}{M}$  over the full range (see text): The straight line hatch pattern denotes the IA1 model; the dotted hatch pattern the IA2 model. The long-dash-short-dash lines represent the free mass values. Data (at  $\theta_{lab} = 19^\circ$ ) are from Ref. [Ca84].

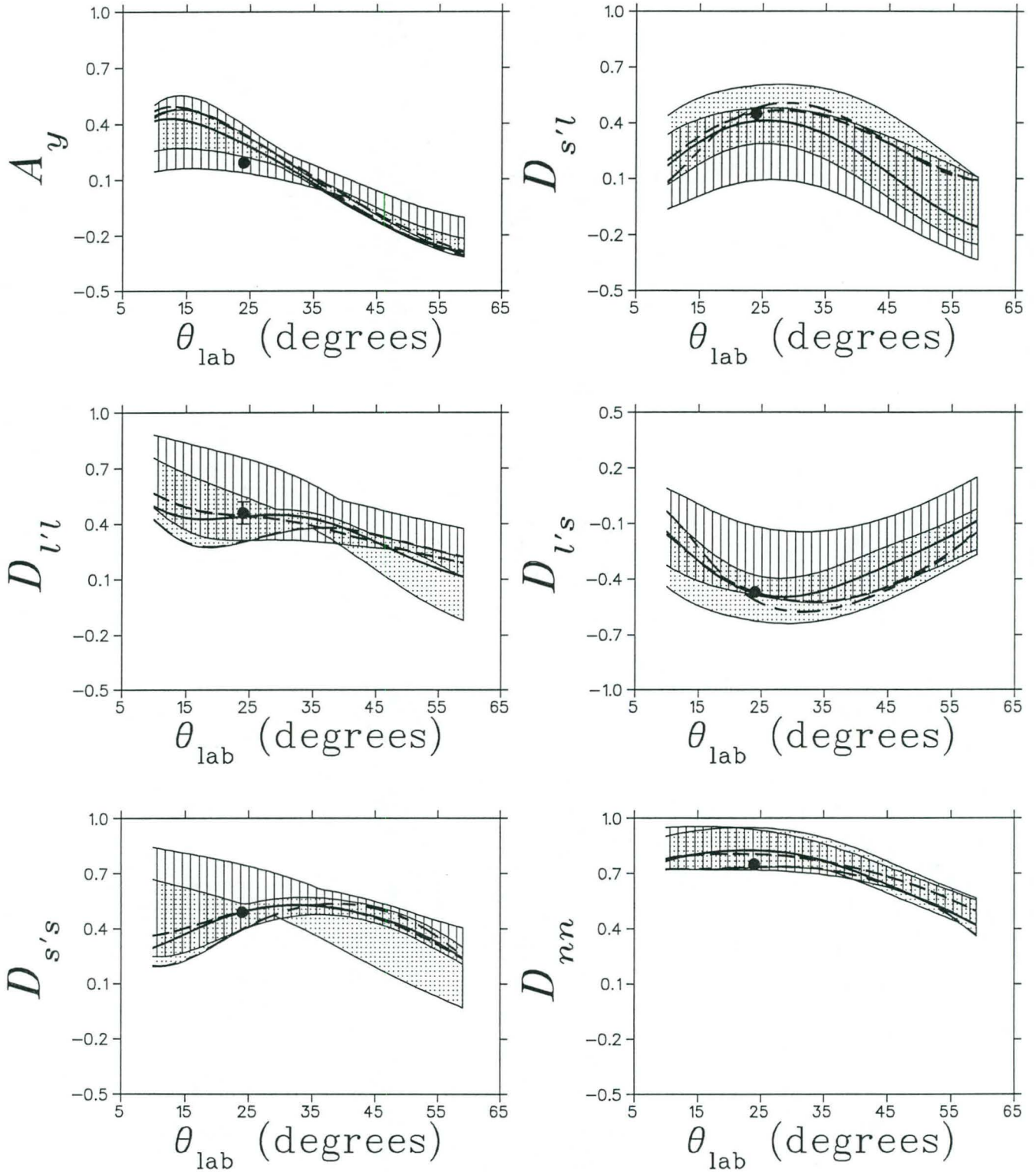


Figure 3.10: Same as Fig. 3.9 but for the reaction  $^{12}\text{C}(\vec{p}, \vec{p}')$  at  $T_{\text{lab}} = 420$  MeV and  $\theta_{\text{lab}} = 24^\circ$ . The data are from Ref. [Ch90].

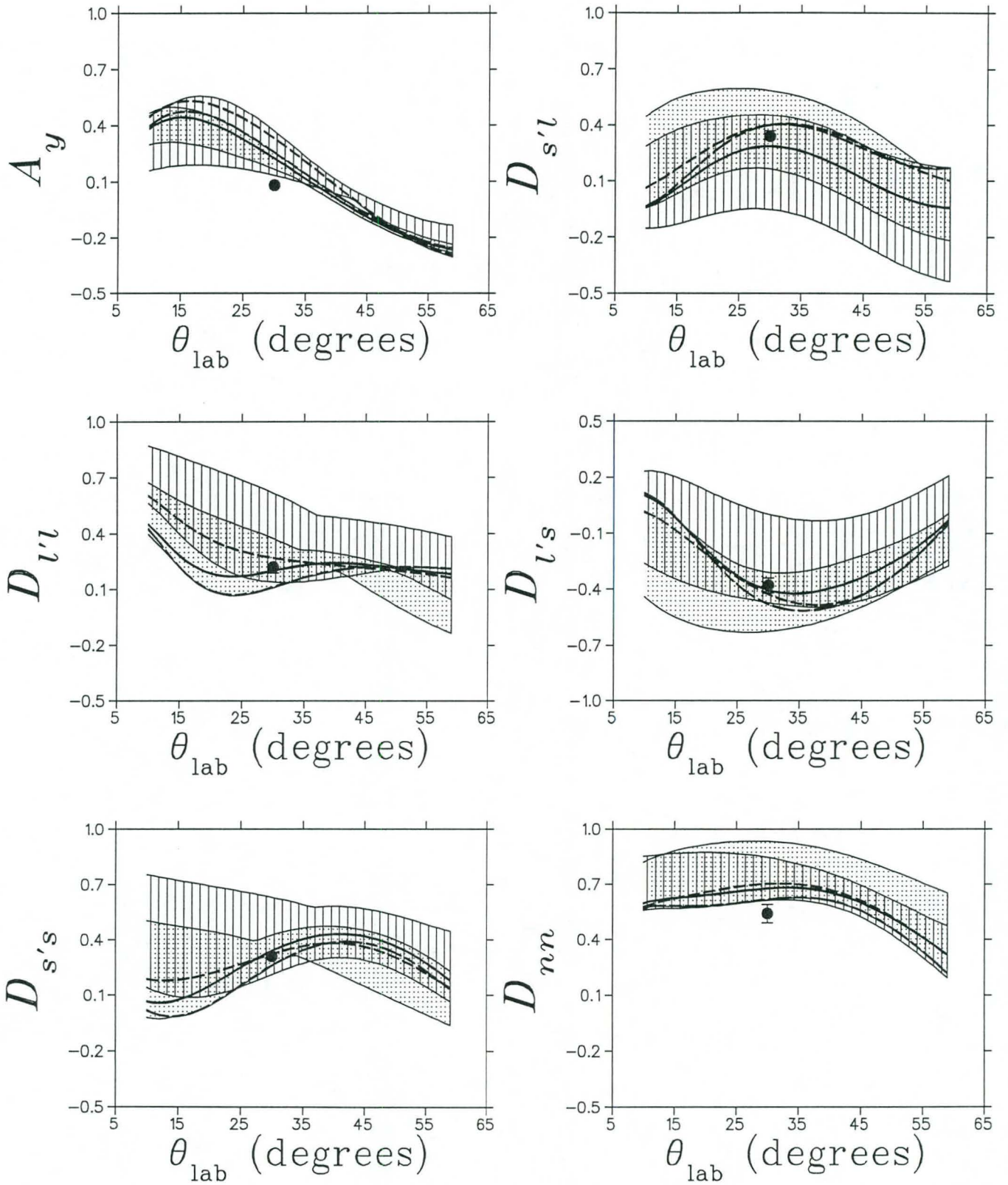


Figure 3.11: Same as Fig. 3.9 but for the reaction  $^{12}\text{C}(\vec{p}, \vec{p}')$  at  $T_{\text{lab}} = 290 \text{ MeV}$  and  $\theta_{\text{lab}} = 30^\circ$ . The data are from Ref. [Ch90].



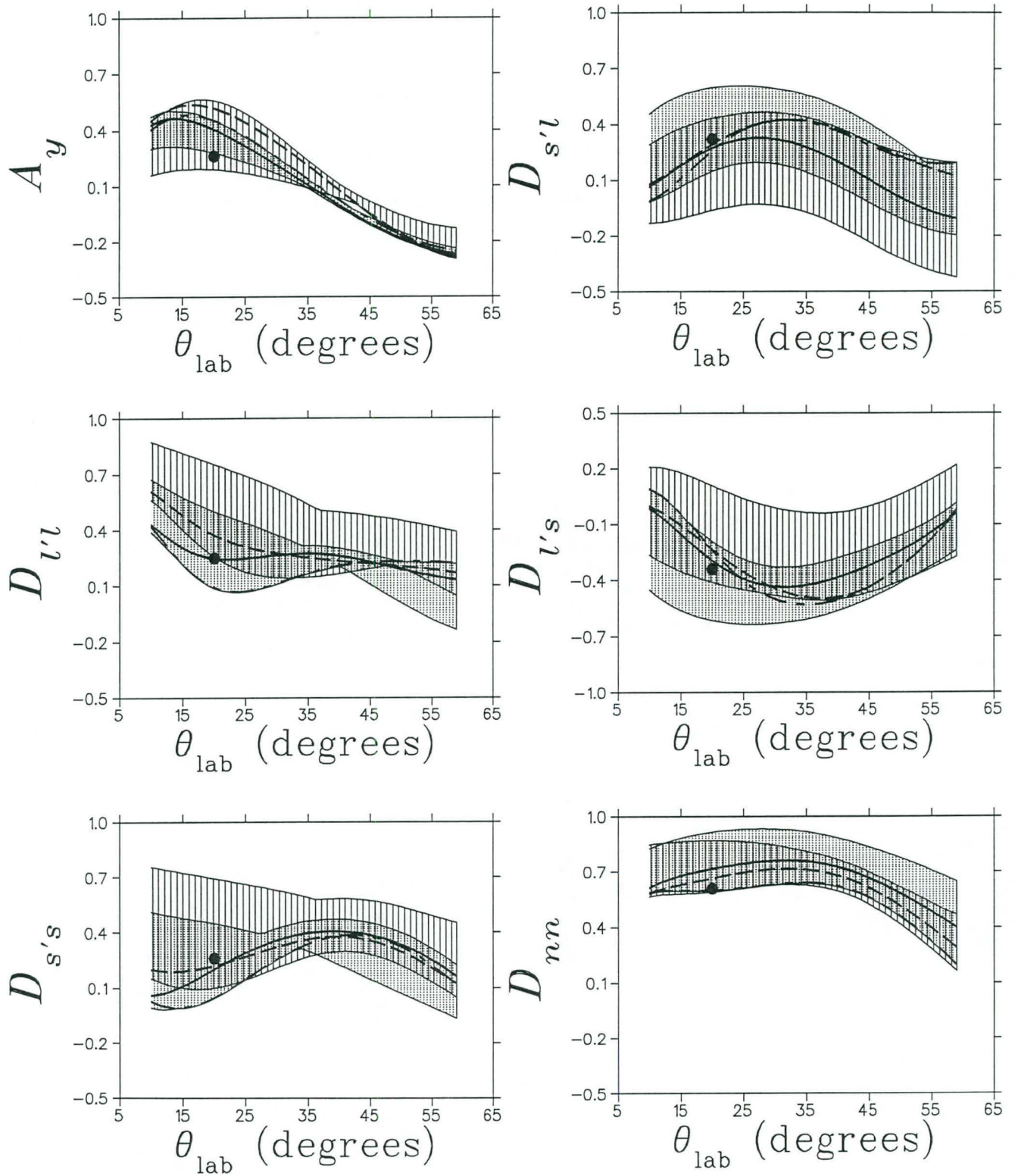


Figure 3.12: Same as Fig. 3.9 but for the reaction  $^{54}\text{Fe}(\vec{p}, \vec{p}')$  at  $T_{\text{lab}} = 290$  MeV and  $\theta_{\text{lab}} = 20^\circ$ . The data are from Ref. [Hä88].

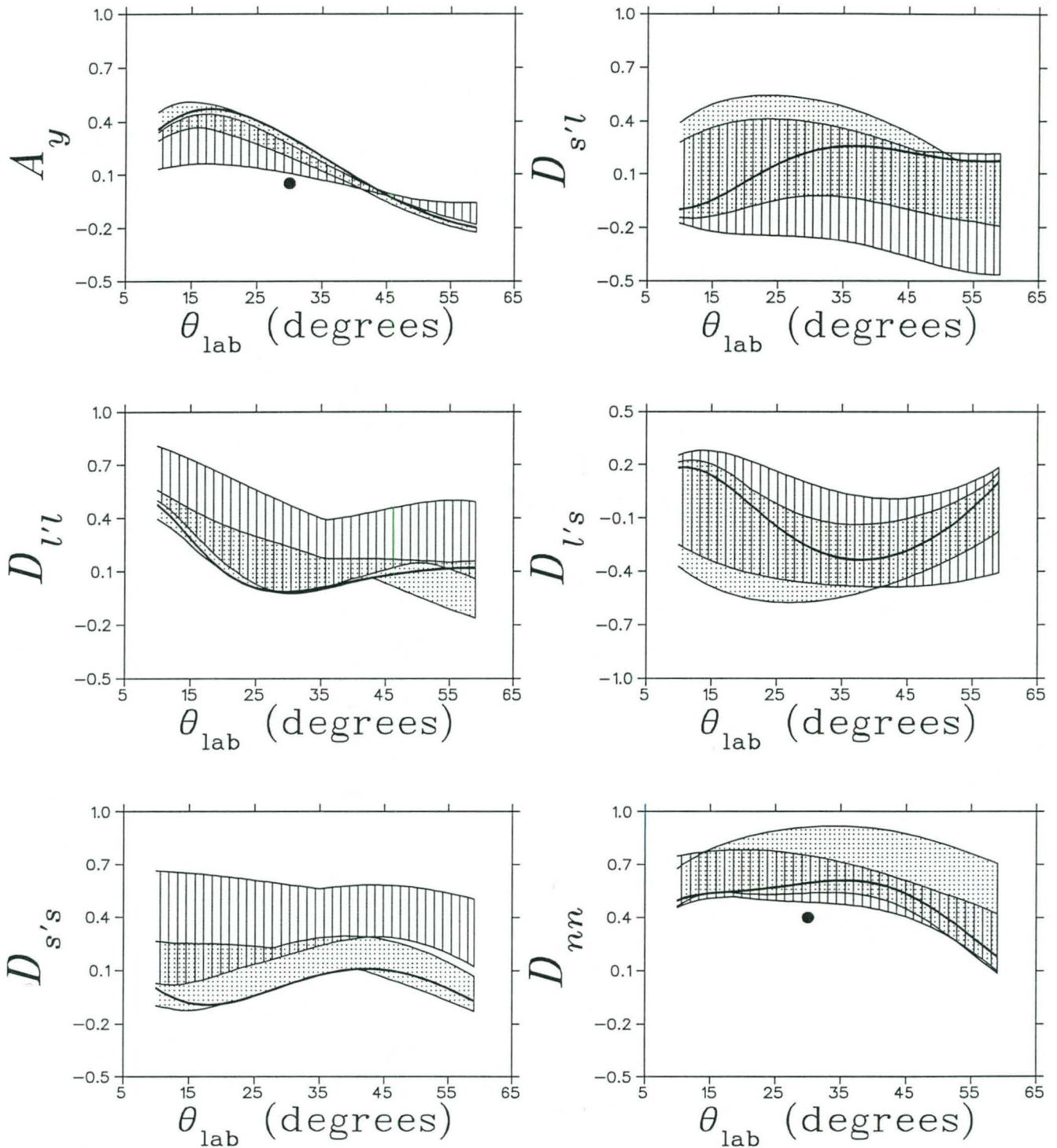


Figure 3.13: For this reaction,  $^{40}\text{Ca}(\vec{p}, \vec{p}')$  at  $T_{\text{lab}} = 200$  MeV and  $\theta_{\text{lab}} = 30^\circ$  only a free mass calculation (denoted by the solid line) was performed due to the lack of a complete set of spin observables. The data are from Ref. [Ca95].

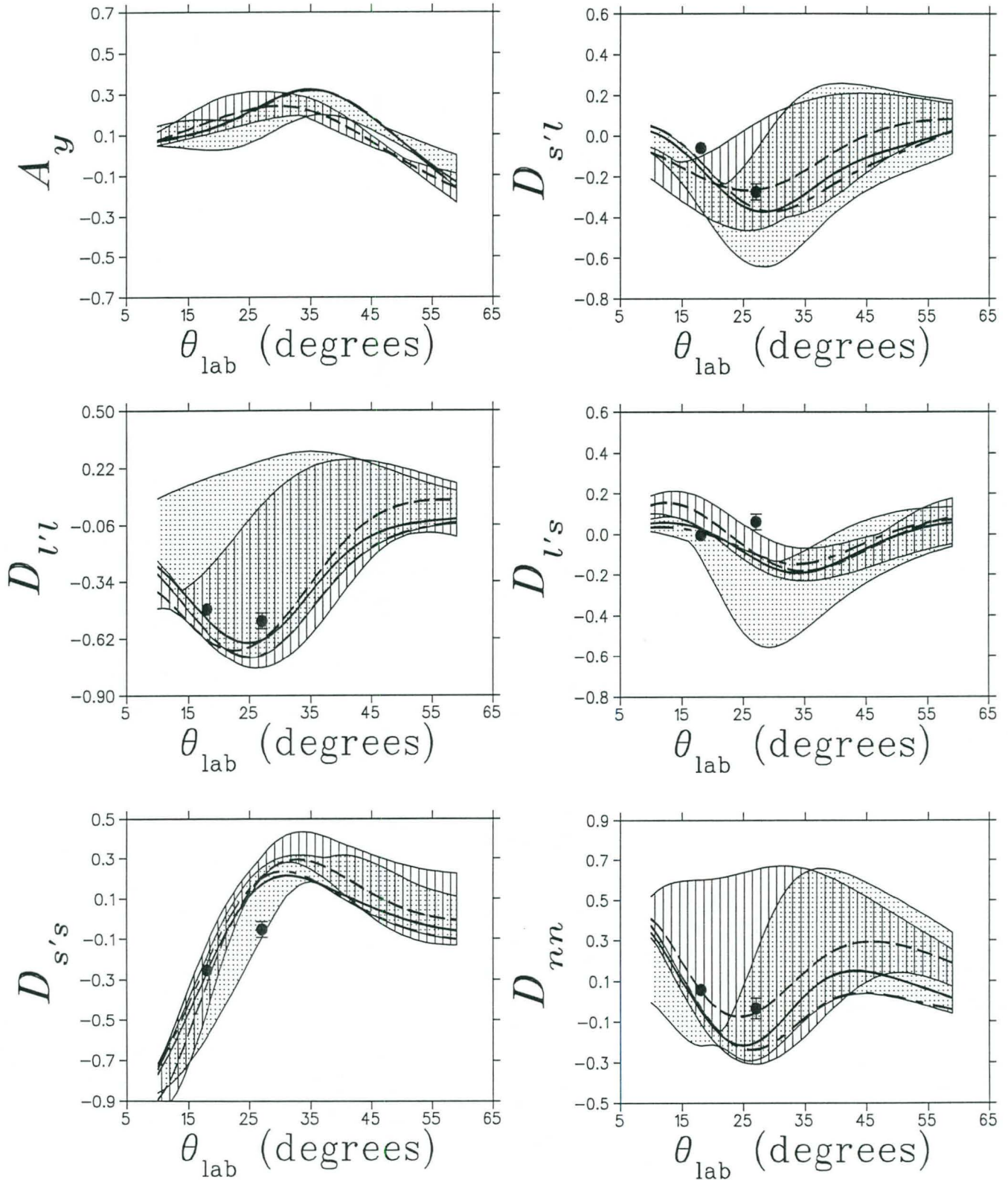


Figure 3.14: Same as Fig. 3.9 but for the reaction  $^{40}\text{Ca}(\vec{p}, \vec{n})$  at  $T_{\text{lab}} = 495$  MeV and  $\theta_{\text{lab}} = 18^\circ$  and  $27^\circ$ . The data are from Ref. [Ta98].



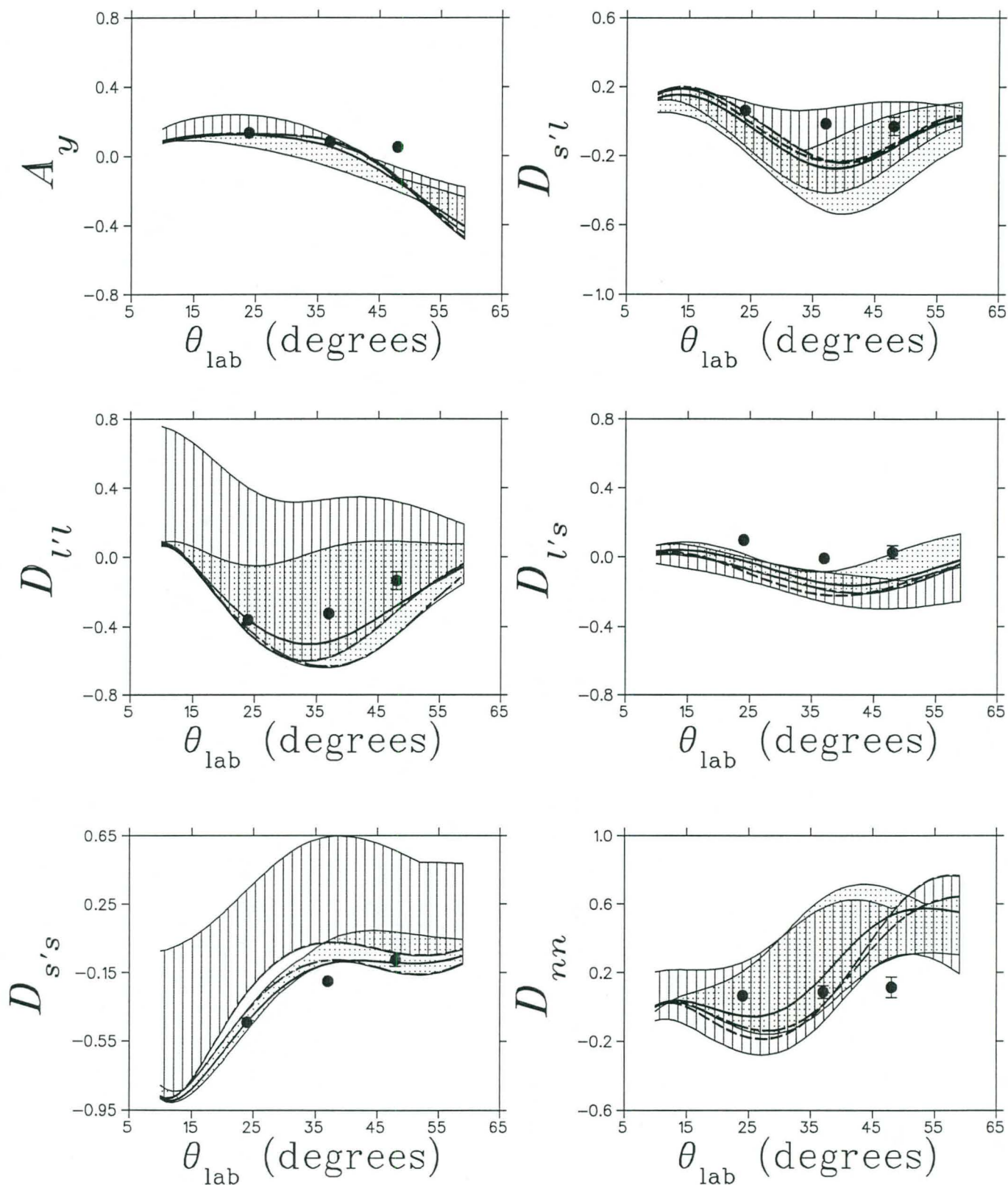


Figure 3.15: Same as Fig. 3.9 but for the reaction  $^{40}\text{Ca}(\vec{p}, \vec{n})$  at  $T_{\text{lab}} = 200$  MeV and  $\theta_{\text{lab}} = 24^\circ, 37^\circ$  and  $48^\circ$ . The data are from Ref. [Ha98].

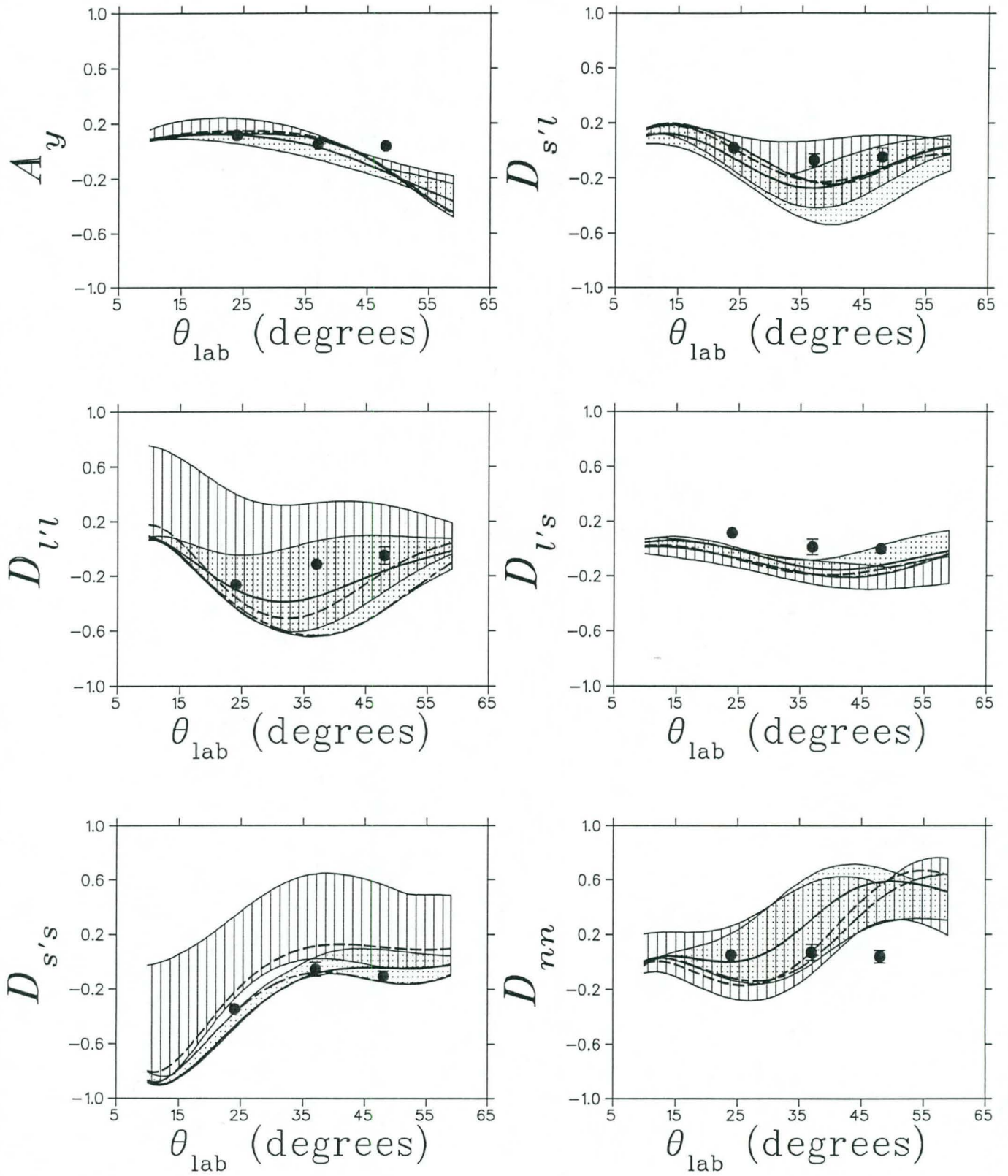


Figure 3.16: Same as Fig. 3.9 but for the reaction  $^{208}\text{Pb}(\vec{p}, \vec{n})$  at  $T_{\text{lab}} = 200$  MeV and  $\theta_{\text{lab}} = 24^\circ, 37^\circ$  and  $48^\circ$ . The data are from Ref. [Ha98].



### 3.5 IA2 versus IA1 predictions with Fermi averaging

When one includes the Fermi motion of the target nucleon one finds that the shape of the effective mass bands stay the same for all practical purposes for all the reactions. We illustrate this in Fig 3.17 which should be compared to Fig 3.9. In the fourth column of Table 3.2 is listed the optimal effective masses for IA1 (first set) and IA2 (second set) extracted at the quasielastic peak taking into account the Fermi motion of the target nucleon. The optimal effective masses differ slightly, however, and one finds for the  $(\vec{p}, \vec{p}')$  reaction that the effective mass of the target nucleon is a little higher than when Fermi motion is neglected. We notice that the effective mass combinations do not vary drastically employing either the IA1 or IA2 representations of  $\hat{F}$ . The optimal sets for both IA1 and IA2 are in general close to the free mass and in this respect they do differ from the sets calculated theoretically. If Fermi motion is neglected then IA2 consistently predicts, for the  $(\vec{p}, \vec{p}')$  reaction, a weak medium effect for the projectile and a stronger medium effect for the target nucleon. This effect is no longer present when the Fermi motion of the target is included: Neglecting Fermi motion for the  $(\vec{p}, \vec{n})$  reaction results in a strong medium effect for both the target and projectile by the IA2 representation. This effect also disappears when the Fermi motion is included: The optimal set is now fairly constant over the energy range 200 MeV to 500 MeV for the  $(\vec{p}, \vec{n})$  reaction. Including the Fermi motion of the target nucleon therefore introduces no discernible differences in the effective mass bands and does not drastically alter the optimal effective mass combinations. All the results and conclusions of Section 3.4.3 are therefore still valid.

### 3.6 Comparison of IA2 predictions to polarization data

In this section we present the RPWIA2 results for the spin observables calculated as a function of energy transfer,  $\omega$ . See Figs 3.18 to 3.30. The solid and dashed lines represent the optimal IA2 and the free mass calculations respectively. The long-dash-short-dash calculation corresponds to  $\frac{M_1}{M}$  and  $\frac{M_2}{M}$  which are taken from Table II in Ref. [Hi94] for the particular reaction and laboratory energy. The optimal set is that combination of effective masses which gives the best value for all experimental spin observables at the quasielastic peak.

The analyzing power for the reaction  $^{40}\text{Ca}(\vec{p}, \vec{p}')$  at  $T_{lab} = 500$  MeV (see Fig 3.18) illustrates very nicely the difference between employing the incomplete IA1 representation of  $\hat{F}$  and the correct IA2 representation of  $\hat{F}$ . Firstly, in the original calculation of Horowitz and Murdock in Ref. [Ho88] it was found that the use of an effective mass for both the projectile and target nucleons moved the theoretical calculation closer to the data and below the free mass calculation for  $A_y$ . This was referred to as the 'quenching effect' in the analyzing power and claimed to be a 'relativistic signature'. In Ref. [Ho88] the SPVAT form of  $\hat{F}$  was used with  $\frac{M_1}{M} = 0.90$  and  $\frac{M_2}{M} = 0.85$ . Fig 3.18 shows that the IA2 representation of  $\hat{F}$  produces a very small quenching effect in  $A_y$  as compared to Fig. 6 of Ref. [Ho88] over the entire range of  $\omega$ . There are two types of effective mass



calculations which must be distinguished in Fig 3.18: On the one hand we employ the effective masses,  $\frac{M_1}{M}$  and  $\frac{M_2}{M}$  which are taken directly from Table II of Ref. [Hi94] for  $^{40}\text{Ca}$  at  $T_{lab} = 500$  MeV and on the other hand we have the IA2 optimal set (in this case  $\frac{M_1}{M} = 1.0$  and  $\frac{M_2}{M} = 0.9$ ). The former calculation with  $\frac{M_1}{M} = 0.892$  and  $\frac{M_2}{M} = 0.817$  (which nearly equals the values of Ref. [Ho88]) is nearly identical to the free mass calculation and the quenching effect is very small and negligible beyond the peak. On the other hand we notice that the IA2 optimal set, (1.0,0.9), nearly corresponds to the free mass combination. We can understand this result as follows: the optimal set is defined as that combination of effective masses which gives the best fit to all experimental spin observables. As the calculation of Ref. [Ho88] also indicates, the  $D_{i'j}$ 's are better described by a free mass calculation. By taking into account the analyzing power, however, the optimal set is now slightly shifted away from (1.0,1.0) to (1.0,0.9) since  $A_y$  does require an effective mass for a better description. The difference between using the SPVAT form of  $\hat{F}$  and a general Lorentz invariant representation of  $\hat{F}$  can now clearly be identified. The results of Ref. [Ho88] indicate that  $A_y$  is better described by an effective mass for the projectile and target while the other  $D_{i'j}$ 's prefer the free mass calculation. The IA2 representation does not lead to such a strong quenching effect in  $A_y$  (hence IA1 gives a better prediction of  $A_y$  than IA2 for  $^{40}\text{Ca}(\vec{p}, \vec{p}')$  at  $T_{lab} = 500$  MeV) but it is consistent in that it predicts very little medium effects for all spin observables, reflected in the fact that the optimal set, (1.0,0.9), nearly corresponds to the free mass combination. One concludes that, even though there may exist some combination of effective masses which leads to a better description of  $A_y$ , it is not necessarily the optimal, which is defined to be that combination which gives the best fit to the data (at the peak) for all spin observables.

The quenching effect becomes smaller as the energy is lowered to 420 MeV (see Fig 3.19) and is entirely negligible at 290 MeV (see Fig 3.20). At  $T_{lab} = 200$  MeV (see Fig 3.22) there is very little medium effect in  $A_y$  and the calculations using a free mass and an effective mass do not predict  $A_y$  at all. For this reaction we did not extract an optimal set due to the lack of a complete set of experimental data. However our previous calculations do show that there is in general not such a large difference between the optimal set and the effective masses taken from Table II in Ref. [Hi94]. We can therefore make the following general statement: The prediction of  $A_y$  for  $(\vec{p}, \vec{p}')$  scattering through the use of an optimal effective mass set becomes poorer as the energy is lowered within the RPWIA2 framework. It is evident from Figs 3.19 to 3.21 that as the energy is lowered, the medium effect in all spin observables is very small and that all three types of calculations give comparable results for  $(\vec{p}, \vec{p}')$  scattering. Figs 3.18 to 3.21 show that the value of  $D_{nn}$  at the quasielastic peak is shifted away from the optimal IA2 theoretical calculation as the energy is lowered. This corresponds to the behaviour in Figs. 3.9 to 3.12 where the data points progressed further from the effective mass bands as the energy is lowered. Referring to Figs 3.23 and 3.24 we notice that, just as in Fig 3.18, IA2 predicts no medium effect in the analyzing power for the reaction  $^{40}\text{Ca}(\vec{p}, \vec{n})$  at  $T_{lab} = 495$  MeV and  $\theta_{lab} = 18^\circ$  and  $27^\circ$ . For the lower energy of  $T_{lab} = 200$  MeV (see Fig 3.25) there is very little medium effect in  $A_y$ . As the angle increases so does the difference between the free mass calculation and an effective mass calculation to the right of the quasielastic



peak (see Figs 3.26 to 3.27) for  $T_{lab} = 200$  MeV. The calculation also gives a fairly good description of the data at this low energy. As for the  $(\vec{p}, \vec{p}')$  observables, there is very little medium effect in the  $D_{ij}$ 's at  $T_{lab} = 495$  MeV, however the comparison with data is now significantly poorer than for the corresponding  $(\vec{p}, \vec{p}')$  observables, especially at  $\theta_{lab} = 27^\circ$ . It is significant that the RPWIA fails at 495 MeV for the  $(\vec{p}, \vec{n})$  reaction since one would expect this to be a favourable energy. A possible cause could be multiple scattering effects since many of the  $D_{ij}$ 's are close to zero in the experimental data. The IA2 prediction of the  $D_{ij}$ 's is fairly good for the reaction  $^{40}\text{Ca}(\vec{p}, \vec{p}')$  at  $T_{lab} = 200$  MeV (see Fig 3.25), except for  $D_{\nu s}$  and  $D_{nn}$ . From Figs 3.26 to 3.27 we notice that the quality of the IA2 prediction of the  $D_{ij}$ 's decreases with an increase in the laboratory scattering angle.

### 3.7 Summary and Conclusions

In this chapter we applied the general Lorentz invariant representation of the NN scattering matrix to the calculation of complete sets ( $A_y, D_{\ell, \ell}, D_{s', s}, D_{\ell, s}, D_{s', \ell}$  and  $D_{nn}$ ) of quasielastic spin observables for both  $(\vec{p}, \vec{p}')$  and  $(\vec{p}, \vec{n})$  scattering. In order to ascertain the degree to which medium effects, i.e. the use of effective projectile and target nucleon masses, can describe the experimental data, we introduced the concept of an effective mass band which is shown in Figs 3.9 to 3.16. The band in each figure represents the range of values of the spin observable in question which is found by varying  $\frac{M_1}{M}$  and  $\frac{M_2}{M}$  over the full range specified in Eq. (3.21). In conjunction with this we extracted an optimal effective mass combination, which is defined as that set of effective projectile and target nucleon masses which gives the best fit to all experimental spin observables for a particular reaction and laboratory kinetic energy, for both  $(\vec{p}, \vec{p}')$  and  $(\vec{p}, \vec{n})$  scattering. These results are summarised in Table 3.2. In order to calculate the effective mass bands and the optimal effective mass combinations we used the values of the spin observables at the quasielastic peak since the spin observables are in general fairly constant with excitation energy. For the reaction at the quasielastic peak we distinguished between the cases where we neglect the Fermi motion of the target nucleon (this corresponds to free NN kinematics) and where we include the Fermi motion of the target nucleon. Neglecting the Fermi motion allows one to do a simple first-order calculation of the effective mass bands and the optimal effective mass combinations as well as comparing IA1- with IA2-based predictions of the spin observables. Inclusion of the Fermi motion of the target nucleon does not lead to results which differ much from the case when Fermi motion is neglected: This is illustrated in Fig 3.17 which must be compared to Fig 3.9. Finally we also presented, in Figs 3.18 to 3.30, the predictions for the spin observables as a function of energy transfer using the IA2 representation of  $\hat{F}$ . Below we summarise the main features of our investigation.

The shape of both the IA1 and IA2 effective mass bands do not vary much over the entire range of  $T_{lab}$  for  $(\vec{p}, \vec{p}')$  scattering. Even though the IA2 effective mass band becomes wider for  $D_{nn}$  as the energy is lowered, the data point lies outside the effective



mass band. The shape of the effective mass bands do vary with energy for the  $(\vec{p}, \vec{n})$  reaction. For  $(\vec{p}, \vec{p}')$  scattering the prediction of  $A_y$  and  $D_{nn}$  at the quasielastic peak by the optimal IA2 curve becomes poorer as the energy decreases. The quenching effect in  $A_y$ , as a function of energy transfer,  $\omega$ , becomes negligible as the incident laboratory energy decreases for  $(\vec{p}, \vec{p}')$  scattering and there is very little medium effect in the analyzing power. The other observables are still fairly well described by the optimal IA2 curve as a function of  $\omega$  and at the quasielastic peak (i.e. as a function of laboratory scattering angle), except for  $D_{nn}$ . The analyzing power for the  $(\vec{p}, \vec{n})$  at  $T_{lab} = 200$  MeV is well described by the optimal IA2 curve, however, due to its strong oscillatory motion it fails to reproduce the  $D_{nn}$  data. The  $(\vec{p}, \vec{n})$  calculations at  $T_{lab} = 495$  MeV display no medium effect in  $A_y$  and very little in the other  $D_{ij}$ 's. Our results clearly indicate that the IA2 formalism does not lead to such strong medium effects as the SPVAT form of  $\hat{F}$ . It should be stressed that a given effective mass combination may well lead to large deviations from the free mass calculation but that this set will not necessarily be the optimal set which is defined as that combination which gives the best fit to all experimental spin observables. This can clearly be seen from the effective mass bands plots. It is in this sense that we say that IA2 does not lead to such strong medium effects. It is also reflected in the fact that the optimal set (see Tabel 3.2) extracted taking into account the Fermi motion of the target nucleon is in general close to the free mass combination for all reactions and laboratory energies. Our results also show that one needs target and projectile relativity (albeit small) to give a reasonable description of the data.

Let us now address the questions which were posed in the introduction of this chapter:

1. *How successful is the effective mass concept in describing quasielastic  $(\vec{p}, \vec{p}')$  and  $(\vec{p}, \vec{n})$  scattering data ?*

For experimental  $(\vec{p}, \vec{p}')$  and  $(\vec{p}, \vec{n})$  data at the quasielastic peak the effective mass concept does provide an adequate description of the following spin transfer coefficients:  $D_{\ell\ell}, D_{s's}, D_{s'\ell}$  and  $D_{\ell's}$  for the energy range 500 MeV to 200 MeV. For the  $(\vec{p}, \vec{p}')$  reaction one obtains an excellent description but the  $(\vec{p}, \vec{n})$  observables are (compared to the  $(\vec{p}, \vec{p}')$  observables) not so well described. The description of  $D_{nn}$  becomes problematic for both  $(\vec{p}, \vec{p}')$  and  $(\vec{p}, \vec{n})$  scattering as the energy is lowered. For the  $(\vec{p}, \vec{p}')$  reaction the data point shifts away from the effective mass band as the energy is lowered while for the  $(\vec{p}, \vec{n})$  reaction the theoretical calculation exhibits a strong oscillatory motion at 200 MeV which causes it to miss the data which are quite constant as a function of laboratory scattering angle. The optimal effective mass does provide a good description of the  $(\vec{p}, \vec{p}')$   $A_y$  data at the quasielastic peak using the IA2 representation of  $\hat{F}$ . It should be emphasised that even though some effective mass combination may describe  $A_y$  well, it will not necessarily be the optimal set. Furthermore, one finds, that as the energy is lowered the  $A_y$  data point shifts away from the effective mass band. Using the optimal set to calculate  $A_y$  as a function of energy transfer  $\omega$ , leads to a poorer description of  $(\vec{p}, \vec{p}')$  scattering data as the energy is lowered, since the optimal set is in general close to the free mass combination. It is important to note that IA2 produces in general very lit-



tle quenching, even when the effective projectile and target nucleon masses differ significantly from the free nucleon mass, which becomes negligible as the energy is lowered to 200 MeV. The  $(\vec{p}, \vec{n})$  data are, however, much better described by the optimal IA2 set.

2. *Is it possible to find a combination of effective projectile and target nucleon masses  $(\frac{M_1}{M}, \frac{M_2}{M})$  which can describe a complete set of spin observables  $\{A_y, D_{ij}\}$  for  $(\vec{p}, \vec{p}')$  and  $(\vec{p}, \vec{n})$  scattering? Will this set be the same for the two types of reactions?*

In general one can find a combination of effective projectile and target masses which describe  $(\vec{p}, \vec{p}')$  and  $(\vec{p}, \vec{n})$  data. One finds, however, that the optimal set fails to describe  $A_y$  for the  $(\vec{p}, \vec{p}')$  reaction. The optimal set for  $(\vec{p}, \vec{p}')$  and  $(\vec{p}, \vec{n})$  scattering are in general fairly close and constant with incident laboratory kinetic energy and target nucleus when the Fermi motion of the target is included as can be seen from the third column of Table 3.2.

3. *How do numerical results based on the IA1 representation of  $\hat{F}$  compare to those utilising the IA2 representation of  $\hat{F}$ ?*

The use of a complete set of NN amplitudes eliminates the arbitrariness of the five-term representation and it provides a theoretical basis for the off-shell parts of the NN interaction which is absent in the SPVAT form of  $\hat{F}$ . However, numerical calculations indicate that at the quasielastic peak, IA1 and IA2 do provide comparable descriptions of the data if one employs the optimal sets for the two representations. One can understand this result as follows: Since the optimal IA2 set is in general very close to the free mass, it indicates that the dominant subclass must be  $\hat{F}^{11}$ , but in this case IA2 is equivalent to IA1. On the other hand, the shape of the effective mass bands are different for the two representations. The IA2 effective mass band is often narrower than the IA1 band for a particular observable and hence IA1 can give a false indication of the predictive power of an  $M^*$  calculation and of the effect of effective projectile and target nucleon masses on the spin observables.

The calculations also show that the  $(\vec{p}, \vec{p}')$  and  $(\vec{p}, \vec{n})$  observables behave very differently and furthermore the individual spin observables are sensitive to different aspects of the model. This emphasises the fact that one should measure complete sets of  $(\vec{p}, \vec{p}')$  and  $(\vec{p}, \vec{n})$  observables for the same target, energy and momentum transfer since these two reactions provide complementary information and place even further restrictions on any model of quasielastic scattering. Our results indicate that the measurement of a complete set of spin observables for low energy  $(\vec{p}, \vec{p}')$  scattering would be extremely useful since this is exactly the place where the RPWIA2 model fails.

In this investigation the effective masses were treated as free parameters and it was found that *no effective mass combination could describe both  $(\vec{p}, \vec{p}')$  and  $(\vec{p}, \vec{n})$  scattering observables*. Even though the IA2 treatment of medium effects (within the RPWIA framework) is the most advanced to date it still fails to describe all observables; the glaring example being the prediction of  $A_y$  for  $(\vec{p}, \vec{p}')$  scattering as the energy is lowered from 500 MeV to 200 MeV. Despite the successes of the Walecka model effective mass concept and

the plane wave approximation the theoretical work should now start to include additional effects like multiple scattering and distortions of the projectile. A theoretical formalism (initially employing the IA1 representation of  $\hat{F}$ ) to include the latter effect has been presented in Ref. [Hi99] but this still needs to be implemented numerically.

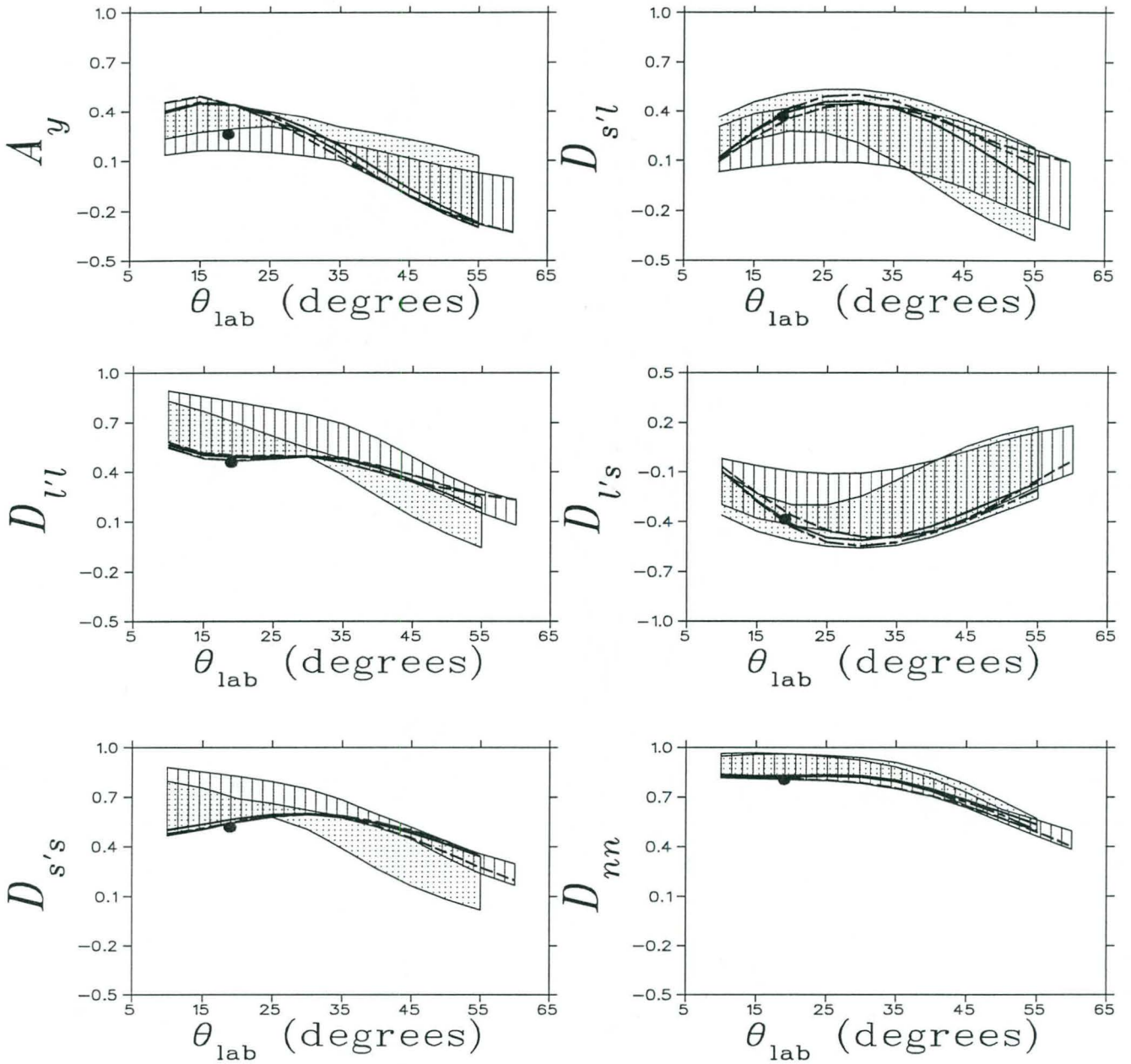


Figure 3.17: Values of  $A_y$  and  $D_{i'j}$  versus  $\theta_{\text{lab}}$  for  $^{40}\text{Ca}(\vec{p}, \vec{p}')$  at  $T_{\text{lab}} = 500$  MeV. This figure includes the Fermi motion of the target nucleon. Compare the shape of the effective mass bands to Fig 3.9 which neglected the Fermi motion of the target nucleon. Solid and dashed lines represent the calculations with optimal effective mass values in respectively the IA2 and IA1 representations. The hatched bands denote the range of values which result from varying  $\frac{M_1}{M}$  and  $\frac{M_2}{M}$  over the full range (see text). The straight line hatch pattern denotes the IA1 model; the dotted hatch pattern the IA2 model. The long-dash-short-dash lines represent the free mass values. Data (at  $\theta_{\text{lab}} = 19^\circ$ ) are from Ref. [Ca84].



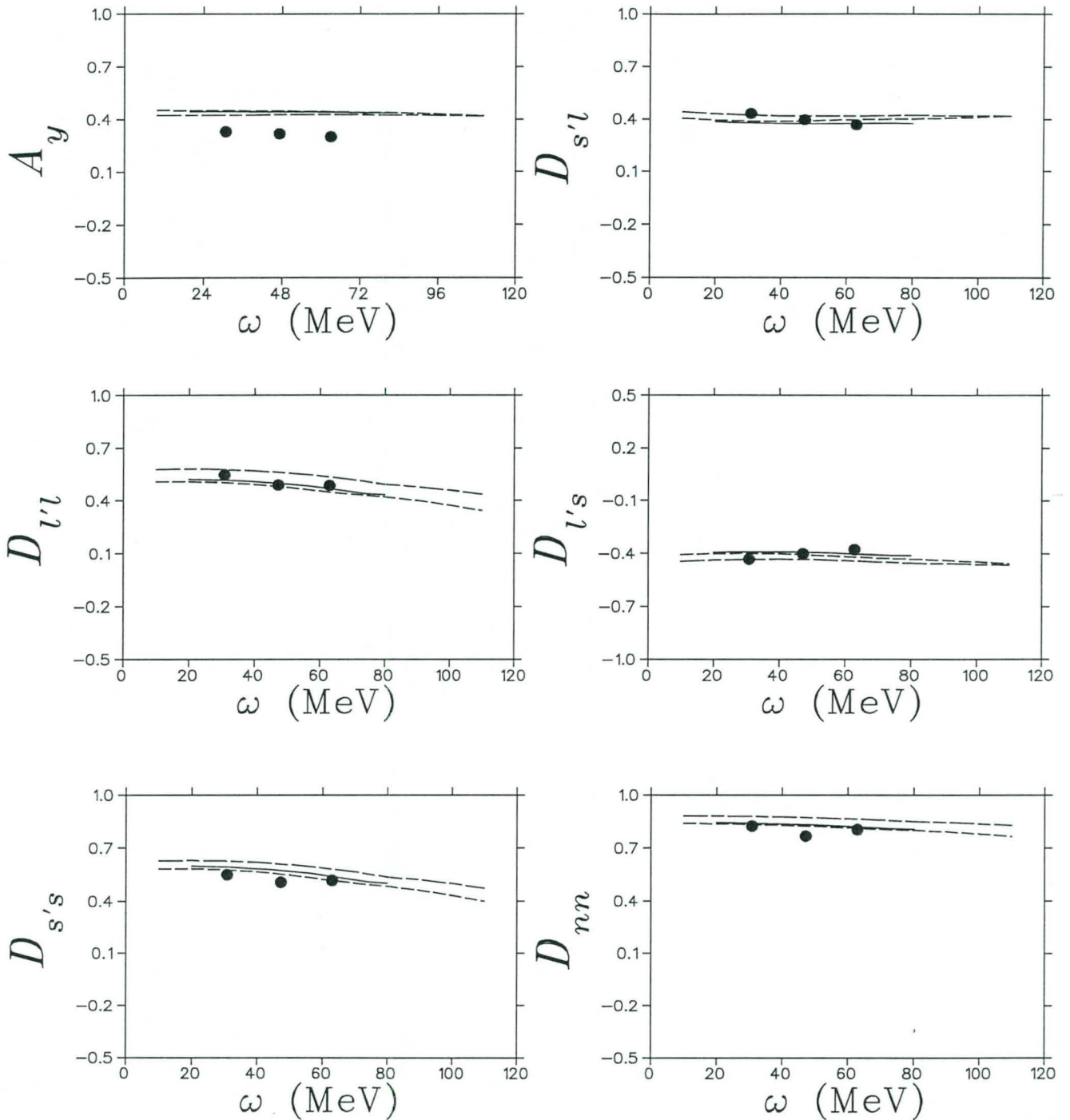


Figure 3.18: Values of  $A_y$  and  $D_{ij}$  versus energy transfer,  $\omega$ , for the reaction  $^{40}\text{Ca}(\vec{p}, \vec{p}')$  at  $T_{\text{lab}} = 500$  MeV and  $\theta_{\text{lab}} = 19^\circ$ . The solid and dashed lines represent the IA2 optimal mass set and the free mass calculations respectively. The long-dash-short-dash line corresponds to the values  $\frac{M_1}{M} = M_{1\text{SC}}^*$  and  $\frac{M_2}{M} = M_{2\text{SC}}^*$  (see text and Ref. [Hi94]), calculated from self-consistent (SC) nuclear potentials. The peak is located at  $\omega \approx 63$  MeV and the data are from Ref. [Ca84].

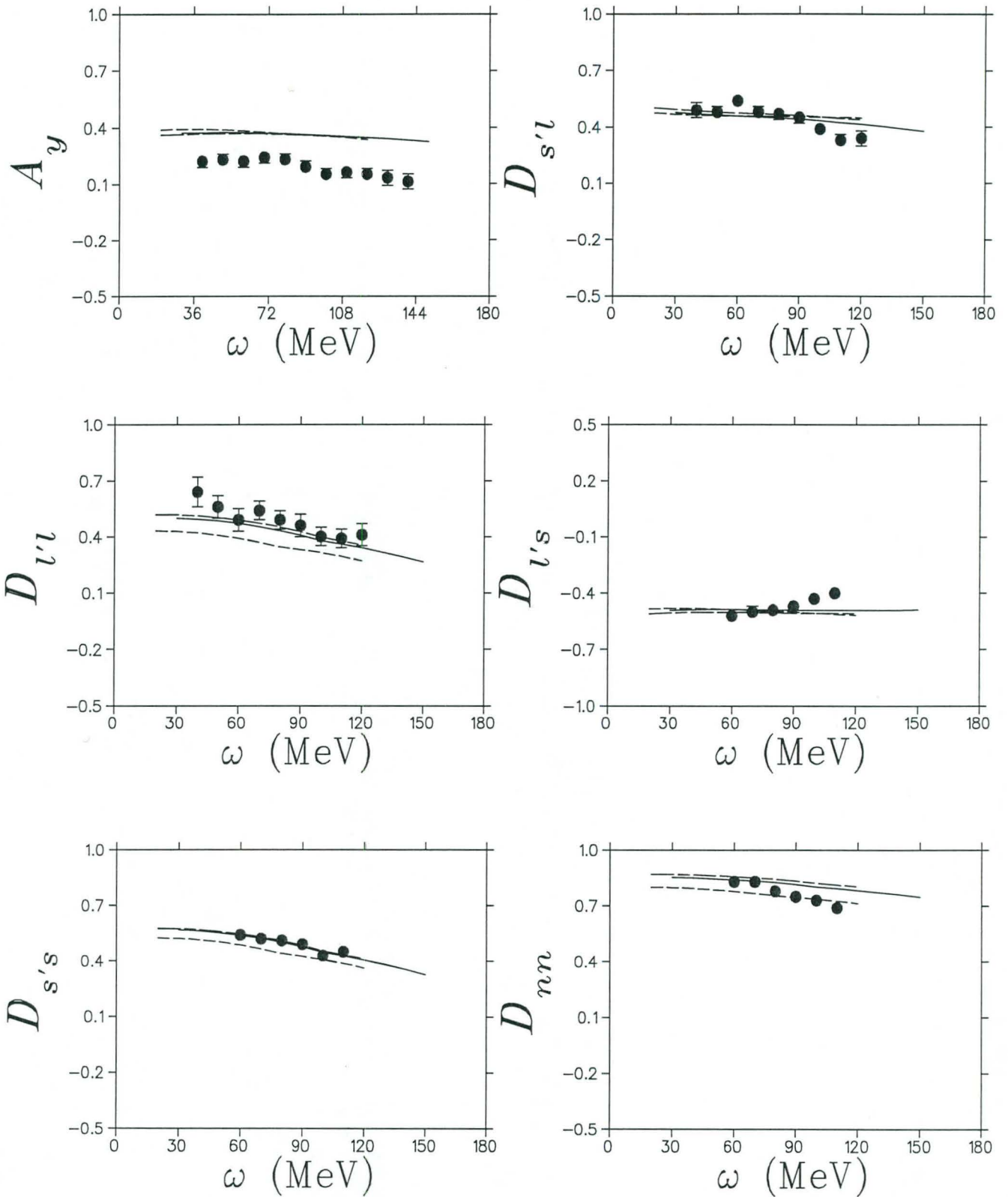


Figure 3.19: Similar to Fig 3.18 for the reaction  $^{12}\text{C}(\bar{p}, \bar{p}')$  at  $T_{\text{lab}} = 420$  MeV and  $\theta_{\text{lab}} = 24^\circ$ . The peak is located at  $\omega \approx 93$  MeV and the data are from Refs. [Ch89, Ch90].

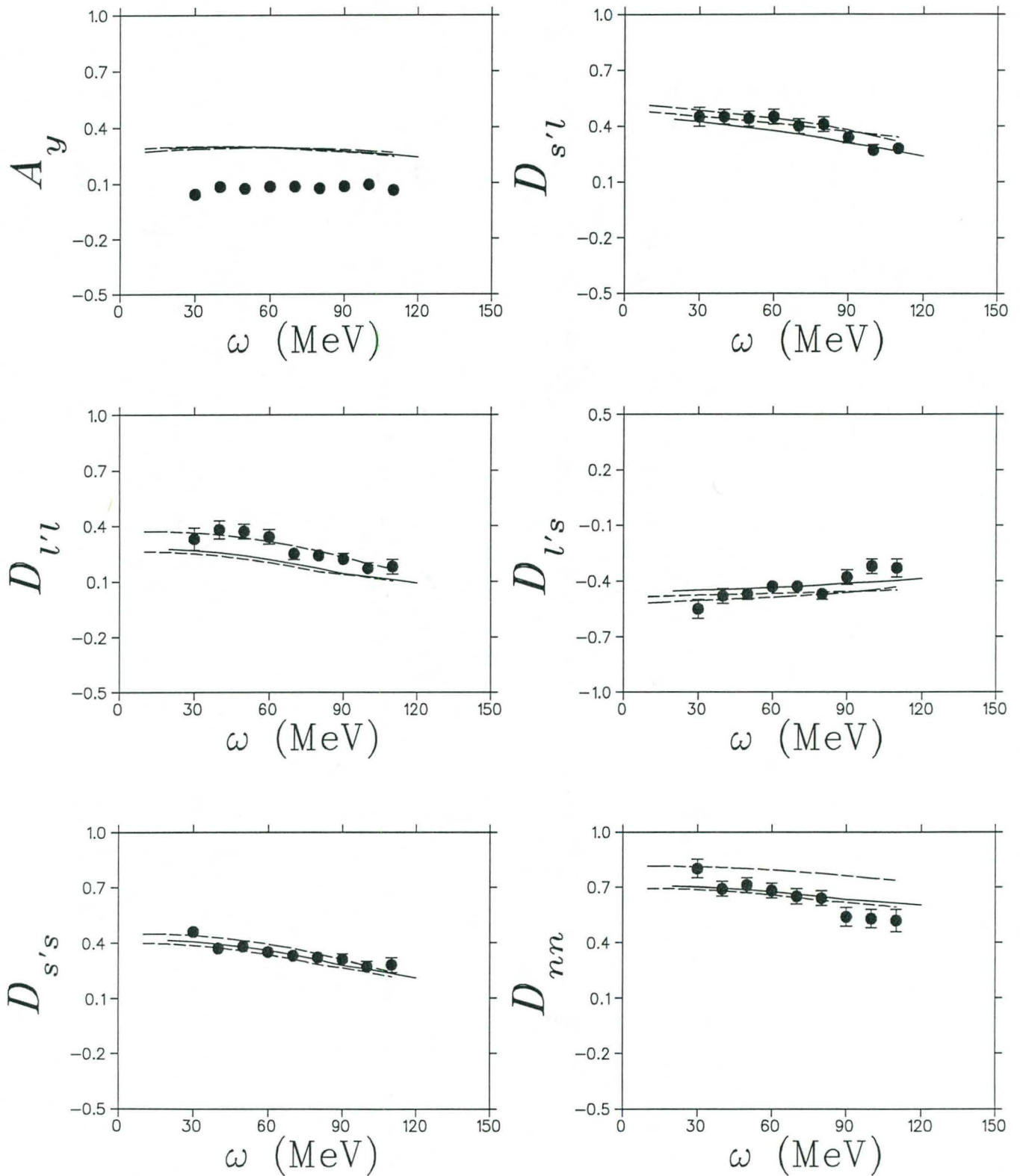


Figure 3.20: Similar to Fig 3.18 for the reaction  $^{12}\text{C}(\bar{p}, \bar{p}')$  at  $T_{\text{lab}} = 290$  MeV and  $\theta_{\text{lab}} = 30^\circ$ . The peak is located at  $\omega \approx 90$  MeV and the data are from Ref. [Ch90].



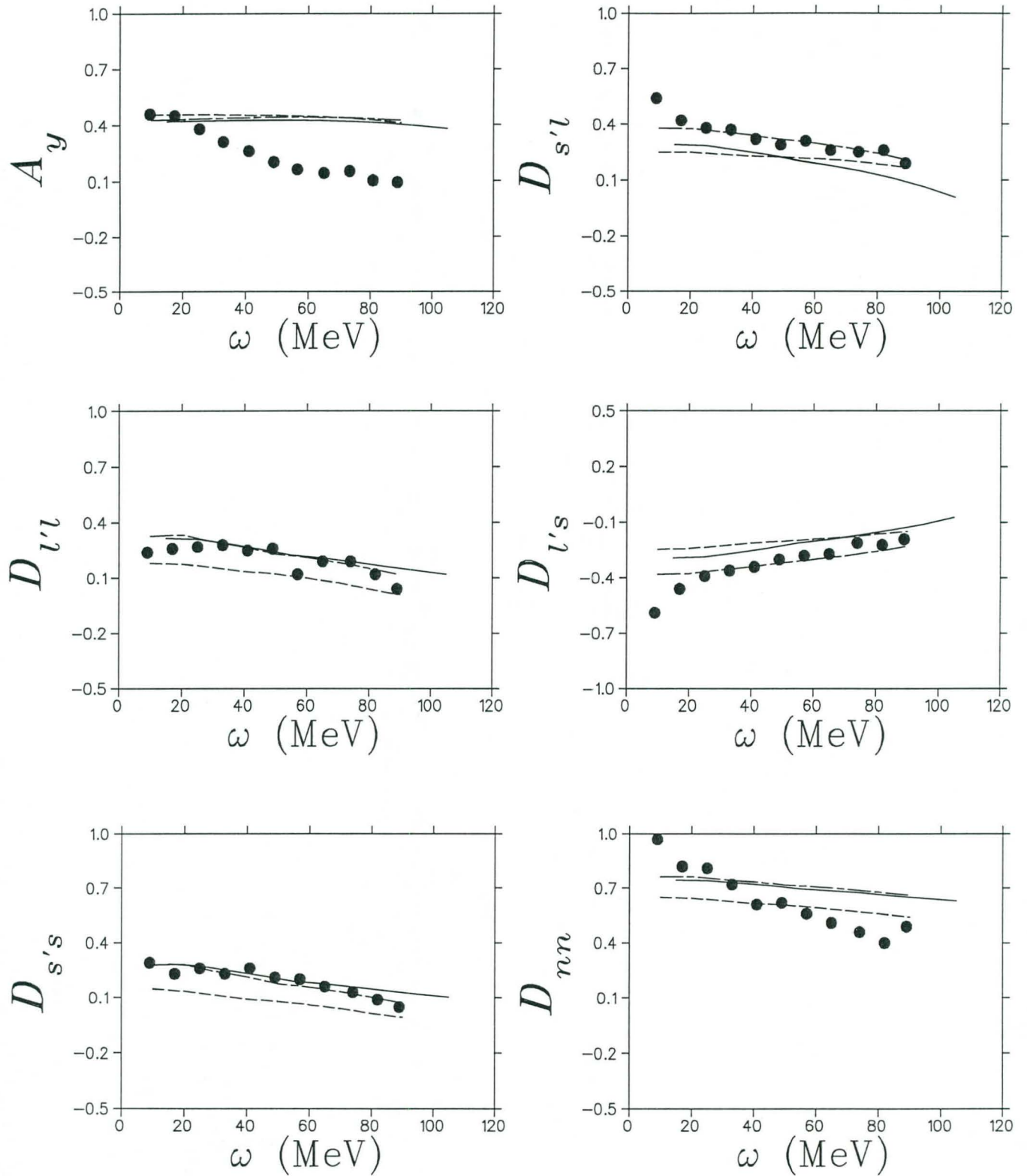


Figure 3.21: Similar to Fig 3.18 for the reaction  $^{54}\text{Fe}(\vec{p}, \vec{p}')$  at  $T_{\text{lab}} = 290$  MeV and  $\theta_{\text{lab}} = 20^\circ$ . The peak is located at  $\omega \approx 40$  MeV and the data are from Ref. [Hä88].

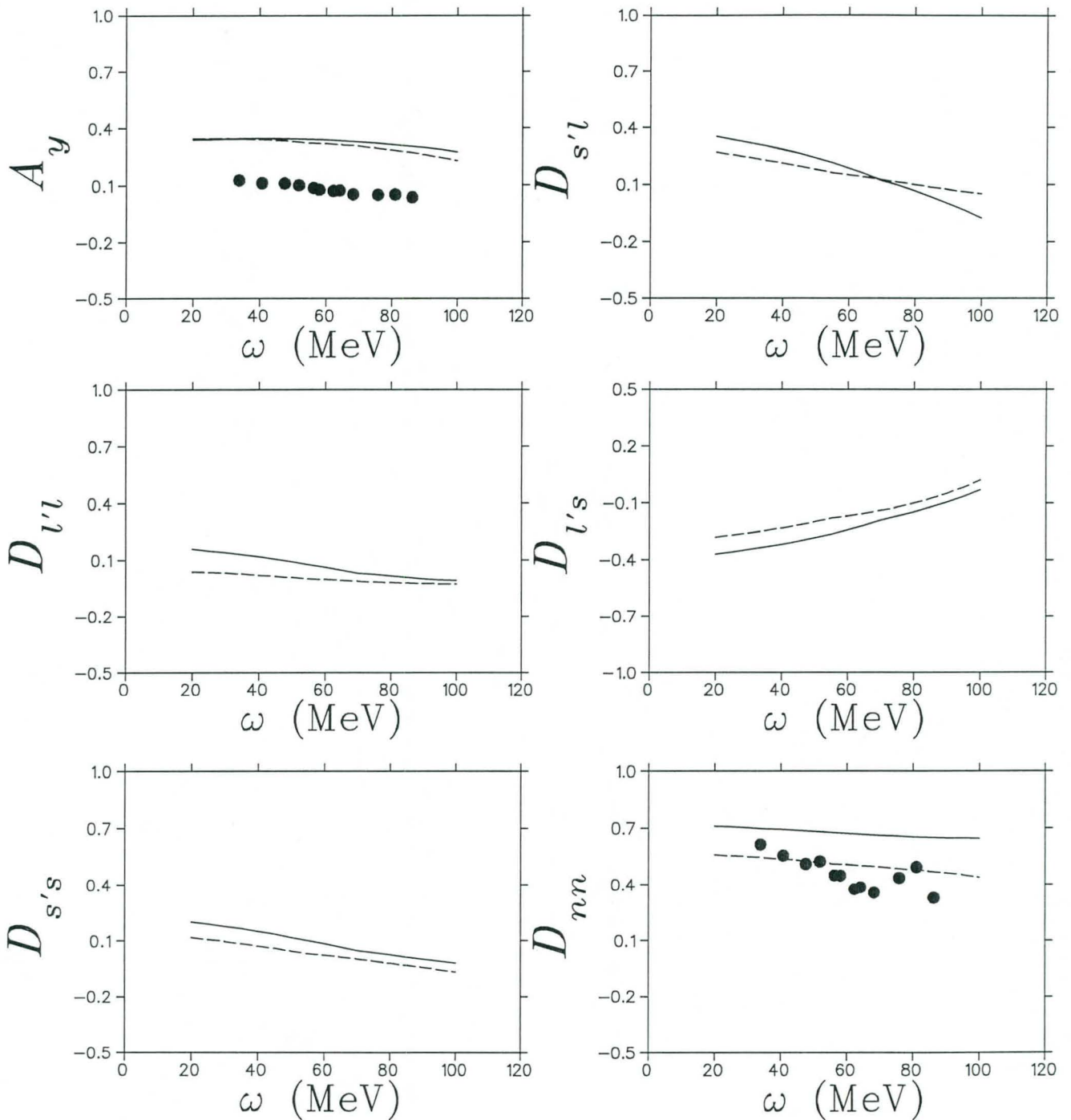


Figure 3.22: For this reaction,  $^{40}\text{Ca}(\vec{p}, \vec{p}')$  at  $T_{lab} = 200$  MeV and  $\theta_{lab} = 30^\circ$ , no optimal set was extracted due to the lack of a complete set of experimental spin observables. The solid line corresponds to the choice,  $\frac{M_1}{M} = M_{1SC}^*$  and  $\frac{M_2}{M} = M_{2SC}^*$  (see Fig. 3.18) while the dashed line refers to the free calculation. The peak is located at  $\omega \approx 64$  MeV and the data are from Ref. [Ca95].

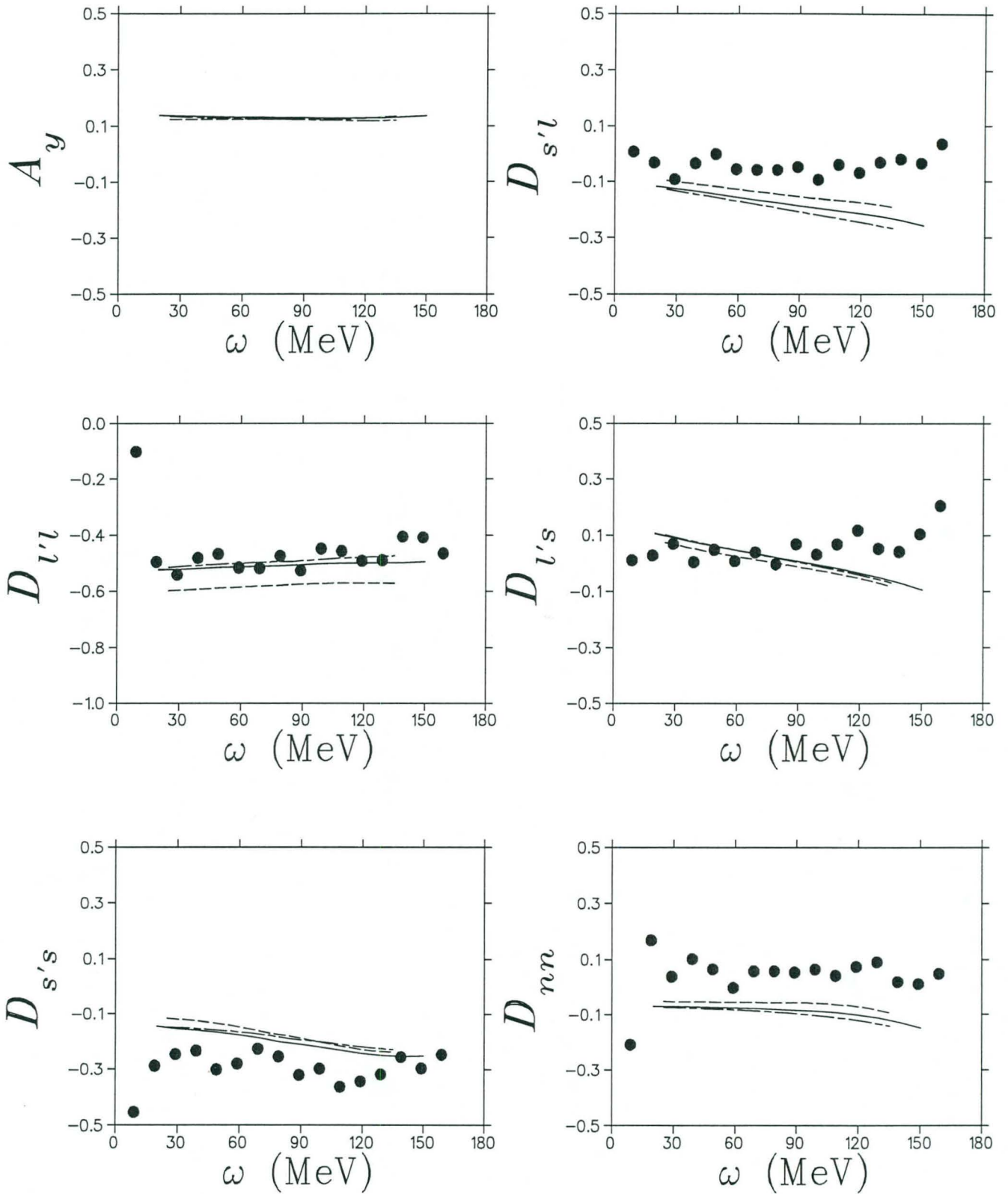


Figure 3.23: Similar to Fig 3.18 for the reaction  $^{40}\text{Ca}(\vec{p}, \vec{n})$  at  $T_{\text{lab}} = 495$  MeV and  $\theta_{\text{lab}} = 18^\circ$ . The peak is located at  $\omega \approx 82$  MeV and the data are from Ref. [Ta98].



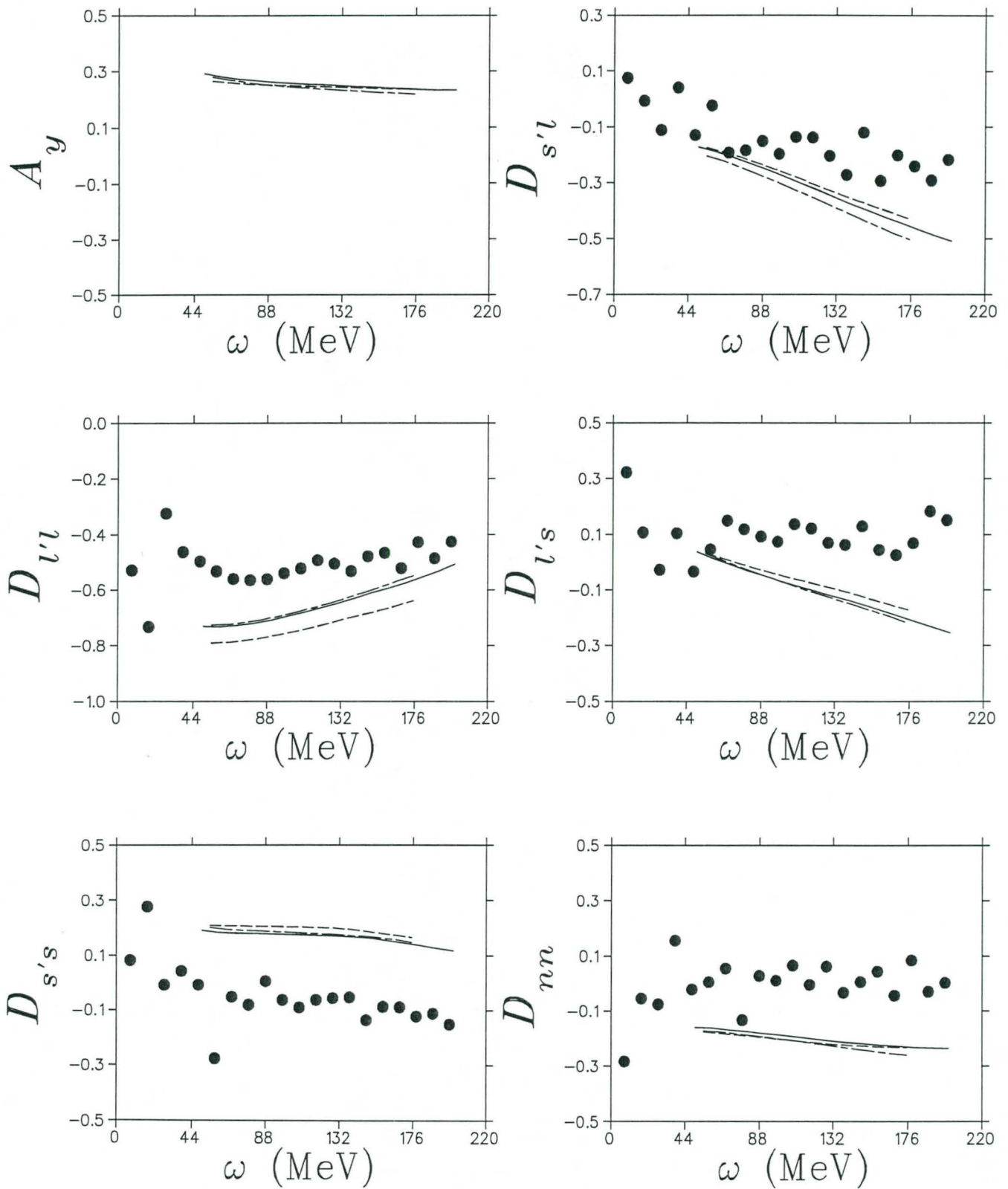


Figure 3.24: Similar to Fig 3.18 for the reaction  $^{40}\text{Ca}(\vec{p}, \vec{n})$  at  $T_{\text{lab}} = 495$  MeV and  $\theta_{\text{lab}} = 27^\circ$ . The peak is located at  $\omega \approx 138$  MeV and the data are from Ref. [Ta98].

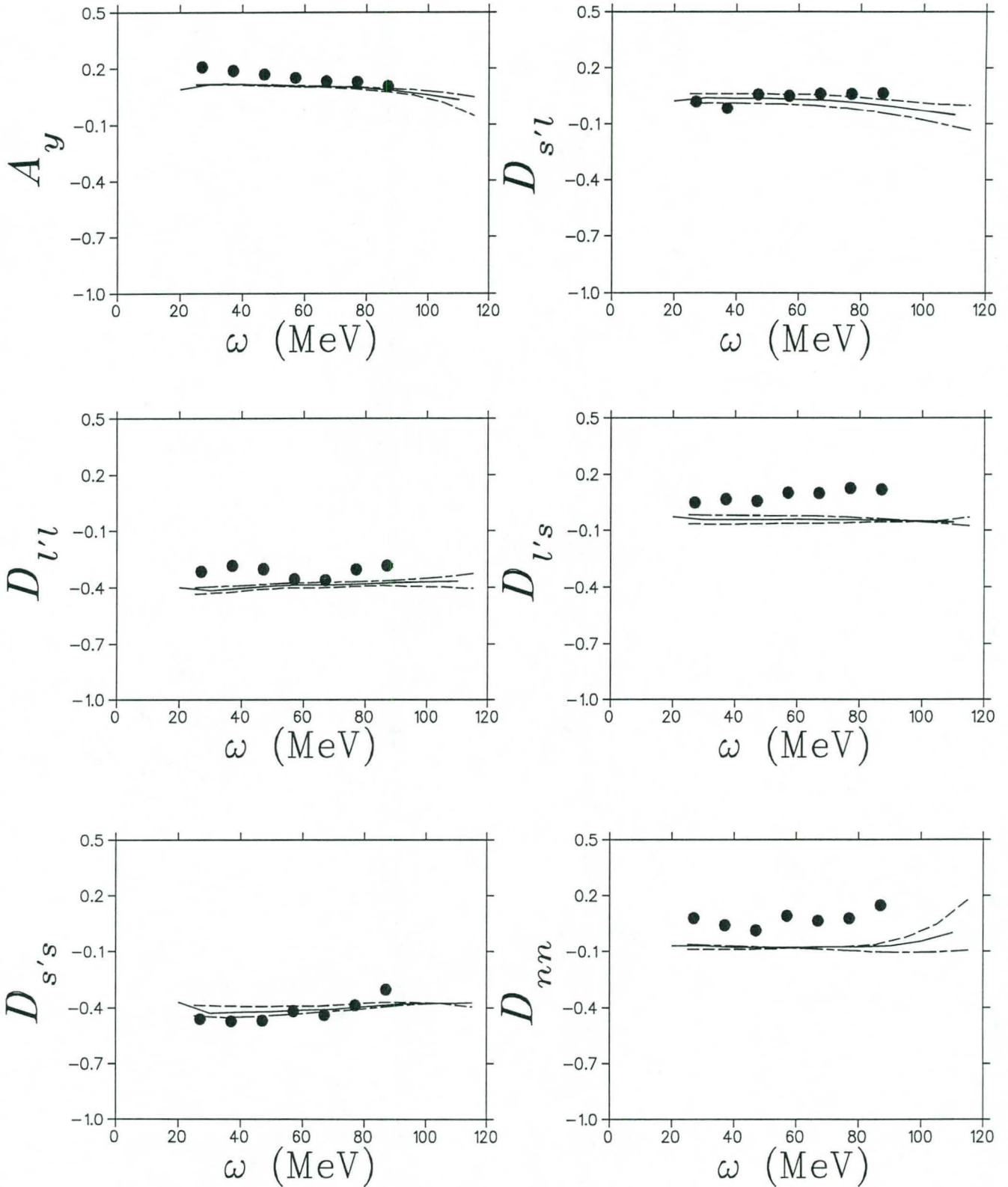


Figure 3.25: Similar to Fig 3.18 for the reaction  $^{40}\text{Ca}(\bar{p}, \bar{n})$  at  $T_{\text{lab}} = 200$  MeV and  $\theta_{\text{lab}} = 24^\circ$ . The peak is located at  $\omega \approx 67$  MeV and the data are from Ref. [Ha98].

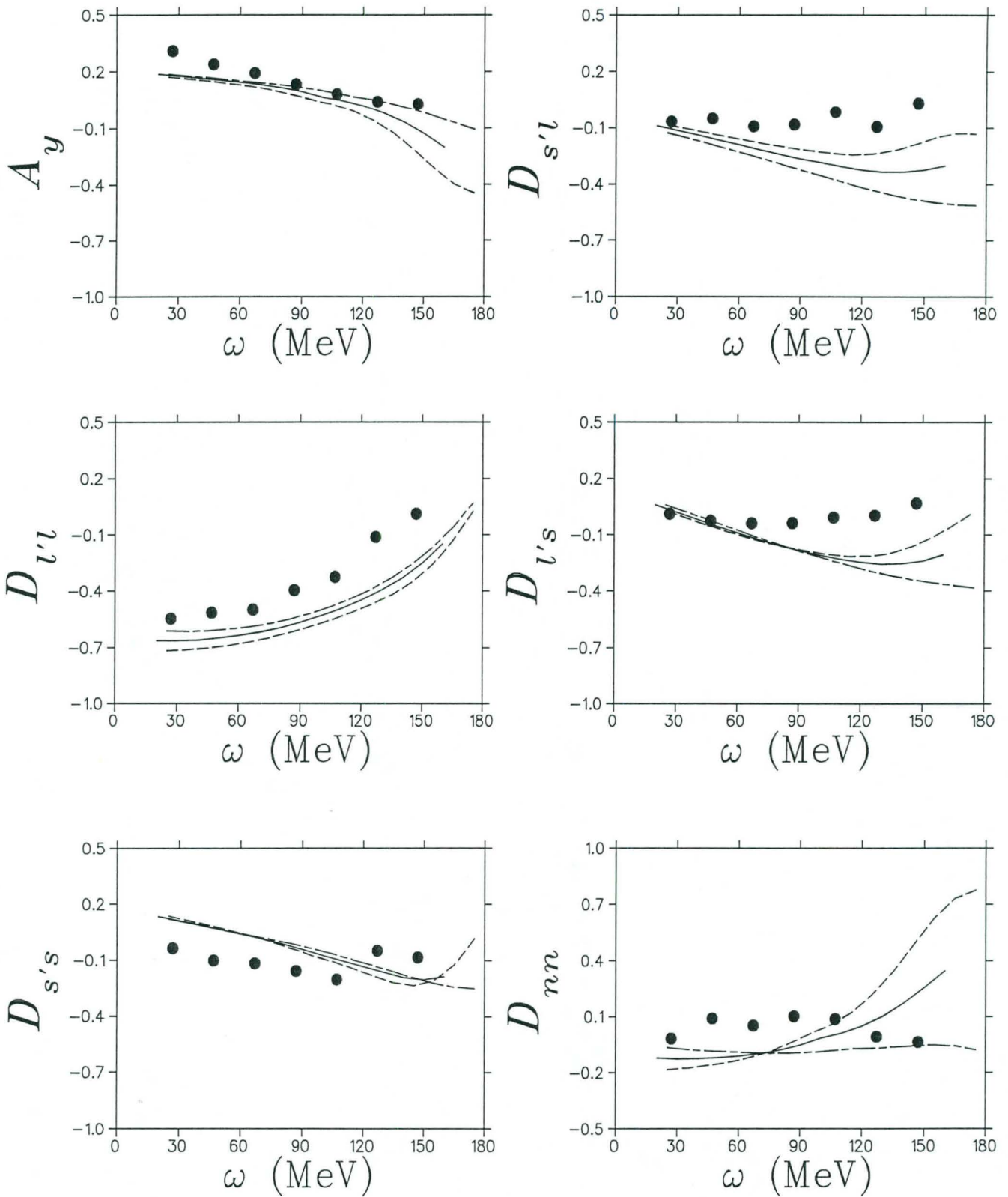


Figure 3.26: Similar to Fig 3.18 for the reaction  $^{40}\text{Ca}(\vec{p}, \vec{n})$  at  $T_{\text{lab}} = 200$  MeV and  $\theta_{\text{lab}} = 37^\circ$ . The peak is located at  $\omega \approx 107$  MeV and the data are from Ref. [Ha98].



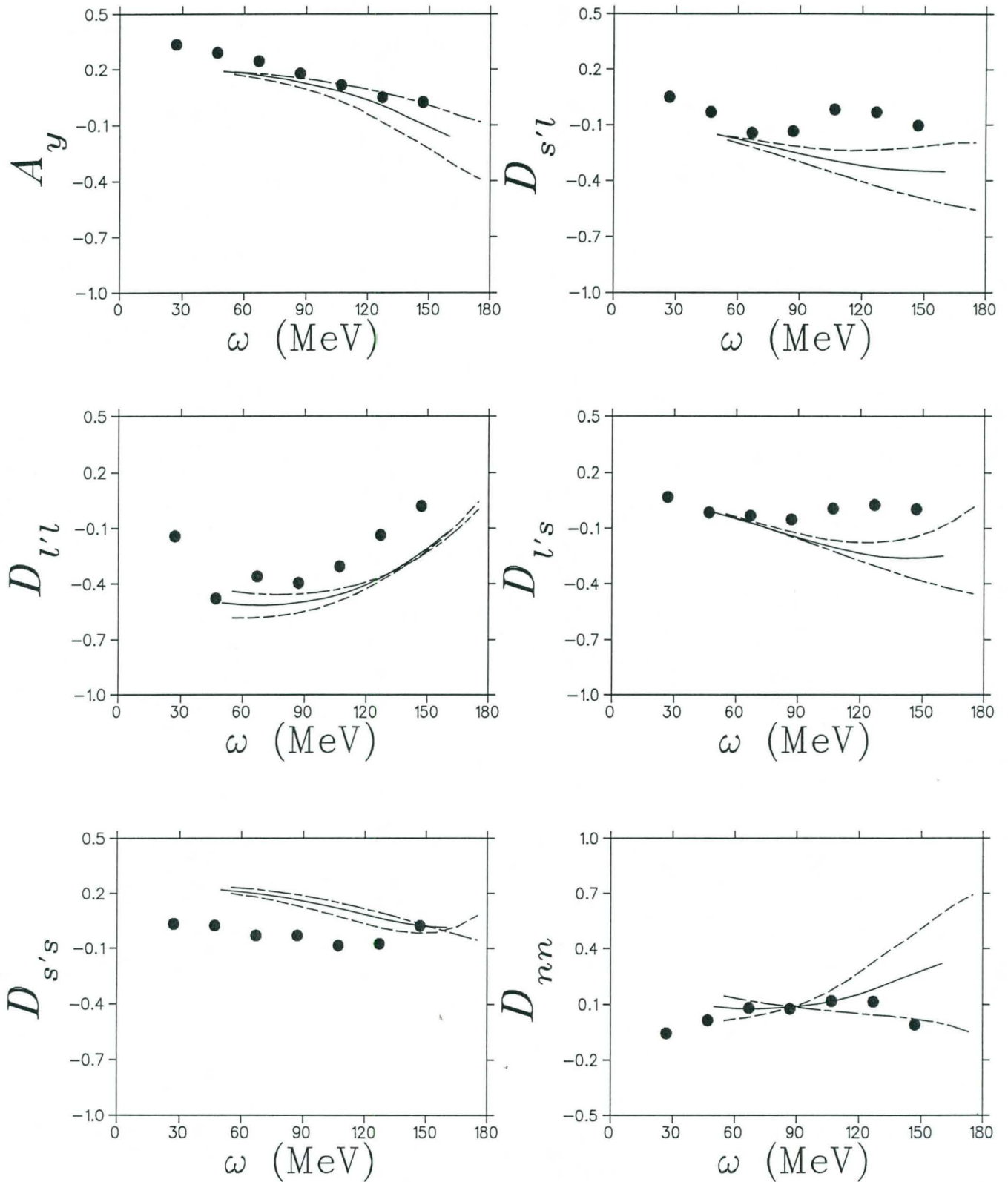


Figure 3.27: Similar to Fig 3.18 for the reaction  $^{40}\text{Ca}(\vec{p}, \vec{n})$  at  $T_{\text{lab}} = 200$  MeV and  $\theta_{\text{lab}} = 48^\circ$ . The peak is located at  $\omega \approx 127$  MeV and the data are from Ref. [Ha98].

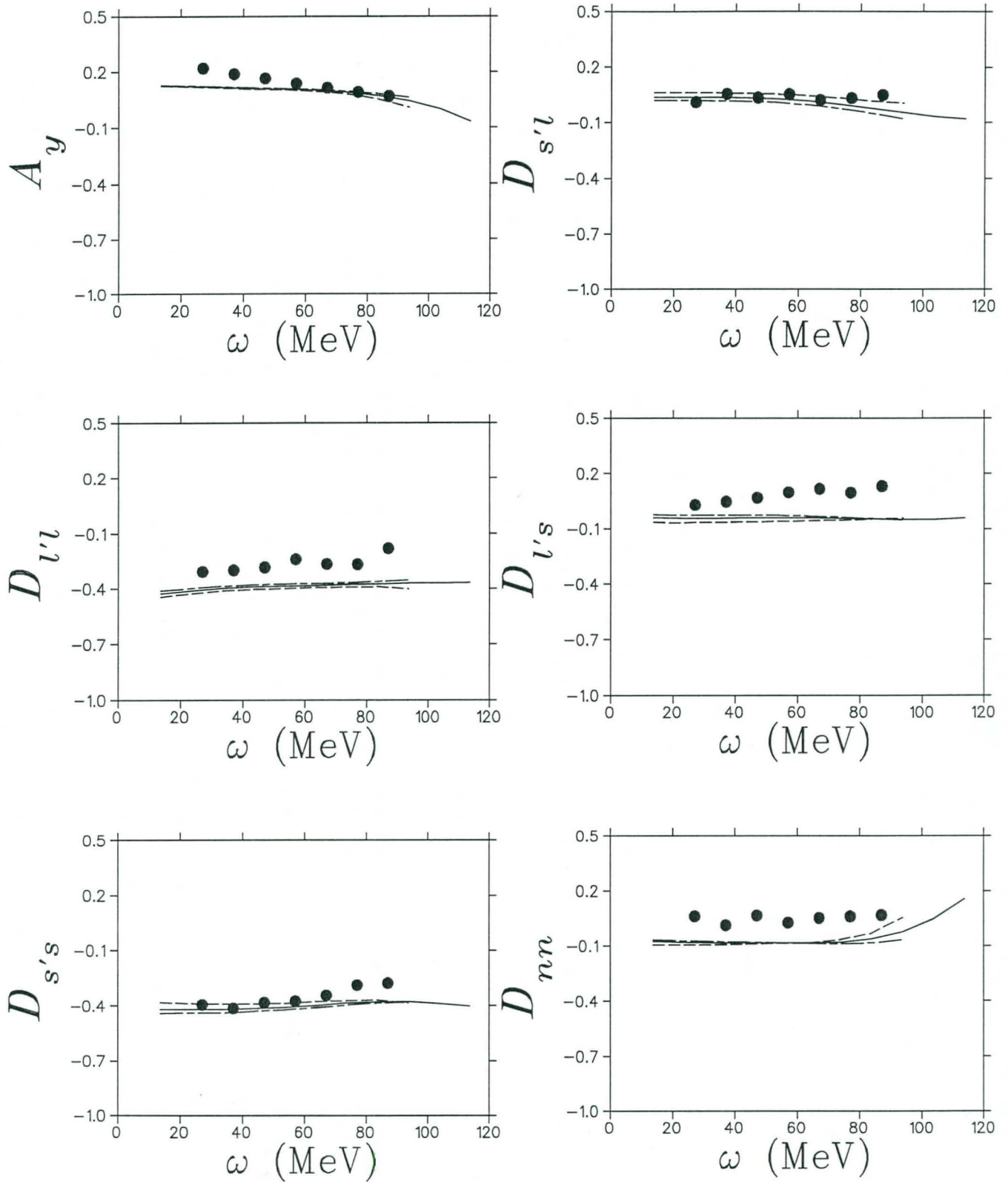


Figure 3.28: Similar to Fig 3.18 for the reaction  $^{208}\text{Pb}(\vec{p}, \vec{n})$  at  $T_{\text{lab}} = 200$  MeV and  $\theta_{\text{lab}} = 24^\circ$ . The peak is located at  $\omega \approx 67$  MeV and the data are from Ref. [Ha98].

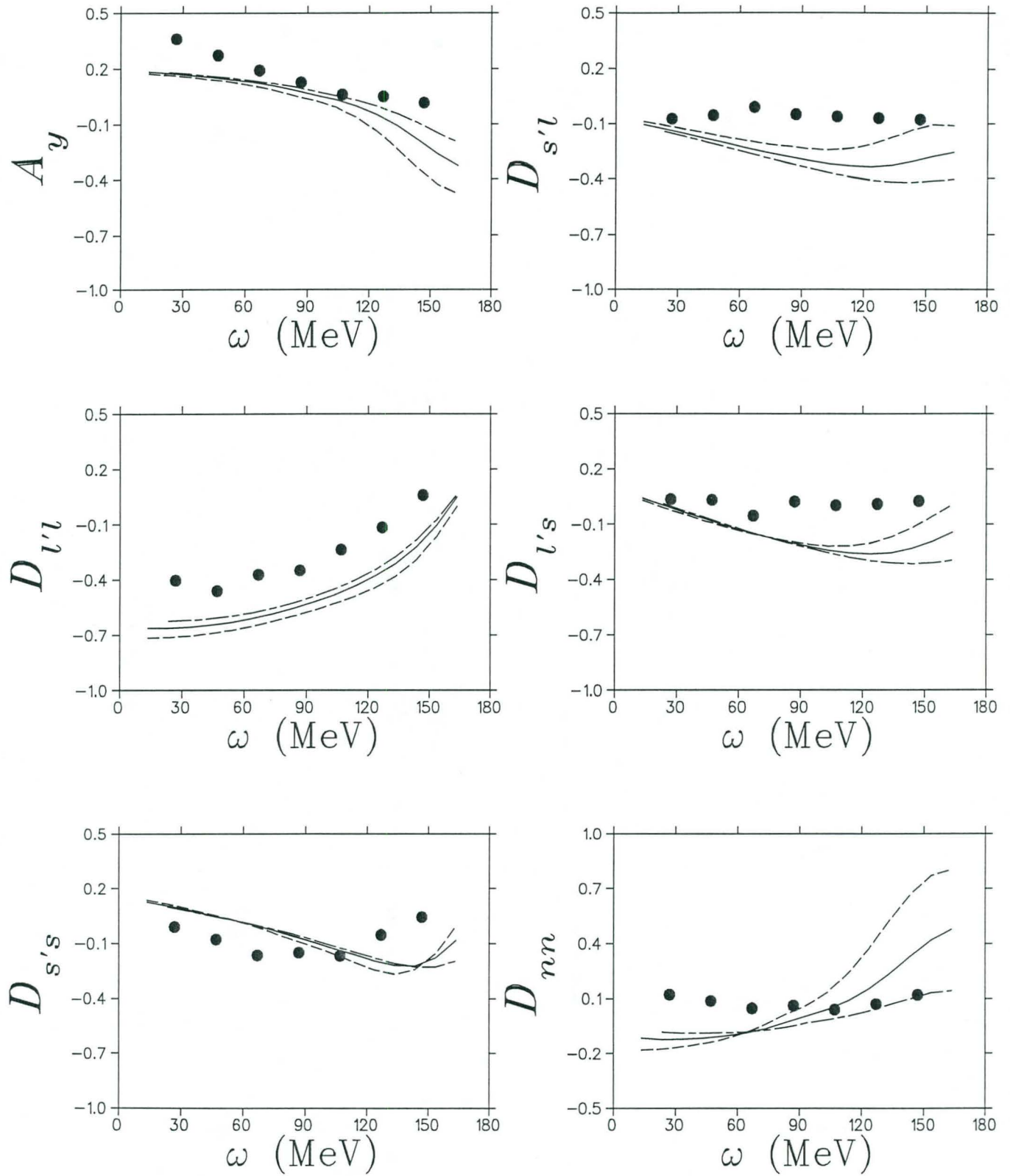


Figure 3.29: Similar to Fig 3.18 for the reaction  $^{208}\text{Pb}(\vec{p}, \vec{n})$  at  $T_{\text{lab}} = 200$  MeV and  $\theta_{\text{lab}} = 37^\circ$ . The peak is located at  $\omega \approx 127$  MeV and the data are from Ref. [Ha98].



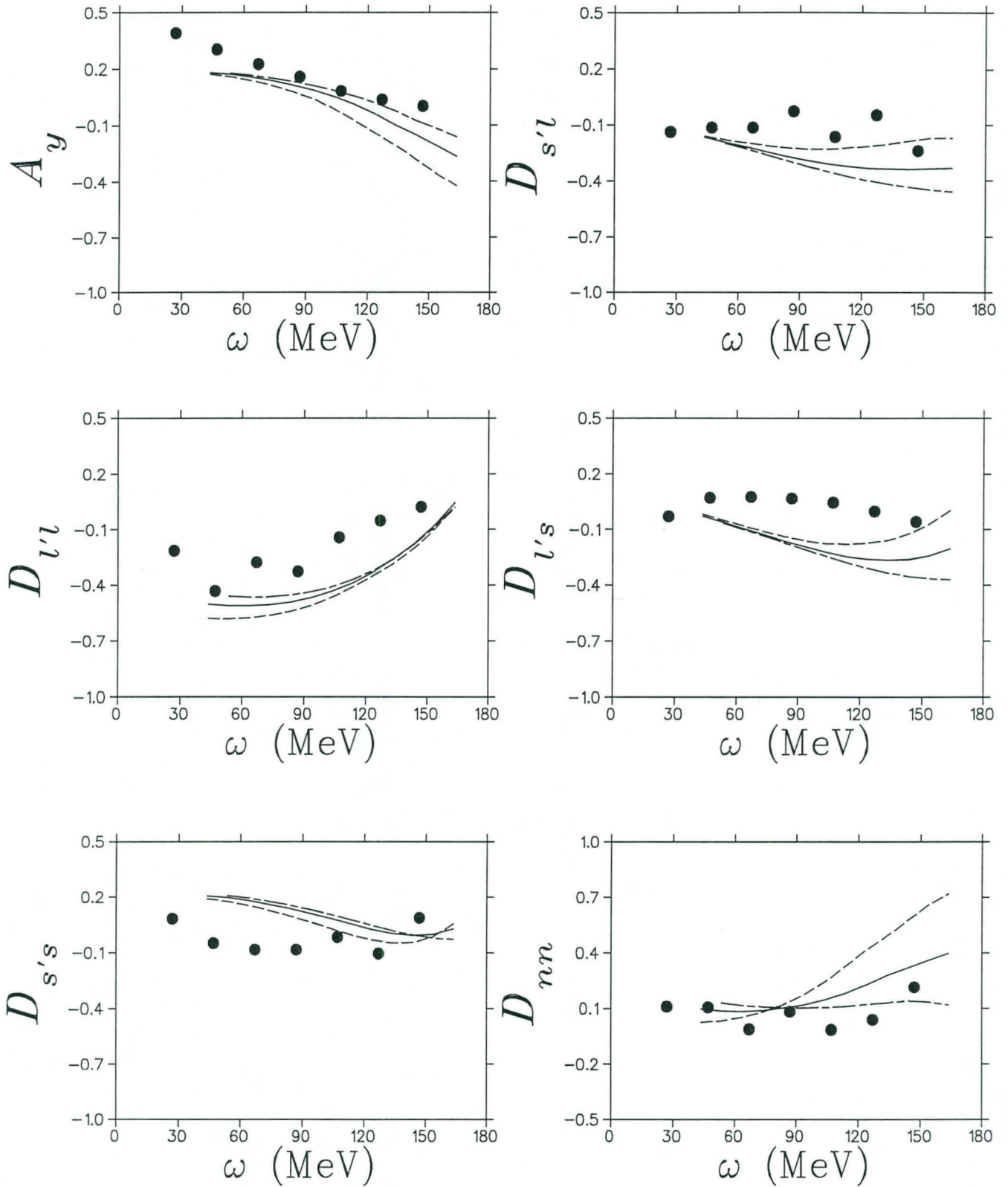


Figure 3.30: Similar to Fig 3.18 for the reaction  $^{208}\text{Pb}(\vec{p}, \vec{n})$  at  $T_{lab} = 200$  MeV and  $\theta_{lab} = 48^\circ$ . The peak is located at  $\omega \approx 127$  MeV and the data are from Ref. [Ha98].

## Appendix A

# Transformation properties of covariants, $\Gamma_n$ , under charge symmetry and time-reversal transformations

### A.1 Transformation properties of covariants, $\Gamma_n$ under a charge symmetry transformation

In this appendix we illustrate how to calculate the transformation properties of the covariants,  $\Gamma_n$  under a charge symmetry transformation.

The *SPVAT* covariants do not contain any momenta and therefore

$$\begin{aligned}\hat{P}_{1'2'}\tilde{S}f_n^{ij}(\underline{s})\Gamma_n(\eta_{ij})\hat{P}_{12}\tilde{S} &= f_n^{ij}(\overset{\leftrightarrow}{\underline{s}})\tilde{S}\Gamma_n(\eta_{ij})\tilde{S} \\ &= f_n^{ij}(\underline{s})\Gamma_n(\eta_{ij}) \quad \forall n = 1\dots 5\end{aligned}$$

where  $\overset{\leftrightarrow}{\underline{s}}$  is a collective index designating the set:

$$\{s_1, s_2, s_3, s_4, s_5, -s_6, -s_7\}$$

since  $s_6$  and  $s_7$  are odd under simultaneous interchange of 1 (1') and 2 (2'). For the other covariants we consider as an example  $\Gamma_6$ .

$$\begin{aligned}\hat{P}_{1'2'}\tilde{S}f_6^{ij}(\underline{s})\Gamma_6(\eta_{ij})\hat{P}_{12}\tilde{S} &= \hat{P}_{1'2'}\tilde{S}f_6^{ij}(\underline{s})[Q_{11,\mu}(I_4 \otimes \gamma^\mu) + Q_{22,\mu}(\gamma^\mu \otimes I_4) + \\ &Q_{21,\mu}(\gamma^\mu \otimes I_4)\tilde{S} + Q_{12,\mu}(I_4 \otimes \gamma^\mu)\tilde{S}]\hat{P}_{12}\tilde{S}.\end{aligned}\quad (\text{A.1})$$

Now

$$\hat{P}_{1'2'}\tilde{S}f_6^{ij}(\underline{s})Q_{11,\mu}(I_4 \otimes \gamma^\mu)\hat{P}_{12}\tilde{S} = \tilde{S}f_6^{ij}(\overset{\leftrightarrow}{\underline{s}})Q_{22,\mu}(I_4 \otimes \gamma^\mu)\tilde{S}$$

under the simultaneous interchange of  $p_1 \rightleftharpoons k_1$  and  $p_2 \rightleftharpoons k_2$  (represented by the operators  $\hat{P}_{12}$  and  $\hat{P}_{1'2'}$ ). Use of Eqs. (2.30) and (2.32) leads to

$$\hat{P}_{1'2'}\tilde{S}f_6^{ij}(\overset{\leftrightarrow}{\underline{s}})Q_{11,\mu}(I_4 \otimes \gamma^\mu)\hat{P}_{1'2'}\tilde{S} = f_6^{ij}(\overset{\leftrightarrow}{\underline{s}})Q_{22,\mu}(\gamma^\mu \otimes I_4).$$

Similar steps can be carried out for the other terms in Eq. (A.1) and therefore

$$\hat{P}_{1'2'}\tilde{S}f_6^{ij}(\underline{s})\Gamma_6(\eta_{ij})\hat{P}_{12}\tilde{S} = f_6^{ij}(\overset{\leftrightarrow}{\underline{s}})\Gamma_6(\eta_{ij}).$$

The same arguments can be made for covariants  $\Gamma_7$  to  $\Gamma_9$  and therefore we can claim that

$$\hat{S}\hat{P}_{1'2'} f_n^{\rho_1\rho_1'\rho_2\rho_2'}(\underline{s}) \Gamma_n(\eta_{ij}) \hat{P}_{12}\tilde{S} = \chi_n f_n^{\rho_1\rho_1'\rho_2\rho_2'}(\overleftrightarrow{\underline{s}}) \Gamma_n(\eta_{ij}) \quad (\text{A.2})$$

where

$$\chi_n = \begin{cases} 1 & \text{if } n = 1\dots 5, 6, 8 \\ -1 & \text{if } n = 7, 9 \end{cases}$$

and

$$\overleftrightarrow{\underline{s}} = \{s_1, s_2, s_3, s_4, s_5, -s_6, -s_7\}.$$

Note in Eq. (A.2) that the order of the rho-spin indices are unchanged.

## A.2 Transformation properties of the covariants, $\Gamma_n$ , under a time-reversal transformation

We first record the following identity:

**Identity 1** *If  $|\tilde{\alpha}\rangle$  and  $|\tilde{\beta}\rangle$  are time-reversed states of  $|\alpha\rangle$  and  $|\beta\rangle$  respectively, i.e.*

$$|\tilde{\alpha}\rangle = \mathcal{T}|\alpha\rangle = |\tilde{\beta}\rangle = \mathcal{T}|\beta\rangle \quad (\text{A.3})$$

where  $\mathcal{T}$  is the time-reversal operator, then

$$\langle\beta|\hat{X}|\alpha\rangle = \langle\tilde{\alpha}|\mathcal{T}\hat{X}^\dagger\mathcal{T}^{-1}|\tilde{\beta}\rangle \quad (\text{A.4})$$

for any linear operator  $\hat{X}$  [Sa85].

We illustrate the calculation of the product

$$\mathcal{T}(\gamma^0 \otimes \gamma^0) \tilde{\Gamma}_n^\dagger(\gamma^0 \otimes \gamma^0) \mathcal{T}^{-1}$$

for the case of  $n = 8$ . From the definition of  $\Gamma_8$  given in Section 2.5.1, it follows that

$$\begin{aligned} \tilde{\Gamma}_8^\dagger(\eta_{ij}) &= \eta_{ij} \tilde{Q}_{11,\mu} (\gamma^{5\dagger} \otimes (\gamma^5 \gamma^\mu)^\dagger) + \eta_{ij} \tilde{Q}_{22,\mu} ((\gamma^5 \gamma^\mu)^\dagger \otimes \gamma^{5\dagger}) + \\ &\quad \eta_{ij} \tilde{Q}_{12,\mu} \tilde{S} (\gamma^{5\dagger} \otimes (\gamma^5 \gamma^\mu)^\dagger) + \eta_{ij} \tilde{Q}_{21,\mu} \tilde{S} ((\gamma^5 \gamma^\mu)^\dagger \otimes \gamma^{5\dagger}) \end{aligned}$$

where Eqs. (2.31) and (2.58) were used. Use of

$$\begin{aligned} \tilde{Q}_{11} &= Q_{11}, & \tilde{Q}_{22} &= Q_{22}, \\ \tilde{Q}_{12} &= Q_{21}, & \tilde{Q}_{21} &= Q_{12}, \end{aligned}$$

$$\gamma^0(\gamma^{5\dagger})\gamma^0 = -\gamma^5$$



and

$$\gamma^0(\gamma^5\gamma^\mu)^\dagger\gamma^0 = \gamma^5\gamma^\mu$$

leads to

$$(\gamma^0 \otimes \gamma^0)\tilde{\Gamma}_8^\dagger(\gamma^0 \otimes \gamma^0) = -(\eta_{ij}Q_{11,\mu}(\gamma^5 \otimes \gamma^5\gamma^\mu) + \eta_{ij}Q_{22,\mu}(\gamma^5\gamma^\mu \otimes \gamma^5) + \eta_{ij}Q_{21,\mu}(\gamma^5\gamma^\mu \otimes \gamma^5)\tilde{S} + \eta_{ij}Q_{12,\mu}(\gamma^5 \otimes \gamma^5\gamma^\mu)).$$

Use of Table 2.4 then leads to

$$\mathcal{T}(\gamma^0 \otimes \gamma^0)\tilde{\Gamma}_8^\dagger(\gamma^0 \otimes \gamma^0)\mathcal{T}^{-1} = -\Gamma_8.$$

Similar reasoning applied to the other covariants allows us to write:

$$\mathcal{T}(\gamma^0 \otimes \gamma^0)\tilde{\Gamma}_n^\dagger(\eta_{ij})(\gamma^0 \otimes \gamma^0)\mathcal{T}^{-1} = \begin{cases} \Gamma_n(\eta_{ij}) & \text{if } n = 1\dots 5, 6 \\ -\Gamma_n(\eta_{ij}) & \text{if } n = 8. \end{cases}$$

Note that  $\Gamma_7$  and  $\Gamma_9$  do not transform simply under a time-reversal transformation [Tj87a].

## Appendix B

### Definition of matrices $t_i$

The  $t$ -matrices referred to in Section 2.5.3 are listed in Table B.1 for the  $SPVAT$  covariants, Table B.2 for covariants  $K_{10}$  to  $K_{11}$  and Table B.3 for covariants  $K_{12}$  to  $K_{13}$ . Even though it is straightforward to calculate traces of these  $t$ -matrices, one only needs to take care with covariants involving the matrix  $\tilde{S}$ . Since  $\tilde{S}$  cannot be written in the form of a Kronecker product, the identity

$$\text{Tr}[(A \otimes B)(C \otimes D)] = \text{Tr}(AC) \text{Tr}(BD) \quad (\text{B.1})$$

will not be useful for covariants  $K_{10}$  to  $K_{13}$  but instead the identity

$$\text{Tr}[(A \otimes B)\tilde{S}(C \otimes D)] = \text{Tr}[ADBC] \quad (\text{B.2})$$

where

$$\begin{aligned} A, B &\equiv 2 \times 4 \text{ matrices,} \\ C, D &\equiv 4 \times 2 \text{ matrices and} \\ \tilde{S} &\equiv 16 \times 16 \text{ matrix.} \end{aligned}$$

Table B.1:  $t$ -matrices for the SPVAT covariants.

covariant	$t$ -matrix
$S = I_4 \otimes I_4$	$t_1 = \bar{\Gamma}_{\rho_1'}(1')\Gamma_{\rho_1}(1)$ $t_2 = \sigma_i \bar{\Gamma}_{\rho_1'}(1')\Gamma_{\rho_1}(1)$
$P = \gamma^5 \otimes \gamma^5$	$t_3 = \sigma_i \bar{\Gamma}_{\rho_1'}(1')\gamma^5 \Gamma_{\rho_1}(1)$
$V = \gamma^\mu \otimes \gamma_\mu$	$t_4 = \bar{\Gamma}_{\rho_1'}(1')\gamma^0 \Gamma_{\rho_1}(1)$ $t_5 = \bar{\Gamma}_{\rho_1'}(1')\gamma^i \Gamma_{\rho_1}(1)$ $t_6 = \sigma_k \bar{\Gamma}_{\rho_1'}(1')\gamma^0 \Gamma_{\rho_1}(1)$ $t_7 = \sigma_k \bar{\Gamma}_{\rho_1'}(1')\gamma^i \Gamma_{\rho_1}(1)$
$A = \gamma^5 \gamma^\mu \otimes \gamma^5 \gamma_\mu$	$t_8 = \bar{\Gamma}_{\rho_1'}(1')\gamma^5 \gamma^i \Gamma_{\rho_1}(1)$ $t_9 = \sigma_k \bar{\Gamma}_{\rho_1'}(1')\gamma^5 \gamma^0 \Gamma_{\rho_1}(1)$ $t_{10} = \sigma_k \bar{\Gamma}_{\rho_1'}(1')\gamma^5 \gamma^i \Gamma_{\rho_1}(1)$
$T = \sigma^{\mu\nu} \otimes \sigma_{\mu\nu}$	$t_{11} = \bar{\Gamma}_{\rho_1'}(1')\sigma^{0i} \Gamma_{\rho_1}(1)$ $t_{12} = \bar{\Gamma}_{\rho_1'}(1')\sigma^{ij} \Gamma_{\rho_1}(1)$ $t_{13} = \sigma_k \bar{\Gamma}_{\rho_1'}(1')\sigma^{0i} \Gamma_{\rho_1}(1)$ $t_{14} = \sigma_k \bar{\Gamma}_{\rho_1'}(1')\sigma^{ij} \Gamma_{\rho_1}(1)$

 Table B.2:  $t$ -matrices for covariants  $K_{10}$  to  $K_{11}$ .

covariant	$t$ -matrices
$K_{10} = Q_{12,\mu}(I_4 \otimes \gamma^\mu) \tilde{S}$	$t_{15} = \bar{\Gamma}_{\rho_1'} \Gamma_{\rho_2} \bar{\Gamma}_{\rho_2'} \gamma^0 \Gamma_{\rho_1}$ $t_{16} = \bar{\Gamma}_{\rho_1'} \Gamma_{\rho_2} \bar{\Gamma}_{\rho_2'} \gamma^i \Gamma_{\rho_1}$ $t_{17} = \sigma_r \bar{\Gamma}_{\rho_1'} \Gamma_{\rho_2} \sigma_s \bar{\Gamma}_{\rho_2'} \gamma^0 \Gamma_{\rho_1}$ $t_{18} = \sigma_r \bar{\Gamma}_{\rho_1'} \Gamma_{\rho_2} \sigma_s \bar{\Gamma}_{\rho_2'} \gamma^i \Gamma_{\rho_1}$ $t_{19} = \sigma_r \bar{\Gamma}_{\rho_1'} \Gamma_{\rho_2} \bar{\Gamma}_{\rho_2'} \gamma^0 \Gamma_{\rho_1}$ $t_{20} = \sigma_r \bar{\Gamma}_{\rho_1'} \Gamma_{\rho_2} \bar{\Gamma}_{\rho_2'} \gamma^i \Gamma_{\rho_1}$ $t_{21} = \bar{\Gamma}_{\rho_1'} \Gamma_{\rho_2} \sigma_s \bar{\Gamma}_{\rho_2'} \gamma^0 \Gamma_{\rho_1}$ $t_{22} = \bar{\Gamma}_{\rho_1'} \Gamma_{\rho_2} \sigma_s \bar{\Gamma}_{\rho_2'} \gamma^i \Gamma_{\rho_1}$
$K_{11} = Q_{21,\mu}(\gamma^\mu \otimes I_4) \tilde{S}$	$t_{23} = \bar{\Gamma}_{\rho_1'} \gamma^0 \Gamma_{\rho_2} \bar{\Gamma}_{\rho_2'} \Gamma_{\rho_1}$ $t_{24} = \bar{\Gamma}_{\rho_1'} \gamma^i \Gamma_{\rho_2} \bar{\Gamma}_{\rho_2'} \Gamma_{\rho_1}$ $t_{25} = \sigma_k \bar{\Gamma}_{\rho_1'} \gamma^0 \Gamma_{\rho_2} \sigma_l \bar{\Gamma}_{\rho_2'} \Gamma_{\rho_1}$ $t_{26} = \sigma_k \bar{\Gamma}_{\rho_1'} \gamma^i \Gamma_{\rho_2} \sigma_l \bar{\Gamma}_{\rho_2'} \Gamma_{\rho_1}$ $t_{27} = \sigma_k \bar{\Gamma}_{\rho_1'} \gamma^0 \Gamma_{\rho_2} \bar{\Gamma}_{\rho_2'} \Gamma_{\rho_1}$ $t_{28} = \sigma_k \bar{\Gamma}_{\rho_1'} \gamma^i \Gamma_{\rho_2} \bar{\Gamma}_{\rho_2'} \Gamma_{\rho_1}$ $t_{29} = \bar{\Gamma}_{\rho_1'} \gamma^0 \Gamma_{\rho_2} \sigma_k \bar{\Gamma}_{\rho_2'} \Gamma_{\rho_1}$ $t_{30} = \bar{\Gamma}_{\rho_1'} \gamma^i \Gamma_{\rho_2} \sigma_k \bar{\Gamma}_{\rho_2'} \Gamma_{\rho_1}$



Table B.3:  $t$ -matrices for covariants  $K_{12}$  to  $K_{13}$ .

covariant	$t$ -matrices
$K_{12} = Q_{12,\mu}(\gamma^5 \otimes \gamma^5 \gamma^\mu) \tilde{S}$	$t_{31} = \bar{\Gamma}_{\rho_1'} \gamma^5 \Gamma_{\rho_2} \bar{\Gamma}_{\rho_2'} \gamma^5 \gamma^0 \Gamma_{\rho_1}$
	$t_{32} = \bar{\Gamma}_{\rho_1'} \gamma^5 \Gamma_{\rho_2} \bar{\Gamma}_{\rho_2'} \gamma^5 \gamma^i \Gamma_{\rho_1}$
	$t_{33} = \sigma_k \bar{\Gamma}_{\rho_1'} \gamma^5 \Gamma_{\rho_2} \sigma_l \bar{\Gamma}_{\rho_2'} \gamma^5 \gamma^0 \Gamma_{\rho_1}$
	$t_{34} = \sigma_k \bar{\Gamma}_{\rho_1'} \gamma^5 \Gamma_{\rho_2} \sigma_l \bar{\Gamma}_{\rho_2'} \gamma^5 \gamma^i \Gamma_{\rho_1}$
	$t_{35} = \sigma_k \bar{\Gamma}_{\rho_1'} \gamma^5 \Gamma_{\rho_2} \bar{\Gamma}_{\rho_2'} \gamma^5 \gamma^0 \Gamma_{\rho_1}$
	$t_{36} = \sigma_k \bar{\Gamma}_{\rho_1'} \gamma^5 \Gamma_{\rho_2} \bar{\Gamma}_{\rho_2'} \gamma^5 \gamma^i \Gamma_{\rho_1}$
	$t_{37} = \bar{\Gamma}_{\rho_1'} \gamma^5 \Gamma_{\rho_2} \sigma_k \bar{\Gamma}_{\rho_2'} \gamma^5 \gamma^0 \Gamma_{\rho_1}$
	$t_{38} = \bar{\Gamma}_{\rho_1'} \gamma^5 \Gamma_{\rho_2} \sigma_k \bar{\Gamma}_{\rho_2'} \gamma^5 \gamma^i \Gamma_{\rho_1}$
$K_{13} = Q_{21,\mu}(\gamma^5 \gamma^\mu \otimes \gamma^5) \tilde{S}$	$t_{39} = \bar{\Gamma}_{\rho_1'} \gamma^5 \gamma^0 \Gamma_{\rho_2} \bar{\Gamma}_{\rho_2'} \gamma^5 \Gamma_{\rho_1}$
	$t_{40} = \bar{\Gamma}_{\rho_1'} \gamma^5 \gamma^i \Gamma_{\rho_2} \bar{\Gamma}_{\rho_2'} \gamma^5 \Gamma_{\rho_1}$
	$t_{41} = \sigma_k \bar{\Gamma}_{\rho_1'} \gamma^5 \gamma^0 \Gamma_{\rho_2} \sigma_l \bar{\Gamma}_{\rho_2'} \gamma^5 \Gamma_{\rho_1}$
	$t_{42} = \sigma_k \bar{\Gamma}_{\rho_1'} \gamma^5 \gamma^i \Gamma_{\rho_2} \sigma_l \bar{\Gamma}_{\rho_2'} \gamma^5 \Gamma_{\rho_1}$
	$t_{43} = \sigma_k \bar{\Gamma}_{\rho_1'} \gamma^5 \gamma^0 \Gamma_{\rho_2} \bar{\Gamma}_{\rho_2'} \gamma^5 \Gamma_{\rho_1}$
	$t_{44} = \sigma_k \bar{\Gamma}_{\rho_1'} \gamma^5 \gamma^i \Gamma_{\rho_2} \bar{\Gamma}_{\rho_2'} \gamma^5 \Gamma_{\rho_1}$
	$t_{45} = \bar{\Gamma}_{\rho_1'} \gamma^5 \gamma^0 \Gamma_{\rho_2} \sigma_r \bar{\Gamma}_{\rho_2'} \gamma^5 \Gamma_{\rho_1}$
	$t_{46} = \bar{\Gamma}_{\rho_1'} \gamma^5 \gamma^i \Gamma_{\rho_2} \sigma_r \bar{\Gamma}_{\rho_2'} \gamma^5 \Gamma_{\rho_1}$

## Appendix C

# Explicit expressions for spin observables in terms of the effective amplitudes, $a_i$ ( $i = 1 - 8$ )

In this appendix we present explicit expressions for the quantities  $\Gamma''$ ,  $\Gamma'$  and  $\Gamma$  in terms of the effective amplitudes  $a_i$  which are related as follows to the effective amplitudes  $b_i$ :

$$\begin{aligned} b_1 &= a_1 \\ b_2 &= \frac{a_2}{m^4}, \\ b_i &= \frac{i}{m^2} a_i \quad \text{for } i = 3, 4 \quad \text{and} \\ b_i &= \frac{1}{m^2} a_i \quad \text{for } i = 5, 6, 7, 8 \end{aligned}$$

where  $m$  denotes the free nucleon mass.

$$\begin{aligned} \frac{1}{g_1^2} \Gamma''(\vec{p}_1, \vec{p}_2, \vec{k}_1, \vec{k}_2) = & \\ & 4 \operatorname{Im}(a_1)^2 + 4 \operatorname{Re}(a_1)^2 + (\vec{N} \cdot \vec{N})^2 \left( \frac{4 \operatorname{Im}(a_2)^2}{m^8} + \frac{4 \operatorname{Re}(a_2)^2}{m^8} \right) + \\ & \vec{N} \cdot \vec{N} \left( \frac{4 \operatorname{Im}(a_3)^2}{m^4} + \frac{4 \operatorname{Re}(a_3)^2}{m^4} + \frac{4 \operatorname{Im}(a_4)^2}{m^4} + \frac{4 \operatorname{Re}(a_4)^2}{m^4} \right) + \left( \frac{4 \operatorname{Im}(a_6)^2}{m^4} + \frac{4 \operatorname{Re}(a_6)^2}{m^4} \right) (\vec{p}_a \cdot \vec{p}_a)^2 + \\ & \left( \frac{8 \operatorname{Im}(a_6) \operatorname{Im}(a_7)}{m^4} + \frac{8 \operatorname{Re}(a_6) \operatorname{Re}(a_7)}{m^4} + \frac{8 \operatorname{Im}(a_6) \operatorname{Im}(a_8)}{m^4} + \frac{8 \operatorname{Re}(a_6) \operatorname{Re}(a_8)}{m^4} \right) \vec{p}_a \cdot \vec{p}_a \vec{p}_a \cdot \vec{q} + \\ & \left( \frac{8 \operatorname{Im}(a_5) \operatorname{Im}(a_6)}{m^4} + \frac{8 \operatorname{Re}(a_5) \operatorname{Re}(a_6)}{m^4} + \frac{8 \operatorname{Im}(a_7) \operatorname{Im}(a_8)}{m^4} + \frac{8 \operatorname{Re}(a_7) \operatorname{Re}(a_8)}{m^4} \right) (\vec{p}_a \cdot \vec{q})^2 + \\ & \left( \frac{8 \operatorname{Im}(a_5) \operatorname{Im}(a_7)}{m^4} + \frac{8 \operatorname{Re}(a_5) \operatorname{Re}(a_7)}{m^4} + \frac{8 \operatorname{Im}(a_5) \operatorname{Im}(a_8)}{m^4} + \frac{8 \operatorname{Re}(a_5) \operatorname{Re}(a_8)}{m^4} \right) \vec{p}_a \cdot \vec{q} \vec{q} \cdot \vec{q} + \\ & \left( \frac{4 \operatorname{Im}(a_5)^2}{m^4} + \frac{4 \operatorname{Re}(a_5)^2}{m^4} \right) (\vec{q} \cdot \vec{q})^2 + \left( \frac{4 \operatorname{Im}(a_7)^2}{m^4} + \frac{4 \operatorname{Re}(a_7)^2}{m^4} + \frac{4 \operatorname{Im}(a_8)^2}{m^4} + \frac{4 \operatorname{Re}(a_8)^2}{m^4} \right) \vec{p}_a \cdot \vec{p}_a \vec{q} \cdot \vec{q} \quad (\text{C.1}) \end{aligned}$$

$$\begin{aligned} \frac{1}{g_1^2} \Gamma'(\vec{p}_1, \dots, \vec{k}_2, \hat{s}_f) = & \\ & \left( \frac{-4 \operatorname{Re}(a_2) \operatorname{Im}(a_4) \vec{N} \cdot \vec{N}}{m^6} + \frac{4 \operatorname{Im}(a_2) \operatorname{Re}(a_4) \vec{N} \cdot \vec{N}}{m^6} - \frac{4 \operatorname{Re}(a_1) \operatorname{Im}(a_3)}{m^2} + \frac{4 \operatorname{Im}(a_1) \operatorname{Re}(a_3)}{m^2} \right) \vec{N} \cdot \hat{s}_f + \\ & \vec{p}_a \cdot (\vec{q} \times \hat{s}_f) \left( \frac{4 \operatorname{Re}(a_6) \operatorname{Im}(a_7) \vec{p}_a \cdot \vec{p}_a}{m^4} - \frac{4 \operatorname{Im}(a_6) \operatorname{Re}(a_7) \vec{p}_a \cdot \vec{p}_a}{m^4} - \frac{4 \operatorname{Re}(a_5) \operatorname{Im}(a_6) \vec{p}_a \cdot \vec{q}}{m^4} + \frac{4 \operatorname{Im}(a_5) \operatorname{Re}(a_6) \vec{p}_a \cdot \vec{q}}{m^4} - \right. \\ & \left. \frac{4 \operatorname{Re}(a_7) \operatorname{Im}(a_8) \vec{p}_a \cdot \vec{q}}{m^4} + \frac{4 \operatorname{Im}(a_7) \operatorname{Re}(a_8) \vec{p}_a \cdot \vec{q}}{m^4} - \frac{4 \operatorname{Re}(a_5) \operatorname{Im}(a_8) \vec{q} \cdot \vec{q}}{m^4} + \frac{4 \operatorname{Im}(a_5) \operatorname{Re}(a_8) \vec{q} \cdot \vec{q}}{m^4} \right) \quad (\text{C.2}) \end{aligned}$$

$$\begin{aligned}
\frac{1}{4g_1^2} \Gamma(\vec{p}_1, \dots, \vec{k}_2, \hat{s}_i, \hat{s}_f) = & \left( \frac{2 \operatorname{Im}(a_2)^2 \vec{N} \cdot \vec{N}}{m^8} + \frac{2 \operatorname{Re}(a_2)^2 \vec{N} \cdot \vec{N}}{m^8} + \frac{2 \operatorname{Im}(a_3)^2}{m^4} + \frac{2 \operatorname{Re}(a_3)^2}{m^4} \right) \vec{N} \cdot \hat{s}_f \vec{N} \cdot \hat{s}_i + \left( \frac{2 \operatorname{Im}(a_2) \operatorname{Im}(a_4) \vec{N} \cdot \vec{N}}{m^6} + \right. \\
& \left. \frac{2 \operatorname{Re}(a_2) \operatorname{Re}(a_4) \vec{N} \cdot \vec{N}}{m^6} - \frac{2 \operatorname{Im}(a_1) \operatorname{Im}(a_3)}{m^2} - \frac{2 \operatorname{Re}(a_1) \operatorname{Re}(a_3)}{m^2} \right) \vec{N} \cdot (\hat{s}_i \times \hat{s}_f) + \vec{p}_a \cdot \hat{s}_f \vec{p}_a \cdot \hat{s}_i \left( \frac{2 \operatorname{Im}(a_6)^2 \vec{p}_a \cdot \vec{p}_a}{m^4} + \right. \\
& \left. \frac{2 \operatorname{Re}(a_6)^2 \vec{p}_a \cdot \vec{p}_a}{m^4} + \frac{4 \operatorname{Im}(a_6) \operatorname{Im}(a_8) \vec{p}_a \cdot \vec{q}}{m^4} + \frac{4 \operatorname{Re}(a_6) \operatorname{Re}(a_8) \vec{p}_a \cdot \vec{q}}{m^4} + \frac{2 \operatorname{Im}(a_8)^2 \vec{q} \cdot \vec{q}}{m^4} + \frac{2 \operatorname{Re}(a_8)^2 \vec{q} \cdot \vec{q}}{m^4} \right) + \\
& \vec{p}_a \cdot \hat{s}_i \left( \frac{2 \operatorname{Im}(a_6) \operatorname{Im}(a_7) \vec{p}_a \cdot \vec{p}_a}{m^4} + \frac{2 \operatorname{Re}(a_6) \operatorname{Re}(a_7) \vec{p}_a \cdot \vec{p}_a}{m^4} + \frac{2 \operatorname{Im}(a_5) \operatorname{Im}(a_6) \vec{p}_a \cdot \vec{q}}{m^4} + \frac{2 \operatorname{Re}(a_5) \operatorname{Re}(a_6) \vec{p}_a \cdot \vec{q}}{m^4} + \right. \\
& \left. \frac{2 \operatorname{Im}(a_7) \operatorname{Im}(a_8) \vec{p}_a \cdot \vec{q}}{m^4} + \frac{2 \operatorname{Re}(a_7) \operatorname{Re}(a_8) \vec{p}_a \cdot \vec{q}}{m^4} + \frac{2 \operatorname{Im}(a_5) \operatorname{Im}(a_8) \vec{q} \cdot \vec{q}}{m^4} + \frac{2 \operatorname{Re}(a_5) \operatorname{Re}(a_8) \vec{q} \cdot \vec{q}}{m^4} \right) \vec{q} \cdot \hat{s}_f + \\
& \vec{p}_a \cdot \hat{s}_f \left( \frac{2 \operatorname{Im}(a_6) \operatorname{Im}(a_7) \vec{p}_a \cdot \vec{p}_a}{m^4} + \frac{2 \operatorname{Re}(a_6) \operatorname{Re}(a_7) \vec{p}_a \cdot \vec{p}_a}{m^4} + \frac{2 \operatorname{Im}(a_5) \operatorname{Im}(a_6) \vec{p}_a \cdot \vec{q}}{m^4} + \frac{2 \operatorname{Re}(a_5) \operatorname{Re}(a_6) \vec{p}_a \cdot \vec{q}}{m^4} + \right. \\
& \left. \frac{2 \operatorname{Im}(a_7) \operatorname{Im}(a_8) \vec{p}_a \cdot \vec{q}}{m^4} + \frac{2 \operatorname{Re}(a_7) \operatorname{Re}(a_8) \vec{p}_a \cdot \vec{q}}{m^4} + \frac{2 \operatorname{Im}(a_5) \operatorname{Im}(a_8) \vec{q} \cdot \vec{q}}{m^4} + \frac{2 \operatorname{Re}(a_5) \operatorname{Re}(a_8) \vec{q} \cdot \vec{q}}{m^4} \right) \vec{q} \cdot \hat{s}_i + \\
& \left( \frac{2 \operatorname{Im}(a_7)^2 \vec{p}_a \cdot \vec{p}_a}{m^4} + \frac{2 \operatorname{Re}(a_7)^2 \vec{p}_a \cdot \vec{p}_a}{m^4} + \frac{4 \operatorname{Im}(a_5) \operatorname{Im}(a_7) \vec{p}_a \cdot \vec{q}}{m^4} + \frac{4 \operatorname{Re}(a_5) \operatorname{Re}(a_7) \vec{p}_a \cdot \vec{q}}{m^4} + \frac{2 \operatorname{Im}(a_5)^2 \vec{q} \cdot \vec{q}}{m^4} + \right. \\
& \left. \frac{2 \operatorname{Re}(a_5)^2 \vec{q} \cdot \vec{q}}{m^4} \right) \vec{q} \cdot \hat{s}_f \vec{q} \cdot \hat{s}_i + \left( \operatorname{Im}(a_1)^2 + \operatorname{Re}(a_1)^2 - \frac{\operatorname{Im}(a_2)^2 (\vec{N} \cdot \vec{N})^2}{m^8} - \frac{\operatorname{Re}(a_2)^2 (\vec{N} \cdot \vec{N})^2}{m^8} - \frac{\operatorname{Im}(a_3)^2 \vec{N} \cdot \vec{N}}{m^4} - \right. \\
& \frac{\operatorname{Re}(a_3)^2 \vec{N} \cdot \vec{N}}{m^4} + \frac{\operatorname{Im}(a_4)^2 \vec{N} \cdot \vec{N}}{m^4} + \frac{\operatorname{Re}(a_4)^2 \vec{N} \cdot \vec{N}}{m^4} - \frac{\operatorname{Im}(a_6)^2 (\vec{p}_a \cdot \vec{p}_a)^2}{m^4} - \frac{\operatorname{Re}(a_6)^2 (\vec{p}_a \cdot \vec{p}_a)^2}{m^4} - \\
& \frac{2 \operatorname{Im}(a_6) \operatorname{Im}(a_7) \vec{p}_a \cdot \vec{p}_a \vec{p}_a \cdot \vec{q}}{m^4} - \frac{2 \operatorname{Re}(a_6) \operatorname{Re}(a_7) \vec{p}_a \cdot \vec{p}_a \vec{p}_a \cdot \vec{q}}{m^4} - \frac{2 \operatorname{Im}(a_6) \operatorname{Im}(a_8) \vec{p}_a \cdot \vec{p}_a \vec{p}_a \cdot \vec{q}}{m^4} - \\
& \frac{2 \operatorname{Re}(a_6) \operatorname{Re}(a_8) \vec{p}_a \cdot \vec{p}_a \vec{p}_a \cdot \vec{q}}{m^4} - \frac{2 \operatorname{Im}(a_5) \operatorname{Im}(a_6) (\vec{p}_a \cdot \vec{q})^2}{m^4} - \frac{2 \operatorname{Re}(a_5) \operatorname{Re}(a_6) (\vec{p}_a \cdot \vec{q})^2}{m^4} - \frac{2 \operatorname{Im}(a_7) \operatorname{Im}(a_8) (\vec{p}_a \cdot \vec{q})^2}{m^4} - \\
& \frac{2 \operatorname{Re}(a_7) \operatorname{Re}(a_8) (\vec{p}_a \cdot \vec{q})^2}{m^4} - \frac{\operatorname{Im}(a_7)^2 \vec{p}_a \cdot \vec{p}_a \vec{q} \cdot \vec{q}}{m^4} - \frac{\operatorname{Re}(a_7)^2 \vec{p}_a \cdot \vec{p}_a \vec{q} \cdot \vec{q}}{m^4} - \frac{\operatorname{Im}(a_8)^2 \vec{p}_a \cdot \vec{p}_a \vec{q} \cdot \vec{q}}{m^4} - \frac{\operatorname{Re}(a_8)^2 \vec{p}_a \cdot \vec{p}_a \vec{q} \cdot \vec{q}}{m^4} - \\
& \frac{2 \operatorname{Im}(a_5) \operatorname{Im}(a_7) \vec{p}_a \cdot \vec{q} \vec{q} \cdot \vec{q}}{m^4} - \frac{2 \operatorname{Re}(a_5) \operatorname{Re}(a_7) \vec{p}_a \cdot \vec{q} \vec{q} \cdot \vec{q}}{m^4} - \frac{2 \operatorname{Im}(a_5) \operatorname{Im}(a_8) \vec{p}_a \cdot \vec{q} \vec{q} \cdot \vec{q}}{m^4} - \frac{2 \operatorname{Re}(a_5) \operatorname{Re}(a_8) \vec{p}_a \cdot \vec{q} \vec{q} \cdot \vec{q}}{m^4} - \\
& \left. \frac{\operatorname{Im}(a_5)^2 (\vec{q} \cdot \vec{q})^2}{m^4} - \frac{\operatorname{Re}(a_5)^2 (\vec{q} \cdot \vec{q})^2}{m^4} \right) \hat{s}_i \cdot \hat{s}_f \tag{C.3}
\end{aligned}$$



## Appendix D

### Exchange covariants, $\tilde{S}$ , $\tilde{P}$ , $\tilde{V}$ , $\tilde{A}$ and $\tilde{T}$ in terms of the $SPVAT$ covariants

The  $SPVAT$  covariants are linearly independent and therefore we may write:

$$\tilde{X} = aS + bP + cV + dA + eT$$

where  $X \in \{S, P, V, A, T\}$  which leads to the following equations for the expansion coefficients:

$$\begin{aligned} a &= \frac{1}{16} \text{Tr}(\tilde{X}) \\ b &= \frac{1}{16} \text{Tr}(P\tilde{X}) \\ c &= \frac{1}{64} \text{Tr}(V\tilde{X}) \\ d &= \frac{1}{64} \text{Tr}(A\tilde{X}) \\ e &= \frac{1}{384} \text{Tr}(T\tilde{X}). \end{aligned}$$

To calculate the traces we can use the identity:

$$\text{Tr}(\tilde{X}) = \text{Tr}(X\tilde{S}) = \text{Tr}(X_1X_2)$$

if  $X = X_1 \otimes X_2$ . This leads to the following matrix relation between the exchange covariants and the  $SPVAT$  covariants:

$$\begin{pmatrix} \tilde{S} \\ \tilde{P} \\ \tilde{V} \\ \tilde{A} \\ \tilde{T} \end{pmatrix} = \frac{1}{4} \begin{pmatrix} 1 & 1 & \frac{1}{2} & -1 & 1 \\ 4 & -2 & 0 & -2 & -4 \\ 12 & 0 & -2 & 0 & 12 \\ -4 & -2 & 0 & -2 & 4 \\ 1 & -1 & \frac{1}{2} & 1 & 1 \end{pmatrix} \begin{pmatrix} S \\ P \\ V \\ A \\ T \end{pmatrix}. \quad (\text{D.1})$$

# Bibliography

- [Ad84] D.L. Adams and M. Bleszynski, Phys. Lett. **136B**, 10 (1984).
- [Am83] R. D. Amado, J. Piekarewicz, D.A. Sparrow and J.A. McNiel, Phys. Rev. C **28**, 1663 (1983).
- [Ar76] L.G. Arnold, B.C. Clark, R.L. Mercer, D.G. Ravenhall and A.M. Saperstein, Phys. Rev. C **14**, 1878 (1976).
- [Ar79] L.G. Arnold, B.C. Clark and R.L. Mercer, Phys. Rev. C **19**, 917 (1979).
- [Ar81] L.G. Arnold, B.C. Clark, R.L. Mercer and P. Schwandt, Phys. Rev. C **23**, 1949 (1981).
- [Bj64] J.D. Bjorken and S. Drell, *Relativistic Quantum Mechanics* (McGraw-Hill, New York, 1964).
- [Bo94] H.F. Boersma and R. Malfiet, Phys. Rev. C **49**, 233 (1994).
- [Br76] G.E. Brown and A.D. Jackson, *The Nucleon-Nucleon Interaction* (North-Holland Publishing Company, Amsterdam, 1976).
- [Ca84] T.A. Carey, K.W. Jones, J.B. McClelland, M. Moss, L.B. Rees, N. Takana and A.D. Bacher, Phys. Rev. Lett **53**, 144 (1984).
- [Ca95] D.S. Carman, *Inclusive and Exclusive Quasifree ( $\vec{p}$ ,  $Np$ ) Reaction Studies from  $^2\text{H}$  and  $^{12}\text{C}$  at 200 MeV*, Ph.D Thesis, Indiana University (1995), unpublished.
- [Ch32] J. Chadwick, Proc. Roy. Soc. (London) **A136**, 692 (1932).
- [Ch98] M. Chaichian and R. Hagedorn, *Symmetries in Quantum Mechanics* (Institute of Physics Publishing, Bristol, 1998).
- [Ch89] C. Chan, T.E. Drake, R. Abegg, D. Frekers, O. Häusser, K. Hicks, D.A. Hutcheon, L. Lee, C.A. Miller, R. Schubank, E.J. Stephenson and S. Yen, J. Phys. G **15**, L55 (1989).
- [Ch90] C. Chan, T.E. Drake, R. Abegg, D. Frekers, O. Häusser, K. Hicks, D.A. Hutcheon, L. Lee, C.A. Miller, R. Schubank and S. Yen, Nucl. Phys. **A510**, 713 (1990).
- [Cl73] B.C. Clark, R.L. Mercer, D.G. Ravenhall and A.M. Saperstein, Phys. Rev. C **7**, 466 (1973).

- [Cl82] B.C. Clark, S. Hamma and R.L. Mercer, in *The Interaction Between Medium Energy Nucleons in Nuclei*, edited by H.O. Meyer, (American Institute of Physics, New York, 1983), p. 260.
- [Fu93] R.J. Furnstahl and S.J. Wallace, *Phys. Rev. C* **47**, 2812 (1994).
- [Go57] M.L. Goldberger, Y. Nambu and R. Oehme, *Ann. Phys.* **2**, 226 (1957).
- [Go60] M.L. Goldberger, M.T. Grisaru, S.W. MacDowell and D.Y. Wong, *Phys. Rev. C* **120**, 2250 (1960).
- [Ha87] M. Haji-Saied, E. Bleszynski, J. Carrol, G.J. Igo, T. Jaroszewicz, A.T.M. Wang, A. Sagle, J.B. McClelland, C.L. Morris, R. Klem, T. Joyce, Y. Makdishi, M. Marshak, B. Mossberg, E.A. Peterson, K. Ruddick and J. Whittaker, *Phys. Rev. C* **36**, 2010 (1987).
- [Ha59] J. Hamilton, *Theory of Elementary Particles*, (Oxford University Press, London, 1959).
- [Hä88] O. Häusser, R. Abegg, R.G. Jeppesen, R. Sawafta, A. Celler, A. Green, R.L. Helmer, R. Henderson, K. Hicks, K.P. Jackson, J. Mildenerger, C.A. Miller, M.C. Vetterli, S. Yen, M.J. Iqbal and R.D. Smith, *Phys. Rev. Lett.* **61**, 822 1988.
- [Ha98] C.L. Hautala, *Measurement of Polarization Observables in the Quasielastic Region on  $^{nat}Ca$  and  $^{nat}Pb$  using the  $(\vec{p}, \vec{n})$  Reaction at 200 MeV*, Ph.D Thesis, Ohio University (1998), unpublished and private communication.
- [Hi89] K.H. Hicks, M.C. Vetterli, A. Celler, R.L. Helmer, R.S. Henderson, K.P. Jackson, R.G. Jeppesen, A. Trudel and S. Yen, *Phys. Rev. C* **40**, 2445 (1989).
- [Hi90] G.C. Hillhouse, *Nuclear Reactions with Polarized Spin- $\frac{1}{2}$  Beams*, M.Sc Thesis (University of Stellenbosch, 1990), unpublished.
- [Hi94] G.C. Hillhouse and P.R. de Kock, *Phys. Rev. C* **49**, 391 (1994).
- [Hi95] G.C. Hillhouse and P.R. de Kock, *Phys. Rev. C* **52**, 2796 (1995).
- [Hi98] G.C. Hillhouse, B.I.S. van der Ventel, S.M. Wyngaardt and P.R. de Kock, *Phys. Rev. C* **57**, 448 (1998).
- [Hi99] G.C. Hillhouse, *Relativistic Descriptions of Polarization Transfer Observables for Quasielastic Proton Scattering*, Ph.D Thesis, University of Stellenbosch (1999), unpublished.
- [Ho85] C.J. Horowitz, *Phys. Rev. C* **31**, 1340 (1985).
- [Ho86] C.J. Horowitz and M.J. Iqbal, *Phys. Rev. C* **33**, 2059 (1986).
- [Ho88] C.J. Horowitz and D.P. Murdock, *Phys. Rev. C* **37**, 2032 (1988).



- [Ho91a] C.J. Horowitz, D.P. Murdock and B.D. Serot in *Computational Nuclear Physics I*, edited by K. Langanke, J.A. Maruhn and S.E. Koonin (Springer-Verlag, Berlin, 1991), p. 129.
- [Ho91b] C.J. Horowitz, in *Proceedings of the International Conference on Spin and Isospin in Nuclear Reactions, Telluride, Colorado, 1991*, edited by S.W. Wissink, C.D. Goodman and G.E. walker (Plenum Press, New York, 1991), p.415.
- [Ja59] M. Jacob and G.C. Wick, *Ann. Phys.* **7**, 404 (1959).
- [Ka90] C. Kalbach, *Phys. Rev. C* **41**, 1656 (1990).
- [Ke94] J.J. Kelly and S. J. Wallace, *Phys. Rev. C* **49**, 1315 (1994).
- [Ma96] O.V. Maxwell, *Nucl. Phys.* **A600**, 509 (1996).
- [Mc83] J.A. McNeil, J.R. Shepard and S.J. Wallace, *Phys. Rev. Lett.* **50**, 1439 (1983).
- [Mc83a] J.A. McNeil, L. Ray and S.J. Wallace, *Phys. Rev. C* **27**, 2123 (1983).
- [Mi72] L.D. Miller and A.E.S. Green, *Phys. Rev. C* **5**, 241 (1972).
- [Mi75] L.D. Miller, *Ann. Phys.* **91**, 40 (1975).
- [Mi76] L.D. Miller, *Phys. Rev. C* **14**, 706 (1976).
- [Mu87] D.P. Murdock and C.J. Horowitz, *Phys. Rev C* **35**, 1442 (1987).
- [Ot97] H. Otsu, *Study of Reaction Mechanisms for (p,n) and (p,p') quasi elastic scatterings*, Ph.D Thesis, University of Tokyo (1997), unpublished.
- [Pa81] M.K. Pal, *Theory of Nuclear Structures* (Scientific and Academic Editions, New Delhi, 1981).
- [Pi86] A. Picklesimer and P.C. Tandy, *Phys. Rev. C* **34**, 1860 (1986).
- [Ra87] A. Rahbar, B. Aas, E. Bleszynski, M. Bleszynski, K. Ganezer, G.J. Igo, F. Irom, B.E. Bonner, O. van Dyck, M.W. McNaughton, J.B. Roberts, C. Hollas, R.D. Ransome and P.J. Riley, *Phys. Lett.* **194B**, 338 (1987).
- [Sa85] J.J. Sakurai, *Modern Quantum Mechanics* (Addison and Wesley Publishing Corporation Incorporated, New York, 1985).
- [Se86] B.D. Serot and J.D. Walecka, in *Advances in Nuclear Physics*, edited by J.W. Negele and E. Vogt (Plenum Press, New York, 1986), Vol. 16.
- [Ta98] T.N. Taddeucci, private communication.
- [Tj85] J.A. Tjon and S.J. Wallace, *Phys. Rev. C* **32**, 1667 (1985).
- [Tj85b] J.A. Tjon and S.J. Wallace, *Phys. Rev. C* **32**, 267 (1985).

- [Tj85a] J.A. Tjon and S.J. Wallace, Phys. Rev. Lett. **54**, 1357 (1985).
- [Tj87] J.A. Tjon and S.J. Wallace, Phys. Rev. C **36**, 1085 (1987).
- [Tj87a] J.A. Tjon and S.J. Wallace, Phys. Rev. C **36**, 280 (1987).
- [Fa83] E.E. van Faassen and J.A. Tjon, Phys. Rev. C **28**, 2354 (1983).
- [Fa84] E.E. van Faassen and J.A. Tjon, Phys. Rev. C **30**, 285 (1984).
- [Wa96] T. Wakasa, *Study of Nuclear Isovector Spin Responses from Polarization Transfer in  $(p,n)$  Reactions at Intermediate Energies*, Ph.D Thesis, University of Tokyo (1996), unpublished.
- [Wa99] T. Wakasa, H. Sakai, K. Hatanaka, H. Okamura, H. Otsu, S. Fujita, T. Nonaka, T. Uesaka, Y. Satou, T. Ohnishi, G. Yokoyama, S. Ishida, N. Sakamoto, M.B. Greenfield, M. Ichimura and K. Kawahigashi, Phys. Rev. C **59**, 3177 (1999).
- [Wa74] J.D. Walecka, Ann. Phys. **83**, 491 (1974).
- [Wa94] L. Wang, X. Yang, J. Rapaport, C.D. Goodman, C.C. Foster, Y. Wang, J. Piekarewicz, E. Sugarbaker, D. Marchlinski, S. de Lucia, B. Luther, L. Rybarczyk, T.N. Taddeucci and B.K. Park, Phys. Rev. C **50**, 2438 (1994).
- [Wo88] S. Wolfram, *MATHEMATICA: A System for Doing Mathematics by Computer* (Addison-Wesley Publishing Company, Inc. New York, 1988).